

UNIVERSITY OF SOUTHAMPTON

FACULTY OF ENGINEERING, SCIENCE & MATHEMATICS

School of Geography

The MERIS Terrestrial Chlorophyll Index

by

Jadunandan Dash

Thesis for the degree of Doctor of Philosophy

October 2005

ABSTRACT

FACULTY OF ENGINEERING, SCIENCE & MATHEMATICS

SCHOOL OF GEOGRAPHY

Doctor of Philosophy**THE MERIS TERRESTRIAL CHLOROPHYLL INDEX**

Jadunandan Dash

The long wavelength edge of the major chlorophyll absorption feature in the spectrum of a vegetation canopy moves to longer wavelengths with an increase in chlorophyll content. The position of this red-edge has been used successfully to estimate, by remote sensing, the chlorophyll content of vegetation canopies. Techniques used to estimate this red-edge position (REP) have been designed for use on small volumes of continuous spectral data rather than the large volumes of discontinuous spectral data recorded by contemporary satellite spectrometers. Also, each technique produces a different value of REP from the same spectral data and REP values are relatively insensitive to chlorophyll content at high values of chlorophyll content.

This thesis reports on the design, evaluation and application of a surrogate REP index for use with spectral data recorded at the standard band settings of the Medium Resolution Imaging Spectrometer (MERIS). This index, termed the MERIS terrestrial chlorophyll index (MTCI) uses data in three red and NIR wavebands centred at 681.25 nm, 708.75 nm and 753.75 nm (bands 8, 9 and 10 in the MERIS standard band setting) to locate the relative position of the red edge. The MTCI is easy to calculate and can be automated. Preliminary indirect evaluation using model, field and MERIS data suggested the sensitivity of MTCI to chlorophyll content, notably at high levels and its insensitivity to spatial resolution and atmospheric effects. As a result this index is now an ESA level-2 product.

Two data sets were used for direct evaluation of the MTCI-chlorophyll content relationship. First, spectral reflectance and chlorophyll content data for spinach and poplar grown under controlled condition in a greenhouse and second, field data for a number of crops grown in sites in southern Spain. This suggests a stronger MTCI-chlorophyll content relationship than REP-chlorophyll content relationship. Due to lack of spatial and temporal chlorophyll content data from a suitably sized plot at MERIS spatial resolution it was not possible to validate the performance of the index with ground data. However, comparison with other vegetation indices available space-borne sensor suggested higher sensitive of MTCI to change in canopy chlorophyll content.

MTCI was used successfully to (i) infer the salt stress in the coastal and near coastal vegetation affected by the 26th December Indian Ocean Tsunami, (ii) monitor the condition of southern Vietnamese forests that had been contaminated by herbicides during the 1960s and 70s and (iii) map landcover in the state of Wisconsin, USA. Future work should emphasise of other regional to global scale applications of the MTCI and validation of MTCI with real ground data at MERIS spatial resolution.

CONTENTS

LIST OF FIGURES.....	vi
LIST OF TABLES.....	xiii
AUTHOR'S DECLARATION	xvi
ACKNOWLEDGEMENTS	xviii
ABBREVIATIONS.....	xx
CHAPTER 1. INTRODUCTION.....	1
1.1. INTRODUCTION.....	1
1.2. OBJECTIVE OF THIS RESEARCH	2
1.3. CHAPTER OVERVIEW	3
CHAPTER 2. LITERATURE REVIEW.....	6
2.1. INTRODUCTION.....	6
2.2. SPECTRAL PROPERTIES OF VEGETATION	6
2.2.1 <i>Visible region</i>	7
2.2.2 <i>NIR region</i>	7
2.2.3 <i>Middle-infrared region</i>	9
2.3. ROLE OF CHLOROPHYLL	9
2.4. THE RED EDGE	10
2.5. REP ESTIMATION TECHNIQUES.....	11
2.5.1 <i>Higher order curve fitting techniques</i>	12
2.5.2 <i>Inverted Gaussian technique</i>	13
2.5.3 <i>Linear interpolation</i>	15
2.5.4 <i>Lagrangian interpolation</i>	17
2.5.5 <i>Rational function</i>	18
2.6. MODELLING	19
2.6.1 <i>Leaf Models</i>	19
2.6.2 <i>Canopy Models</i>	24
2.6.3 <i>Combined models</i>	29
2.7. SPECTRAL MEASUREMENT TECHNIQUES FOR VEGETATION.....	31
2.7.1 <i>Laboratory Spectrometers</i>	32
2.7.2 <i>Field Spectrometers</i>	35
2.7.3 <i>Airborne imaging spectrometers</i>	37
2.7.4 <i>Space-borne imaging spectrometers</i>	47
2.7.4.1. <i>The Moderate Resolution Imaging Spectroradiometer</i>	48
2.7.4.2. <i>The Medium Resolution Imaging Spectrometer</i>	51
2.8. UNCERTAINTIES IN RED EDGE CHLOROPHYLL RELATIONSHIP	60
2.8.1 <i>Leaf area index</i>	60
2.8.2 <i>Fluorescence</i>	61

2.8.3 Chlorophyll a/b ratio.....	62
2.8.4 Viewing geometry.....	63
2.8.5 Soil and understorey.....	63
2.8.6 Senescence.....	65
2.8.7 Absorption due to other leaf components	65
2.9. APPLICATION OF THE RED EDGE	66
2.9.1 Vegetation productivity	66
2.9.2 Stress	67
2.9.3 Land contamination.....	70
2.9.4 Leaf nitrogen concentration	71
2.9.5 Possible spectroscopic bio-signature for extraterrestrial planets.....	71
CHAPTER 3. MERIS TERRESTRIAL CHLOROPHYLL INDEX: DESIGN AND INITIAL EVALUATION	73
3.1. INTRODUCTION.....	73
3.2. DESIGNING A CHLOROPHYLL INDEX	75
3.3. MTCI EVALUATION METHODS	76
3.3.1 Model data.....	76
3.3.2 Field data	77
3.3.3 MERIS data	77
3.4. MTCI EVALUATION RESULTS.....	78
3.4.1 Model data.....	78
3.4.2 Field data	78
3.4.3 MERIS data	80
3.5. DISCUSSION AND CONCLUSION.....	84
CHAPTER 4. UNDERSTANDING MTCI.....	85
4.1. INTRODUCTION.....	85
4.2. UNDERSTANDING THE SPECTRAL DATA	85
4.2.1 Reflectance spectrum of a leaf.....	85
4.2.2 Canopy reflectance.....	88
4.2.3 Satellite (MERIS) spectra	90
4.2.3.1. Effect of Landcover.....	90
4.2.4 Signal-to-noise ratio of MERIS data	91
4.2.4.1. Introduction.....	91
4.2.4.2. Methods of estimating SNR	92
4.2.4.3. Geostatistical Method.....	92
4.2.4.4. Estimating the SNR of MERIS.....	94
4.2.4.5. Results and discussion.....	97
4.2.4.6. Conclusion	101
4.3. EFFECT OF NON CANOPY VARIABLE ON MTCI.....	101
4.3.1 Introduction.....	101

4.3.2 <i>Simulated spectral data</i>	103
4.3.2.1. Methods of evaluation.....	104
4.3.2.2. Effect of soil brightness on MTCI.....	106
4.3.2.3. Effect of viewing angle	108
4.3.2.4. Effect of atmosphere	109
4.3.3 <i>Using real MERIS data</i>	112
4.3.3.1. Effect of data processing on MTCI	112
4.3.3.2. Effect of spatial resolution	119
4.3.3.3. Effect of aerosol load	120
4.4. CONCLUSION.....	122
CHAPTER 5. DIRECT MTCI EVALUATION.....	124
5.1. INTRODUCTION.....	124
5.2. EVALUATION OF MTCI WITH GREENHOUSE DATA	124
5.2.1 <i>Introduction</i>	124
5.2.2 <i>Spinach (Spinacia oleracea) data</i>	125
5.2.2.1. Experimental design.....	125
5.2.2.2. Canopy measurements.....	126
5.2.2.3. Canopy data processing.....	131
5.2.2.4. Statistical significance of data.....	135
5.2.2.5. Leaf measurements.....	138
5.2.3 <i>Poplar (Populus deltoids) data</i>	140
5.2.3.1. Canopy measurements.....	140
5.2.3.2. Leaf measurements.....	141
5.2.4 <i>Results and discussion for spinach</i>	142
5.2.4.1. Relation between chlorophyll content and reflectance in individual MERIS Bands	142
5.2.4.2. Effect of chlorophyll content.....	144
5.2.4.3. Problem with the Lagrangian Interpolation technique.....	145
5.2.4.4. Relation between different REP for MERIS	149
5.2.4.5. Effect of chlorophyll a:b.....	150
5.2.4.6. Effect of LAI	152
5.2.4.7. Effect of Irradiance.....	154
5.2.4.8. Moving from leaf to canopy.....	157
5.2.4.9. Conclusions.....	159
5.2.5 <i>Results and discussion for poplar</i>	160
5.2.5.1. Effect of chlorophyll content.....	160
5.2.5.2. Effect of irradiance.....	161
5.2.5.3. Conclusion	164
5.3. EVALUATION WITH FIELD DATA	165
5.3.1 <i>Introduction</i>	165
5.3.2 <i>Study site and data used</i>	165
5.3.3 <i>Relation of MTCI and REP with chlorophyll content</i>	166
5.4. CONCLUSION.....	168

CHAPTER 6. INDIRECT MTCI EVALUATION (VALIDATION)	170
6.1. INTRODUCTION	170
6.2. COMPARISON WITH MGVI	171
6.2.1 <i>Spatial comparison</i>	171
6.2.1.1. United Kingdom, Ireland and northern France data	172
6.2.1.2. Analysis with Wisconsin data	173
6.2.2 <i>Temporal comparison</i>	174
6.3. COMPARISON WITH MODIS VEGETATION INDICES	178
6.3.1 <i>Spatial comparison</i>	181
6.3.2 <i>Temporal comparison</i>	181
6.3.2.1. Image comparisons	183
6.3.2.2. Histogram comparison	185
6.4. CONCLUSION	187
CHAPTER 7. APPLICATION OF MTCI-I	189
7.1. INTRODUCTION	189
7.2. LEVEL-2 MERIS PRODUCT	189
7.2.1 <i>Implementation of MTCI in the MERIS processor</i>	190
7.2.2 <i>Mathematical description of the algorithm</i>	193
7.2.3 <i>Conclusion</i>	195
7.3. LAND COVER CLASSIFICATION USING MULTI-TEMPORAL MERIS VEGETATION INDICES	195
7.3.1 <i>Introduction</i>	195
7.3.2 <i>MERIS vegetation indices</i>	198
7.3.3 <i>Data and methods</i>	200
7.3.4 <i>Results and discussion</i>	207
7.3.5 <i>Conclusions</i>	214
7.4. CONCLUSION	214
CHAPTER 8. APPLICATION OF MTCI-II	216
8.1. INTRODUCTION	216
8.2. ASSESSMENT OF VEGETATION CONDITION IN THE TSUNAMI AFFECTED COASTAL REGION	216
8.2.1 <i>Introduction</i>	216
8.2.2 <i>Study area and remotely sensed data</i>	217
8.2.2.1. MERIS data	218
8.2.2.2. SRTM data	219
8.2.3 <i>Analysis and results</i>	220
8.2.3.1. Change detection	220
8.2.3.2. MTCI change in relation to elevation	221
8.2.4 <i>Conclusion</i>	223
8.3. PRESENT VEGETATION CONDITION IN THE HERBICIDE SPRAYED FORESTS OF SOUTHERN VIETNAM IN THE 1960S AND EARLY 1970S	224

8.3.1 Introduction.....	224
8.3.2 Data used.....	226
8.3.2.1. Herbicide spraying data.....	226
8.3.2.2. MERIS data.....	230
8.3.3 Results and discussion.....	230
8.3.4 Summary.....	233
8.4. CONCLUSION.....	233
CHAPTER 9. CONCLUSION.....	234
9.1. INTRODUCTION.....	234
9.2. SUMMARY.....	234
9.2.1 Red Edge Position.....	235
9.2.2 The MERIS Terrestrial Chlorophyll Index.....	235
9.2.3 Evaluation of MERIS data.....	236
9.2.4 Evaluation of MTCI.....	237
9.2.5 Application of MTCI.....	238
9.3. CHRONOLOGY OF MTCI DEVELOPMENT.....	238
9.4. FUTURE WORK.....	239
9.4.1 Further understanding the MTCI.....	240
9.4.1.1. Use of other multi angular and fine spectral resolution satellite data.....	240
9.4.1.2. MERIS spectral campaign.....	241
9.4.2 Validating the MTCI.....	242
9.4.3 Continuing on going research.....	242
9.4.3.1. Long term monitoring of tsunami region.....	242
9.4.3.2. Comparison with MODIS.....	244
9.5. CONCLUSION.....	244

List of Figures

Figure 1.1. Arrangement and description of chapters in this thesis.....	5
Figure 2.1. A typical leaf reflectance spectrum indicating the major spectral features.....	8
Figure 2.2. Inverted Gaussian technique, with red edge curve fit parameters indicated: the reflectance maximum (R_s), the reflectance minimum (R_o), the spectral position of the reflectance minimum (λ_o), the spectral position of the curve inflection (λ_p) and the Gaussian curve width parameter σ	14
Figure 2.3. Linear interpolation technique, indicating the red edge inflection point (R_i) and the red edge position (REP).....	16
Figure 2.4. The three point Lagrangian interpolation technique to determine the red edge position, indicating the REP along the derivative curve.....	17
Figure 2.5. Schematic diagram of a dual beam spectrometer.....	33
Figure 2.6. A spectral reflectance curve of vegetation with MERIS bands in the red edge region.....	53
Figure 2.7. Arrangement of optical modules, folding mirror and Earth viewing windows (Adapted from ESA 2005).....	55
Figure 2.8. Relationship between stress factors, chlorophyll content, wilting and location of red edge.....	68
Figure 3.1. (a) Vegetation reflectance spectra at four chlorophyll contents overlain with the position of MERIS bands 8, 9 and 10. (b) Relation between the MERIS terrestrial chlorophyll index (MTCI) and red edge position (REP) for four chlorophyll contents.....	77
Figure 3.2. (a) Reflectance spectra for MERIS data at the standard band positions, simulated using the LIBSAIL model for a wide range of chlorophyll contents; (b) relation between chlorophyll content and MTCI for the same range of chlorophyll contents and (c) relation between REP and chlorophyll content for the same range of chlorophyll contents.....	81
Figure 3.3 Sensitivity of REP and MTCI calculated from field reflectance spectra to variation in chlorophyll content for (a) Douglas-fir and (b) maple...	81






Figure 3.4. Relation between REP and MTCI, estimated using continuous spectra and MERIS standard band settings for field reflectance data of Douglas-fir and maple.....	82
Figure 3.5 MERIS images of southern England (a) land cover map of the study area (New Forest) with the black box indicating the sub-scene (6.3 km x 6.3 km) containing vegetation with the assumed relatively high and low chlorophyll content that was selected for quantitative analysis;(key : Heath  Woodland  Meadows & Agricultural land  Urban  Water ); (b) False colour composite image of bands 10, 8 and 6; (c) classified (unsupervised) image; (d) NDVI image, colour key in table 2; (e) REP image, colour key in table2; (f) MTCI image, colour key in table3.2.	84
Figure 3.6 Relationships between (a) NDVI and MTCI; (b) REP and MTCI and (c) REP and NDVI for a subscene of MERIS data (Figure3. 5a) containing heath and woodland.....	85
Figure 4.1. Leaf reflectance (a) and derivative (b) spectra for two leaf samples (leaf 1 with chlorophyll concentration 251 mg m^{-2} and leaf 2 with chlorophyll concentration 458 mg m^{-2}).....	87
Figure 4.2. Canopy reflectance spectra (a) and derivative spectra (b) for two canopies. (Canopy 1 having LAI= 0.9 chlorophyll concentration 163 mg m^{-2} and canopy 2 having LAI= 0.5 and chlorophyll concentration 336 mg m^{-2}).....	89
Figure 4.3. Change in reflectances from leaf to satellite (MERIS) level due to the influence of different variables.....	90
Figure 4.4 Radiances recorded at MERIS sensor for four landcovers (points in the graph indicate the MERIS band position).....	91
Figure 4.5. A generalised semivariogram showing the nugget variance.	94
Figure 4.6. The radiance and SNR for MERIS data of the Eastern Mediterranean (table 4.2).....	98
Figure 4.7. The radiance and SNR for MERIS data of the western English channel (table 4.2).....	99
Figure 4.8. The radiance and SNR for MERIS data of central African forest (table 4.2).....	99
Figure 4.9. The radiance and SNR for MERIS data of Northern Ireland grassland (table 4.2).....	100

Figure 4.10 The radiance and SNR for MERIS data of Eastern Saharan soil (table 4.2).....	101
Figure 4.11. The SNR for five landcovers (table 4.2).	101
Figure 4.12 Illustrated relationships between maximum and minimum value of MTCI as a function of chlorophyll content as a effect of a non-canopy variable Vc1. Maximum Vc1 curve (solid) is the relationship between MTCI and chlorophyll content for maximum value of Vc1 and minimum Vc1 curve (dotted) is the relationship between MTCI and chlorophyll content for minimum value of Vc1.....	106
Figure 4.13. Maximum and minimum MTCI among five soils (type=2, 3, 4, 5, 6) and LAI of 1 and LAI of 5 for a nadir view angle and a 0° solar angle.....	109
Figure 4.14. Maximum and minimum MTCI from all view angle (-80° to +80°) and LAI of 1 and LAI of 5 for soil type 6 and a 0° solar angle.....	110
Figure 4.15. MTCI and Delta MTCI (Δ MTCI) for 4 atmospheric conditions and two LAIs: (a) viewing angle of 0°; (b) viewing angle of -80°; (c) viewing angle of +80°.	113
Figure 4.16. Evaluating the effect of data processing on MTCI; (a) MTCI estimated from L1 data, (b) MTCI estimated from normalised surface reflectance data (L2) and (c) difference image.....	116
Figure 4.17. Comparison of MTCI estimated from L1 and L2 data for (a) grassland and (b) woodland.....	117
Figure 4.18. Temporal comparison of MTCI estimated from L1 and L2 data for (a) Hainich; (b) Loobos and (c) New Forest.....	120
Figure 4.19. SD of MTCI at eight spatial resolutions.....	121
Figure 4.20 Effect of atmospheric aerosol load on MTCI.....	122
Figure 5.1. (a) One week old spinach seedlings in the greenhouse and (b) information record used in the greenhouse.....	126
Figure 5.2. Spectral measurement pattern for a tray.....	128
Figure 5.3. Flow diagram of SPAD-502 processing steps.....	130
Figure 5.4. SPAD measurement points on a leaf.....	131
Figure 5.5. Correlation between SPAD values with chlorophyll a concentration (a) and chlorophyll b concentration (b) for spinach.....	135

Figure 5.6. Estimation of LAI from a digital photo (a) Extraction of IFOV image, (b) digitisation of individual leaf and (c) estimation of area.....	136
Figure 5.7. Variation of chlorophyll concentration (a), LAI (b) and chlorophyll content (c) through out the experiment.....	137
Figure 5.8. Correlation between SPAD values with chlorophyll a concentration (a) and chlorophyll b concentration (b) for poplar.....	142
Figure 5.9. Spectral reflectance at MERIS standard band setting for a wide range of chlorophyll content.....	142
Figure 5.10. Relation between chlorophyll content and reflectance in MERIS band 7(a), band 8 (b), band 9 (c), band 10 (d) and band 12 (e).....	144
Figure 5.11. Relationship between chlorophyll content and SR (a), NDVI (b), REP estimated by maximum of first derivative (c), REP estimated by linear interpolation (d), REP estimated by Lagrangian interpolation (e) and MTCI (f) for spinach.....	146
Figure 5.12. Reflectance spectra at MERIS standard band setting for cases where Lagrangian interpolation over estimated the REP (a) and derivative spectra (b).....	147
Figure 5.13. Reflectance spectra at MERIS standard band setting for cases where Lagrangian interpolation did not over estimate the REP (a) and derivative spectra (b).....	148
Figure 5.14. Relationship between chlorophyll content and REP estimated by Lagrangian interpolation using band 11 (a) and not using band 11(b).....	149
Figure 5.15. Relationship between REP estimated by different methods and chlorophyll content.	150
Figure 5.16. Relationship between REP estimated by (a) maximum of first derivative and linear interpolation; (b) maximum of first derivative and Lagrangian interpolation.....	151
Figure 5.17. Canopy reflectance spectra for different chlorophyll a:b.....	152
Figure 5.18. Relationship between chlorophyll a:b and SR (a), NDVI (b), REP estimated by maximum of first derivative (c), REP estimated by linear interpolation (d), REP estimated by Lagrangian interpolation (e) and MTCI (f) for spinach.....	153
Figure 5.19. Canopy reflectance spectra of spinach for different LAI.....	153

Figure 5.20. Relationship between LAI and SR (a), NDVI (b), REP estimated by maximum of first derivative (c), REP estimated by linear interpolation (d), REP estimated by Lagrangian interpolation (e) and MTCI (f) for spinach.....	155
Figure 5.21. Spectral reflectance spectra (a) for spinach at two levels of irradiance.....	155
Figure 5.22. Relationships between chlorophyll concentration and SR (a), NDVI (b), REP estimated using the maximum of first derivative (c), REP estimated using linear interpolation (d), REP estimated using Lagrangian interpolation (e) and MTCI (f) at two levels of irradiance for spinach.....	156
Figure 5.23. Effect of scaling up on relationship between chlorophyll content and REP estimated by linear interpolation (a), Lagrangian interpolation (b) and MTCI (c) for spinach.....	160
Figure 5.24. Relationship between chlorophyll content and SR (a), NDVI (b), REP estimated by maximum of first derivative (c), REP estimated by linear interpolation (d), REP estimated by Lagrangian interpolation (e) and MTCI (f) for poplar.....	162
Figure 5.25. Spectral reflectance spectra for poplar at three levels of irradiance.	163
Figure 5.26. Relationships between chlorophyll content and SR (a), NDVI (b), REP estimated using the maximum of first derivative (c), REP estimated using linear interpolation (d), REP estimated using Lagrangian interpolation (e) and MTCI (f) at three levels of irradiance for poplar.....	164
Figure 5.27. MERIS spectral reflectances for different crops.....	167
Figure 5.28. Relationship between SR(a); NDVI(b); REP estimated using linear interpolation (c); REP estimated by Lagrangian interpolation(d) and MTCI(e) with chlorophyll content for different crops in the filed site.....	168
Figure 6.1 MTCI (left) and MGVI (right) images of United Kingdom, Ireland and northern France acquired on 18 th April 2003 showing two regions where there was considerable difference between MGVI and MTCI values.....	172
Figure 6.2 MTCI (left) and MGVI (right) images of Wisconsin, USA acquired on 18 th August 2003.....	173
Figure 6.3. Time series of MGVI and MTCI for (a) (a) Hainich; (b) Loobos; (c) New Forest and (d) Pavia.....	176

Figure 6.4. Correlation between MGVI and MTCI for (a) (a)Hainich; (b) Loobos; (c) New Forest and (d) Pavia.....	178
Figure 6.5. MERIS and MODIS bands overlain on a modelled vegetation spectrum.....	179
Figure 6.6. MTCI and MODIS VI for United Kingdom and Ireland. (a) MTCI estimated from MERIS data acquired on 18 th April 2003 , (b) NDVI and (c) EVI for MODIS data acquired on 17 th Aril 2003.....	183
Figure 6.7. MTCI derived from MERIS data, EVI and NDVI derived from MODIS data acquired in three dates for Wisconsin, USA, MTCI and MODIS VIs images are different in size because they have different spatial resolution....	185
Figure 6.8. Histograms for MTCI (a); EVI (b) and NDVI derived from MODIS data(c) for data acquired in three dates for Wisconsin.....	187
Figure 7.1. MERIS level 2 processing for land.....	192
Figure 7.2 Reflectance of sediment laden water in MERIS red and NIR wavebands for two points in the Mekong River, Cambodia.....	193
Figure 7.3. MERIS level 2 MTCI computation (step 2.8) in the MERIS processor.....	194
Figure 7.4. Description of <i>Algorithm 2.8</i> used for MTCI calculation.....	195
Figure 7.5. Study area for landcover classification.....	201
Figure 7.6. Landcover map of the study area derived from Landsat TM data.....	202
Figure 7.7. Vegetation indices image of the study area: (a) MTCI in August; (b) MTCI in September; (c) MGVI in August and (d) MGVI in September; (e) chlorophyll range.....	204
Figure 8.1. Location of the study area in western Thailand.....	219
Figure 8.2. Elevation image of the study area generated from SRTM data.....	221
Figure 8.3. MTCI image of the study area (a) pre-tsunami; (b) post-tsunami.....	223
Figure 8.4. Difference between pre and post-tsunami MTCI images.....	223
Figure 8.5. Pre and post-tsunami MTCI for terrain with an elevation (a) between 10 m and 25 m and (b) greater than 100 m.....	224
Figure 8.6 Herbicide used during 1965 to 1971 on the forest of southern Vietnam by (a) type and (b) year.....	226

Figure 8.7. Plot of a flight path corresponding to a spraying mission started at (602100E,1875700N) and ended at (614800E,1879900N) of the UTM zone 48N with its estimated area of influence.....	229
Figure 8.8 Flow diagram of HERBS file processing.....	230
Figure 8.9 Herbicide concentration map of southern Vietnam (units of 1 km^{-2} over 7 years).....	232
Figure 8.10 Herbicide concentration map (units of 1 km^{-2} over 7 years) (a) and MTCI map (b) for a sub section of the study area.....	232
Figure 8.11 Herbicide concentration and MTCI along a transect.....	233
Figure 8.12 Relationship between MTCI and herbicide concentration for selected forested sites in southern Vietnam.....	233
Figure 9.1. MERIS standard bands and proposed Venus bands are overlain on model vegetation spectra.....	240
Figure 9.2. Tsunami affected area in Sri Lanka (a), MTCI before tsunami (22-12-2004) (b) and MTCI after tsunami (17-02-2005) (c).....	244
Figure 9.3. Cloud free MERIS data available for the eastern Sri Lanka (figure 9.2.).....	244

List of Tables

Table 2.1. Characteristic spectral features of foliar biochemicals (adapted from Curran, 1980).	9
Table 2.2. Performances of different techniques for locating the REP (modified from Dawson and Curran, 1998).....	12
Table 2.3. Characteristic of some selected airborne spectrometers.....	41
Table 2.4. Different data acquisition modes for CASI (NERC, 2005).....	42
Table 2.5 .Use of airborne imaging spectrometer data for vegetation studies.....	44
Table 2.6. Spaceborne imaging spectrometers.....	46
Table 2.7. MODIS spectral channels (MODIS web, 2005).....	49
Table 2.8. Technical specification of MODIS (MODIS web, 2005).....	50
Table 2.9. MERIS band positions.....	54
Table 2.10. MERIS performance summary (Adapted from ESA, 2005).	57
Table 2.11. MERIS data products (Adapted from ESA, 2005).....	58
Table 3.1. Input variables for LIBSAIL model.....	79
Table 3.2 . Key for NDVI, REP and MTCI images in figure 3.4.....	84
Table 4.1. Comparison of advantages and disadvantages of five most commonly used method to estimate image SNR (Smith and Curran, 1999).....	93
Table 4.2. MERIS image data user to estimate SNR.....	97
Table 4.3. Approximate SNR for different wavelength with different irradiance.....	102
Table 4.4 Leaf and canopy variables used to simulate data for the evaluation of MTCI.....	105
Table 4.5 Non leaf and canopy variables used to simulate data for the evaluation of MTCI.	105
Table 4.6. Leprieur parameter (LP) for MTCI as a function of soil brightness for different values of LAI.....	108
Table 4.7. Leprieur parameter (LP) for MTCI as a function of view angle for different values of LAI.....	109
Table 4.8. Test site description.....	119
Table 4.9. Relative influence of various non-canopy variables on the MTCI.....	123
Table 5.1 Specification of GER-1500 field spectrometer.....	127

Table 5.2. Total number of LAI, chlorophyll concentration and spectral reflectance measurements undertaken during the experiment.....	129
Table 5.3. Minolta SPAD system specifications.....	130
Table 5.4. Statistical significance values from ANOVA for chlorophyll concentration, LAI chlorophyll content through out the experiment.....	138
Table 5.5. Coefficient of determination of different estimators with chlorophyll content, chlorophyll a:b and LAI.....	145
Table 5.6. The coefficient of determination for correlations between chlorophyll concentration and reflectance indices at two levels of irradiance (and their statistical significance) for spinach.....	157
Table 5.7. The coefficient of determination for correlations between chlorophyll content and reflectance indices at three levels of irradiances (and their statistical significance) for poplar.....	165
Table 6.1. Description of study sites used for the temporal comparison between MTCI and MGVI.....	174
Table 7.1. List of Variables used in the MTCI algorithm (figure 7.4) in the MERIS processor.....	195
Table 7.2. The land cover classes and number of pixels extracted from each class for the analyses. Note that Agricultural land –I contains the vegetation type present on the field in August and September (e.g. corn) and Agricultural land –II contains the vegetation type harvested from the field by September (e.g. forage crop).....	206
Table 7.3. Wilks’ lambda coefficients derived from the MERIS data acquired in August.....	207
Table 7.4. Wilks’ lambda coefficients derived from the MERIS data acquired in September.....	207
Table 7.5. Wilks’ lambda coefficients derived from the combined August and September MERIS data sets.....	208
Table 7.6. Confusion matrix for the classification by discriminant analysis using data acquired in the MERIS spectral wavebands in August. Wavebands selected: B1, B3, B5, B8, B9, B10, B12, B13 and B14. Overall accuracy = 66.74%.....	211

Table 7.7. Confusion matrix for the classification by discriminant analysis using data acquired in the MERIS spectral wavebands in September.	
Wavebands selected: B1, B2, B10, B12 and B13. Overall accuracy = 55.92%...	211
Table 7.8. Confusion matrix for the classification by discriminant analysis using data acquired in the MERIS spectral wavebands in August and September. Wavebands selected: B1, B5, B7, B8, B9, B10 and B12 from August and B1, B7, B10 and B12 from September. Overall accuracy = 69.02%.	212
Table 7.9. Confusion matrix for the classification by SVM using data acquired in the MERIS spectral wavebands in August. Wavebands used: B1, B3, B5, B8, B9, B10, B12, B13 and B14. Note $C=14$ and $\gamma=9$. Overall accuracy = 67.57%.....	212
Table 7.10. Confusion matrix for the classification by SVM using data acquired in the MERIS spectral wavebands in September. Wavebands used: B1, B2, B10, B12 and B13. Note $C=250$ and $\gamma=30$. Overall accuracy = 61.33%.	213
Table 7.11. Confusion matrix for the classification by SVM using data acquired in the MERIS spectral wavebands in August and September. Wavebands used: B1, B5, B7, B8, B9, B10 and B12 from August and B1, B7, B10 and B12 from September. Note $C=400$ and $\gamma=30$. Overall accuracy = 68.81%.....	213
Table 7.12. Confusion matrix for the classification by discriminant analysis using the vegetation index product data for August and September. Overall accuracy = 67.20%.....	214
Table 7.13. Confusion matrix for the classification by the SVM using the vegetation index product data for August and September. Note $C= 3$ and $\gamma= 8$. Overall accuracy = 73.18%.....	214
Table 8.1. Remotely sensed data used in this study: MERIS is the Medium Resolution Imaging Spectrometer on board ESA’s Envisat and SIR-C is the Space-borne Imaging Radar-C on board NASA’s Shuttle Radar Topography Mission (SRTM).....	220
Table 8.2 Herbicide sprayed during the defoliation mission.....	226
Table 9.1. Chronology of development of the MTCTI.....	240
Table 9.2 .proposed band positions in the special spectral campaign.....	243

Journal papers

1. DASH, J. and CURRAN, P. J., 2004, The MERIS Terrestrial Chlorophyll Index. *International Journal of Remote Sensing*, 25, pp-5003-5013.
2. CURRAN, P. J, DASH. J. and LLEWELLYN, G. M, 2005, The Indian Ocean Tsunami: Use of the MERIS (MTCI) data to detect salt stress on near coastal vegetation. *International Journal of Remote Sensing* (Accepted).
3. DASH, J and CURRAN, P. J., 2005, Evaluation of the MERIS Terrestrial Chlorophyll Index (MTCI). *Advances in Space Research* (Accepted).
4. DASH, J. and CURRAN, P. J., 2005, Relationship between herbicide concentration during the 1960s and 1970s and the contemporary MERIS Terrestrial Chlorophyll Index (MTCI) for southern Vietnam. *International Journal of Geographical Information Science* (Submitted).
5. DASH, J., TALLIS, M., CURRAN, P. and TAYLOR, G., 2005, The relationship between irradiance and the red edge position of a leaf. *New Phytologist* (Submitted).

Conference Proceedings

1. DASH, J. and CURRAN, P. J., 2003, Design and preliminary evaluation of the MERIS Terrestrial Chlorophyll Index. *Proceeding of RSPS Annual Conference, "Scales and Dynamics in Observing the Environment"*, Nottingham, UK (CD Rom).
2. DASH, J. and CURRAN, P. J., 2004, MTCI: The MERIS Terrestrial Chlorophyll Index. *Proceeding of First MERIS Users Workshop*, ESA SP- 549, Frascati, Rome, Italy (CD Rom).
3. DASH, J. and CURRAN, P. J., 2004, Evaluation of the MERIS Terrestrial Chlorophyll Index. *Proceedings of 2004 IEEE Geosciences and Remote Sensing Symposium*, 1, pp-254 – 257, IEEE, Anchorage, Alaska, USA (available online at <http://ieeexplore.ieee.org/>).
4. CURRAN, P. J. and DASH, J., 2004, ESA's new land product: the MERIS Terrestrial Chlorophyll Index. *Proceedings of Airborne Imaging Spectroscopy Workshop*, Belgium Science Policy Office, Bruges, Belgium (CD Rom).
5. CURRAN, P. J. and DASH, J., 2004, Evaluation of the MERIS Terrestrial Chlorophyll Index. *Proceeding of Envisat and ERS Symposium*, ESA, Salzburg, Austria (CD Rom).
6. DASH, J., CURRAN, P. J. and LLEWELLYN, G. M., 2005, Indian Ocean tsunami: the use of MERIS (MTCI) data to detect salt stress on near coastal-vegetation, *Proceeding of RSPS Annual Conference, "Measuring, Mapping and Managing a Hazardous World"*, Nottingham, UK (CD Rom).
7. DASH, J., TALLIS, M., CURRAN, P. and TAYLOR, G., 2005, The relationship between irradiance and the red edge position of a leaf , *Proceeding of RSPS Annual Conference, "Measuring, Mapping and Managing a Hazardous World"*, Nottingham, UK (CD Rom).
8. DASH, J. and CURRAN, P. J., 2005, Effect of herbicide contamination on the MERIS Terrestrial Chlorophyll Index for the forests of southern Vietnam, *Proceeding of RSPS Annual Conference, "Measuring, Mapping and Managing a Hazardous World"*, Nottingham, UK (CD Rom).
9. DASH, J. and CURRAN, P. J., 2005, Application and evaluation of the MERIS Terrestrial Chlorophyll Index, *Proceeding of the MERIS/AASTER Users Workshop*, Frascati, Rome, Italy (CD Rom).

Page xviii missing

Page ix missing

Abbreviations

ACCP: Accelerated Canopy Chemistry Program
AIS: Airborne Imaging System
ANOVA: Analysis of variance
AOI: Area of Influence
ARVI: Atmospherically Resistance Vegetation index
ASD: Analytical Spectral Device
ATBD: Algorithm Theoretical Basis Document
AVIRIS: Airborne Visible/Infrared Imaging Spectrometer
BRDF: Bidirectional Reflectances Distribution Function
CASI: Compact Airborne Spectrographic Imager
CHRIS: Compact High Resolution Imaging Spectrometer
DA: Discriminant Analysis
DART: Discrete Anisotropic Radiative Transfer
DPi: Double Peak optical index
EVI: Enhanced Vegetation Index
FAPAR: Fraction of Absorbed Photosynthetically Active Radiation
GEMI: Global Environmental Monitoring Index
GIFOV: Ground-projected Instantaneous-Field-Of-View
HIRIS: High Resolution Imaging Spectrometer
IGM: Inverted Gaussian model
LAI: Leaf Area Index
LIBERTY: Leaf Incorporating Biochemistry Exhibiting Reflectance and Transmittance Yield
LOPEX: Leaf Optical Property Experiment
LP: Leprieur Parameter
MASER: MODIS/ASTER Airborne Simulator
MCRM: Multispectral Canopy Reflectance Model
MERIS: MEdium Resolution Imaging Spectrometer
MGVI:MERIS Global Vegetation Index
MODIS: MOderate Resolution Imaging Spectroradiometer
MTCI: MERIS Terrestrial Chlorophyll Index
NDVI: Normalised Difference Vegetation Index

NEAL : Noise Equivalent change in radiance, L

NEDT: Noise Equivalent Differences in Temperature

PVI: Perpendicular Vegetation Index

REP: Red Edge Position

ROI: Region of Interest

RVI: Ratio-Based Vegetation Index

RVSI: Red-edge Vegetation Stress Index

SAIL: Scattering by Arbitrary Inclined Leaves

SAVI: Soil Adjusted Vegetation Index

SAVI: Soil Adjusted Vegetation Index

SIR-C: Spaceborne Imaging Radar-C

SLOP: Stochastic model for Leaf Optical Properties

SMAC: Simplified Methods for Atmospheric Correction

SNR: Signal to Noise Ratio

SPECTRA: Surface Process and Ecosystem Changes Through Response Analysis

SR: Simple Ratio

SRTM: Shuttle Radar Topography Mission

SVM: Support Vector Machine

TM: Thematic Mapper

TOAVI: Top of Atmosphere Vegetation Index

TSAVI: Transformed Soil Adjusted Vegetation Index

WDVI: Weighted Distance Vegetation Index

YI: Yellowness Index

Chapter 1. Introduction

1.1. Introduction

Remote sensing is a discipline-independent technique used by researchers to obtain indirect information for identifying, classifying and estimating various features in our environment. Earlier definitions in 1970s to early 1980s called it a technique for recording objects as an image; later narrower definitions emphasized the use of the technique (Curran, 1987). One of the definitions is: “remote sensing is the science and art of obtaining information about an object, area, or phenomenon through the analysis of data acquired by a device that is not in contact with the object, area, or phenomenon under investigation” (Lillesand and Kiefer, 1987).

Monitoring and evaluation of terrestrial environments requires the assessment of vegetation. Remote sensing techniques have traditionally provided this information at a wide range of spatial and temporal scales (Boyd and Danson, 2005). However, the nature of the remotely sensed data required for assessment of vegetation depends on the level of information users want to obtain; these levels can be characterised by asking three levels of ecological questions (Curran, 2001): “What is the vegetation there? How much vegetation is there? and what is the condition of that vegetation?”

First two questions can be answered using broad band sensors whereas the third question requires data in narrow wavebands. Remotely sensed data recorded in narrow visible/near visible wavebands can be used to estimate foliar biochemical content at local to regional scales. This information can, in turn, be used to quantify, understand and support the management of vegetated environments.

Chlorophyll is one of the more important foliar biochemicals and the content within a vegetation canopy is related positively to both the productivity of that vegetation and the

depth and width of the chlorophyll absorption feature in reflectance spectra. The long wavelength (red) edge of this absorption feature moves to even longer wavelengths with an increase in chlorophyll content (Curran et al., 1990, Filella and Peñuelas, 1994, Munden et al., 1994). Study of the red edge and its movement requires reflectance data for a vegetation canopy with fine spectral resolution in red and near infra red wavelengths. Such data can be collected by laboratory and field spectroradiometers and airborne imaging spectrometers. However, monitoring vegetation condition at a global scale requires such data at satellite level and this has been possible by the launch of few space-borne imaging spectrometer during last five years. Two most widely used ones are: the MEdium Resolution Imaging Spectrometer (MERIS) on board of ESA's Envisat and the MOderate Resolution Imaging Spectroradiometer (MODIS) on board of NASA's Terra and Aqua mission. MODIS does not have those bands in the red edge region that are need to estimate the red edge position (REP), where as MERIS has 5 bands in the red edge region. Two techniques have been used to estimate the REP on discontinuous (simulated) MERIS spectra: Lagrangian interpolation (Dawson 2000) and linear interpolation (Clevers et al. 2002). However, (i) each technique produces a different value of REP from the same set of data, (ii) neither of the techniques offer the automated, one-step procedure that would be required for the processing of large volume data at, for example, a ground receiving station and (iii) due to the asymptotic relationship between REP and chlorophyll content the REP is not an accurate indicator of chlorophyll content at high chlorophyll contents. This lead to the idea of designing a new index for estimating chlorophyll content at regional to global scales.

1.2. Objective of this research

This research was focused on the following:

- To design a chlorophyll index which should (i) use the MERIS bands situated in the REP, (ii) easy to calculate from MERIS data and (iii) sensitive to wide range of chlorophyll content.
- To understand the performance of the index under the effect of major non canopy variables, which include the soil background reflectance, viewing geometry and the atmosphere.
- To evaluate the index with a range of chlorophyll content data at different scales: leaf to satellite and validate the index with wide range of spatial and temporal variation in chlorophyll content.
- To provide some suitable application of the index for understanding and managing the vegetated terrain at a regional to global scale.

1.3. Chapter overview

Chapter organisation and links between individual chapters is presented in figure 1.1.

Chapter 2 reviews the literature on various methods of estimation of red edge (maximum of first derivative spectrum, curve fitting, linear interpolation and Langrangian interpolation), different leaf, canopy and combined models used for obtaining reflectance spectra over leaf or canopy, different spectral measurement techniques, application of red edge (e.g. determination of plant stress) and uncertainty in the red edge:chlorophyll relationship.

Chapter 3 reports on the design and preliminary evaluation of a surrogate REP index for use with spectral data recorded at the standard band settings of the Medium Resolution Imaging Spectrometer (MERIS). This index, termed the MERIS terrestrial chlorophyll index (MTCI) was evaluated using model spectra, field spectra and MERIS data. Further evaluation of the MTCI was proposed.

Chapter 4 reports the performance of the MTCI under changing conditions of soil

background reflectance, viewing geometry, atmosphere and data processing. It also describes the change in the nature of spectral reflectance of vegetation while moving from leaf to satellite level.

Chapter 5 evaluates the MTCI for a wide range of chlorophyll content data obtained from a greenhouse experiment involving two species: spinach and poplar. It also reports, for the first time, on the effect of changing levels of irradiance on the leaf reflectance spectra, thereby, on the red edge and chlorophyll relationship.

Chapter 6 describes an indirect evaluation of the performance of MTCI through spatial temporal comparison with other available vegetation indices from current space-borne spectrometers; they include the MGVI derived from MERIS data and Enhanced Vegetation Index (EVI) and Normalised Differential Vegetation Index (NDVI) derived from MODIS data.

Chapter 7 provides the processing steps that were included in the MERIS processor at the ESA to produce MTCI as a standard level 2 land product. It also demonstrates the application of multi temporal MERIS vegetation indices (MTCI and MGVI) for the mapping of landcover.

Chapter 8 reports on two possible regional scale application of MTCI. First, identification of salt stress in the near coastal vegetation of Phuket, Thailand one of the areas affected by the Indian Ocean tsunami on 26th December 2005; second, the assessment of current vegetation condition in the forests of southern Vietnam that were affected by the ‘defoliation mission’ between January 1961 and September 1971.

Chapter 9 summarises the research and proposed some possible future research on the MTCI.

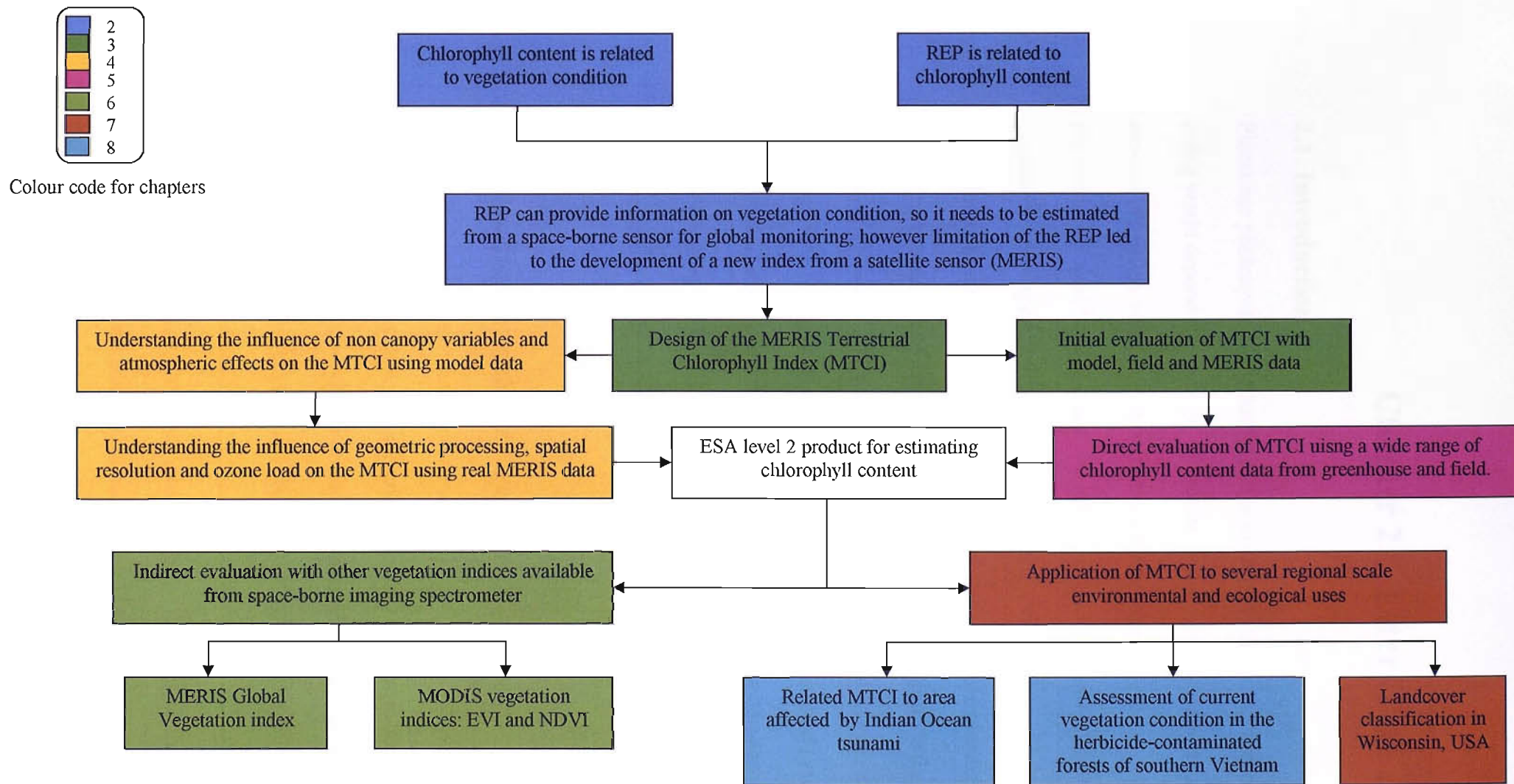


Figure 1.1. Arrangement and description of chapters in this thesis.

Chapter 2. Literature review

2.1. Introduction

Plants use photosynthesis to harness solar energy for the production of food. The rest of the living world depends upon them. Therefore, when modelling the ecosystem of a region, the amount of healthy vegetation is required. Field techniques used to determine the physiological conditions of plants are labour intensive, can be destructive and are inaccurate when applied to a large area (Wulder, 1998). As a result it is difficult to obtain physiological information on plants at a global scale. Remote sensing techniques enable researchers to use the spectral properties of vegetation to estimate the amount of vegetation (Treitz and Howarth, 1999) and the physiological condition of vegetation (Carter, 1993; Johnson, 1999, Smith et al., 2004; Li et al., 2005). These methods are non-destructive and have the advantage of repetitive coverage. During last three decades remotely sensed data from various sensors has been used to monitoring vegetation parameters, particularly, forest resources (Boyd and Danson, 2005).

2.2. Spectral properties of vegetation

Understanding remotely sensed data requires knowledge of reflectance properties of features on Earth's surface. The spectral reflectance of vegetation contains absorption features that are the result of electron transitions and vibrational stretching of organic and inorganic bonds. The main chemical constituents of leaves include chlorophyll, water, nitrogen and carbon containing compounds, comprising primarily protein, lignin and cellulose. Out of these chlorophyll is associated with the process of photosynthesis and together with water, temperature, nutrient availability, CO₂ and sunlight; determines the

rate of primary productivity. Therefore, chlorophyll is an important driver for the whole ecosystem (Munden et al., 1994).

When incoming radiation interacts with vegetation, some of it is reflected, some absorbed and rest is transmitted. A typical reflectance spectrum (figure 2.1) of a vegetation canopy can be subdivided into 3 parts, visible (400- 700 nm), near-infrared (NIR) (701 – 1300 nm) and middle-infrared (1301- 2500 nm).

2.2.1 Visible region

Chlorophyll is the major absorber of radiation in the visible region. Chlorophylls are of two types, chlorophyll-a and chlorophyll-b; chlorophyll-a content is usually two to three times that of chlorophyll-b and dominates absorption in 600-700 nm wavelengths (Lichtenthaler, 1987). Other leaf pigments also have an important effect on the visible spectrum. For example, the yellow to orange-red pigment, carotene, has a strong absorption in the 350 - 500 nm range and is responsible for the colour of some flowers and fruits as well as leaves without chlorophyll. The red and blue pigment, xanthophyll, has strong absorption in the 350-500 nm range and is responsible for the leaf colour in autumn.

2.2.2 NIR region

In the near-infrared spectral domain (701-1300 nm), leaf structure explains the optical properties. Near-infrared spectral region can be divided into two major spectral sub-regions: first, between 701 and 1100 nm, where reflectance is high, except in two minor water-related absorption bands (960 and 1100 nm) and second, between 1100 and 1300 nm, which corresponds to the transition between high near-infrared reflectance and water-related absorption bands of the middle infrared (Fig. 1). There is strong reflectance between 701 to 1000 nm (NIR) region in the spongy mesophyll cells located in the interior

or back of a leaf, within which light reflects mainly at cell wall/air space interfaces (Gausmann, 1974). Leaf pigments and cellulose are transparent to near-infrared wavelengths and therefore leaf absorption in the near-infrared region is very small. In this region, there is typically a reflectance plateau in the leaf spectrum. The level of this plateau is dependent on the internal leaf structure as well as the space in the mesophyll that in turn determines the interfaces with different refraction indices (air or water- cells). Leaf reflectance increases for more heterogeneous cell shapes and contents as well as with increasing number of cell layers, number of intercell spaces and cell size. This reflectance is therefore dependent on the relative thickness of mesophyll. The intensity of NIR reflectance is commonly greater than from most inorganic materials, so vegetation appears bright in NIR wavelengths.

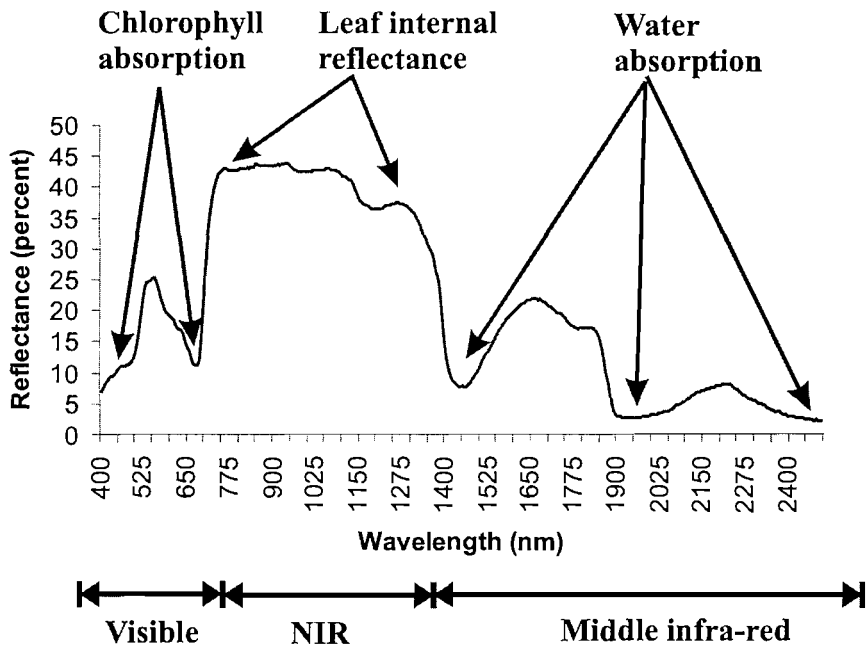


Figure 2.1. A typical leaf reflectance spectrum indicating the major spectral features.

2.2.3 Middle-infrared region

The middle-infrared region contains information about the absorption of radiation by water, cellulose and lignin etc. The protein molecules are made up of carbon, hydrogen and oxygen and nitrogen atoms. Thus nitrogen status can be inferred indirectly by studying the absorption feature in that region (Baret and Fourty, 1997). Other biochemicals, which contribute to absorption in middle infra-red wavelengths, are starches, sugars, lipids and minerals. Curran (1989) presented a list of forty-four absorption features in the visible and near-infrared wavelengths which were related to foliar biochemical constituents.

The relations between multispectral reflectance and vegetation amount to six wavebands (Curran, 1980) summarised in table 2.1.

Waveband	Waveband width (nm)	Characteristics	Relation to vegetation amount
Ultraviolet/blue	350-500	Strong chlorophyll and carotene absorption	Strong negative
Green	500-600	Reduced level of pigment absorption	Weak positive
Red	600-700	Strong chlorophyll absorption	Strong negative
Red edge	700-740	Transition between strong absorption and strong reflectance	Weak negative
Near-infrared	740-1300	High vegetation reflectance	Strong positive
Middle-infrared	1300-2500	Water, cellulose and lignin absorption	Not specific

Table 2.1. Characteristic spectral features of foliar biochemicals (adapted from Curran, 1980).

2.3. Role of chlorophyll

Chlorophyll plays an important role in determining the physiological status of a plant. The chlorophyll *concentration* of leaves can be defined as the amount of chlorophyll per unit weight of leaf (mg g^{-1}) or as a percentage of leaf weight (% dry weight). It is often

impractical to estimate the chlorophyll concentration at the leaf level by using remote sensing techniques because of its variable distribution in a canopy. Therefore, reflectance from the canopy is more sensitive to the chlorophyll *content* of the canopy than the *concentration* of individual leaves (Curran et al., 1995). For example, the chlorophyll content can be defined as chlorophyll within an area covered by one pixel (measured in g) (Jago et al., 1999).

Various methods have been developed to estimate the chlorophyll concentration of leaves (Datt, 1998; Gitelson and Merzlyak, 1998; Mariotti et al., 1996) and content of canopies (Daughtry et al., 2000; O'Neill et al., 2002; Peterson et al., 1988). As two major features occur in a reflectance spectra of a canopy (i.e., chlorophyll absorption in the red region and scattering due to internal cell structure in the NIR region) so majority of researchers have used reflectances in these wavelength regions to establish a relationship between chlorophyll content and reflectance of a canopy. Most of the methods for the purpose of this chapter can be classified into two groups, one using some index of vegetation (e.g. RVI (Ratio-Based Vegetation Index) (Jordan, 1969); NDVI (Normalised Differential Vegetation Index) (Rouse et al., 1974; Ustin, 1999); SAVI (Soil Adjusted Vegetation Index) (Huete, 1988) and other vegetation indices (Broge and Leblanc, 2001)) and the other using the 'red edge' (Barton, 2001; Blackburn, 1998; Curran et al., 1990; 1995; Gupta et al., 2001; Pinnar and Curran, 1996).

2.4. The red edge

The red edge is a region within the red-NIR transition zone of a vegetation reflectance spectrum and marks the boundary between absorption due to chlorophyll in the red region and scattering due to leaf internal structure in the NIR region (Horler et al., 1983). The red edge position (REP) can be defined as the maximum of the first derivative of the reflectance spectra of a leaf (Horler et al., 1983; Curran et al., 1990). According to the

Beer-Lambert law a negative exponential correlation exists between chemical concentration and absorption. Therefore an increase in chlorophyll concentration increases absorption. This in turn will cause both broadening and deepening of the absorption feature (Filella and Peñuelas, 1994; Curran et al., 1995) and a movement of the REP to longer wavelengths. This change in the REP can be used to estimate the amount of chlorophyll both in a leaf and over a canopy (Munden et al., 1994; Pinar and Curran, 1994; Railyan and Korobov, 1993).

2.5. REP estimation techniques

Mathematically, REP is the maximum of the first derivative spectrum in the red edge region. The derivative spectrum can be estimated by

$$D_{\lambda(i)} = \frac{R_{\lambda(i)} - R_{\lambda(i-1)}}{\Delta\lambda} \quad (2.1)$$

Where, $R_{\lambda(i)}$ and $R_{\lambda(i-1)}$ are reflectances at wavelength i and $(i-1)$ respectively. The REP estimated using the maximum of first derivative method is accurate if the sensor has fine spectral resolution and also this process eliminates/reduces the source of variability, for example, background reflectance from the reflectance spectra (Horler et al., 1983; Demetriades-Shah, 1990). However, an accurate estimation of REP using maximum of first derivative method requires both spectral continuity and fine spectral resolution of the reflectance spectra (Dawson and Curran, 1998). To overcome this dependency on spectral sampling intervals researchers suggested different techniques for REP estimation. Most commonly used techniques include (i) higher order curve fitting techniques (Demetriades-Shah, 1990); (ii) an inverted Gaussian technique (Bonham-Carter, 1988; Miller et al., 1990); (iii) a linear interpolation technique (Guyot et al., 1988, Danson and Plummer,

1995), (iv) a Lagrangian interpolation technique (Dawson and Curran, 1998) and (v) using rational function technique (Baranoski and Ronke, 2005) . Performances of these techniques are given in table 2.2.

Requirements	Linear Interpolation	Inverted Gaussian	Lagrangian interpolation	Curve fitting	Maximum of first derivative	Rational
Fine Spectral resolution	Medium	Medium	Low	High	High	High
Number of bands in red-edge)	4	3	3/4	Many	Many	3
High band continuity	Low	Low	Low	High	High	low
Requires derivative spectra	Low	Low	High	Low	High	High
Uses a modelled relationship	High	High	Medium	Medium	Low	medium

Table 2.2. Performances of different techniques for locating the REP (modified from Dawson and Curran, 1998).

2.5.1 Higher order curve fitting techniques

Baret et al. (1992) proposed a polynomial equation for estimating the REP using three spectral bands. They used model simulations to select optimal spectral bands at 672 nm (R_1), 710 nm (R_2) and 780 nm (R_3) and subsequently fit a polynomial equation to the maximum of the second derivative (equation 2.2).

$$REP = C_0 + C_1 R_1 + C_2 R_2 + C_3 R_3 + C_4 R_1^2 + C_5 R_2^2 + C_6 R_3^2 + C_7 R_1 R_2 + C_8 R_1 R_3 + C_9 R_2 R_3 + C_{10} R_1 R_2 R_3 \quad (2.2)$$

Where C_0 to C_{10} are the constants to be determined through iteration.

Broge and Leblanc (2001) proposed a sixth order polynomial function for estimating the REP. The polynomial was described by (equation 2.3)

$$R(\lambda) = C_0 + C_1 \lambda + C_2 \lambda^2 + C_3 \lambda^4 + C_5 \lambda^5 + C_6 \lambda^6 \quad (2.3)$$

The REP is determined by identifying the root of the second derivative of the polynomial, where λ is considered to be close to 720 nm, depending upon the nature of the curve (Borge and Leblanc, 2001).

Computationally these higher order curve fitting techniques are complex. However, they will capture the potential asymmetry of the red edge, where as other methods, for example, the inverted Gaussian will average out such asymmetry (Broge and Leblanc, 2001).

2.5.2 Inverted Gaussian technique

Hare et al. (1984) suggested that the shape of a vegetation reflectance spectra in the red edge region can be approximated by an inverted Gaussian function; this approach was used to derive the inverted Gaussian model (IGM) for estimating the REP. Variables of IGM includes the central wavelength (λ_0), reflectance minimum (R_0) of the chlorophyll absorption region that occur at approximately 680 nm (figure 2.2). The IGM describes the variation of reflectance, R , as a function of wavelength (λ).

$$R(\lambda) = R_s - (R_s - R_0) \exp \left[-\frac{(\lambda - \lambda_0)^2}{2\sigma^2} \right] \quad (2.4)$$

Where, R_s is the ‘shoulder’ reflectance (at approximately 800 nm)

R_0 is the minimum reflectance at the chlorophyll absorption feature

σ is the Gaussian shape parameter

For N data points in the red edge region, the problem is to determine R_s , R_0 , σ and λ_0 that minimises the sum of the squared deviation of the fitted curve, $R'(\lambda)$ from the observed reflectance, $R(\lambda)$.

$$\sum_{i=1}^N [R_i(\lambda) - R'_i(\lambda)]^2 \rightarrow \text{minimum} \quad (2.5)$$

Then REP can be defined as the

$$REP = \lambda_0 + \sigma$$

(2.6)

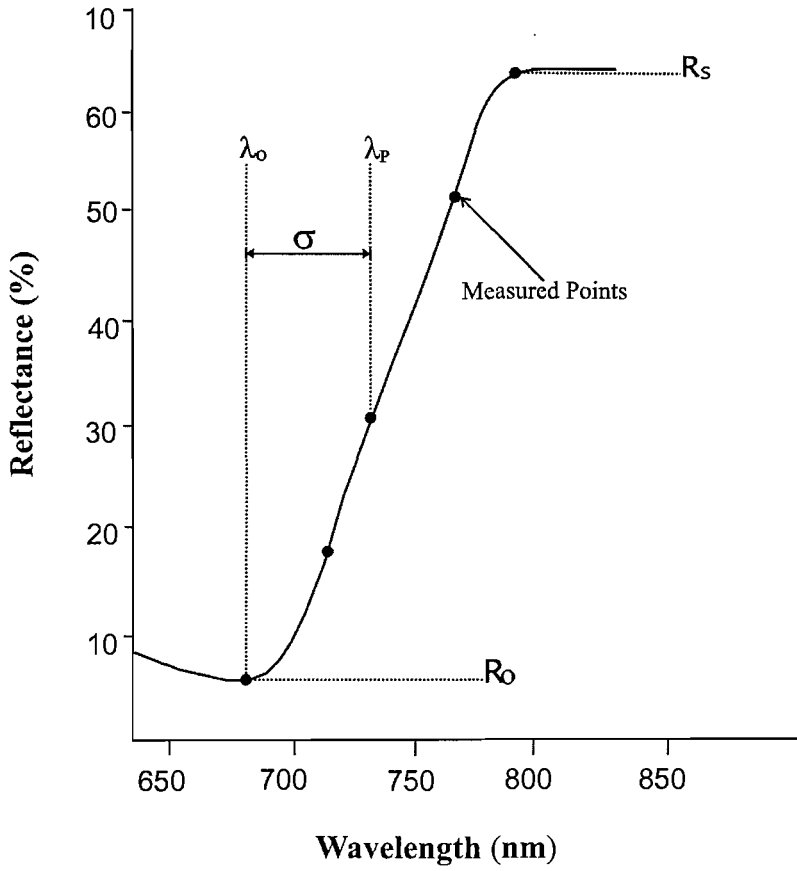


Figure 2.2. Inverted Gaussian technique, with red edge curve fit parameters indicated: the reflectance maximum (R_s), the reflectance minimum (R_0), the spectral position of the reflectance minimum (λ_0), the spectral position of the curve inflection (λ_p) and the Gaussian curve width parameter σ .

Miller et al. (1990) suggested a linear fitting approach which was computationally more efficient than (i) the iterative optimisation fitting procedure as described above and (ii) non-linear fitting methods, for example, Gauss-Newton differential-correlation technique (Bonham-Crater, 1988). Details of these fitting procedures and a number of software subroutines were described by Bonham-Crater (1988). Despite the lack of theoretical basis, the IGM has a shape that effectively characterised the shape of the red edge and can be fitted to laboratory and field measurements of vegetation spectra. IGM has

been used widely for the estimation of REP (Lucas et al., 2000; Miller et al., 1990; Patel et al., 2001; Zarco-Tejada and Miller, 1999).

Vegetation canopy spectra contain information on shadow, soil and understorey reflectance, which affect the accuracy with which REP can be estimated for the canopy alone. These effects coupled with the need to know pre-determined points like R_0 and R_s , weakens the argument for using IGM for estimation of REP (Dawson and Curran, 1998).

2.5.3 Linear interpolation

Guyot et al. (1988) proposed a linear interpolation technique for estimating the REP. They assumed that the red edge could be represented as a straight line on a spectrum between reflectance at 670 nm and 780 nm. Reflectances at 670 nm and 780 nm were then used to calculate the reflectance of the inflection point and a linear interpolation technique was used to calculate the wavelength of this inflection point (figure 2.3). So there are two steps: first, calculation of reflectance at the inflection point (equation 2. 7) and second, calculation of the REP (equation 2.8).

$$R_i = \frac{(R_{670} + R_{780})}{2} \quad (2.7)$$

Where R_i is the reflectance at wavelength i.

$$REP = 700 + 40 \frac{(R_i - R_{700})}{(R_{740} - R_{700})} \quad (2.8)$$

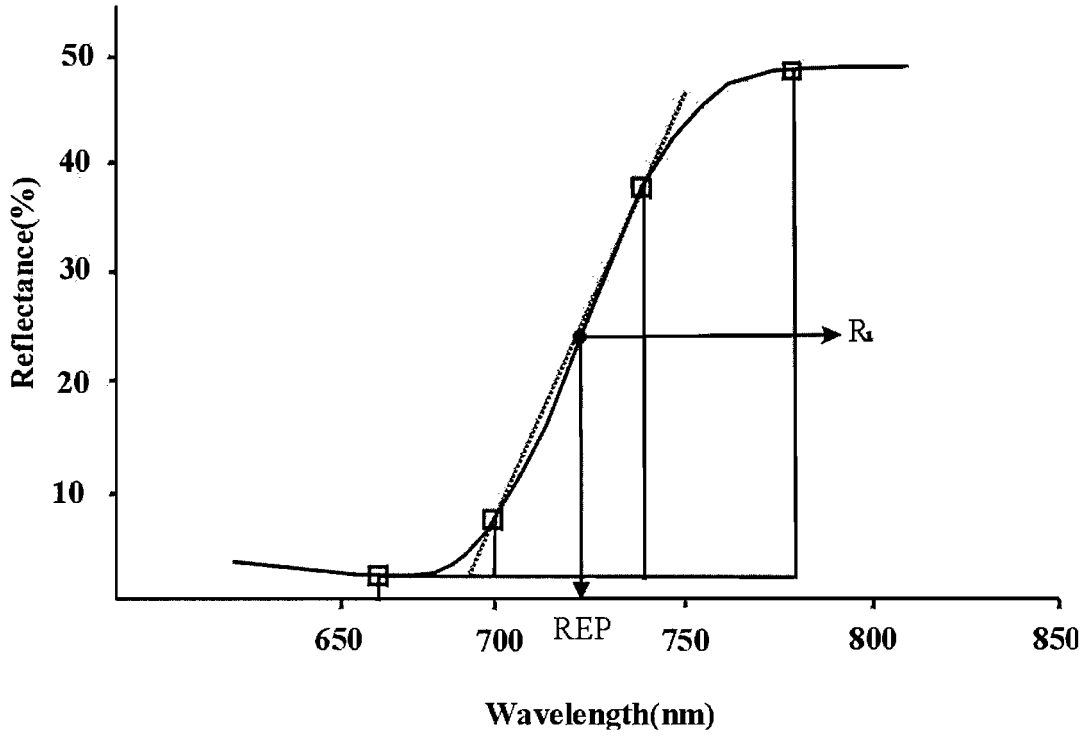


Figure 2.3. Linear interpolation technique, indicating the red edge inflection point (R_i) and the red edge position (REP).

Danson and Plummer (1995), used a slightly different wavelengths and the following equation for estimating the reflectance at the REP (equation 2.9) and calculation of REP (equation 2.10).

$$R_i = \frac{(R_{673} + R_{780})}{2} + R_{673} \quad (2.9)$$

Where R_i is reflectance at wavelength i .

$$REP = 700 + 40 \frac{(R_i - R_{700})}{(R_{740} - R_{700})} \quad (2.10)$$

The linear interpolation technique is conceptually and computationally simple (Guyot et al., 1988). However, in some cases this can result in a loss of useful spectral details.

2.5.4 Lagrangian interpolation

Dawson and Curran (1998) proposed a technique based on three point Lagrangian interpolation (Jeffrey 1985) for the estimation of REP. This uses a second order polynomial fit to the first derivative vegetation reflectance spectrum and reflectance in three wavebands: the band with maximum first derivative reflectance and two adjoining bands. REP is:

$$REP = \frac{A(\lambda_i + \lambda_{i+1}) + B(\lambda_{i-1} + \lambda_{i+1}) + C(\lambda_{i-1} + \lambda_i)}{2(A + B + C)} \quad (2.11)$$

$$\text{Where, } A = \frac{D\lambda_{(i-1)}}{(\lambda_{i-1} - \lambda_i)(\lambda_{i-1} - \lambda_{i+1})}, \quad B = \frac{D\lambda_{(i)}}{(\lambda_i - \lambda_{i-1})(\lambda_i - \lambda_{i+1})},$$

$$C = \frac{D\lambda_{(i+1)}}{(\lambda_{i+1} - \lambda_{i-1})(\lambda_{i+1} - \lambda_i)}$$

In this case $D\lambda_{(i-1)}, D\lambda_{(i)}, D\lambda_{(i+1)}$ are the first derivative reflectances corresponding to wavebands $\lambda_{(i-1)}, \lambda_{(i)}, \lambda_{(i+1)}$ respectively ($\lambda_{(i)}$ is the band with maximum first derivative reflectance with $\lambda_{(i-1)}$ and $\lambda_{(i+1)}$ representing the bands either side of it).

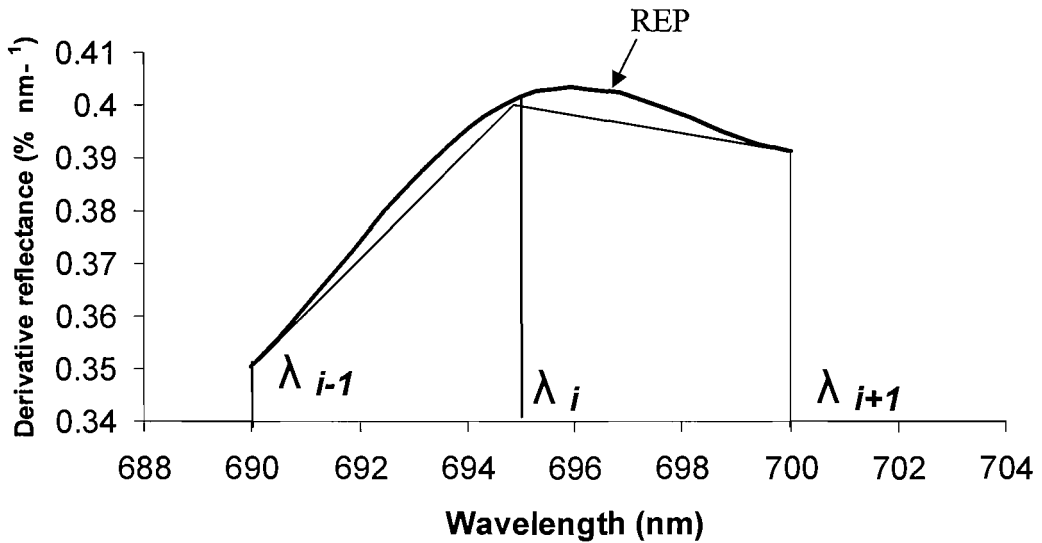


Figure 2.4. The three point Lagrangian interpolation technique to determine the red edge position, indicating the REP along the derivative curve.

The advantages of Lagrangian interpolation are: (i) wavebands used for the estimation of REP need not be spaced equally; (ii) the use of first derivative spectrum minimises interpolation errors and (iii) it is computationally one of the simpler curve fitting techniques. However, Clevers et al. (2002) reported a ‘jumping’ feature in a nonlinear REP/chlorophyll content relationship derived using Lagrangian interpolation.

2.5.5 Rational function

Recently Baranoski and Ronke (2005) proposed a red edge estimation technique based on the rational function. They assumed the reflectance in the red edge region can be classified into three regions : (i) region of low and relatively low reflectance; (ii) the red edge region and (ii) region of high and relatively constant reflectance. These features could be approximated by a rational function:

$$f(\lambda) = \frac{a + b\lambda + c\lambda^2}{1 + c\lambda + d\lambda^2}$$

Four conditions could be used to estimate the five parameters a,b,c,d and e as

$$f(\lambda_l) = \rho_l$$

$$f'(\lambda_l) = 0$$

$$f(\lambda_h) = \rho_h$$

$$f'(\lambda_h) = 0$$

Where λ_l and ρ_l are wavelength and reflectance at lower bound and λ_h and ρ_h are wavelength and reflectance at the upper bound of the red edge. Input at another point, centre of the red edge (λ_c, ρ_c) is required to estimate the REP.

The accuracy of the REP depends on the accuracy of picking the three points mentioned above. REP estimated by rational function has two advantage: (i) rational functions tends

to spread the approximate error more evenly over the approximation interval, thus allowing error to be distributed evenly and (ii) this technique could be automated by using the fixed values for three input wavelengths (680 nm, 725 nm and 770 nm).

Baranoski and Ronke (2005) found a relative error of less than 1% in comparing the REP estimated using the rational function and actual REP for 80 spectra. However, this technique needs to be compared with the REP estimated by other techniques.

2.6. Modelling

Reflection modelling of vegetation leaf or canopy uses a description of leaf optical and/or structural properties to understand reflectance. Modelling has been proved to be a powerful tool for understanding light interaction with leaf/canopy and to infer ecological condition from reflectances measured over a canopy. This theoretical understanding will lead to development of more reliable remote sensing information about vegetation. Current models can be divided into leaf models, canopy models and combined models.

2.6.1 Leaf Models

Leaf models (Jacquemoud and Baret, 1990; Dawson et al., 1998) have the physical and biochemical properties of leaves as input and reflectance spectra as output of the model. Several models have been developed that link leaf reflectance, leaf structure and leaf biochemical constituents. Leaf models generally assume that leaf internal structure (cell wall, cytoplasm etc.) have a definite shape and optical properties and the resultant reflectance is the combined effect of light interaction with these structures. Four of the more commonly used leaf reflectance models are described here.

- PROSPECT

Allen et al. (1969) proposed a plate model of leaf reflectance for a typical compact leaf, where the optical properties are characterised by an effective index of reflection and an effective index of absorption. Later Allen and Richardson (1970) extended this plate model to N layers and describe the internal structure by a void area index (VAI).

PROSPECT proposed by Jacquemoud and Baret (1990) is based on Allen's plate model (which uses the radiative transfer function) and describes leaf optical properties from 400 nm to 2500 nm wavelength of electromagnetic radiation.

The PROSPECT model is based upon the following assumptions:

- A plant leaf is a transparent plate with rough plane parallel surfaces.
- A plant leaf is composed of N horizontal layers separated by N-1 air spaces.
- Light fluxes are isotropic.
- There is a uniform distribution of water, pigment and structure inside a leaf.

The PROSPECT model has four major input variables: refractive index of the leaf material, incidence angle, transmission coefficient and number of layers in a leaf. In addition to these it also require information about leaf biochemical constituents which includes chlorophyll a+b content, water content and dry mater content. The reflectance and transmittance are calculated for each individual layer and the sum gives the total reflectance (Jacquemoud et al., 1996). By inverting the PROSPECT model leaf variables can be estimated from leaf optical measurements. The PROSPECT model was upgraded (Jacquemoud et al., 1996) to include leaf biochemical constituents. In the upgraded version PROSPECT takes into account the absorption, reflection and transmission coefficients for chlorophyll, water and other leaf pigments along with the other variables in its older version.

- LIBERTY

LIBERTY (Leaf Incorporating Biochemistry Exhibiting Reflectance and Transmittance Yield) model was proposed by Dawson et al. (1998). LIBERTY adopts Melamade's theory of light interaction with suspended powder (Melamade, 1963) to model leaf optical properties at the cellular level (Dawson et al., 1998). LIBERTY uses the radiative transfer function, where the total reflectance of a leaf or stacked leaves will be the sum of the scattered radiation fluxes emerging in upward direction from a horizontal surface. The model is based on the following assumptions:

- Internal structure of leaves consists of spherical particles whose surfaces scatter radiation according to the Lambert cosine law.
- All leaf cells have the same mean diameter.
- Cells are separated from each other by air gaps.
- Leaf surface is horizontal.

Reflectance for an individual leaf cell is estimated by considering absorption coefficient of the cell medium (which depends on the biochemical constituents present in the leaf) and internal and external scattering. Then the total reflectance can be calculated by aggregating all reflections from individual cells. The model can be extended into multiple layers by considering air gaps between cell layers (Dawson et al., 1998). Input variables to LIBERTY models includes the cell structural variables (cell diameter, intercellular air spaces, leaf thickness), absorption features (absorption due to baseline, absorption due to albino) and major chemical contents of a leaf (water, chlorophyll, nitrogen, lignin). Using these input variables LIBERTY can estimate the reflectance spectra over stacked leaves and reflection and transmission spectra over a single leaf. By inverting the model absorption coefficients, biochemical and biophysical variables can be obtained directly from high resolution remote sensing data (Dawson et al., 1997). Braton (2001) used the LIBERTY model for simulating a reflectance spectrum over a leaf to study the influence of

heterogeneity in chlorophyll distribution on leaf reflectance. LIBERTY can be used with other canopy model to estimate the reflectance spectra over a canopy (Dawson et al., 1998).

- RAYTRAN

Ray-tracing techniques require a detailed description of leaf geometric properties as well as knowledge of the mechanisms involved in the scattering and absorption of light at different amount of leaf tissue and at different wavelengths. Various assumptions must be made on the shape and size of the cells and on their spatial arrangement in tissues, if efficient numerical computations are to be performed repetitively (Gibson and Ashby, 1995).

RAYTRAN based on Monte Carlo ray-tracing, can be used to compute radiation transfer in this virtual three-dimensional leaf. This tool was designed initially to investigate radiation transfer problems in terrestrial environments at a variety of spatial scales (Govaerts and Verstraete, 1994).

According to this model, incident rays can be either collimated to simulate direct illumination or distributed angularly to represent diffuse light. Rays are generated in the forward direction, i.e., from the light source to the scene, and tracked from interaction to interaction throughout the leaf cell structure, until the ray is absorbed or escapes from the leaf. Reflectance of a membrane can be calculated with the Fresnel formulas using the refractive-index differences between two media (Govaerts and Verstraete, 1994). Ray path statistics are accumulated to compute the bi-directional reflectance and transmittance factors.

Govaerts and Verstraete (1998) investigated the propagation of light in a typical dicotyledon leaf using RAYTRAN model. They assigned cells of different tissues appropriate morphologies, water and chlorophyll content and each cell constituent is

characterized by an index of refraction and an absorption coefficient . The influence of the roughness of the epidermis on the reflection and absorption of light was investigated, and simulation results confirmed that convex cells in the epidermis focus light on the palisade parenchyma and increase the absorption of radiation (Govaerts and Verstraete, 1998).

- SLOP

SLOP (Stochastic model for Leaf Optical Properties) proposed by Maier et al. (1999) describes the radiative transfer of light within leaf as a stochastic process. It calculates the reflection, transmission, and absorption of light by leaves in the spectral region from 400 nm up to 2500 nm. The model treats the radiative transfer of diffuse light as transitions of light with weighted probabilities according to the theory of homogeneous Markov chains (Tucker and Garratt, 1977). The leaves are divided in several compartments analogous to the well-known leaf structure. In a Markov chain, photon states are represented by two states, illumination state and absorbing state. In Markov chains the temporal development occurs in discrete time steps. This is expressed mathematically by matrix multiplications. The elements of the so-called ‘transition-matrix’ are the probabilities for the transitions between the different states.

Transition probabilities are calculated using Beer’s law from the optical parameters (i.e. specific absorption and scattering coefficient of different constituents), concentration of these constituents and the geometrical dimensions (Maier et al., 1999). The specific absorption coefficients of chlorophyll are also a major input constituent to the SLOP model. In this model water is treated as an absorbing constituent, therefore its influence on leaf internal structure and thus, on the scattering is ignored. SLOP can be used to distinguish between the reflection from the upper and the lower leaf side (Maier et al., 1999).

- LEAFMOD

Leaf Experimental Absorptivity Feasibility MODEL (MODEL) proposed by Ganapol et al. (1998) is a leaf radiative transfer model. One dimensional radiative transfer function is used to represent the leaf material with homogenous optical properties. The model is based on the following assumptions:

- Leaf is one dimensional and extends to infinity in transverse direction.
- Scattering is isotropic from cellwalls .
- Leaf interior is a homogenous mixture of biochemicals.

Input variables to LEAFMOD includes: leaf thickness and optical characteristics(i.e., absorption and scattering coefficients). For these inputs LEAFMOD generates an estimate of leaf reflectance and transmittance. In the inverse mode it computes the total leaf absorption and scattering coefficients from measured reflectance, transmittance and leaf thickness. LEAFMOD exact inversion was performed on spectral measurement from the Leaf Optical Property Experiment (LOPEX) archive (Hosgood, 1995) to examine the absorption feature response to pigment concentration.

2.6.2 Canopy Models

Canopy models (Verhoef, 1984; Suits, 1972) have the canopy structural properties (e.g. LAI (leaf area index), Leaf angle distribution etc.), background reflectance, Sun-sensor geometry and leaf optical properties as input and reflectance spectra as output. Goel (1988) divided vegetation canopy models into four distinct classes:

- a) Geometrical models (Otterman model (Otterman, 1981)); the canopy is assumed to consist of geometrical objects of known shape (cylinder, sphere etc.), dimension and optical properties.

- b) Turbid medium models (SAIL model, (Verhoef, 1984)); the canopy is assumed to be a parallel planer finitely extended medium comprising small absorbing and scattering particles with given optical properties.
- c) Hybrid models (FLIGHT model, (North, 1996)); the vegetation canopy is assumed to be geometrically shaped plants, the elements of these plants are treated as absorbing and scattering particles.
- d) Ray tracing models (Ross-Marshak model, (Ross and Marshak, 1987)); the arrangements and orientation of leaves are simulated on a computer and Monte-Carlo ray tracing techniques are used to estimate the reflectance flux over a vegetation canopy.

Some of the earliest vegetation reflectance models were based on Kubelka-Munk (K-M) theory (Allen and Richardson, 1970). The K-M approximation of radiative transfer function (Chandrasekhar, 1950) is a four flux approximation for a parallel plane medium (Kubelka and Munk, 1931). In this approximation diffuse flux is in form of two monochromatic fluxes, travelling downward and upward in the medium and perpendicular to the medium. Similarly, specular radiation is described by two more fluxes. One of the earliest models was developed by Allen and Richardson (1970), who used a two flux K-M approximation of the upward and downward diffuse fluxes. Allen et al. (1969) used a three flux K-M approximation by adding the downward specular flux and compared its performance with that of previous model of Allen et al. (1969). Prior to the work of Suits (1972) vegetation reflection models did not consider solar and viewing angles or canopy architecture. Suits (1972) used a four flux and nine parameter K-M approximation of the radiative transfer function, where the canopy was assumed to be a homogenous mixture of horizontal and vertical diffusely reflecting and transmitting elements. In this model vegetation canopy

elements are projected into a horizontal and a vertical plane. The total reflectance includes consideration of (i) leaf hemispherical reflectance, (ii) leaf hemispherical transmittance and (iii) solar zenith angle. The fourth flux added by Suits is radiance in the direction of observation. An angular component was added to the Suits model by Verhoef (1984). The resultant SAIL (Scattering by Arbitrary Inclined Leaves) model describes the extinction and scattering of a radiant flux by leaf layers.

- SAIL

The SAIL model of canopy reflectance is a modification of the Suits model. This model also applies the 4 fluxes and nine parameter solution of K-M approximation (Verhoef, 1984). The model is based on the following assumptions:

- Canopy is horizontal and infinitely extended.
- Canopy components are small and leaves are flat.
- Leaf layer is homogenous.
- Distribution of leaf orientation can be described by a leaf area orientation distribution function.
- Leaf azimuth angles exhibit a random distribution.

To describe canopy morphology Verhoef (1984) used the Leaf Area Index (LAI), leaf inclination density and layer thickness. In addition to the nine parameters described by Suits in his model, SAIL calculates two other parameters: extinction efficiency and scattering efficiency. Extinction efficiency is defined as the capability of a leaf to intercept radiant flux (Verhoef, 1984), whereas the scattering efficiency is a function of both incident and scattered flux. From the SAIL model it can be shown that each leaf inclination angle generates its own characteristic spatial pattern of intercepting and scattering radiation.

The SAIL model is used widely in remote sensing research for investigating the reflectance properties of vegetation canopies (Danson, 1998). The SAIL model can be inverted to estimate biophysical variables such as biomass, LAI and vegetation cover (Goel and Thompson, 1984). The inverted SAIL model was used successfully to simulate the crop residue reflectance from wheat in visible and near infrared wavelengths (Su et al., 1997). SAIL model was used by Daughtry et al., (2000) for simulating canopy reflectance for variable background reflectances, LAI and leaf chlorophyll concentration. They found that, variations in background reflectances and LAI confounded the detection of the relatively subtle difference in canopy reflectance due to change in leaf chlorophyll concentration. Guerif and Duke (1998) combine the SUCROS (Simple and Universal CROp growth Simulator) a crop growth model with SAIL for estimation of sugar beat yield.

- DART

Gastellu-Etchegorry et al. (1996) proposed the DART (Discrete Anisotropic Radiative Transfer) model that simulates radiative transfer in a heterogenous 3-D scene. The whole scene was divided into small rectangular building blocks. The optical properties of the building block are represented by individual scattering function of the elements in the block and are directly input into the model. The model simulation is a two step process: First, the cell is illuminated with direct solar radiation and within cell multiple scattering is simulated. Second, interception and scattering of previously scattered radiation, in this case atmospheric radiation is input. Output of the DART model comprises: Bidirectional Reflectances Distribution Function (BRDF) of the canopy, radiation components associated with leaf volume and surface (Gastellu-Etchegorry et al., 1996). DART model

has been used successfully to estimate canopy spectral reflectances over homogenous canopies (Gastellu-Etchegorry et al., 1996).

- MCRM

The MCRM (Multispectral Canopy Reflectance Model) developed by Kuusk (1994) describes the directional reflectance of a homogenous canopy over 400 nm -2500 nm of the spectral range. Three models have been integrated into this model: (i) leaf optical model PROSPECT (Jacquemoud and Baret, 1990), (ii) soil reflectance spectrum (Price, 1990) and (iii) skylight spectral ratio (McCartney, 1976).

The set of model input variables includes 4 structural variables, 4 geometrical and illumination variables and 5 variables representing the optical properties of leaves and soil. Structural variables include: Leaf area index (LAI), relative linear size of the leaves, modal leaf inclination and eccentricity of the elliptical distribution of leaf normals. Geometrical and illumination variables include: solar zenith angle, view zenith angle, relative view azimuth and Angström turbidity factor. Optical variables include: leaf pigment concentration, leaf water equivalent, the number of elementary layers inside a leaf, the ratio of refractive indices of the leaf surface wax and internal material and the weights of the price function (Price, 1990). The number of input variables of the model does not depend on the number of spectral band used.

Kusk (1995) also inverted the MCRM model with canopy reflectance data measured by Ranson et al., (1985). The inversion was carried out in two steps. First: values of the optical variables were fixed at typical values of vegetation and the structural variables estimated. Second: estimated structural values were assumed and optical variables estimated. There was a good agreement between the estimated and measured variables

(Kusk, 1995). The MCRM is computationally faster and can be inverted easily on relatively large sets of reflectance data.

Kusk and Renhua (1997) estimated LAI and canopy chlorophyll concentration by inverting the MCRM. In their study the MCRM model was inverted on a Landsat Thematic Mapper scene. MCRM has also been used successfully to estimate the understorey reflectance for Scots pine stands (Rautiainen et al., 2003).

- FLIGHT

North (1996) developed the three dimensional forest light interaction model, FLIGHT (Forest LIGHT) for estimating the spectral BRDF of discrete forest stands using a hybrid geometric/radiative transfer model. The model utilises Monte Carlo ray tracing to simulate photon transport within the discontinuous environment of the forest canopy. Macro structure variables determine the geometry of each stand, including crown shape and size. Within each crown envelope, foliage microstructure is approximated by mean value of leaf area density, leaf angle distribution, leaf size and leaf reflectance and transmittance. The effect of woody bark and twigs are modelled similarly as opaque foliage, while a second cone is used to represent the trunk. Individual photon trajectories are traced from solar source, through successive interaction to a pre-determined sensor view angle. Each photon interacting with foliage within a crown, or with trunk and understorey surfaces, is absorbed or scattered in new direction. Anisotropic scattering functions are used to model the diffuse sky radiance component and interaction with the soil understorey (North, 1996).

2.6.3 Combined models

These are a combination of a leaf model and a canopy model. However, sometimes other models e.g., geometrical models can also be combined with either leaf or canopy models.

In this combined approach the output of the leaf models are input to the canopy model.

Five commonly used combined models are considered below.

- PROSAIL

This is a combined model constituting PROSPECT as the leaf model and SAIL as the canopy model. PROSAIL was used to simulate reflectance spectra over a vegetation canopy (Jacquemoud et al., 1995) and to estimate LAI (Chaurasia and Dadhwal, 2002).

- LIBSAIL

This is a combination of the LIBERTY leaf model and SAIL canopy model. The influences on reflectance spectra of the background (e.g., vegetation understory) have been evaluated using a spectral mixture model of LIBSAIL outputs (Llewellyn and Curran, 2001).

- GEOSAIL

The GeoSail model combines a geometric model, which calculates the amount of shadowed and illuminated components in a scene, with the SAIL model, which calculates the reflectance and transmittance of the tree crowns. Scene reflectance is determined in the model by calculating an area-weighted average of three landscape components: illuminated canopy, illuminated background, and shadowed background. The simplicity of this model is a result of the assumption that single values for the reflectance and transmittance of light by canopy clumps are enough to provide a reasonable overall description of scene reflectance and absorption. The geometric part of GeoSail uses the model

developed by Jasinski (1990) for the limiting case where the shadows cast by clumps of vegetation are very small relative to the size of the area observed (Jasinski and Eagleson, 1989; Jasinski, 1990; Jasinski and Eagleson, 1990).

Rowland et al. (2000) described an experiment where data from GeoSAIL were used to train a neural network, which was later used for the estimation of forest LAI.

- LCM2

Ganapole et al. (1999) developed a combined model called LCM2 (Leaf/Canopy Model version 2), to generate vegetation canopy reflectance as a function of leaf biochemistry, leaf morphology, leaf thickness, soil reflectance and canopy architecture. This combines the LEAFMOD leaf model and a dense canopy radiative transfer model, CANMOD. The model was used to reconstruct fresh-leaf reflectance and transmittance profiles for 38 different monocot and dicot species.

- FLIGHT and LIBERTY

Dawson et al. (1999) coupled FLIGHT with LIBERTY and varied LAI, canopy closure, understorey reflectance, foliar water and lignin cellulose content to evaluate the sensitivity of canopy spectra to variation in foliar biochemical content. The study identified wavelength regions related to both water and lignin-cellulose that was persistent at both leaf and canopy scales. Dawson (2000) simulated a reflectance spectrum over a vegetation canopy, in the MERIS standard band setting, by integrating LIBERTY with FLIGHT.

2.7. Spectral measurement techniques for vegetation

To estimate the foliar biochemical content of vegetation canopies remotely a fundamental advance was required in instrumentation and techniques of analysis. This came about in 1970s, with the development of imaging spectrometers, instruments that combined the spatial aspects of remote sensing and the analytical techniques of spectroscopy (Curran,

2001). Spectrometry is the measurement of the interaction of electromagnetic radiation with matter and the use of these measurements to deduce the properties of material (Banwell, 1994). It is the extension of human vision and a non-destructive way of determining information about a material (Birth and Hecht, 1987). It may be possible to estimate the biochemical concentration of foliage within vegetation canopies over large areas by combining remotely sensed and spectroscopic measurements (Curran, 1989). Spectrometers have been used in laboratory [Perstorp NIRSystem 6500 spectrometer (Kupiec and Curran, 1995)], field [Spectron SE590 Spectroradiometer (Blackburn, 1998); Geophysical Environmental Research IRIS Mark IV (Jago et al., 1999)], air [Compact Airborne Spectrographic Imager (CASI) (Niemann, 1995); Airborne Visible/Infrared Imaging Spectrometer (AVIRIS) (Zagolski et al., 1996)] and space [MOderate Resolution Imaging Spectroradiometer (MODIS) (Justice and Townshend, 2002); MEdition Resolution Imaging Spectrometer (MERIS) (Curran and Steele, 2002)] studies to develop and modify techniques for estimating variables related to the condition and amount of vegetation.

2.7.1 Laboratory Spectrometers

To understand the interaction of radiation with a material a device is required which can measure the amount of radiation absorbed in individual wavebands over a range of wavelengths. A simplest form of device known as a spectrograph (Svanberg, 1992) can be used to demonstrate the occurrence of absorption features. This device takes light from a source and splits it into its spectrum via a dispersing element. However, for quantitative measurements of the absorption of radiation by material a more complex instrument, known as a spectrometer is required. The most common instrument emits radiation at specific wavelengths which can be varied across a specific wavelength range (figure 2.5). This instrument consists of a source, normally a quartz halogen tungsten filament lamp, which produces a continuous spectrum that covers the required wavelength range and a

monochromator that separates out a narrow waveband of radiation (Svanberg, 1992). The monochromator contains a set of optical devices, such as slits, mirrors and lenses, and a dispersing element, either a prism or a diffraction grating. The sample is therefore illuminated by narrow wavebands of radiation that leaves the monochromator. A photoconductive detector (e.g. lead sulphide) records the intensity of the radiation that has interacted with the sample in relation to its wavelength. Spectrometers often work as a dual beam principle where radiation leaving the monochromator is alternatively directed to the sample and a reference. This allows corrections to be made for the effect of the source and the instrument. The viewing geometry and the position of the sample within the spectrometer will depend on the sample type and the measurements to be made (Hollas, 1992). An example of a dual beam spectrometer is described below.

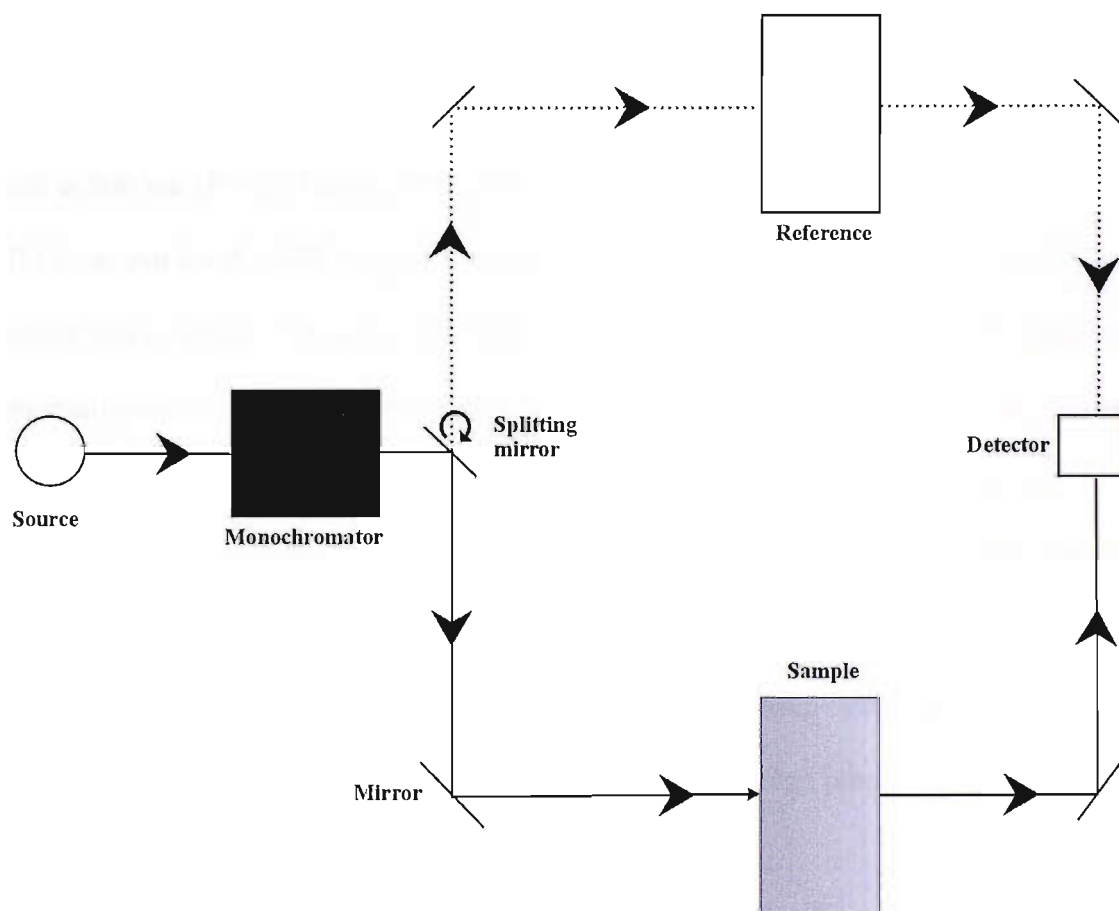


Figure 2.5. Schematic diagram of a dual beam spectrometer.

A variety of different laboratory spectrometers are now available and each has a different function. Example of such instruments includes Perkin Elmer Lambda 19 Spectrometer, S106 Spectrophotometer.

- Perkin Elmer Lambda 19 spectrometer

This is a computer driven, dual beam, double monochromator ratio recording spectrometer. For UV work and auto calibration it has a deuterium lamp and for visible and NIR wavelengths a tungsten halogen lamp. Mirrors reflect radiation into a chopper assembly that rotates to alternately bring a mirrored segment, a window segment and a dark segment into the radiation beam. The mirror segment direct radiation from a reference and the dark segment blocks the radiation beam and creates a dark signal for internal calibration (Perkin Elmer, 1991). The Lambda 19 can provide a nominal slit width of 0.1 nm for visible and 0.2 nm for NIR. For a nominal wavelength bandwidth of 1 nm the spectral resolution is 0.99 nm at 400 nm, 0.93 nm at 600 nm, 0.91 nm at 656.1 nm and 0.86 nm at 800 nm (Perkin Elmer, 1991). The instrument accuracy for the UV/visible range is ± 0.15 nm and for the NIR range is ± 0.6 nm. Repeatability is less than 0.02 nm in UV/visible range and less than 0.08 nm in the NIR range (determined by the standard deviation of ten measurements). Calibration of the Perkin-Elmer instrument is performed using internal radiometric and spectral calibration standards and a BaSO₄ standard. Instrumental corrections are performed as necessary, according to sample mounting and measurement type (Hosgood et al., 1994).

Hosgood et al. (1994) used a Perkin-Elmer Lambda 19 double-beam spectrophotometer for measuring the reflectance and transmittance in leaf optical properties experiment (LOPEX).

2.7.2 Field Spectrometers

Field spectrometers are becoming more convenient as user interfaces are improved and as the instruments become smaller and more efficient (Milton, 2000). A variety of different field spectrometers are now available and each has a different functionality. Examples of such instruments includes Spectron SE90 Spectroradiometer, GER 1500, GER 3700, Analytical Spectral Device (ASD).

- Spectron SE590 spectroradiometer

The Spectron SE590 spectroradiometer is a lightweight, rapid scanning field instrument capable of collecting narrow bandwidth spectra over the range 400 nm to 1100 nm. It collects spectra sequentially from the target and the reference, taking approximately one second to measure a spectrum. The typical delay between measurement of the target and reference with the Spectron SE590 is 10 seconds. The reference spectrum may be collected from either a calibrated panel or (using a second optical head) a cosine receptor. Data may be stored on miniature digital tapes provided with the unit, or directly to a portable computer.

A Spectron SE590 spectroradiometer was used to measure the reflectance over Douglas-fir, a part of the NASA's Accelerated Canopy Chemistry Program (ACCP) (Yoder and Johnson, 1999). A Spectron SE590 spectroradiometer was fitted with a cosine corrected receptor for obtaining data in seven spectral channels, chosen as input to a neural network for estimating the optimisation of bands (Milton et al., 2001).

- GER 1500

The GER 1500 operates as a computer driven field spectrometer with a spectral range of 300 nm to 1100 nm (GER, 2005). It operates in both single beam and in double beam

mode. Single beam mode uses a single spectrometer in a standard manner with alternate measurements of a target and reference, while dual beam mode uses two spectrometers to record near-simultaneous measurements of the target and reference. Dual beam mode requires frequent inter calibration of reference measurements between the two spectrometers but is quicker than single beam mode if there are two or more persons available to record the measurements. It also reduces inaccuracy incurred from changes in atmospheric and solar conditions between target and the reference measurements. The GER 1500 has a sampling interval of 1.5 nm and a spectral band width of 3 nm. Fore-optics to provide a cone of acceptance field-of-view at 3°, 15° and 2 pi with a fiber optic link to the instrument is available. It has a wavelength accuracy of ± 1 nm. GER 1500 has been used extensively in the field for collecting spectral data for various applications. Some of the examples are to: predict nitrogen and chlorophyll concentration at leaf and canopy scale (Yoder and Pettigrew-Crosby, 1995); undertake spectral on mixing of hyperspectral data (Tseng, 1999); estimate the red-edge of soil contaminated grassland (Llewellyn et al., 2001) and to identify the spatial variability in cotton growth (Sudbrink et al., 2003).

- Analytical spectral devices (ASD) FieldSpec FR

The ASD FieldSpec FR is a portable field spectrometer with a spectral range of 350 nm to 2500 nm (ASD, 2005). A 512 element photo diode array with long pass filter is used for the measurements. This provides a sampling interval of 1.4 nm and a spectral resolution 3 nm at 700 nm and 10 nm above 700 nm. Fore-optics to provide a cone of acceptance field-of-view at 25° and pass the light to instrument through a fiber optics bundle of 1.2 m length. The instrument has a 16 bit encoding with 12 for charge couple device (CCD) (ASD, 2005).

ASD FieldSpec FR has been used to: relate hyperspectral vegetation indices with crop characteristics (Thenkabail et al., 2000) and to investigate the effect of chlorophyll fluorescence (Zarco-Tejada et al., 2003).

2.7.3 Airborne imaging spectrometers

Airborne imaging spectrometers provide a flexible operational and experimental remote sensing tool with a fine spectral and spatial resolution (Wulder, 1998). One of the earliest systems to provide airborne imaging spectrometry for civil use was the Airborne Imaging System (AIS) (Vane et al., 1984) developed and designed at the NASA JPL. The AIS could record radiance in 128 contiguous bands over the spectral range of 1200-2400 nm. Over the last decades a large number of airborne imaging spectrometers have been developed and used to acquire contiguous spectra over land and water (Treitz and Howarth, 1999). This includes Airborne Visible/Infrared Imaging Spectrometer (AVIRIS) (Vane et al., 1993), Compact Airborne Spectrographic Imager (CASI) (Anger et al., 1996) and MASER (MODIS/ASTER Airborne Simulator) (<http://masterweb.jpl.nasa.gov>). Some of the better known airborne imaging spectrometers are given in Table 2.3. Airborne spectrometric data have been used to estimate biophysical variables (Hall et al., 1996), age of forest stands (Niemann, 1995), canopy biochemical composition (Elvidge et al., 1993) (table 2.5). For the purpose of vegetation study CASI data (Jago et al., 1999; Niemann, 1995; Gong et al., 1995) and AVIRIS data (Roberts et al., 1993; Elvidge et al., 1993; Kupiec and Curran, 1995) have been used widely because of their availability.

- Compact Airborne Spectrographic Imager (CASI)

CASI was developed by Itres Research (<http://www.itres.com>), Canada and has been operational since 1989. It is a two dimensional CCD based push broom imaging spectroscope (NERC, 2005). A fore-optic lens with 54.4° Field-of-View (FOV) is used to provide optimal focusing across the CASI wavelength range. Incoming radiation entering the lens can be varied equivalent to aperture of f 11, f 8, f 5.6 and f 4. The CASI sensor can record data in a wavelength range of 405-950nm over 288 channels at a spectral sampling rate of 1.8 nm. A distinguishing feature of this system is its programmable band positioning system, where wavelength regions can be selected by the users before data acquisition. Data can be acquired by either 1) spatial mode, or 2) spectral mode, or 3) enhanced spectral mode, or 4) full frame mode. A comparison of different mode of data collection by CASI sensors is given in table 2.4.

CASI sensors have been used for a wide range of ecological and environmental applications ranging from atmospheric monitoring (Singh et al., 1997) to bathymetric mapping (George, 1997). Neiman (1995) used the CASI data for determining forest strand age based on a shift in the red edge position and change in NDVI. Goel et al. (2003) detected the nitrogen level and weed infestation in corn crop by applying the Artificial Neural Network and decision tree to CASI data. Further uses of CASI data for vegetation analysis are given in table 2.5.

- Airborne Visible/Infrared Imaging Spectrometer (AVIRIS)

AVIRIS was developed and designed at NASA JPL (<http://aviris.jpl.nasa.gov/>) and has been operational since 1987 (Vane et al., 1993). It is a whisk-broom imaging spectrometer and contains a linear array of detectors. AVIRIS was deigned to acquire data in the region of 400 nm -2500 nm over 224 contiguous channels. At an operating altitude of 20km, it has

a spatial resolution of 20m. This sensor consists of a scanner, four spectrometers and a calibration system (Porter and Enmark, 1987; Vane et al., 1993). There is one spectrometer for each of visible, near infrared and two for shortwave infrared regions of the spectrum.

Laboratory and in-flight calibration of AVIRIS data ensures a high level of calibration accuracy. Laboratory calibration aims to : 1) determine the central wavelength of light falling on each detector and 2) determine band width and distribution of AVIRIS spectral channels (Vane et al., 1993). During the in-flight calibration surface reflectance measurements are performed on a uniform surface followed by atmospheric correction. These atmospherically corrected values are then compare with spectral data recorded by a field spectrometer over the same area and their data are corrected accordingly.

Sensor	Number of bands	Spectral resolution (nm)	Spectral coverage (nm)	Spatial resolution (m)	Period of operation	Reference/ Website
Advanced Solid-state Array Spectrometer (ASAS)	62	10	404-1020	3.3- 6.6 (across track) 3 (along track)	1987 to 1993	NASA GSFC http://asas.gsfc.nasa.gov/asashome.html
Airborne Imaging Spectrometer for Applications+ (AISA+)	244	2.9	400-970	1.41, 1.02	1997 to present	Spectral Imaging Ltd., Finland http://www.specim.fi/products-aisa.html
Airborne Imaging System 1 (AIS 1)	128	9.3	1200-2400	8	1984 to 1987	NASA JPL
Airborne Imaging System 2 (AIS 2)	128	10.6	800-2400	8	1986 to 1987	NASA JPL
Airborne Multi-angle Imaging SpectroRadiometer (AirMISR)	4	variable	446.4 - 866.4	7 (across track) 6 (along track)	2001 to present	NASA JPL http://www-misr.jpl.nasa.gov/mission/air.html
Airborne Visible/Infrared Imaging Spectrometer (AVIRIS)	224	variable	400-2500	20	1987 to present	NASA JPL http://aviris.jpl.nasa.gov/
Compact Airborne Spectrographic Imager (CASI) (modified to CASI-2)	288	3	385-905 400-1000 (CASI 2)	0.5 -10	1989 to present	ITRES Research Limited, Canada http://www.itres.com/docs/casi2.html
Digital Airborne Imaging Spectrometer (DAIS 7915)	32 8 32 1 6	variable	400-1000 1500-1800 2000-2500 3000-5000 8000-12600	3-20 (depending on flight height)	1995 to present	German Aerospace Center. http://www.op.dlr.de/dais/dais-scr.htm
Geophysical Environmental research Imaging Spectrometer (GERIS)	63	variable	400-2500	<0.5	1994 to present	The Geophysical and Environmental Research Corporation, Millbrook, New York http://www.ger.com/ie.html

Hyper spectral Digital Imagery Collection Experiment (HYDICE)	210	10.2	400-2500	1 to 4 varies with altitude	1995 to present	Naval Research Laboratory http://rsd-www.nrl.navy.mil/7213/IR/hydice.html
HYMAP	126	Variable (10-20)	450-2500	3to10 varies with altitude	1998 to present	HyVista Corporation, 22 Delhi Rd, North Ryde NSW 2113, Australia http://www.hymap.com/main.htm
MODIS Airborne Simulator (MAS)	50	variable	550-14300	50	1992 to present	NASA ARC http://mas.arc.nasa.gov/
MODIS/ASTER Airborne Simulator (MASTER)	50	variable	400-13000	10-30 DC8* 50 ER 2 5-25 B200	2000 to present	NASA ARC & JPL http://masterweb.jpl.nasa.gov/
Multispectral Infrared and Visible imaging Spectrometer (MIVIS)	20 8 64 10	variable	431-833 1150-1550 1985-2479 8210-12700		1994 to present	Sensytech, Inc., Newington, VA. http://www.sensysotech.com/Imaging/MIVIS.html
Probe 1	128	15-17 13-16 13-17 15-20	440-900 890-1350 1400-1800 1950-2500	5-10	1997 to present	Earth Search Sciences, Inc., Kalispell, Montana. http://www.earthsearch.com/Earth_Search's_Probe_1_Sensor.htm
Reflective Optics System Imaging Spectrometer (ROSIS)	128	4	400-900	variable	1991 to present	German Aerospace Center. http://www.op.dlr.de/ne-oe/fo/rosis/home.html
Scanning imagery Spectroradiometer (SIS)	32	15	430-800	Not available	1974-1979	NASA

Table 2.3. Characteristic of some selected airborne spectrometers.

Acquisition mode	Description	Data specification		Used for	Other information
		Pixels per scene	Channels		
Spatial	Records data in all spatial dimensions	512	Maximum 18	Mineral identification, foliar biochemical study	User can provide own band specification
Spectral	Records full spectral profile	Maximum 39	288	Application related to high spectral and low spatial coverage	Missing spatial pixel problem, but using scene recovery channel (SRC) this can be solved.
Enhanced spectral	Full 3D data cube can be alternatively sliced into a single block of 101 adjacent spatial pixels imaged for all spectral channels.	131	288	Can not be used in low altitude terrain	Integration time is much longer than for Spatial Mode.
Full frame	Records in all spatial and spectral channel	512	288	This mode is normally used for laboratory calibration.	Not used for data acquisition in flight due to high integration time.

Table2.4. Different data acquisition modes for CASI (NERC, 2003)

Data	Study area	Species	Aim	Method	Result	Reference
Helicopter mounted Barnes Modular Multiband Radiometer (MMR)	Boreal coniferous forest (super National forest(SNF), near Ely, Minnesota)	Black spruce (<i>Picea mariana</i>) Jack pine (<i>Pinus banksiana</i>) trembling aspen (<i>Populus tremuloides</i>)	To study the correlation of biophysical variables (LAI, Biomass, net primary productivity) with reflectance	Used spectral mixture analysis where the pixel level reflectance of various vegetation components can be computed as a linear combination of aggregated radiometric element (sunlit chemistry, sunlit background and shadow reflectance) used two geometrical optical models : 1) cylindrical and 2) cone model of canopy geometry	Strong correlation coefficients observed between biophysical variables and radiative fraction of sunlit canopy, sunlit background and shadows.	Hall et al., 1996
AVIRIS	Gainesville, Florida	Slash pine (<i>Pinus elliottii</i>)	To determine the correlation between foliar biochemical concentration and AVIRIS spectra	Selected wavelengths of AVIRIS spectra were entered into a forced entry multi-variant liner regression (Norusis, 1992)	Strong correlation coefficient found between lignin, nitrogen , cellulose and AVIRIS first derivative spectra	Dawson et al.,1995
CASI	Sooke watershed, British Columbia, Canada	Costal Douglas-fir (<i>Pseudotsuga menziesii</i>) Western recedar (<i>Thuja plicata</i>)	To determine forest stand age	Used 3 method to estimate forest stand age a) study of continuous radiance spectrum (430- 950 nm), b) determining spectral band ratio (NDVI, R_{550}/R_{675} , R_{750}/R_{675}) and c) shift of red edge position.	Spectral band ratio was found more suitable for discrimination between stands of different age than other two methods.	Niemann, 1995
AVIRIS	Les Landes (South-west France)	Maritime pines (<i>Pinus pinaster</i>)	To estimate canopy chemistry (nitrogen, lignin and cellulose)	Determine predictive equations for nitrogen, cellulose and lignin and spectral reflectance from laboratory spectra. These relationships were applied to AVIRIS data for deriving canopy chemistry.	Relatively large correlation between nitrogen (55 per cent), cellulose (63 per cent) with reflectance and poor for lignin (30 per	Zagolski et al., 1996

AVIRIS	Land strip between sand hill road and Stanford linear accelerator	Pine (<i>Pinus radiata</i>)	To detect trace quantities of vegetation.	First used aerial photographs to determine the percent vegetation cover and then determine the red edge from AVIRIS data and study the shift in the red edge position compared to ground having no vegetation	cent) are found when the predictive equations were applied to AVIRIS data Trace quantities of vegetation were detected accurately up to a low vegetation cover of 4.8 per cent.	Elvidge et al., 1993
AVIRIS	Gainesville and Alachua county, Florida	Slash pine (<i>Pinus elliottii</i>)	To study the change in absorption feature for different foliar biochemicals while moving from leaf to canopy scale.	Two numerical ratios 'laboratory reflectance ratio' (mean of laboratory reflectance spectra of needles over fertilised plot were divided by laboratory reflectance spectra of controlled plots) and 'AVIRIS reflectance ratio' (calculated by the same process as laboratory reflectance ratio) was calculated.	Canopy effects were large in the middle infrared (1482-1789nm) and in far-infrared (2020-2260nm) where as the effect was minor in visible(400-761nm) and the effect were negligible in near-infrared (761.5-1136.3nm)	Kupiec and Curran, 1995

Table 2.5 .Use of airborne imaging spectrometer data for vegetation studies.

Name	Carrying satellite	Launch date	No. of spectral channels	Spectral coverage (nm)	Spatial resolution (m)	Swath width (km)	reference
HYPERION	Earth Observation-1	November 24, 2000	220	400-2500	30	7.5	http://eo1.gsfc.nasa.gov/Technology/Hyperion.html
CHRIS (Compact High Resolution Imaging Spectrometer)	Proba (Project for On-Board Autonomy)	October 22, 2001	19 at a time	425-1050	20	15	http://www.esa.int/export/esaMI/Proba_web_site/
MODIS (Moderate resolution Imaging Spectroradiometer)	Earth observing system (EOS), Terra	December 18, 1999	36	620-14385	250 m (bands 1-2) 500 m (bands 3-7) 1000 m (bands 8-36)	2330 (cross track) 10 (along track)	http://modis.gsfc.nasa.gov/
MERIS (Medium Resolution Imaging spectrometer)	Envisat	March 1, 2002	15 (programmable)	390-1040	300 (Full resolution) 1200 (Reduced resolution)	1150 (across track)	http://envisat.esa.int/dataproducts/meris/CNTR.htm
GLI (Global Imager)	ADEOS-II (Advanced Earth Observing Satellite -II)	To be launched	36	375-1250	250	1600	http://www.eoc.nasda.go.jp/guide/satellite/sendata/gli_e.html

ARIES (Australian Resource Information and Environmental Satellite)	NA	To be launched	32 32	400-1100 2000-25000	30	15	http://www.tec.army.mil/tio/ARIES.htm
SPECTRA	Not yet decided	To be launched	200 (selectable)	450-2350	50	50	http://www.esa.int/export/esaLP/ESACZLJUWSC_futuremissions_0.html
Venus	Not yet decided	To be launched in 2008	12	395-920	5.3	27.5	personal Communication (Karnieli, 2005)

Table 2.6. Spaceborne imaging spectrometers.

2.7.4 Space-borne imaging spectrometers

At present there are several space-borne imaging spectrometers either operational or in the developmental stage (table 2.6). The first civil imaging spectrometer to be designed for use in orbit was the Shuttle Imaging Spectrometer (SIS) (Herring, 1987) and was considered as the next step after AVIRIS. SIS was a push broom imaging spectrometer which would record 404 ground pixels. At normal flight height of 250km the field-of-view of SIS would have given it a swath of 12 km and a Ground-projected Instantaneous-Field-Of-View (GIFOV) of 30 m. Unfortunately the Challenger accident caused the SIS project to be cancelled, on the other hand, it led to the development of the High Resolution Imaging Spectrometer (HIRIS). The HIRIS was designed to fly on the space station polar platform, part of the NASA Earth Observing Station (EOS) programme (Vane, 1987). HIRIS was similar to SIS in spatial and spectral design. It had 192 wavebands in the range of 400 nm – 2500 nm, a band width of approximately 10 nm and a swath width of 24 km. This was followed by a few others in the last decade. Moreover the launch of Hyperion (<http://eo1.gsfc.nasa.gov/Technology/Hyperion.html>) on NASA Terra mission on 21st November, 2000, opened way to the development of other spaceborne imaging spectrometers (e.g., CHRIS, SPECTRA) (Curran, 2001). The Surface Process and Ecosystem Changes Through Response Analysis (SPECTRA) mission to be launched by ESA in near future, is an imaging spectrometer which will be used to further develop our understanding of the interaction of terrestrial ecosystem with the atmosphere (Tobehn et al., 2003). SPECTRA can acquire data over 200 selectable wave bands in visible and NIR wavelength with a spatial resolution of 50 m (ESA, 2005). At present there are three imaging spectrometers in space which are being used by researchers for vegetation study: MODIS (Moderate Resolution Imaging Spectroradiometer), MERIS (Medium Resolution Imaging Spectrometer) and CHRIS (Compact High Resolution Imaging Spectrometer).

2.7.4.1. The Moderate Resolution Imaging Spectroradiometer

a) Introduction

NASA's Moderate Resolution Imaging Spectroradiometer (MODIS) was onboard of the Terra mission launched in 1999. From its launch till date MODIS data were being used for various land (Townshend and Justice, 2002; Roy et al., 2002), ocean (Hoge and Lyon, 2002) and atmospheric (Heymsfield et al., 2002) applications.

b) Technical Specification

(i) Spectral resolution

MODIS records radiation in 36 discontinuous wavebands with variable band width within 400 nm – 14500 nm range of the electromagnetic spectrum (table 2.7).

(ii) Geometric Properties

- Earth coverage

MODIS is a whisk broom scanning imaging radiometer consisting of a cross-track scan mirror, collecting optics, and a set of linear arrays with spectral interference filters located in four focal planes. The collecting optical system consists of a two-mirror off-axis a focal telescope which directs energy to four refractive objective assemblies; one for each of the VIS, NIR, middle infrared and far infrared spectral regions covering a total spectral range of 400 nm to 14400 nm. It has a repeat period of 1 to 2 days.

- Spatial resolution

MODIS has 3 spatial resolutions at nadir; they are 250 m, 500 m and 1000 m. Two bands are imaged at a nominal resolution of 250 m at nadir, with five bands at 500 m and the remaining 29 bands at 1000 m. A $\pm 55^\circ$ scanning pattern at the Terra orbit of 705 km achieves a 2,330 km swath and provides global coverage every one to two days (MODIS, 2003).

Band	Bandwidth (nm)	Spectral Radiance (W/m ² μm ⁻¹ sr ⁻¹)	SNR or NEDT *	Primary Use
1	620 - 670	21.8	128	Land/Cloud/Aerosols Boundaries
2	841 - 876	24.7	201	
3	459 - 479	35.3	243	
4	545 - 565	29.0	228	Land/Cloud/Aerosols Properties
5	1230 - 1250	5.4	74	
6	1628 - 1652	7.3	275	
7	2105 - 2155	1.0	110	
8	405 - 420	44.9	880	Ocean Colour/ Phytoplankton/ Biogeochemistry
9	438 - 448	41.9	838	
10	483 - 493	32.1	802	
11	526 - 536	27.9	754	
12	546 - 556	21.0	750	
13	662 - 672	9.5	910	
14	673 - 683	8.7	1087	
15	743 - 753	10.2	586	Atmospheric Water Vapor
16	862 - 877	6.2	516	
17	890 - 920	10.0	167	
18	931 - 941	3.6	57	
19	915 - 965	15.0	250	Surface/Cloud Temperature
20	3660 - 3840	0.45(300K)	0.05	
21	3929 - 3989	2.38(335K)	2.00	
22	3929 - 3989	0.67(300K)	0.07	
23	4020 - 4080	0.79(300K)	0.07	Atmospheric Temperature
24	4433 - 4498	0.17(250K)	0.25	
25	4482 - 4549	0.59(275K)	0.25	
26	1360 - 1390	6.00	150	Cirrus Clouds Water Vapor
27	6535 - 6895	1.16(240K)	0.25	
28	7175 - 7475	2.18(250K)	0.25	Cloud Properties
29	8400 - 8700	9.58(300K)	0.05	
30	9580 - 9880	3.69(250K)	0.25	Ozone
31	10780 - 11280	9.55(300K)	0.05	
32	11770 - 12270	8.94(300K)	0.05	Surface/Cloud Temperature
33	13185 - 13485	4.52(260K)	0.25	
34	13485 - 13785	3.76(250K)	0.25	Cloud Top Altitude
35	13785 - 14085	3.11(240K)	0.25	
36	14085 - 14385	2.08(220K)	0.35	

* Radiometric performances of Band (20-36) are measured by NEDT.

Table 2.7. MODIS spectral channels (MODIS web, 2005).

Scan Rate	20.3 rpm, cross track
Swath	2330 km (cross track) by 10 km (along track at nadir)
Dimensions	
Telescope	17.78 cm diam. off-axis, afocal (collimated), with intermediate field stop
Size	1.0 x 1.6 x 1.0 m
Weight	228.7 kg
Power	162.5 W (single orbit average)
Data Rate	10.6 Mbps (peak daytime); 6.1 Mbps (orbital average)
Quantization	12 bits
Spatial	250 m (bands 1-2)
Resolution	500 m (bands 3-7) 1000 m (bands 8-36)
Design Life:	6 years

Table 2.8. Technical specification of MODIS (MODIS,2005).

(iii) Radiometric properties

The MODIS radiometric sensitivity is measured as signal to noise (SNR) and/or noise equivalent differences in temperature (NEDT). Desired SNR/NEDT for different spectral bands are given in table 2.7. Each of the MODIS bands has a unique maximum radiance. The full-scale signal of each of the MODIS bands was measured during thermal vacuum testing performed as a part of pre-flight calibration (Barnes et al., 1998). Maximum spectral radiance for each of the spectral band is given in table 2.7.

c) Calibration

The MODIS design includes four onboard calibration modules: (1) a solar diffuser; (2) solar diffuser stability monitor; (3) spectral radiometric calibration assembly and (4) blackbody (Barnes et al., 1998). The solar diffuser is located behind a deployable door on the forward or along-track wall of the MODIS. The diffuser fills the entrance aperture and is viewed each scan line. For monitoring the spectral diffuser reflectance independently a solar diffuser stability monitor is used. It is a 5 cm diameter integrating sphere with nine

spectral filter and silicon detector pairs on its inner wall and an opto-mechanical front end that enables the system to successively view the illuminated solar diffuser, a dark region and the sun. The Spectral Radiometric Calibration Assembly is used to monitor on-orbit spectral, spatial, and radiometric performance. The device includes a source assembly, a spectrometer and an output collimator. The black body is a V-groove design with 45 included angles that has been black anodized to give an effective emissivity of 0.992. The black body provides dc restoration (a known radiance level; zero for reflected solar bands and black body temperature for thermal bands) (Barnes et al., 1998).

d) Data products

Since the Terra launch in December 1999, the MODIS Science Team has made significant progress in characterizing the performance of the first MODIS instrument, providing the MODIS instrument data (Level 1B), generating and assessing the quality of higher order geophysical products (Levels 2, 3 and 4), initiating product validation and preparing for the launch of the second MODIS instrument on the EOS Aqua platform (Justice et al., 2002). MODIS land products includes: a) surface reflectance; b) land surface temperature; c) albedo and land surface BRDF products; d) MODIS vegetation indices; e) fire products; f) snow, lake ice and sea ice product and g) land cover change products. Results from the first year of MODIS LAI and fPAR data are summarized (Myneni et al., 2002).

2.7.4.2. The Medium Resolution Imaging Spectrometer

a) Introduction

After the successful demonstration of the potential of the CZCS (Coastal Zone Colour Scanner) for ocean application, ESA's ocean colour working group in 1984 conceived the idea of developing a new European imaging spectrometer for ocean applications. This

sensor was to have a fine spectral and radiometric resolution, coarse spatial resolution and high repeativity. In 1987 ESA released the technical specification of this new sensor and named it as MERIS (MEdium Resolution Imaging Spectrometer).

b) Land applications

Because of its fine spectral and moderate spatial resolution, MERIS can be used to monitor the terrestrial environment at regional to global scales (Verstraete et al., 1999).

The following land applications were expected from the MERIS data:

- a) Vegetation indices: High radiometric and spectral resolution of MERIS data would enable the researchers to develop new algorithms for vegetation indices (Verstraete and Pinty, 1996). One of such example is the MTCI (MERIS Terrestrial Chlorophyll Index), which is described in detail in the next chapter.
- b) Red edge: This could be calculated using this sensor's 5 bands in the red edge region (figure 2.6). This could be used to estimate chlorophyll content over land. Among these bands, band 8, 9 and 10 are used to estimate MTCI (a surrogate red edge index) (explained in chapter3).
- c) Fraction of Absorbed Photosynthetically Active Radiation (FAPAR): this provides information on the capacity of plants to absorb light. This could be estimated easily from MERIS data using the algorithm developed by Govaerts et al. (1999).

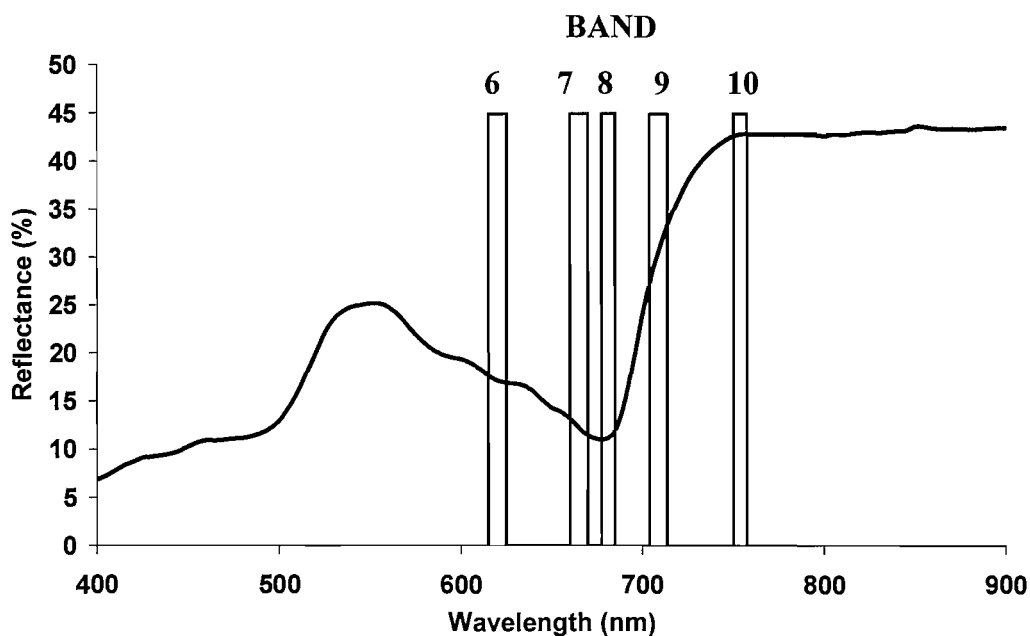


Figure 2.6. A spectral reflectance curve of vegetation with MERIS bands in the red edge region (band 8, 9 and 10 are used to estimate MTCI).

c) Technical Specification

(i) *Spectral resolution*

MERIS records radiation in 15 discontinuous wavebands with variable band width (2.5-20 nm) within 390 nm – 1040 nm range of the electromagnetic spectrum (table 2.9). Unlike other imaging spectrometers, the band centre and width of MERIS bands are programmable in-flight. This allows the users to define specific band centre and width for specific applications. A detailed description about the development of MERIS bands is given in Curran and Steele (2005).

Band no	Band center (nm)	Width (nm)	Environmental variable of interest
1	412.5	10	Yellow substance and detrital pigments
2	442.5	10	Chlorophyll absorption maximum
3	490	10	Chlorophyll and other pigments
4	510	10	Suspended sediment, red tides
5	560	10	Chlorophyll absorption minimum
6	620	10	Suspended sediment
7	665	10	Chlorophyll absorption and fluorescence reference
8	681.25	7.5	Chlorophyll fluorescence peak
9	708.75	10	Atmospheric correction
10	753.75	7.5	Oxygen absorption reference
11	760.625	3.75	Oxygen absorption R-branch
12	778.75	15	Aerosols, vegetation
13	865	20	Aerosols correction over ocean
14	890	10	Water vapour absorption reference
15	900	10	Water vapour absorption, vegetation

Table 2.9. MERIS band positions.

(ii) *Geometric Properties*

- Earth coverage

MERIS is a pushbroom sensor with five optical modules arranged symmetrically about nadir, each containing a two dimensional charged couple device (CCD) array. These optical modules are positioned in a fan shape so that the viewing aperture converges towards each other (figure 2.7). The field-of-view (FOV) of each module is 14° and FOV of the whole instrument is 68.5° , thus allowing slight overlap between each module. From the platform altitude of 799 km it has a swath of 1150 km and a complete global coverage within 3 days.

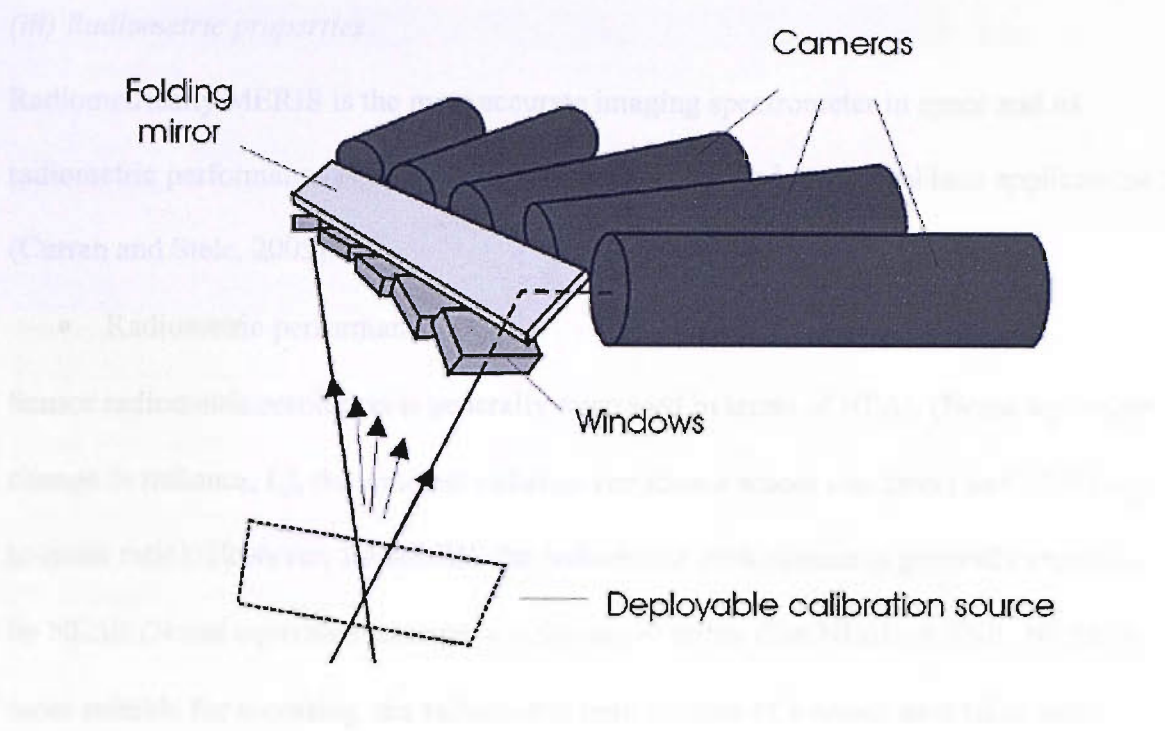


Figure 2.7. Arrangement of optical modules, folding mirror and Earth viewing windows (Adapted from ESA 2005).

- Spatial resolution

MERIS has dual spatial resolution: Full resolution (FR) (300 m at nadir) and reduced resolution (RR) (1200 m at nadir). The full resolution data are used mainly for coastal and land applications, while reduced resolution data are used mainly for large area ocean and atmospheric applications. Previously MERIS data were designed to operate in FR mode for 20 minutes per orbit because of power restrictions. However, this was reviewed later as it produces excessive coverage for areas dominated by ocean (e.g., Pacific Ocean) and inadequate coverage for areas dominated by land (e.g., Asia). Therefore acquisition of FR data are now distributed over each duty cycle rather than each orbit, to enable coverage of all land and coastal areas (Curran and Steele, 2005).

(iii) *Radiometric properties*

Radiometrically MERIS is the most accurate imaging spectrometer in space and its radiometric performance is beyond that of a sensor required for typical land applications (Curran and Steele, 2005).

- Radiometric performance

Sensor radiometric resolution is generally expressed in terms of NE Δ L (Noise equivalent change in radiance, L), the smallest radiance variation a sensor can detect and SNR (signal-to-noise ratio). However, for MERIS the radiometric performance is generally expressed by NE Δ R (Noise equivalent change in reflectance) rather than NE Δ L or SNR. NE Δ R is more suitable for accessing the radiometric performance of a sensor as it takes into account the contribution of atmosphere, solar radiation and solar zenith angle to change in signal measured by sensor. NE Δ R and NE Δ L are related by the following equation.

$$NE\Delta R = \frac{\beta}{E_s \cos \theta_s} \bullet NE\Delta L \quad (2.15)$$

Where, β is the atmospheric degradation factor, a function of illumination and viewing condition, E_s is extraterrestrial solar irradiance, θ_s is the solar zenith angle.

MERIS has NE Δ R of $2 \times 10^{-4} \text{ Wm}^2 \text{ sr}^{-1} \mu\text{m}^{-1}$.

- Dynamic range

Dynamic range is the ratio of maximum measurable signal to minimum detectable signal. A high dynamic range is required for recording the radiometric difference between dark ocean and bright clouds (Rast et al., 1999). Table 2.10 produce the dynamic range and some other radiometric properties of MERIS.

Geometric image quality	
Field of view	68.5° centred around nadir
Swath width	1150 km
Localisation accuracy	400 m (without the use of land mark)
Spatial resolution	FR- 300 m RR- 1200 m
Band to band registration	<0.1 FR pixel
Spectrometric image quality	
Spectral range	390 nm – 1040 nm
Spectral sampling interval	1.25 nm
Spectral resolution	1.8 nm
Band transmission capacity	15 bands programmable in position and width
Band width	Programmable from 1.25 nm up to 30 nm
Band centre knowledge	<0.6 nm
Radiometric image quality	
Radiometric accuracy	< 2% in reflectance
Dynamic range	Up to bright clouds (100 % reflectance)
Signal to noise ratio	1650:1 (@412.5 nm) for typical ocean signal
Polarisation sensitivity	< 0.3 % over full spectral range
Orbital signal stability	< 0.05%
Interface budgets	
Mass	200 kg
Power	175 W
Data rate	RR: 0.2 Mb s ⁻¹ FR: 3.0 Mb s ⁻¹

Table 2.10. MERIS performance summary (adapted from ESA, 2005).

d) Calibration

To meet the desired level of accuracy, the data should be corrected for any non-uniformities and distortions introduced by the measuring system (Bézy et al., 2000). Three in-flight calibrations are performed on MERIS data (ESA, 2005):

- Dark calibration: During the dark calibrations, the signal is recorded with the Earth and Sun aperture closed.
- Gain calibration: In the gain calibration, a white diffuser plate, Sun-illuminated, is inserted at the cross over point of the field-of-view of camera 5. The diffuser provides a reflectance standard across the entire spectral range and field-of-view.

- Wavelength calibration: This is achieved by using another diffuser plate (pink Spectralon™ panel) featuring well-known absorption peaks. From this calibration, the spectral position of any spectral band can be derived.

e) Data products

MERIS Primary data products include calibrated instantaneous reflectance in each band in both full and reduced resolution; where as secondary products could include vegetation amount and chlorophyll concentration. In general level-1 data contain top of atmospheric radiances, level-2 data contain atmospherically corrected top-of-canopy reflectances and geophysical products and biophysical products (e.g., LAI, MERIS global vegetation index (MGVI) (Gobron et al., 1999)) and level-3 data will contain derived products (e.g. mosaic of fPAR). Table 2.11 lists MERIS data products according to ESA (2005).

Product ID	Product Name	Application
MER_RR__0P	Reduced Resolution Level 0	Not generally available to users
MER_FR__0P	Full Resolution Level 0	
MER_CA__0P	Calibration Level 0	
MER_RV__0P	Reduced Field of View Level 0	
MER_RR__1P	Reduced Resolution Level 1	Serve as the basis for level 2 processing
MER_FR__1P	Full Resolution Level 1	Application in atmospheric modeling, land use monitoring, ocean colour monitoring, vegetation indices, and others
MER_RR__2P	Reduced Resolution Geophysical	Ocean, land or atmosphere characterization at 1040 by 1160 m pixel spatial resolution
MER_FR__2P	Full Resolution Geophysical	Climatology, meteorology, environmental monitoring, etc.
MER_LRC_2P	Extracted Cloud Thickness and Water Vapour for Meteorological Users	Intended only for meteorological applications
MER_RRC_2P	Extracted Cloud Thickness and Water Vapour	Intended for meteorological applications
MER_RRV_2P	Extracted Vegetation Indices	Intended for near real time land monitoring
MER_RR__BP	Browse Product	Support queries to a MERIS archive for land, sea, ice or cloud features, to be viewed from a remote user terminal

Table 2.11.MERIS data products (Adapted from ESA, 2005).

f) MERIS and the REP

As it was demonstrated earlier (figure 2.7) in the standard band setting, MERIS has 5 discontinuous wavebands in the red edge region with band centres at 665 nm, 681.25 nm, 708.75 nm, 753.75 nm and 760.625 nm. Two techniques have been used to estimate the REP on discontinuous (simulated) MERIS spectra: Lagrangian interpolation (Dawson 2000) and linear interpolation (Clevers et al. 2002) (see previous section (2.5) for detailed description). However these methods are subject to confirm with real MERIS data.

- Linear interpolation method for MERIS data

The linear interpolation technique can be modified for MERIS using wavebands 7 and 12 with centres at 665 nm and 778.75 nm. Equations 2.6 and 2.7 become

$$R_i(MERIS) = \frac{(R_{Band7} + R_{Band12})}{2} = \frac{(R_{665} + R_{778.75})}{2} \quad (2.16)$$

Where $R_i(MERIS)$ is reflectance at the inflection point for MERIS data.

$$\begin{aligned} REP(MERIS) &= 708.75 + 45 \frac{(R_i(MERIS) - R_{Band9})}{(R_{Band10} - R_{Band9})} \\ &= 708.75 + 45 \frac{(R_i(MERIS) - R_{708.75})}{(R_{753.75} - R_{708.75})} \end{aligned} \quad (2.17)$$

The linear interpolation technique is computationally simple and (Clevers et al., 2002) reported it to be a robust method for estimating REP. However, a correction needs to be made to allow for the occurrence of an oxygen absorption band near 753.75 nm (one of the wavebands used in interpolation).

- Lagrangian Interpolation for MERIS

Dawson (2000) showed that Lagrangian interpolation technique could be used to detect a shift in the REP for simulated MERIS data in standard band positions. However, Clevers et

al. (2002) reported a ‘jumping’ feature in a nonlinear REP/chlorophyll content relationship derived using Lagrangian interpolation. This was thought to be due to the ‘not unusual’ occurrence of more than one peak in the first derivative spectrum. As a result Lagrangian interpolation, if used operationally, would require manual confirmation of contented first derivative reflectance maximum, thus making it a semi-automatic two step procedure.

2.8. Uncertainties in Red edge chlorophyll relationship

Despite the theoretical relationship between the REP and chlorophyll content of a vegetation canopy, several researchers have pointed out the variability of this relationship (Horler et al., 1980). This variability may be caused by variability in: Leaf area index (LAI) (Danson and Plummer, 1995), fluorescence (Buschmann and Lichtenthaler, 1998; Zarco-Tejada et al., 2000), chlorophyll a/b ratio (Curran et al., 1990), absorption due to different pigment (Curran et al., 1991), viewing geometry (Treitz and Howarth, 1999), soil and understorey (Blackburn and Milton, 1995) and senescence (Raillyan and Korobov, 1993). Following paragraphs describe the influence of these variables on the red edge:chlorophyll relationship.

2.8.1 Leaf area index

Leaf area index (LAI) is defined as the total leaf area per unit ground surface (Herwitz et al., 1989). LAI is a very important variable in terrestrial ecosystems (Chen et al., 1997), because light interception, gas exchange, photosynthesis and biomass production are closely related with LAI (Peterson et al., 1988; Herwitz et al., 1989; Nemani et al., 1993). Many studies reported the correlation between red and NIR reflectance with LAI (Franklin, 1986; Peterson et al., 1988; Gong et al., 1995). There is a negative relationship between red radiance and LAI and a weak positive relationship between NIR radiance and LAI (Danson and Curran, 1993). Danson and Plummer (1995) found that in addition to chlorophyll

content, REP was influenced by LAI. This is because, chlorophyll content varies with the amount of chlorophyll in the vegetation and the amount of vegetation. Therefore, if chlorophyll concentration is constant then an increase in LAI will alter the REP. They reported a near linear relationship between REP and LAI. Fillela and Peñuelas (1994) correlated different red edge variable (amplitude of red edge peak in the first derivative reflectance curve at 703 nm, sum of the first derivative reflectance amplitude between 680 and 780 nm, maximum amplitude of red edge peak in the first derivative curve and the wavelength of red edge peak) with LAI and chlorophyll. They found the area of the red edge peak was very well correlated with LAI. Pu et al. (2003) correlated LAI with REP estimated with different techniques (4- point interpolation, polynomial fitting, Lagrangian interpolation and IG modelling). They reported a low correlation between these two if the REP is estimated by Lagrangian interpolation compared with REP estimated by other methods.

2.8.2 Fluorescence

During the process of photosynthesis some electrons in the chlorophyll molecule jump to a more excited state by absorbing radiation. The electrons then drop to a lower level by decaying energy. If this energy is not used in photosynthesis or transmitted to other molecules then they decay to a ground state by emission of fluorescence of lower energy (Lawler, 1993). This fluorescence has a maximum reflection at 690 nm (Lichtenthaler et al., 1987). Zarco-Tejada et al. (2000) demonstrated chlorophyll fluorescence and effects on leaf level reflectance and transmittance. These effects could be quantified using radiative transfer theory and the Fluorescence-Reflectance-Transmittance (FRT) leave radiative transfer model. Subsequent studies demonstrated quantitatively that chlorophyll fluorescence could be detected with the Compact Airborne Spectrographic Imager (CASI)

(Zarco-Tejada et al., 2001). Zarco-Tejada et al. (2003) detected a double-peak feature at 690-710 nm spectral regions seen in the derivative reflectance. They concluded that this feature was due to the combined effects of fluorescence and low chlorophyll (a+b) contents on stressed vegetation. They proposed a double peak optical index (DPi):

$$DPi = \frac{D_{688} * D_{710}}{D_{697}^2} \quad (2.18)$$

Where D_{688} , D_{697} , D_{710} are derivative reflectance at 688 nm, 697 nm and 710 nm respectively. A strong correlation was observed between the double peak optical index (DPi) and fluorescence measured by a fluorometer (Zarco-Tejada et al., 2003).

The fluorescence yield at a wavelength of 690 nm is only a few percent of the absorbed energy and this is partially reabsorbed by chlorophyll before it reaches the leaf surface. However, as chlorophyll content decreases this reabsorption decreases, resulting in a slight 'blue shift', i.e. movement of the red edge to shorter wavelength (Bushman and Lichtenthaler, 1998).

2.8.3 Chlorophyll a/b ratio

The ratio of chlorophyll-a to chlorophyll-b is approximately 3:1 (Sharp, 1983). However, this relation changes with illumination, e.g. in bright illumination the ratio may be 2:1 (Anderson, 1986). Chlorophyll a should have a greater influence on REP than chlorophyll b because its absorption maxima is approximately 20 nm more than chlorophyll b (Curran et al., 1990). Most studies have evaluated the REP shift against total chlorophyll because the influence of the chlorophyll a/b is difficult to observe (Horler et al., 1983). However, the size and direction of REP shift is not always consistent with a reduction of total chlorophyll (Banninger, 1991).

2.8.4 Viewing geometry

Solar radiation incident on the top-of-canopy is composed of two components, direct and diffuse. The direct component is one which has not been scattered or absorbed by the atmosphere, whilst the diffuse component is radiation which has been scattered in a downward direction. The direction of direct flux is characterised by the solar zenith and the azimuth angles. As the solar zenith angle increases from horizontal, there is an increase penetration of the solar radiation into the canopy, thus reducing the canopy reflectance (Treitz and Howarth, 1999). For vegetation canopies which are not 'closed', the sensor and the view zenith angle will determine the amount of soil background that is visible to the sensor. As the angular elevation of view increases towards the vertical more of the soil background and less on the vegetation are seen (Suits, 1972). Variation in Sun-sensor geometry affects the signals viewed by sensors. As the sensor direction moves away from anti solar direction two effects cause the reflectance to decrease: (i) the relative proportion of shadow surface increases in the sensors field of view and (ii) the proportion of the leaf surfaces in the anti-solar direction increases, producing decrease in solar irradiance on the surface. When either or both solar or viewing directions assume large zenith angles, the tree crowns are more likely to be illuminated and visible than the lower layers and thus the scene appears to be brighter. These effects jointly affect the vegetation reflectance spectra and they are not the actual representation of the reflectance due to interaction with biomass. As a result they introduce some ambiguity in the estimation of the red edge position as the overall signal is a mixture of the vegetation reflectance and background information.

2.8.5 Soil and understorey

The bidirectional reflectance of a vegetation canopy can be affected significantly by soil background (Curran, 1982). Different soils and soil moisture contents produce different

canopy reflectances. If the reflectance of soil is similar to the reflectance of vegetation in a particular wavelength then the relation between reflectance and pigment concentration at that wavelength will be weak. On a light coloured soil with strong near infrared reflectance, the relationship between near infrared reflectance and vegetation amount is less than on a dark soil with a low infrared reflectance (Curran, 1982). As soil reflectance is roughly a linear function, it should not affect the slope of the reflectance spectrum. Therefore, this effect can be removed for REP calculated using the derivative spectrum (Demetriades-Shah et al., 1990). However, background reflectance varies non-linearly with wavelength, it will introduce a source of variability to the REP. Abrupt changes in REP have been recorded where the background is organic and for low canopy covers of *Pinus elliotti* (slash pine) (Curran et al., 1990). The contribution of the background has also been demonstrated for deciduous canopies where changes in the red edge wavelength region were associated with a transfer of dominant scene elements from bark and litter to a photosynthetically active canopy, through out the growing season (Blackburn and Milton, 1995).

Forest floors are also associated with different understorey vegetation and these produce a different spectral reflectance as compared to the main vegetation canopy. An essential input for any canopy model is a good estimate of the average understorey reflectance. Llewellyn and Curran (2001) studied the effect of mixing an overstorey canopy and understorey canopy (based on a combined leaf and canopy model) on the REP and other vegetational indices. REP was observed to be more sensitive to understorey effects when its overstorey had a low optical thickness and REP was more sensitive to chlorophyll content than LAI. Curran et al. (1990) found that REP recorded over a canopy of live pine needles was influenced by the lower REP contribution of vegetated understorey and litter layer of dead pine needles.

2.8.6 Senescence

As vegetation senesces the infrared reflectance does not decrease significantly; however the breakdown of leaf pigments, for example, chlorophyll cause a rise in blue and red reflectance. Railyan and Korobor (1993) examined changes in the red edge position of *Triticale* over growing season and found that the REP varied with developmental stage. At earlier growth stage, the red edge moved from shorter to longer wavelengths (a shift of about 5nm was observed); while later they found a shift back to shorter wavelengths. Miller et al. (1991) studied the seasonal patterns in red edge position for both deciduous and coniferous trees. They detected four phases of REP for deciduous trees: (i) an early rapid increase (Julian day 140-155); (ii) a sustained period where the REP moved to longer wavelengths (Julian day 156- 222); (iii) a variable period where the REP moved to shorter wavelengths (Julian day 223-250) and (iv) a period of accelerating decline (Julian day 251-290). However, for coniferous species the seasonal pattern for the REP is a gradual shift towards longer wavelengths (Miller et al., 1991).

2.8.7 Absorption due to other leaf components

Leaves contain several pigments, besides chlorophyll, that absorb radiation in the region of red edge; these could alter the REP independently of chlorophyll concentration (Curran et al., 1990). One such non-chlorophyll pigment is amaranthin, which is found in the leaves of *Amaranthus*. This absorbs radiation in the region of red edge and affects the red edge-chlorophyll relationship (Curran et al., 1991). A strong correlation reported between chlorophyll concentration and REP when the concentration of amaranthin is low. However, for high chlorophyll concentration there was no relationship between red edge and

chlorophyll concentration and increase in amaranthin concentration moves the red edge to longer wavelengths (Curran et al., 1991).

2.9. Application of the red edge

A strong red edge-chlorophyll relationship has been noted for a variety of vegetation types, sugar maple (Vogelmann et al., 1993), slash pine (Curran et al., 1995), conifer stand (Dawson et al., 1998), grass (Pinar and Curran, 1996) and winter wheat (Munden et al., 1994). An increase or decrease in the amount of chlorophyll will affect the resulting vegetation canopy spectra. As a result there will be a shift of the REP to longer or shorter wavelengths. This implies that REP can be used to estimate the amount of chlorophyll at the canopy level (Horler et al., 1983; Filella and Peñuelas, 1994; O'Neill et al., 2002). Using the estimated chlorophyll amount, information about physiological and biochemical condition of the vegetation can be derived. The following paragraphs describe the application of REP to different environmental conditions, plant biophysical status and, most interestingly, a possible bio-signature for extraterrestrial plants.

2.9.1 Vegetation productivity

According to Reeves et al. (2005) estimation of vegetation productivity using remotely sensed data has generally two approaches: (i) use of the spectral reflectance to estimate the amount of absorbed photosynthetically active radiation (APAR) (Choudhury, 1987) and (ii) establishing an empirical relationship between spectral reflectance and productivity (Wylie, 1995). The first approach is likely to be more successful in predicting biomass across variable climatic regimes, while the second approach is useful in estimating live biomass. As chlorophyll is one of the ingredients for photosynthesis so the estimation of

chlorophyll can in turn give information on the productivity. In a well managed cereal crop the concentration of chlorophyll is related directly to yield (Reeves et al., 1993), so the remote sensing of chlorophyll concentration offers the possibility of estimating cereal yield. A remotely sensed measure of reflectance at the absorption wavelength of chlorophyll has limited suitability for estimating yield as it couples with the effects of chlorophyll content, leaf mass and other effects like variable radiances, ground reflectance and the Sun-sensor geometry (Curran, 1982). However the REP is sensitive to these factors in the vegetation reflectance spectrum. Therefore it can be used to estimate the crop yield through the chlorophyll content.

2.9.2 Stress

Vegetation stress may be defined as any factor that reduces the productivity below the optimum value (Steven et al., 1990). Stress may result from a change in the physiochemical condition of the environment, pests or pathogens. Detection of vegetation stress from remotely sensed data is based on studying the change of reflection spectra over a vegetation canopy change in time (Adams et al., 1999). The effect of vegetation stress on reflectance spectra has been studied in relation to heavy metals (Horler et al., 1980), arsenic and selenium (Milton et al., 1989), stress agents of biological origin (*Phylloxera* infestation (Johnson, 1999), powdery mildew disease, senescence (Carter, 1993)), water deficiency (Yang and Su, 2000). Horler et al. (1980) detected a shift in the long wavelength edge of chlorophyll absorption to shorter wavelengths as a result of stress. Similar effects have been observed as a result of disease (Johnson, 1999) and water deficiency (Yang and Su, 2000). Milton et al. (1989) found the same as Horler et al., (1980) for plants stressed with arsenic whereas they found an opposite in the shift of chlorophyll absorption feature i.e., toward the higher wavelength side for plants stressed by

selenium. Vegetation stress results in chlorosis (yellowing of leaves) (Adams et al., 1999) due to the destruction of chlorophyll (Horler et al., 1980). Carter (1993) in an experiment with various stressed and species of plant noted an increase in visible reflectance particularly in wavebands centred near 510 nm and 710 nm in response to stress, regardless of stress agents and vegetation type. The relationship between stress factors, chlorophyll content, wilting and location of REP is described in figure 2.8.

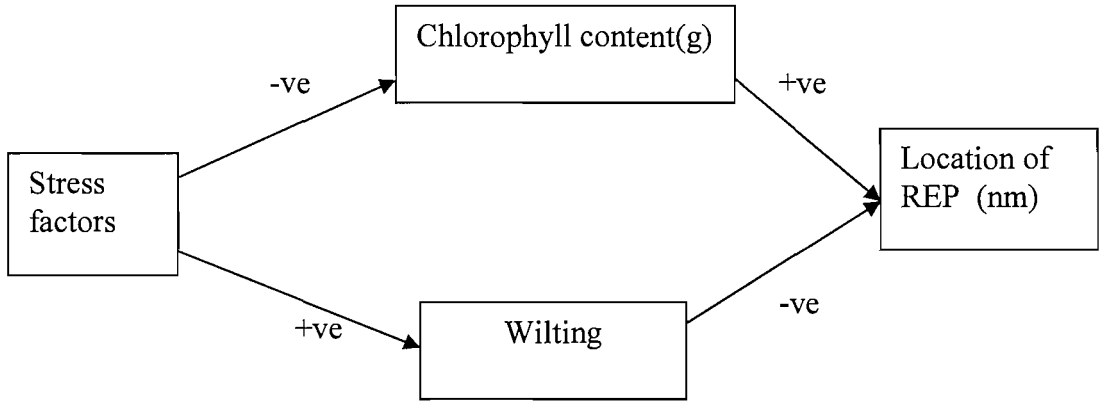


Figure 2.8. Relationship between stress factors, chlorophyll content, wilting and location of red edge.

The shift in red edge position and resulting change in the shape of the reflectance curve can be quantified using indices and algorithms e.g., red-edge vegetation stress index (RVSI) (Merton, 1998), tricoder algorithm (Clark et al., 1993) and yellowness index (Adams et al., 1999). The well established REP methods as described in section 2.5. can also be used to identify stress in plant. For identifying a single red edge bases descriptor for vegetation stress analysis Merton (1998) computed Red-edge Vegetation Stress Index (RVSI). Where RSVI is defined as

$$RSVI = \left(\frac{R_{714} + R_{752}}{2} \right) - R_{733} \quad (2.18)$$

Where R_{714} , R_{752} , R_{733} are vegetation canopy reflectance measured at 714 nm, 752 nm and 733 nm respectively. Positive values of RVSI indicate an increase in the degree of relative

vegetation stress, negative values indicate a decrease in the degree of relative vegetation and stress values, zero values indicate a transition between stressed and unstressed.

Merton (1998) observed a 'break point' occurring at 716 nm along the red edge. Below this point red edge curves have a concave shape and beyond this point curves may a) show increase in reflectance resulting in an asymptotic curve or b) continued as near linear or c) show a decrease in reflectance followed by an increase resulting in a cuspid curve. RVSI was used to measure the spectral concavity in the red edge curve as a displacement in reflectance values between the data mid point and mean reflectance between modelled red edge break point and start of the NIR plateau (Merton, 1998).

Adams et al. (1999) developed the Yellowness Index (YI) to estimate chlorosis in the leaves in stressed plants. In their experiment with Soya been plants treated with Mn they found a noticeable change in reflectance between 550 nm and 650 nm and used the second derivative of reflectance spectra to define YI:

$$YI \propto \frac{R_{\lambda_{-1}} - 2R_{\lambda_0} + R_{\lambda_{+1}}}{\Delta\lambda^2} \cong \frac{d^2 R}{d\lambda^2} \quad (2.19)$$

Where R_{λ_0} is the central wavelength of the red edge region, $R_{\lambda_{-1}}$ is the lower wavelength, $R_{\lambda_{+1}}$ is the higher wavelength and $\Delta\lambda$ is the difference between maximum and minimum wavelength in the reflectance spectra between 550 nm and 650 nm. Higher YI values will result from a more stressed plant (Adams et al., 1999).

There is a change in REP due to vegetation stress, but estimating stress requires fine spectral resolution in red and the NIR wavelengths (Horler et al., 1980; Clark et al., 1993). However, although stress has been estimated using AVIRIS data (Clark et al., 1993, Li et al., 2005), Johnson (1999) found it difficult to distinguish pre-visual stress in vegetation using the REP.

Several studies have reported the use of red edge to identify vegetation stress due to natural fuel leakage (Smith et al., 2004; Li et al., 2005). Smith et al., (2004) reported an increase in visible reflectance and decrease in NIR reflectance as a result of exposure to natural gas. Pre-visual stress was detected using the ratio of derivative reflectance in the red edge region: 725 nm and 705 nm. This ratio was low for vegetation affected by natural gas. Li et al., (2005) reported a 20 nm shift in the REP in a year for the vegetation exposed to oil spill at the Jornada experimental range in New Mexico using AVIRIS data.

2.9.3 Land contamination

Contamination of land by heavy metals and non organic anthropogenic waste can lead to decrease in chlorophyll concentration of the overlying vegetation. Therefore, remotely sensing the degree of land contamination will rely on an understanding of the link between land contamination, chlorophyll concentration of the overlying vegetation and the REP (Jago et al., 1999, Clevers et al., 2004). A qualitative relationship has been reported between the REP and the level of land contamination (Llewellyn et al., 2000; 2001). In their study of the effect of hydrocarbon contamination of soil on the grassland, Llewellyn et al. (2001), found that grassland on highly contaminated soil had a shorter wavelength REP than on uncontaminated grassland. They also observed that grassland with low levels of soil contamination tended to be more homogenous in terms of species canopy and background component, while the grassland with high levels of contamination tended to have two short wavelength REP peaks and a frequent alteration between the two REP peaks. Clevers et al. (2004) found a significant negative correlation between the REP estimated using the maximum of first derivative method and heavy metal concentration in the soil of the flood plain of the River Wall in the Netherlands.

2.9.4 Leaf nitrogen concentration

Nitrogen provides a crucial input to the production of protein and chlorophyll, which are essential for plant development and yield. However the ability to estimate leaf nitrogen concentration depends on the influence of individual or the functional groups of foliar constituents on the overall reflectance spectra (Lucas et al., 2000). Several empirical studies have derived spectrally based estimates of nitrogen concentration in fresh leaves (Curran et al., 1992; Yoder and Pettigrew-Crosby, 1995). Johnson (2001) reported a decrease in NIR reflectance by 1.8 % and transmittance up to 3.7 %, with a change in slope of $\pm 0.02 \text{ \% nm}^{-1}$ due to change in nitrogen of 0.5% in fresh leaves. REP have been used to estimate the leaf nitrogen concentration in ryegrass (Lamb et al., 2002) and in a coniferous forest plantation (Lucas et al., 2000). Lamb et al. (2002) found a double peak ($\sim 705 \text{ nm}$ and $\sim 725 \text{ nm}$) in the derivative spectrum, which shifted to longer wavelength with increasing LAI. This red edge was observed to account for 60 % of the variance in the leaf nitrogen concentration. However Lucas et al. (2000) observed no significant relationship between the REP and leaf nitrogen concentration, which they explained, might be attributed due to limited chlorophyll/nitrogen range of the sample. On the other hand, a strong correlation between LAI and REP and LAI and leaf nitrogen concentration was observed. Based on that they developed a predictive relationship to estimate leaf nitrogen indirectly from an estimate of LAI derived from the REP.

2.9.5 Possible spectroscopic bio-signature for extraterrestrial planets

Spectroscopic bio-signatures are indicative of a planetary environment that is considered to be either hospitable to life or has a strong probability of life.

Research in the detection of possible bio-signature in extraterrestrial planets is quite recent, but interest in the spectroscopic signature of planetary vegetation has a long history (Seager et al., 2005). As Earth is the only planet known to have life, all techniques fused in

the search of life on extrasolar planets were tested on it. One of the emerging and possible techniques is the study of Earthshine (Seagan et al., 1993). Earthshine is sunlight that has been scattered by Earth towards the Moon and then back to Earth. This can be recorded by a CCD camera. The rough lunar surface makes the Moon a diffuse reflector with each point on the Moon reflecting spatially integrated illumination from the Earth. The viewing portion on the Earth is the sunlight illuminated portion of Earth as seen from the Moon. Recent spectral observation of Earthshine has detected a weak vegetation red edge around 700 nm (Woelf et al., 2002). Arnold et al., (2002) also reported a weak vegetation red edge signal from the Earthshine observation on several different dates. In their experiment, Earthshine from the evening crescent moon was measured from America and the Atlantic ocean, where as Earthshine on the morning crescent moon was measured from Europe and Asia. They estimated the vegetation red edge (VRE) as

$$\text{VRE} = \frac{r_I - r_R}{r_R} \quad (2.20)$$

Where r_I and r_R are the mean reflectances in the [600; 670 nm] and [740; 800 nm] windows in the Earthshine spectrum.

Some minerals, for example, Sulphur may produce a false red edge (Seager et al. 2005) which may misled the interpretation of the spectroscopic signature. However, temporal variability of this spectroscopic signature may be able to separate the vegetation signatures.

Chapter 3. MERIS Terrestrial Chlorophyll Index: Design and initial evaluation

3.1. Introduction

Remotely sensed data recorded in narrow visible/near visible wavebands can be used to estimate foliar biochemical content at local to regional scales (Curran 1989, Curran et al. 1997). This information can, in turn, be used to quantify, understand and manage vegetated environments (Curran 2001, Johnson 1999, Lamb et al. 2002). Chlorophyll is one of the more important foliar biochemicals and the content within a vegetation canopy is related positively to both the productivity of that vegetation and the depth and width of the chlorophyll absorption feature in the reflectance spectra. The long wavelength (red) edge of this absorption feature moves to even longer wavelengths with an increase in chlorophyll content (Curran et al. 1990, Filella and Peñuelas 1994, Munden et al. 1994) and the red edge position (REP) can be defined as the point of maximum change in reflectance along this edge (Horler et al. 1983). However, there are two problems with the use of REP to estimate foliar chlorophyll content from a spaceborne sensor. First, the methods used to estimate REP have been designed for use on continuous spectra without thought for standardisation or automation (Dawson and Curran 1998). Second, REP is not an accurate indicator of chlorophyll content at high chlorophyll contents because of the asymptotic relationship between REP and chlorophyll content (Jago et al. 1999, Munden et al. 1994).

The MEdium Resolution Imaging Spectrometer (MERIS), one of the payloads on Envisat, is radiometrically the most accurate imaging spectrometer in space (Curran and Steele 2003). It has 15 programmable (2.5 nm-20 nm wide) wavebands in the region of 390 nm - 1040 nm and a spatial resolution of 300 m. Because of its fine spectral and

moderate spatial resolution and three day repeat cycle, MERIS is a potentially valuable sensor for the measurement and monitoring of terrestrial environments at regional to global scales (Verstraete et al. 1999). In the standard band setting, it has 5 discontinuous wavebands in red and near infrared (NIR) wavelengths with band centres at 665 nm, 681.25 nm, 708.75 nm, 753.75 nm and 760.625 nm. Two techniques have been used to estimate the REP on discontinuous MERIS spectra: Lagrangian interpolation (Dawson 2000) and linear interpolation (Clevers et al. 2002).

Lagrangian interpolation:

Dawson and Curran (1998) proposed a technique based on three point Lagrangian interpolation (Jeffrey 1985) for the estimation of REP. This uses a second order polynomial fit to the first derivative vegetation reflectance spectrum and reflectance in three wavebands: the band with maximum first derivative reflectance and two adjoining bands. Detail description about this technique is given in section 2.5.4.

Linear interpolation:

Guyot et al. (1988) proposed a linear interpolation technique for estimating the REP. They assumed that reflectance at the red edge could be estimated by half of the reflectance between 670 nm and 780 nm. Reflectances at 670 nm and 780 nm were then used to calculate the reflectance of the inflection point and a linear interpolation technique was used to calculate the wavelength of this inflection point. Detail description about this technique is given in section 2.5.3.

Undoubtedly, other REP techniques will be applied to MERIS data for the estimation of chlorophyll content. However, (i) there remains no generally accepted technique for estimation of REP and (ii) each technique produces a different value of REP from the same set of data. In this thesis a new index for estimating chlorophyll content from MERIS data has been proposed as a surrogate for REP.

3.2. Designing a chlorophyll index

Two criteria for the design of a chlorophyll index using MERIS data are: first, it should be easy to calculate from MERIS data recorded at the standard band setting and second, it should be sensitive to a wide range of chlorophyll contents. Illustrative vegetation reflectance spectra from model output are given in Figure 3.1a, with chlorophyll content increasing from spectrum 1 to spectrum 4. An increase in absorption due to an increase in chlorophyll content is seen in the wavelength range 650 - 700 nm. Reflectance increases sharply as we move from MERIS band 8 to band 10 for a particular chlorophyll content (Figure 3.1a). However, comparison of the four reflectance spectra reveals two important features: (i) with an increase in chlorophyll content the difference in reflectance between band 8 and band 9 decreases gradually and (ii) with an increase in chlorophyll content the difference in reflectance between band 9 and band 10 increases gradually.

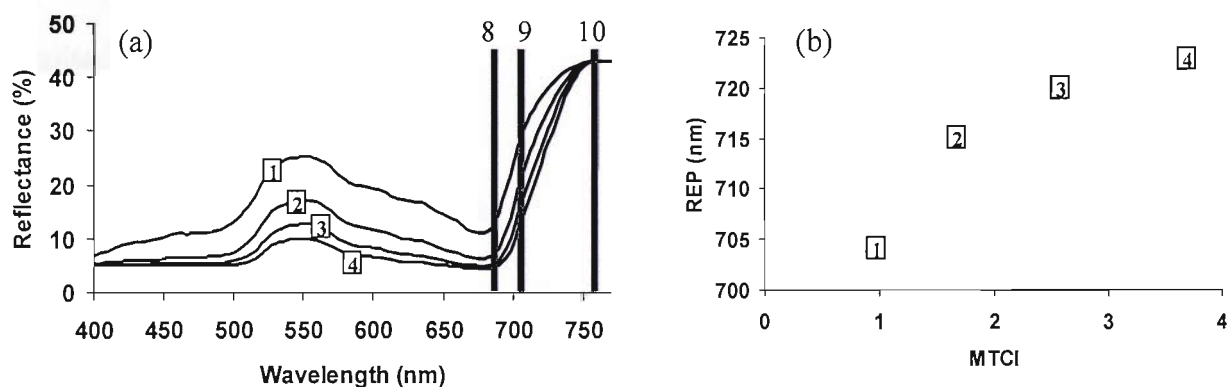


Figure 3.1. (a) Vegetation reflectance spectra at four chlorophyll contents overlain with the position of MERIS bands 8, 9 and 10. (b) Relation between the MERIS terrestrial chlorophyll index (MTCI) and red edge position (REP) for four chlorophyll contents.

A new index, the MERIS Terrestrial Chlorophyll Index (MTCI) is a ratio of the difference in reflectance between band 10 and band 9 and the difference in reflectance between band 9 and band 8 of the MERIS standard band setting.

$$\begin{aligned}
MTCI &= \frac{R_{Band10} - R_{Band9}}{R_{Band9} - R_{Band8}} \\
&= \frac{R_{753.75} - R_{708.75}}{R_{708.75} - R_{681.25}}
\end{aligned} \tag{3.1}$$

Where $R_{753.75}$, $R_{708.75}$, $R_{681.25}$ are reflectance in the centre wavelengths of the MERIS standard band setting.

Figure 3.1b illustrates the relation between MTCI and REP for the four spectra in Figure 3.1a. The REP calculated using linear interpolation is illustrated here because of its simplicity, however, REP calculated using Lagrangian interpolation provided similar, albeit linearly offset, results. It can be seen that there is little change in REP but large change in MTCI between high chlorophyll contents. This implies that MTCI is more sensitive to change in chlorophyll content at high chlorophyll contents than is REP.

Data from vegetation reflectance models (based on radiative transfer theory) and laboratory and field measurements of leaves and canopies respectively were used to evaluate the MTCI quantitatively. Real MERIS data were used to evaluate the MTCI qualitatively.

3.3. MTCI evaluation methods

3.3.1 Model data

LIBSAIL, a combination of LIBERTY (Leaf Incorporating Biochemistry Exhibiting Reflectance and Transmittance Yield (Dawson et al. 1998)) and SAIL (Scattering by Arbitrary Inclined Leaves (Verhoef 1984)) was used to generate canopy reflectance spectra (400-2500 nm, spectral resolution of 5nm) for a wide range of chlorophyll contents. The variables input to the combined model are given in table 3.1.

3.3.2 Field data

Canopy reflectance spectra and canopy chlorophyll content data had been collected for monospecific canopies formed from Douglas-fir (*Pseudotsuga menziesii*) and bigleaf maple (*Acer macrophyllum*) seedlings as a part of NASA’s 1992-1993 ACCP (Accelerated Canopy Chemistry Program) (Yoder and Johnson 1999).

Model and field reflectance data were averaged according to the band centre and band width of the MERIS standard bands to obtain the reflectance data used to calculatate REP (Equation 3.5) and MTCI (Equation 3.6).

LIBSAIL variables	Values
Chlorophyll content (mg m-2)	10,20,50,100,150,200,250,300,350,400
Average internal cell diameter (µm)	30
Inter cellular airspace determinant (unit less)	0.005
Leaf thickness (unit less)	3
Base line absorption (unit less)	0.0004
Albino leaf absorption (unit less)	2
Leaf water content (gm m-2)	100
Lignin or cellulose content (gm m-2)	30
Nitrogen content (gm m-2)	1
Solar zenith angle (°)	0.0
Mean leaf inclination (°)	30
Leaf Area Index	1

Table 3.1. Input variables for LIBSAIL model.

3.3.3 MERIS data

A subset of a MERIS image acquired on 19th October 2002 was extracted for the New Forest, Hampshire, UK. The area comprises coniferous and deciduous woodland along with heath, meadows, agricultural land, urban areas and water. The data were atmospherically corrected and converted to top-of-canopy reflectance using the Simplified Methods for Atmospheric Correction (SMAC) (Rahman and Dedieu 1994).

3.4. MTCI evaluataion results

3.4.1 Model data

Vegetation reflectance obtained from LIBSAIL spectra for simulated MERIS band positions over a wide range of chlorophyll contents (10 mg m^{-2} to 300 mg m^{-2}) are shown in Figure 3.2a. An increase in chlorophyll content was associated with increased absorption in red wavelengths but the amount of absorption was less at high chlorophyll contents than low chlorophyll contents. Estimated MTCI and REP for each spectrum are given in Figures 3.2b and 3.2c respectively.

The asymptotic relationship between REP and chlorophyll content (Figure 3.2c) suggested insensitivity to high chlorophyll contents; however, the near-linear relationship between MTCI and chlorophyll content (Figure 3.2b), suggested sensitivity to high chlorophyll contents.

3.4.2 Field data

For Douglas-fir (Figure 3.3a), the coefficients of determination (r^2) were 0.64 and 0.62 between chlorophyll content and first MTCI and second REP. Similarly, for maple (Figure 3.3b) the coefficients of determination (r^2) were 0.72 and 0.62 between chlorophyll content and first MTCI and second REP. In both the cases, the regression line between MTCI and chlorophyll content had a slightly steeper slope than the regression line between REP and chlorophyll content. This suggested that MTCI was more sensitive than REP to chlorophyll content.

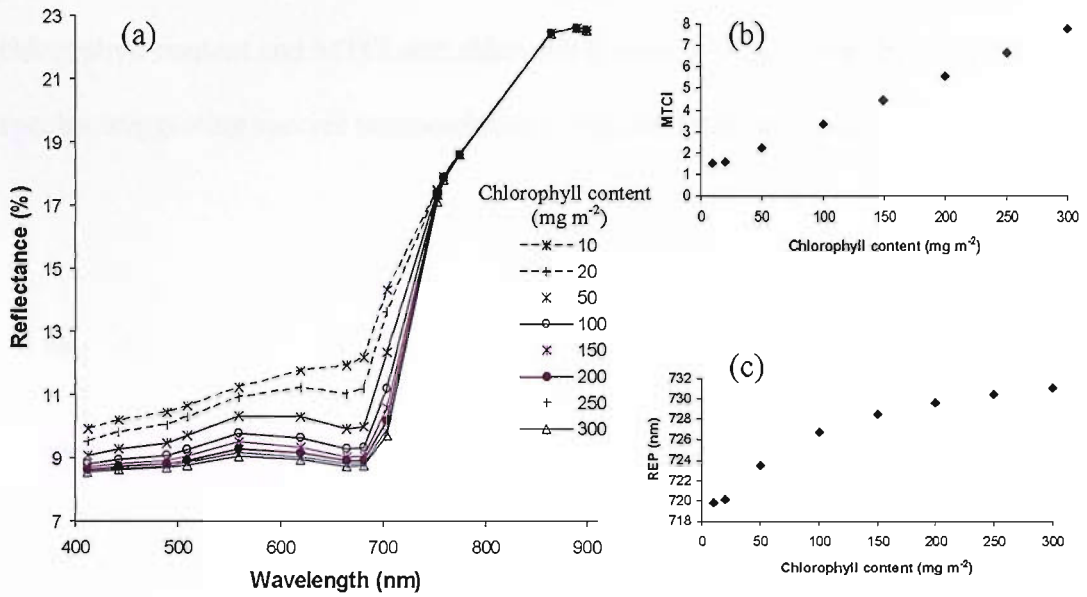


Figure3. 2. (a) Reflectance spectra for MERIS data at the standard band positions, simulated using the LIBSAIL model for a wide range of chlorophyll contents; (b) relation between chlorophyll content and MTCI for the same range of chlorophyll contents and (c) relation between REP and chlorophyll content for the same range of chlorophyll contents.

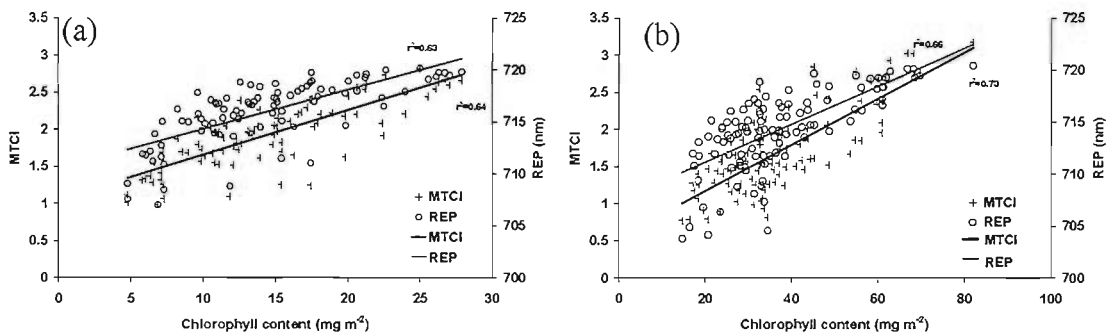


Figure 3.3 Sensitivity of REP and MTCI calculated from field reflectance spectra to variation in chlorophyll content for (a) Douglas-fir and (b) maple.

The relationship between REP and MTCI was determined using both continuous (2 nm spacing between bands) reflectance spectra and reflectance at the MERIS standard band settings (Figure 3.4). REP and MTCI were correlated strongly (r^2 greater than 0.99 and 0.98 for Douglas-fir and maple respectively) for values derived using both continuous reflectance spectra and reflectance at the MERIS standard band settings. However, reflectance at the MERIS standard band settings resulted in higher values of REP (Dawson 2000) because of the large spectral interval between the MERIS bands 9 and 10 (centres

located at 705 nm and 753.75 nm). Interestingly, the relationship between REP and chlorophyll content and MTCI and chlorophyll content was almost the same for the two species, suggesting species independence of the two relationships.

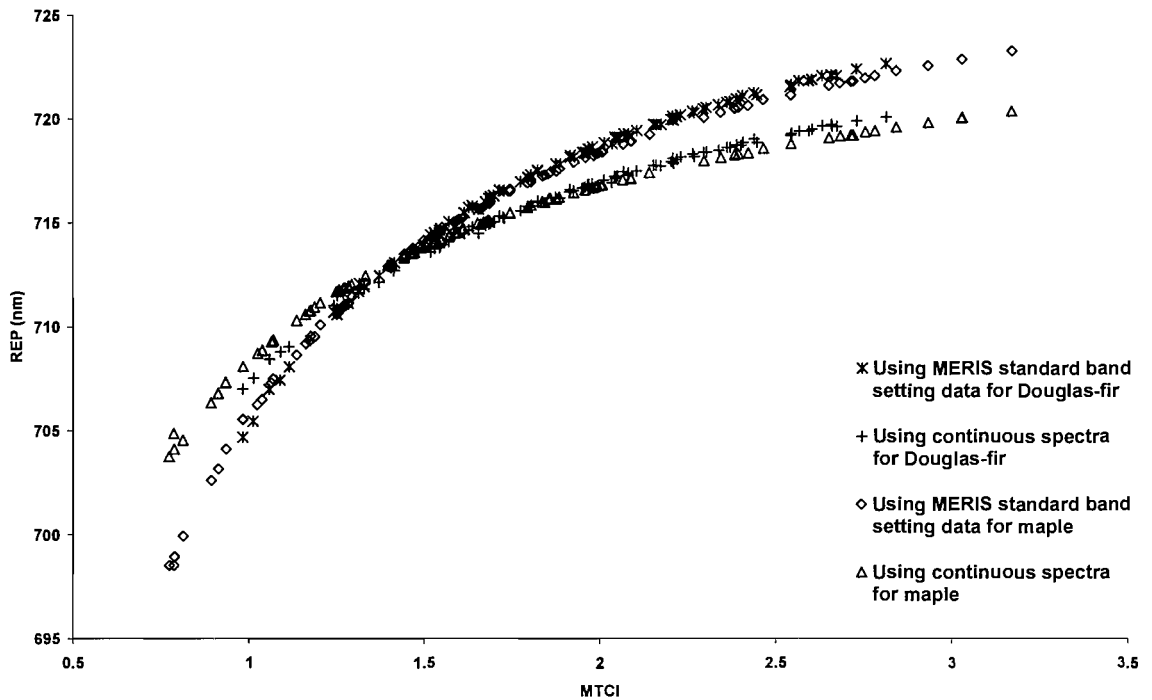


Figure 3.4. Relation between REP and MTCI, estimated using continuous spectra and MERIS standard band settings for field reflectance data of Douglas-fir and maple.

3.4.3 MERIS data

For illustrative purposes a false colour composite from MERIS data was generated using band 10 data as red, band 8 data as green and band 6 data as blue (Figure 3.5b) and the data were classified using an unsupervised algorithm (Isodata) (Figure 3.5c).

Analysis of the MERIS data is presented in two forms: first, images of NDVI (for convenience), REP and MTCI and second, graphical representations of relations between NDVI, REP and MTCI for both heath and woodland. The NDVI image (Figure 3.5d) delineated three broad zones (i) vegetated with high NDVI (and assumed high chlorophyll content) in woodland areas near the image centre, (ii) vegetated with intermediate NDVI

(and assumed lower chlorophyll content) in heath, meadows and agricultural land towards for example, the western edge of the image and (iii) non-vegetated with, for example, low or negative NDVI values in urban and coastal areas. The REP image (Figure 3.5e) identified some variation within these broad NDVI zones; however, the MTCI image (Figure 3.5f) identified greater variation within the broad NDVI zones and this level of variation did not decline with increasing NDVI. This suggested that MTCI was likely to be more sensitive than REP to high values of NDVI and thereby chlorophyll content.

Relationships between NDVI, REP and MTCI were illustrated (Figure 3.6) for a 6.3 km x 6.3 km image subscene (Figure 5.5a) comprising heath and woodland. For heath (assumed relatively low chlorophyll content) there was a near-linear relationship between NDVI and MTCI, but woodland areas (assumed high chlorophyll content) there was little change in NDVI with change in MTCI (Figure 3.6a). The relationship between REP and MTCI (Figure 3.6b) was strong and little influenced by the assumed chlorophyll content. As the NDVI had an asymptotic relationship with MTCI in Figure 3.6a, so the REP was shown to have an asymptotic relationship with NDVI in Figure 3.6c. Together the three graphs in Figure 3.6 point to the value of MTCI as a surrogate for REP that is sensitive to variability in chlorophyll content over a wide range of chlorophyll contents.

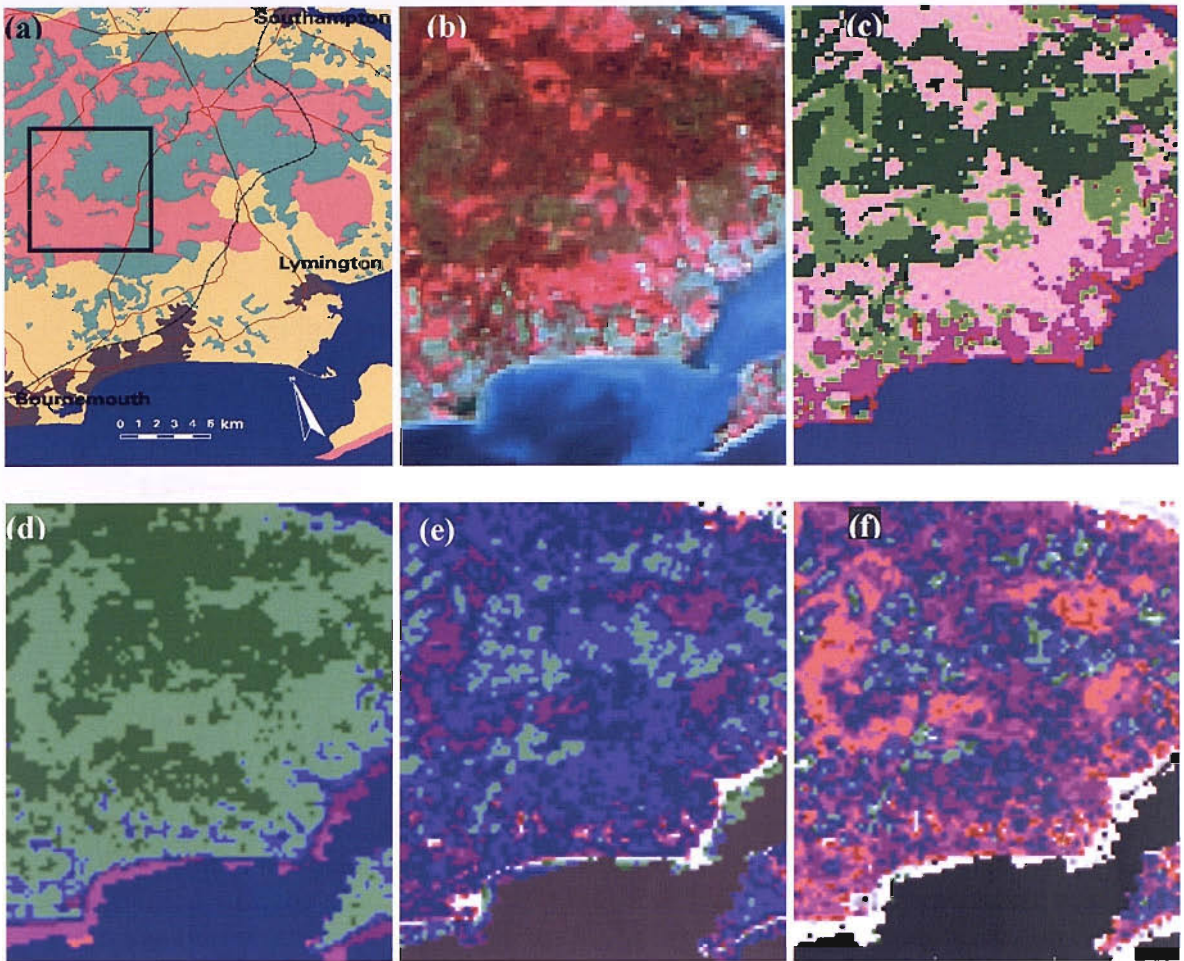


Figure 3.5 MERIS images of southern England (a) land cover map of the study area (New Forest) with the black box indicating the subscene (6.3 km x 6.3 km) containing vegetation with the assumed relatively high and low chlorophyll content that was selected for quantitative analysis;(key : ■ Heath ■ Woodland ■ Meadows & Agricultural land ■ Urban ■ Water); (b) False colour composite image of bands 10, 8 and 6; (c) classified (unsupervised) image; (d) NDVI image, colour key in table 2; (e) REP image, colour key in table2; (f) MTCI image, colour key in table3.2.

Colour	NDVI		REP		MTCI	
	min.	max.	min.	max.	min.	max.
■	-0.4	-0.2370	705	707.37	1	1.2
■	-0.2371	-0.0740	707.38	709.75	1.21	1.4
■	-0.0741	0.0890	709.76	712.12	1.41	1.6
■	0.0891	0.2520	712.13	714.5	1.61	1.8
■	0.2521	0.4149	714.51	716.87	1.81	2.0
■	0.4150	0.5779	716.88	719.25	2.01	2.2
■	0.5780	0.7409	719.26	721.62	2.21	2.4
■	0.7410	0.9039	721.63	724	2.41	2.6

Table3.2 . Key for NDVI, REP and MTCI images in figure .

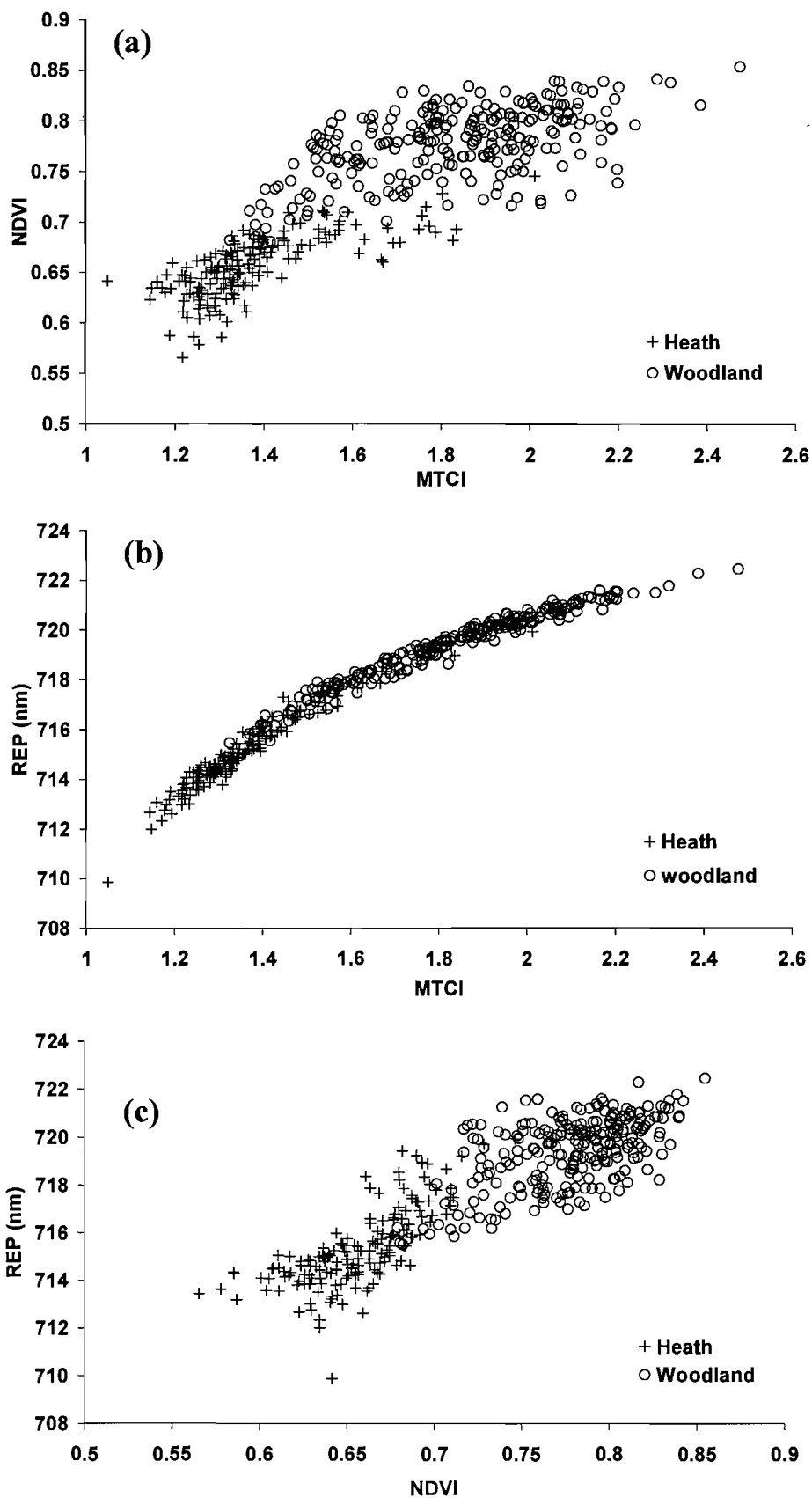


Figure 3.6 Relationships between (a) NDVI and MTCI; (b) REP and MTCI and (c) REP and NDVI for a subsample of MERIS data (Figure 3.5a) containing heath and woodland.

3.5. Discussion and conclusion

The relation between REP and MTCI was asymptotic and remained the same for model, field and MERIS data. The MTCI fulfilled the design criteria (section 3.2) in that it was easy to calculate from MERIS data recorded at the standard band setting and was sensitive to a wide range of chlorophyll contents. It had four characteristics that are relevant here:

1. Comparing the chlorophyll indices, there was only one MTCI value for each pixel unlike the REP value which will vary with method employed.
2. Calculation of the MTCI could be automated readily, as it involved one step and no manual intervention.
3. Should it be necessary REP can be estimated from MTCI, as a strong relationship exists between REP and MTCI.
4. MTCI was more sensitive than REP to high chlorophyll contents.

In conclusion: the MTCI appeared to be a most suitable index for the estimation of chlorophyll content with MERIS data. Further investigation of the performance of MTCI with changing canopy and non canopy variable for a wide range of data are now required.

Chapter 4. Understanding MTCI

4.1. Introduction

The previous chapter discussed the design and initial evaluation of MTCI, which suggested higher sensitivity of MTCI to canopy chlorophyll content than REP. As described in section 2.8 spectral reflectance in the red edge region depends on various canopy and non canopy variables, these includes soil reflectance, atmospheric effects and Sun-sensor geometry. The nature of these data recorded at the sensor also depends on the spectral and spatial resolution of the sensor. Therefore, understanding the performance of MTCI requires understanding the following: (i) data used to estimate MTCI and (ii) the effect of non canopy-variables on MTCI.

4.2. Understanding the spectral data

4.2.1 Reflectance spectrum of a leaf

A typical leaf reflectance spectrum in visible and NIR wavelengths exhibits two important behaviours: a strong absorption in visible and high scattering in the NIR wavelengths. The physical structure of leaves (layered structure of cells and air gaps in between) is designed to scatter light and therefore, absorption occurs only due to the absorption by specific pigments. Chlorophyll is a major pigment that absorbs light in red wavelengths; increase in chlorophyll concentration is related to deepening and widening of this absorption feature (figure 4.1).

In the NIR region leaves are highly reflective, because of a leaf's construction. The inside of a leaf is made of water filled cells with surrounding air gaps. Part of the light entering a leaf reflects off from the cell wall and the other part enters into the

cell. Inside the cell (except the wavelength of pigment absorption) light keeps scattering until it exits the cell. Light scattering inside a cell is due to

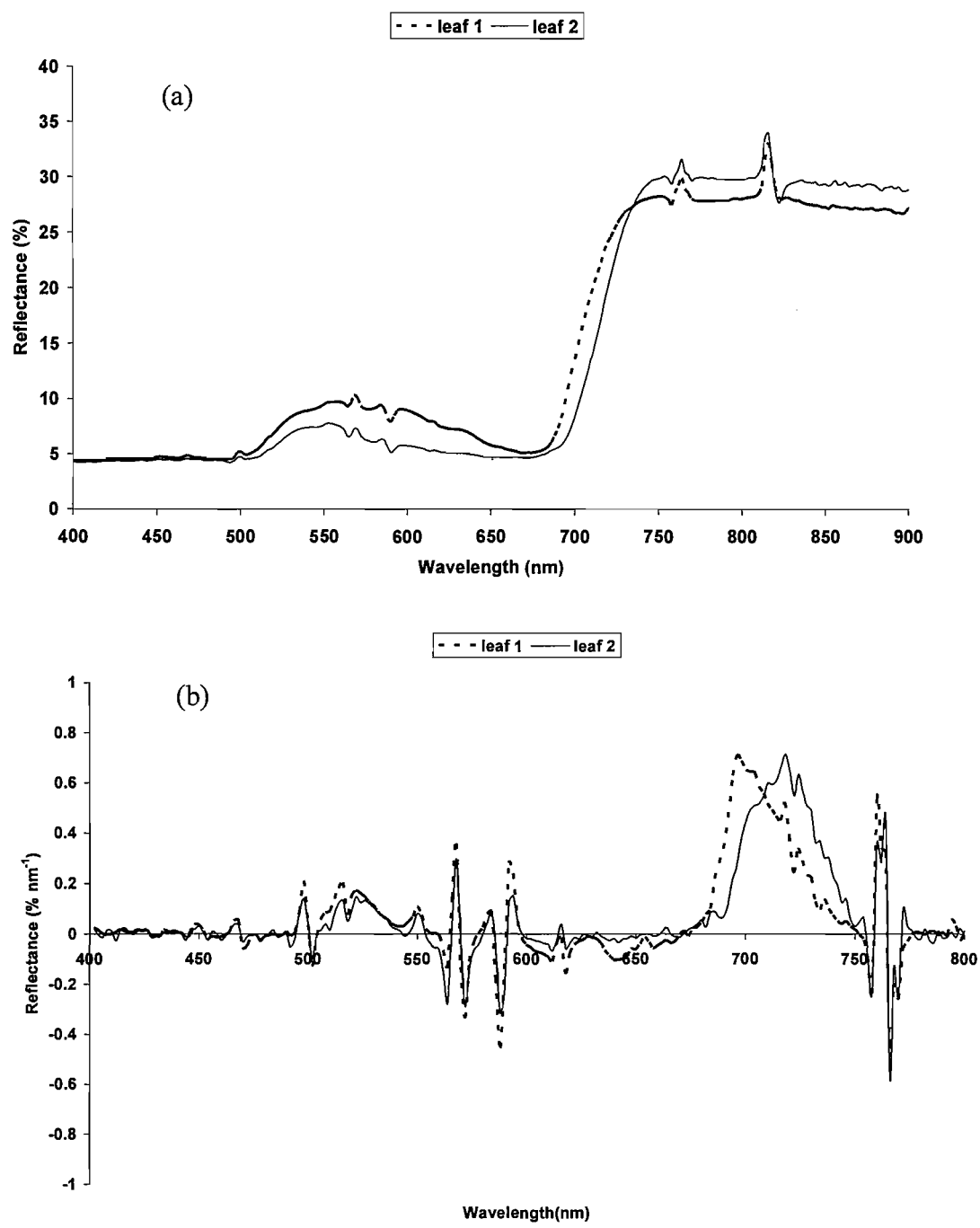


Figure 4.1. Leaf reflectance (a) and derivative (b) spectra for two leaf samples (leaf 1 with chlorophyll concentration 251 mg m^{-2} and leaf 2 with chlorophyll concentration 458 mg m^{-2}) from data obtained from greenhouse experiment (explained in chapter 5).

two factors: the change in refractive index between the water filled cells and surrounding air gaps (1.33 for water and 1.00 for air) and size of the cell's organelles which is less than the wavelength of the light entering the cell prompts Rayleigh or Mie scattering. The leaf surface also contributes to the reflectance due to presence of leaf surface wax.

REP is the point of maximum change in the red and NIR region of the vegetation spectrum. Therefore, a derivative spectrum could be able to determine the REP. Figure 4.1b represents the derivative spectrum for two leaf spectra: Leaf 1 (chlorophyll concentration 251 mg m^{-2}) and leaf 2 (chlorophyll concentration 458 mg m^{-2}). A prominent REP was found for both leaf samples and it shifted 22 nm with increase in chlorophyll concentration.

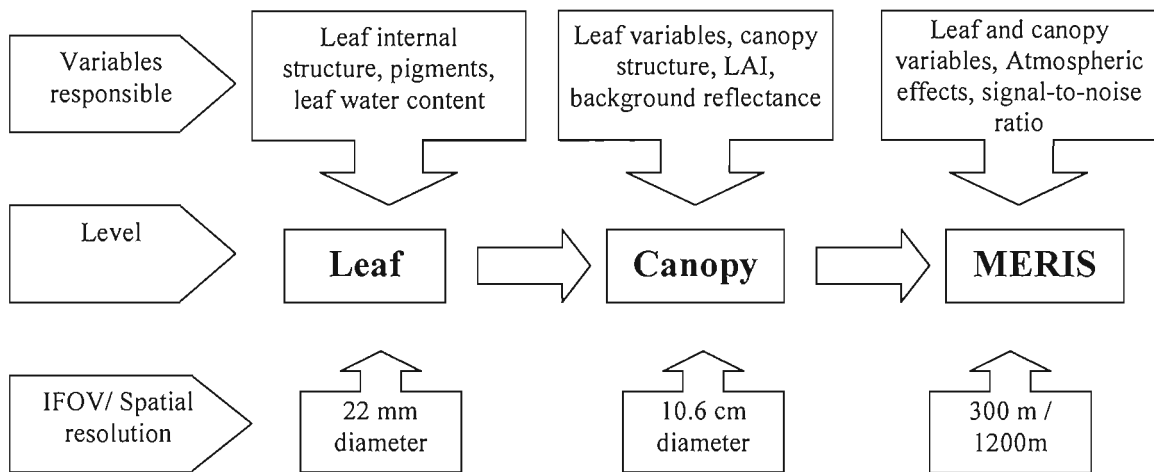


Figure 4.2. Change in reflectances from leaf to satellite (MERIS) level due to the influence of different variables.

4.2.2 Canopy reflectance

Reflectance measured at the top of the canopy is generally less than the reflectance of a leaf. Because of two major factors: (i) Top-of-canopy reflectance is affected by various canopy and non canopy factors and (ii) the sensor IFOV increases (figure 4.2). When compared to a leaf the canopy has lower reflectance in visible wavelengths that is approximately half as it reduces reflectance at NIR wavelengths. Figure 4.3a represents two canopy spectra: canopy 1 having LAI= 0.9 chlorophyll content 146 mg and canopy 2 having LAI= 0.5 and chlorophyll content 168 mg. The canopy reflectance of these spectra is less than 15 % of the leaf spectra. Increase in LAI results in increase in reflectance in NIR region. However, there has little change in the absorption in red region (figure 4.3).

Because the chlorophyll content (total amount of chlorophyll) in the sensor IFOV, i.e., product of chlorophyll concentration and LAI, is nearly same for both canopies. Therefore, the REP of a canopy is more strongly related to chlorophyll content of the canopy than chlorophyll concentration of individual leaf with in the canopy. As compared to a leaf the canopy derivative spectra (figure 4.3) (i) are less in amplitude and (ii) do not show a prominent shift in REP.

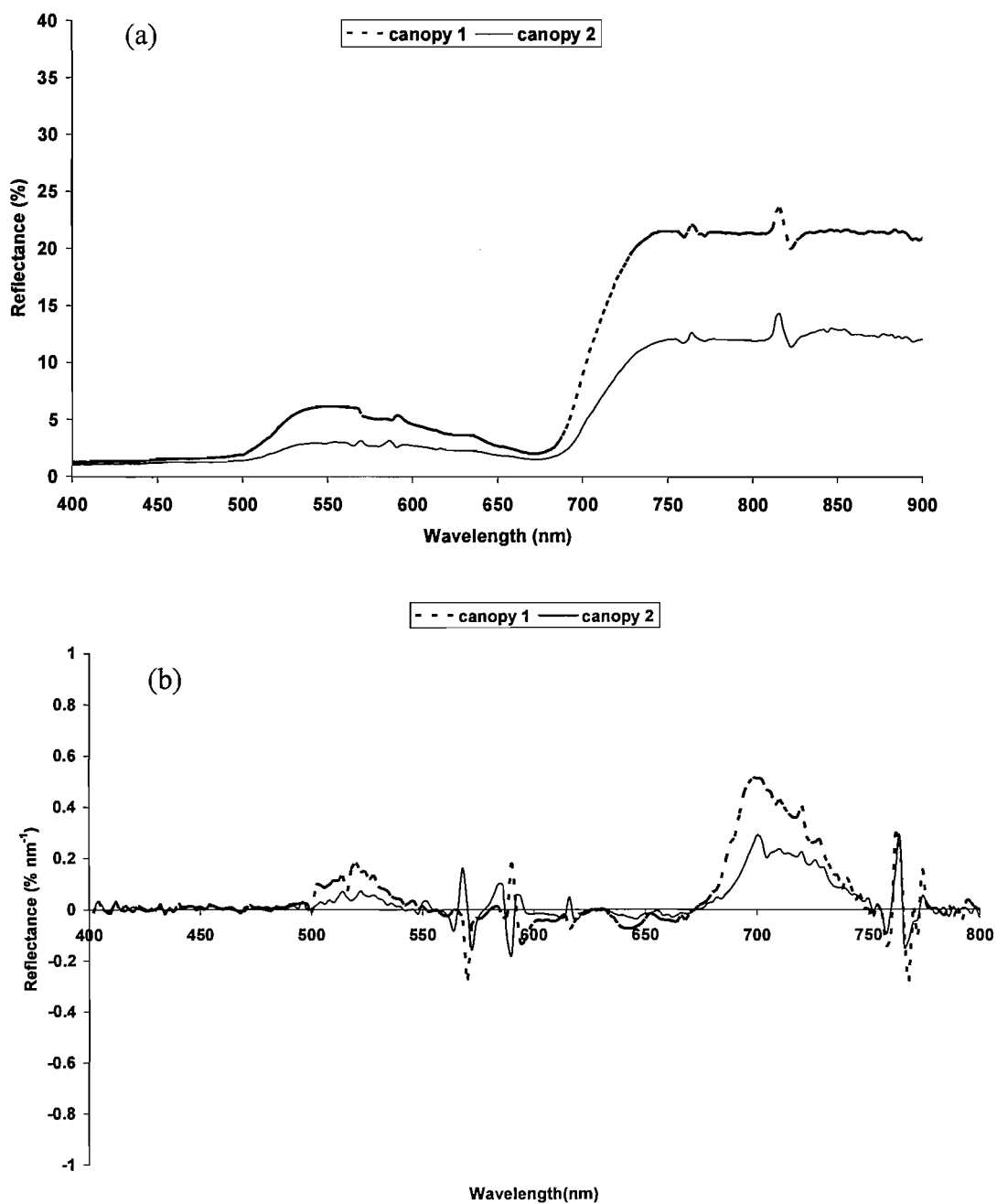


Figure 4.3. Canopy reflectance spectra (a) and derivative spectra (b) for two canopies. (Canopy 1 having LAI= 0.9 chlorophyll concentration 163 mg m⁻² and canopy 2 having LAI= 0.5 and chlorophyll concentration 336 mg m⁻²) from data obtained from greenhouse experiment (explained in chapter 5).

4.2.3 Satellite (MERIS) spectra

Data recorded at satellite (MERIS) level have two major differences from data at canopy level (figure 4.2): (i) effect of atmosphere has been added to the data and (ii) it has a coarse spatial and spectral resolution. The type of landcover seen by the sensor and the signal-to-noise ratio of the instrument also influence the data recorded at satellite level.

4.2.3.1. Effect of Landcover

Each landcover produces a different spectral signature at MERIS sensor. Radiance recorded at MERIS sensor for four landcovers is given in figure 4.4. In this particular example radiance for water decreases with an increase in wavelength. Radiance for soil increases in visible wavelengths from green to red and then there is a little change in radiance at NIR wavelengths. For vegetation classes (woodland and grassland) there is a clear red edge , however, the radiance for woodland is less than grass land.

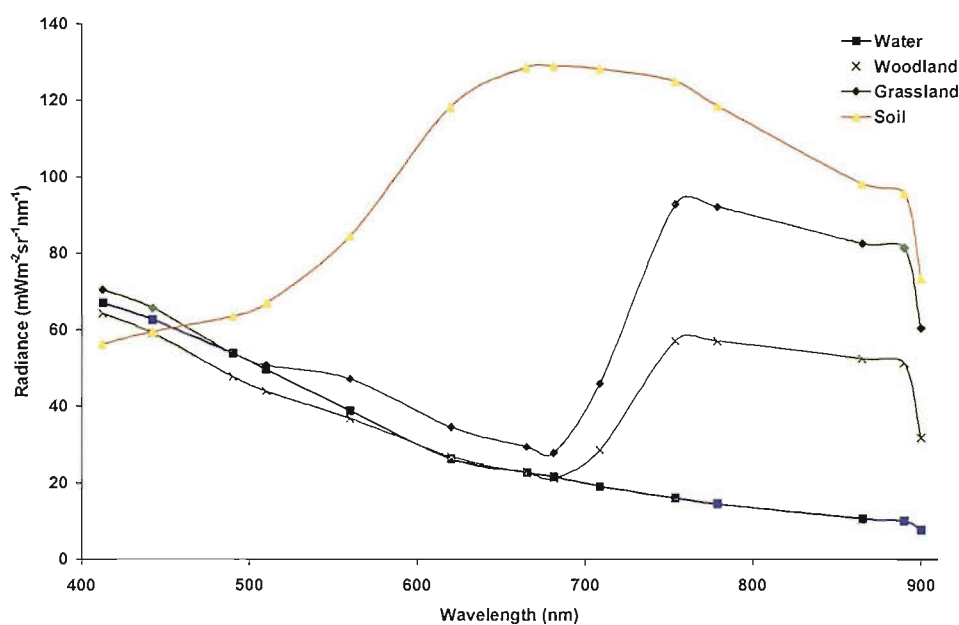


Figure 4.4 Radiances recorded at MERIS sensor for four landcovers (points in the graph indicate the MERIS band position).

4.2.4 Signal-to-noise ratio of MERIS data

4.2.4.1. Introduction

Like all remotely sensed data, MERIS data comprise two components: signal (information related to the object being sensed) and noise (variation unrelated to the object being sensed). This variation may be caused by the instrument, the platform or the atmosphere. If MERIS data were used to estimate environmental variables using only spectral properties, then the amount of noise in the data would be very important as the accuracy of the estimate would be inversely related to the level of the noise. Therefore knowledge of amount of noise present in the data is a prerequisite to analysis. Three approaches have been used to estimate the amount of noise in the data produced by a remote sensing instrument: (i) repeated measurement of a standard scene in the laboratory; this omits the effects of platform and atmospheric noise; (ii) repeated measurement of a standard ground area while in orbit, this requires a flat homogenous area and related atmospheric data at the time of overpass and (iii) analysis of the end product. Using the end product (i.e. the image) for estimating noise is the most convenient approach for a user.

Noise can be represented by the signal-to-noise ratio (SNR) (Lo, 1986), which is given by

$$SNR = \frac{SIGNAL}{NOISE}$$

SNR is proportional to data quality; the higher the SNR the greater the data quality.

MERIS is now in its third year of orbit but little attention has been given to the estimation of data noise or to consider the effect of this noise on the estimation of environmental variables.

4.2.4.2. Methods of estimating SNR

The most commonly used methods for the estimation of image SNR are: (i) homogenous area (Fujimoto et al., 1989); (ii) nearly homogenous area (Boardman and Goetz, 1991); (iii) geostatistics (Curran and Dungan, 1989); (iv) homogeneous block (Gao, 1993) and (v) multiple wavebands (Roger and Arnold, 1996). Each method varies in the amount of data, processing time and manual intervention required (table 4.1).

Each method has its drawbacks (e.g., the homogenous area method will have its noise estimates inflated by interpixel variability (Dungan and Curran, 1989)) and each method produces a different SNR from the same dataset (Smith and Curran, 1999). Therefore, care is needed when choosing a method and when interpreting SNRs estimated by others.

Method	Data amount	Processing time	User input	Effect of spatial variation
Homogenous area	Small	Short	More	High
Nearly homogenous area	Medium	Medium	Medium	Medium
Geostatistics	Medium	Short	Medium	Medium
Homogenous block	Large	Long	Little	Medium
Multiple waveband	Large	Long	Little	Low

Table 4.1. Comparison of advantages and disadvantages of five most commonly used method to estimate image SNR (Smith and Curran, 1999).

The geostatistical method has the advantage of using reasonable assumptions and is easy to apply; therefore it was used in the estimation of SNR from MERIS data.

4.2.4.3. Geostatistical Method

Curran and Dungan (1989) developed the geostatistical method for estimating noise using the variogram (Isaaks and Srivastava, 1989). The variogram is produced from a

transect of pixels where the response R , at pixel number x along the transect, has been extracted at $x=1,2,\dots,n$. The relation between a pair of pixels separated by h pixels (the lag distance) can be given by the variance of the difference between all such pairs. The semivariance $\gamma(h)$ for pixels at distance h apart is given by half their expectation squared difference (Webster and Oliver, 2000)

$$\gamma(h) = \frac{1}{2} E[\{R(x_i) - R(x_i + h)\}^2]$$

Within the transect there will be m pairs of observation separated by the same lag (h), then semivariance can be estimated by

$$\bar{S} = \frac{1}{2m} \sum_{i=1}^m \{R(x_i) - R(x_i + h)\}^2$$

The semivariogram is the function that relates semivariance to lag (figure 4.5) (Webster and Oliver, 2000). Three important aspects of semivariogram are: the sill (asymptotic upper bound value of $\gamma(h)$); the nugget variance (C_0) (extrapolated value of $\gamma(h)$ when $h=0$); and the spatially dependent structural variance (C) (sill minus nugget variance) (figure 4.5)

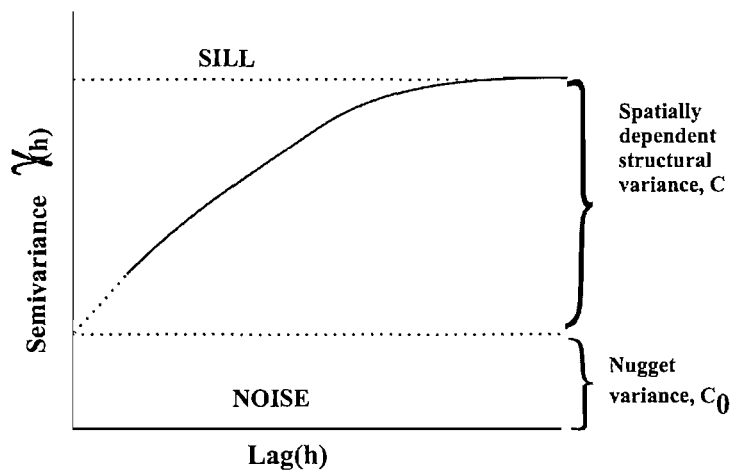


Figure 4.5. A generalised semivariogram showing the nugget variance.

The nugget variance is a good estimator of the spatially independent noise variance. Because, at the limit of $\gamma(h)$, when h approaches 0, the nugget variance does not have a spatial component and is comprised entirely of sensor noise and intrapixel variability. The statistical justification for one dimensional model was given by Curran and Dungan (1989). They showed that the square root of nugget variance can be used as an estimator of the standard deviation of the random noise and intrapixel variability, and thereby SNR can be estimated as

$$SNR = \frac{\bar{R}}{\sqrt{C_0}}$$

where \bar{R} is the average pixel response (brightness) along the transect.

This method is based on following assumptions:

1. The variation in pixel response is related to the lag and not to their location.
2. The orientation of the transect will not affect the variogram.
3. The image has a fixed spatial resolution
4. Scene does not contain much variation in information.

These assumptions can be met if the transects were chosen from a same land cover type. The transect should also be long enough to produce adequate number of statistically significant lags for the production of a semivariogram.

4.2.4.4. Estimating the SNR of MERIS

SNR of MERIS estimated using geostatistical method could depend on 3 major variables: signal, sensor noise and non sensor noise. Signal depends on landcover type and sensitivity of the sensor. Therefore, five landcover classes: clear ocean water, ocean water with sediment, grassland, woodland and soil were analysed to find if there was any landcover effect on the SNR (table 4.2).

The presence of chlorophyll and/or suspended sediment in ocean water will alter the signal and therefore, the SNR. Hence, two ocean water sites were used for the estimation of SNR: water in the eastern Mediterranean Sea with low chlorophyll concentration (figure 4.6) and water in the western English Channel with high chlorophyll concentration (figure 4.7).

We know that the more the vegetation amount the higher the NIR reflectance and the lower the red reflectance. Therefore, amount of vegetation will alter the signal and hence, the SNR; so, two different vegetation types were used to estimate the SNR: tropical evergreen broadleaved forest with a very high chlorophyll content (figure 4.8) and grassland of Northern Ireland with medium chlorophyll content (figure 4.9). The eastern Sahara was used to estimate SNR over bare soil (figure 4.10).

Sun-sensor geometry and atmospheric conditions may contribute to non-sensor noise and thereby, affect the radiances recorded by the instrument. However, the difference between both conditions was not large enough between different scenes to make an effect on SNR estimation. Estimation of SNR using the geostatistical method involved two steps: First, data selection and pre-processing and second, estimation of the SNR for each waveband of MERIS data.

(i) *Data selection and pre-processing*

A reduced spatial resolution (1200m) MERIS image for each landcover was selected as this is the most commonly used form of MERIS data. Each image was geocorrected using the ground control points supplied by the data provider and Level-1 radiance was used to estimate the signal-to-noise ratio.

No	Location	Landcover of Interest	Date of acquisition
1	Eastern Mediterranean Sea	Ocean water with very low chlorophyll concentration (Ocean 1)	31.07.2002
2	Western English channel	Ocean water with medium chlorophyll concentration (Ocean 2)	18.04.2003
3	Central Africa	Evergreen broadleaf forest	05.01.2004
4	Northern Ireland	Grassland	18.04.2003
5	Eastern Sahara	Bare soil	05.01.2004

Table 4.2. MERIS image data used to estimate SNR.

(ii) *Estimating the SNR*

Four 75-100 pixel long transects (running N-S, E-W, NE-SW, NW-SE) were located in each landcover (table 4.2) for 15 MERIS wavebands to minimise angular variability (if any) in the SNR. SNR was estimated for each transects using the following three steps:

- (i) Estimation of the average pixel response (\bar{R}) along the transect and semivariogram for each waveband.
- (ii) Determination of nugget variance (C_0) by extrapolating the slope of the semivariogram towards the origin for each waveband. The smallest lags were considered and this extrapolation was obtained by using either one model or a combination of authorised models (Webster and Oliver, 2000).
- (iii) Plot of \bar{R} (average for four transects) versus wavelength and SNR (average for four transects) versus wavelength for each landcover.

4.2.4.5. Results and discussion

Plots for SNR for each MERIS wavebands and landcover were generated and compared with radiance for each land cover type. As noted by other researchers (e.g., Smith and Curran, 1999; Curran and Dungan, 1989) SNR will vary with signal and signal varies with landcover, this was also observed in this study.

If signal decreases then one would expect SNR to decrease as there is less signal per unit of noise. The same was observed in this study: SNR was highest in the blue band (centred at 412.5 nm) and lowest for near infra red (NIR) band (centred at 900 nm) irrespective of the chlorophyll concentration. However, presence of chlorophyll in the ocean water resulted in a low SNR for all MERIS bands (figure 4.6 and 4.7). For nearly clear ocean water the SNR in the blue band (centred at 412.5 nm) was 1622 which was nearly same as specified during the design of sensor (ESA, 2004).

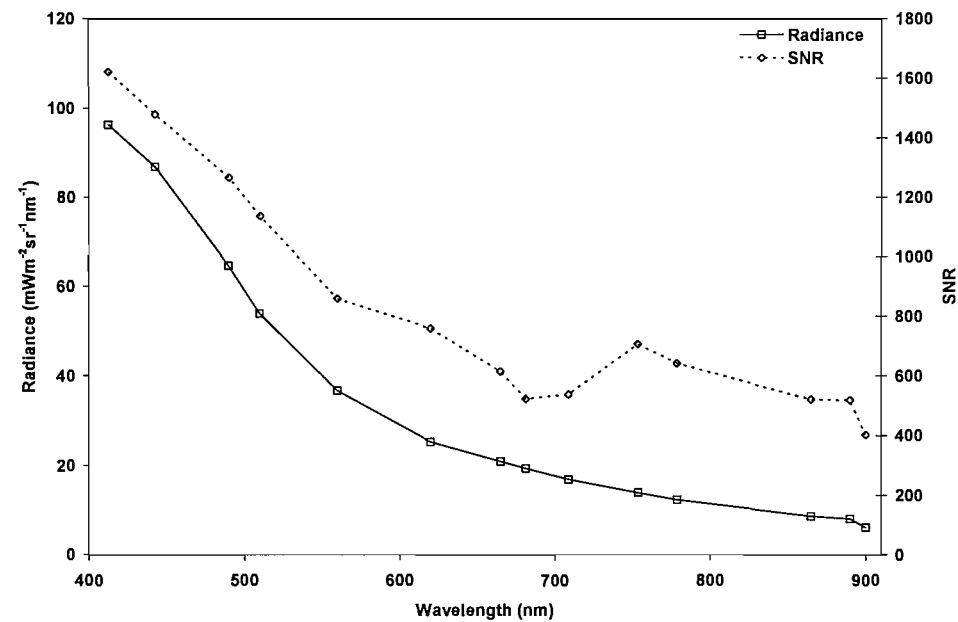


Figure 4.6. The radiance and SNR for MERIS data of the Eastern Mediterranean (table 4.2).

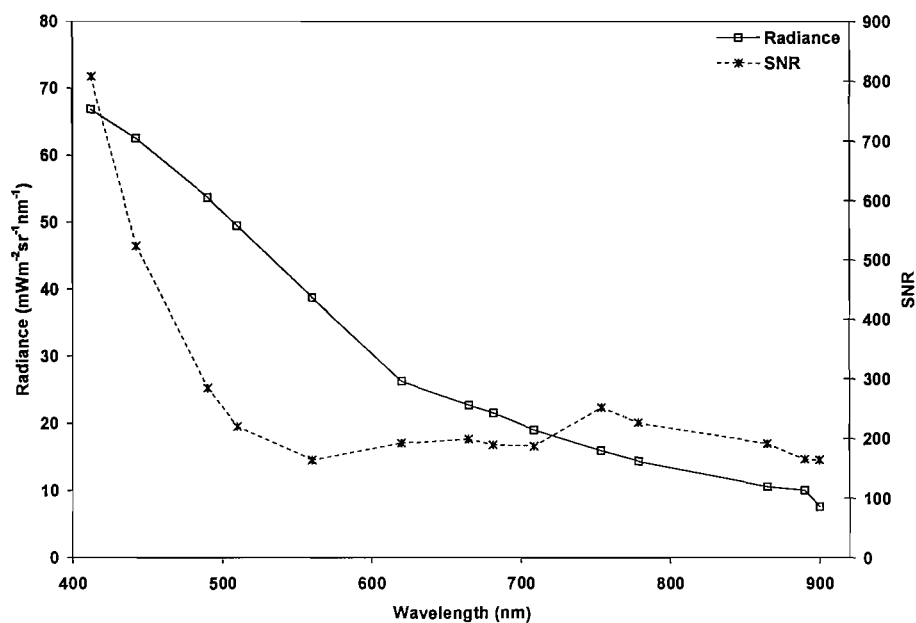


Figure 4.7. The radiance and SNR for MERIS data of the western English channel (table 4.2).

Like the ocean water, the SNR for vegetation was highest in the blue band (centred at 412.5 nm) and lowest in the NIR band (centred at 900 nm) and this was the case irrespective of chlorophyll content. However, an increase in chlorophyll content resulted in an increase in the SNR in the visible wavebands and had very little effect in the NIR wavebands (figure 4.8 and 4.9).

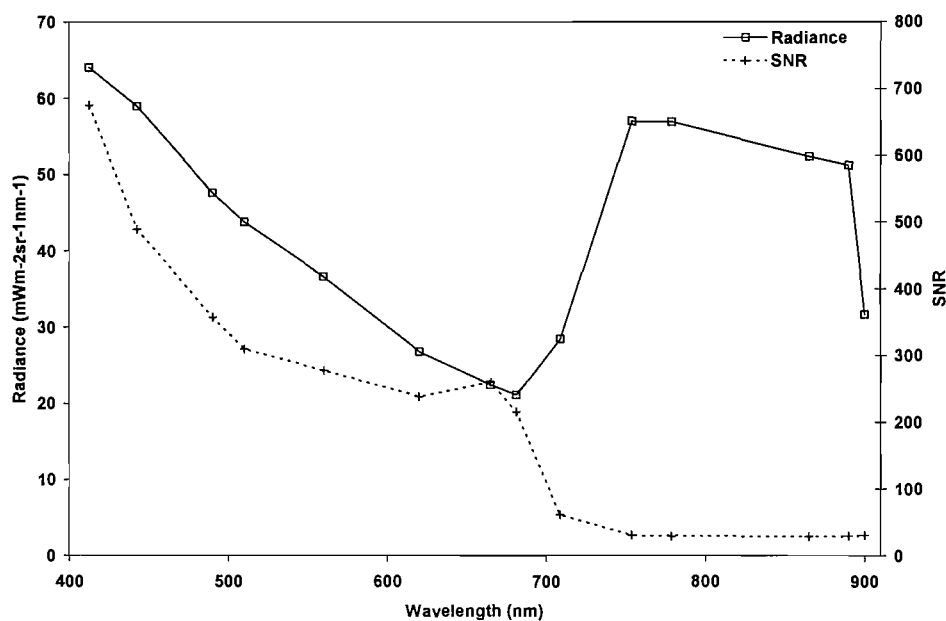


Figure 4.8. The radiance and SNR for MERIS data of central African forest (table 4.2).

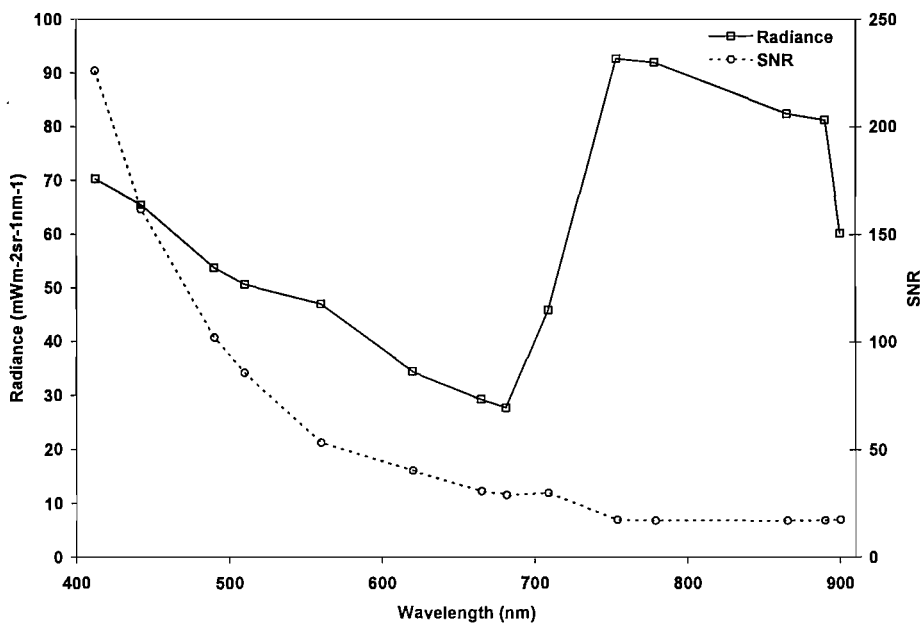


Figure 4.9. The radiance and SNR for MERIS data of Northern Ireland grassland (table 4.2).

Like other landcover the SNR for soil was high in visible and low in NIR wavebands. In general, bare soil had the lowest SNR in visible wavebands and intermediate SNR in NIR wavebands compared to the other five landcovers (figure 4.10).

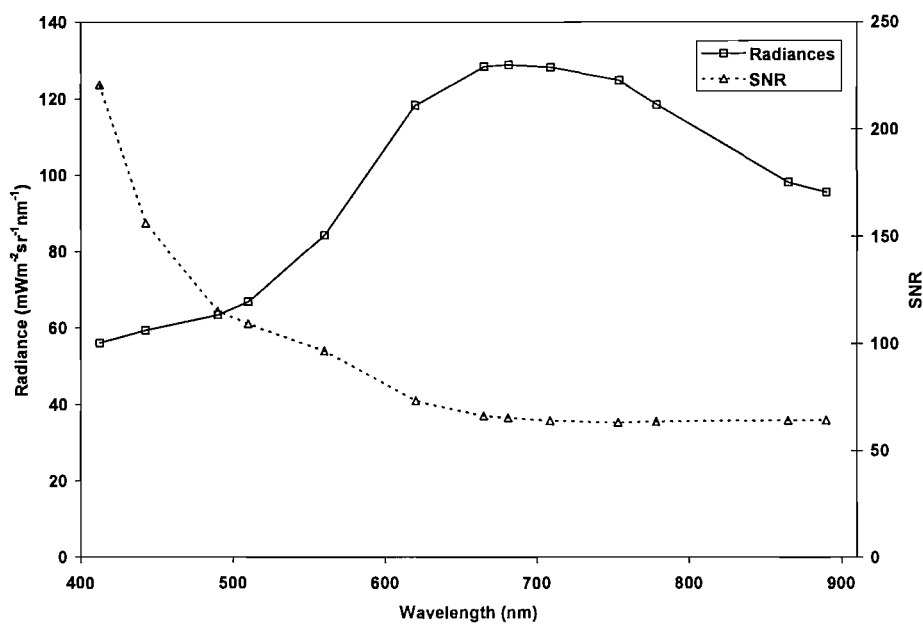


Figure 4.10 The radiance and SNR for MERIS data of Eastern Saharan soil (table 4.2).

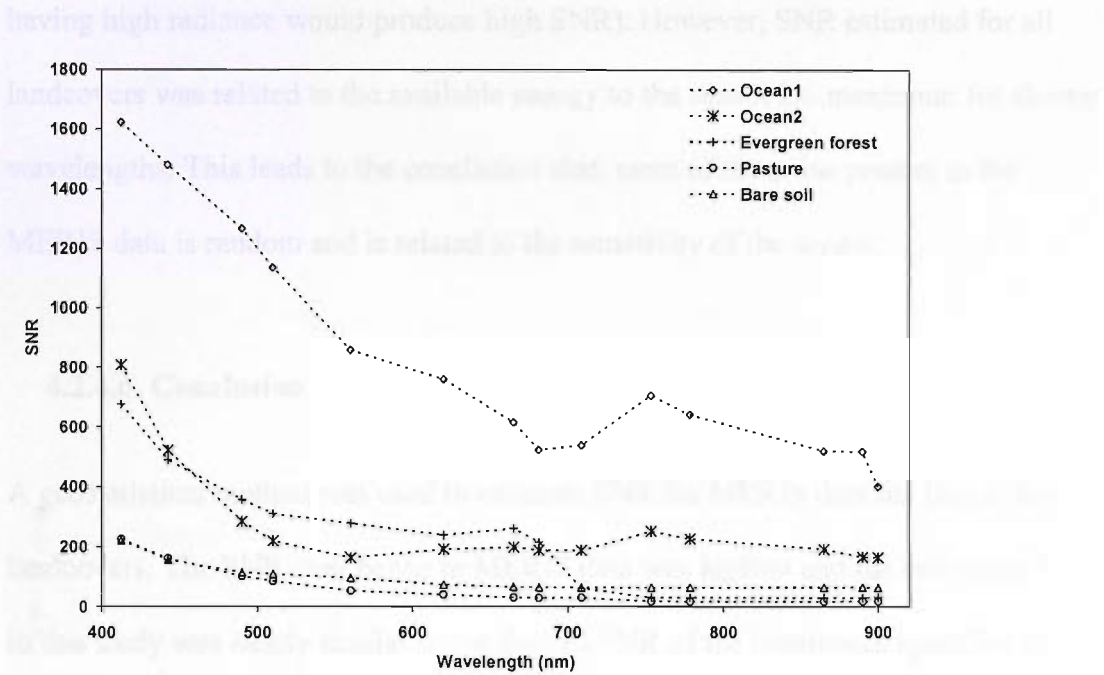


Figure 4.11. The SNR for five landcovers (table 4.2).

SNR estimated for all five landcovers followed a similar trend (figure 4.11), i.e. highest SNR in visible wavelengths and lowest in NIR wavelengths irrespective of landcover type. The SNR decrease with increase in available energy (table 4.3).

		Wavelength		
Radiance ↑		Blue	Green/Red	NIR
	Bright	1400	200	50
	Medium	400	200	100
	Low	-	-	500
Decrease in SNR with energy available →				

Table 4.3. Approximate SNR for different wavelength with different radiance.

It indicated that the noise was not fixed for the instrument; if it was the case, then one would anticipate a strong relationship between SNR and radiance (e.g. bright surface

having high radiance would produce high SNR). However, SNR estimated for all landcovers was related to the available energy to the sensor i.e. maximum for shorter wavelengths. This leads to the conclusion that, most of the noise present in the MERIS data is random and is related to the sensitivity of the sensor.

4.2.4.6. Conclusion

A geostatistical method was used to estimate SNR for MERIS data for five different landcovers. The SNR over ocean in MERIS data was highest and the estimated SNR in this study was nearly similar to the desired SNR of the instrument specified in the design criteria. However, SNR estimated in this study was landcover dependent and most of the noise present in MERIS data was random. Most importantly, SNR was not related directly to the signal, but was related strongly to the sensitivity of the instrument.

4.3. Effect of non canopy variable on MTCI

4.3.1 Introduction

For a given sensor three major non-canopy variables can influence the remotely sensed reflectance from a vegetation canopy in red and NIR wavelengths and consequently, the MTCI. They are: a) soil brightness; b) viewing angle and c) atmospheric condition.

The bidirectional reflectance of a vegetation canopy can be affected significantly by soil background (Price, 1990). Different soils and soil moisture contents produce different reflectances for a composite of soil and vegetation scene. For example, if the reflectance of soil is similar to the reflectance of vegetation in a particular wavelength then the relation between reflectance and pigment content at

that wavelength will be weak. Likewise on a light coloured soil with high near infrared reflectance, the relationship between NIR reflectance and vegetation amount will be less than on a dark coloured soil with a low NIR reflectance (Curran, 1980, Verma et al., 2002). Vegetation indices have been developed to minimise this effect, for example, the soil adjusted vegetation index (SAVI) (Huete, 1988).

The directional variation in reflectance depends on the nature of the material from which the radiation is reflected. The less Lambertian a surface is, the greater is the variation in the signal with view angle. Since most of the Earth's surface is not Lambertian, the reflectance recorded at the sensor varies in response to solar zenith and view angle (Middleton, 1991). Variation in solar-zenith angle alters canopy illumination and optical thickness, variation in sensor view angle alters the amount of vegetation viewed and the signal from vegetation/background in the sensor field of view (Epiphanio and Huete, 1995). As a result a given amount of vegetation may produce different reflectances and in turn different spectral indices, for example, an increase in solar zenith angle increases NDVI for same amount of vegetation (Huete et al., 1992). Kirchner et al., (1982) simulated reflectance data in red and NIR at satellite altitude for solar zenith angle and atmospheric condition and they found that off nadir viewing effects were more pronounced in the red than in NIR region.

The atmosphere exerts considerable influence on vegetation reflectance recorded by space-borne sensor and the biophysical variables estimated from that reflectance (Huete and Jackson, 1987). Two main atmospheric processes: scattering and absorption modify the angular distribution and the amount of radiation coming from the target. To minimise this effect researchers have developed different spectral indices, for example, Atmospherically Resistant Vegetation Index (ARVI) (Kaufman and Tanré; 1992), Global Environmental Monitoring Index (GEMI) (Pinty and

Verstraete, 1992). The effect of these variables on the estimation of MTCI was evaluated using simulated spectral data from model output and real MERIS data.

4.3.2 Simulated spectral data

A combination of LIBERTY (Leaf Incorporating Biochemistry Exhibiting Reflectance and Transmittance Yield (Dawson et al., 1998)) and a semi-discrete model (Gobron et al., 1997) was used to generate canopy reflectance spectra (400-2500 nm, spectral resolution of 5 nm) for a wide range of canopy (table 4.4) and non-canopy variables (table 4.5). A semi-discrete model was used because it has an advantage of describing vegetation canopy properties as a function of variable which can be physically measured, i.e. the number and orientation of the leaves within a canopy; the height of the canopy; and the spectral reflectance and transmittance at leaf level. In addition, the semi-discrete model can generate reflectance data for various view and zenith angle relatively quickly than other canopy models with known canopy parameters.

variables	Values
Chlorophyll content (mg m^{-2})	10-400 with 10 increments
Average internal cell diameter (μm)	30
Intercellular airspace determinant (unitless)	0.005
Leaf thickness (unitless)	3
Base line absorption (unitless)	0.0004
Albino leaf absorption (unitless)	2
Leaf water content (g m^{-2})	100
Lignin or cellulose content (g m^{-2})	30
Nitrogen content (g m^{-2})	1
Leaf Area Index (unit less)	1 -5 with increment of 1
Leaf Angle Distribution (unitless) (using Bunnik's function)	1
Height of canopy (m)	2
Number of leaves per unit volume	3184

Table 4.4 Leaf and canopy variables used to simulate data for the evaluation of MTCI.

Variables	Values
Sensor view angle(°)	-80 to +80 with 10 increments
Sun zenith angle (°)	0 to 40 with 10 increments
Sun azimuth angle(°)	0,180
Soil type (Price, 1995)	2, 3,4,5,6

Table 4.5 Non leaf and canopy variables used to simulate data for the evaluation of MTCI.

Model data were averaged according to the band centre and band width of the MERIS standard bands to obtain the reflectance data, used to calculate MTCI.

4.3.2.1. Methods of evaluation

Performance of MTCI for soil brightness and viewing angle was evaluated by using an approach based on the signal-to-noise ratio (SNR) of data (Leprieur et al, 1994), here after will be called as ‘Leprieur method’ and for atmospheric effect was evaluated by using an approach based on differential MTCI.

3.1.1.1. Leprieur method

In this approach ‘signal’(s) corresponds to difference between the average MTCI value for maximum chlorophyll content and the average MTCI for minimum chlorophyll content.

$$S(MTCI) = \overline{MTCI(Ch_{\max})} - \overline{MTCI(Ch_{\min})}$$

where Ch_{\max} and Ch_{\min} are the maximum and minimum chlorophyll content. From the user’s perspective, MTCI should be sensitive to chlorophyll content and insensitive to non-canopy variables (described above).

Theoretically there is a near linear relationship between MTCI and chlorophyll content (Dash and Curran, 2004). Let’s say one non-canopy variable ($Vc1$), (for

example, change in soil brightness), affects the relationship and there is a non linear relationship between chlorophyll content and MTCI.

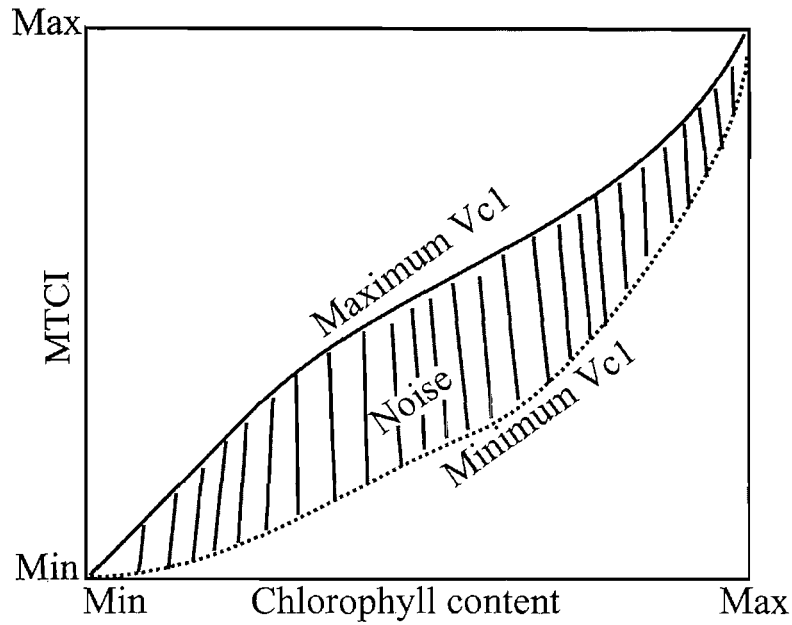


Figure 4.12 Illustrated relationships between maximum and minimum value of MTCI as a function of chlorophyll content as a effect of a non-canopy variable Vc1. Maximum Vc1 curve (solid) is the relationship between MTCI and chlorophyll content for maximum value of Vc1 and minimum Vc1 curve (dotted) is the relationship between MTCI and chlorophyll content for minimum value of Vc1.

Illustrative relationships between MTCI and chlorophyll content for (averaged) maximum and minimum value of Vc1 are given in figure 4.12. If Vc1 had no effect on MTCI then the two curves (i.e. maximum Vc1, minimum Vc1) should superimpose. But this is not the case in figure 4.12. Therefore, the area between the maximum and minimum curve is considered to be resulted due to the effect of Vc1 and can be termed as ‘noise’ (N) due to Vc1. Mathematically it can be estimated as

$$N(MTCI) = \int_{Ch_{min}}^{Ch_{max}} [\max(MTCI(Ch_i)) - \min(MTCI(Ch_i))] dCh$$

Therefore, the signal-to-noise ratio termed as the ‘Leprieur parameter’ (LP) here after as the evaluator of the index for a particular variable is defined as

$$LP(MTCI) = \frac{S(MTCI)}{N(MTCI)}$$

High LP suggests less sensitivity of MTCI to a particular variable and low LP suggests high sensitivity of MTCI to the variable.

Differential MTCI method

Any change in reflectance in band 8 (say $\Delta B8$), band 9 (say $\Delta B9$) and band 10 (say $\Delta B10$) as a result of changing atmospheric conditions will affect MTCI (say $\Delta MTCI$).

Therefore, the relationship between MTCI and $\Delta MTCI$ was used to evaluate the sensitivity of MTCI to changing atmospheric conditions.

$$MTCI = f(B8, B9, B10)$$

$$\Delta MTCI = f(\Delta B8, \Delta B9, \Delta B10)$$

The partial derivative form will be

$$\Delta MTCI = \frac{\partial f}{\partial B8} dB8 + \frac{\partial f}{\partial B9} dB9 + \frac{\partial f}{\partial B10} dB10$$

Solving the equation

$$\Delta MTCI = \frac{(B9 - B8) - (B10 - B9)}{(B9 - B8)^2} \Delta B9 + \frac{(B10 - B9)}{(B9 - B8)^2} \Delta B8 + \frac{1}{(B9 - B8)^2} \Delta B10$$

Low $\Delta MTCI$ indicates less sensitivity of MTCI to change in atmospheric condition.

4.3.2.2. Effect of soil brightness on MTCI

Figure 4.13 shows the overall sensitivity of MTCI to soil brightness and chlorophyll content by displaying the maximum and minimum value of MTCI estimated for five soils (table 4.5) and two LAIs, i.e. LAI=1 and LAI=5. For LAI=1 the variation between the maximum and minimum curve increases with increasing chlorophyll content. However, for LAI=5 both maximum and minimum curves superimpose.

LAI	1	2	3	4	5
LP	6.45	7.29	10.12	17.76	35.19

Table 4.6. Leprieur parameter (LP) for MTCI as a function of soil brightness for different values of LAI.

A decrease in the difference between the maximum and minimum curves resulted in a decrease in ‘noise’, which in turn, produced a high Leprieur parameter. LP estimated for five soil brightness was lowest for LAI of 1 and it gradually increased with increase in LAI with a maximum for LAI of 5 (table 4.6).

.

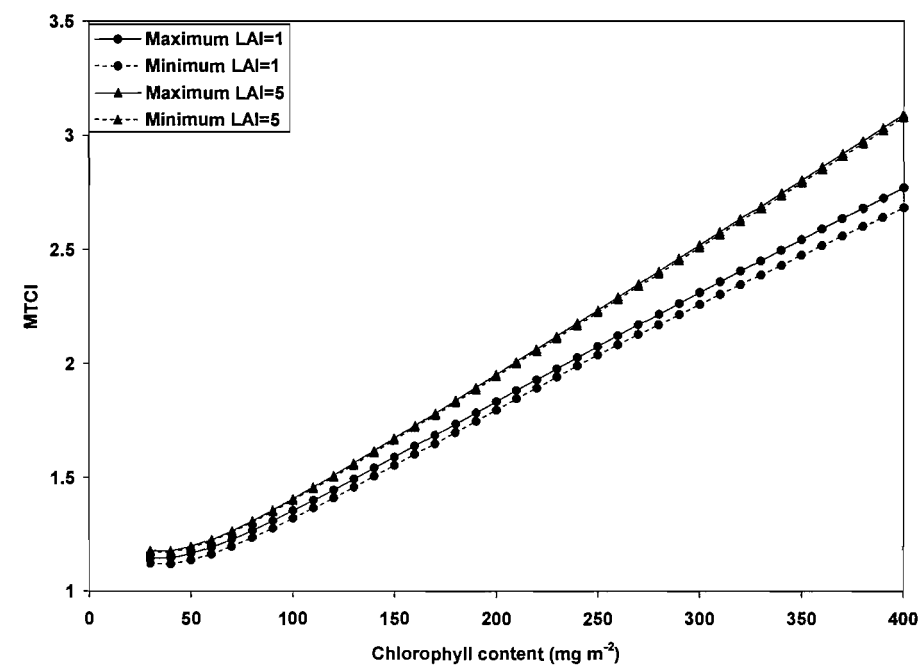


Figure 4.13. Maximum and minimum MTCI among five soils (type=2, 3, 4, 5, 6) and LAI of 1 and LAI of 5 for a nadir view angle and a 0° solar angle.

Reflectance spectra collected over canopy consists of two components: (i) reflection from the canopy and (ii) reflection from the background. For low LAI, there is less

reflection from canopy and more reflection from background. Therefore, the change in MTCI was mainly due to change in background reflectance. However, with increase in LAI the amount of background reflectance decreases, thus making MTCI less sensitive to change in soil brightness. For higher LAI, MTCI is nearly insensitive to change in soil brightness. So for all LAI, LP was greater than 5, which indicates that MTCI is nearly insensitive to change in soil brightness.

4.3.2.3. Effect of viewing angle

The reflectance in bands 8, 9 and 10 changes differently with a change in the sensor viewing angle. Therefore, the MTCI values change with change in sensor viewing angle. Leprieur method was used to evaluate the sensitivity of MTCI for change in viewing angle.

LAI	1	2	3	4	5
LP	2.56	2.56	2.62	2.64	2.64

Table 4.7. Leprieur parameter (LP) for MTCI as a function of view angle for different values of LAI.

Figure 4.14 shows the overall sensitivity of MTCI to viewing angle and chlorophyll content by displaying maximum and minimum value of MTCI estimated for view angle -80° to +80° and two LAIs i.e. LAI of 1 and LAI of 5. For both LAIs, variations between maximum and minimum curve increased with increase in chlorophyll content. The Leprieur parameter was low and there was very little change in the Leprieur parameter for different values of LAI (table 4.7).

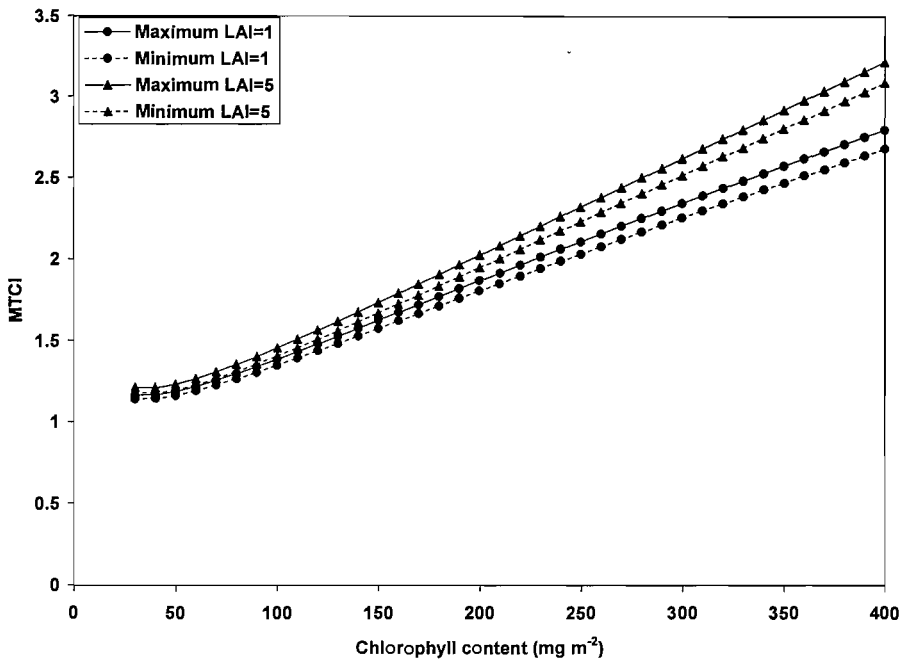


Figure 4.14. Maximum and minimum MTCI from all view angle (-80° to $+80^{\circ}$) and LAI of 1 and LAI of 5 for soil type 6 and a 0° solar angle.

Low Leprieur parameter suggests high ‘noise’ resulted from a large difference between maximum MTCI values averaged for all viewing angles (-80° to $+80^{\circ}$) and minimum MTCI averaged for all viewing angles (-80° to $+80^{\circ}$) for a given LAI. Therefore, the MTCI value could be different for given chlorophyll content with change in viewing angle, suggesting a sensitivity of MTCI to change in viewing angle. However, MTCI estimated for viewing angles -30° to $+30^{\circ}$ resulted in a reasonably high Leprieur parameter (approximately 7) suggesting a limited sensitivity to viewing angle -30° to $+30^{\circ}$. Therefore, this should be considered while estimating MTCI for different viewing angles.

4.3.2.4. Effect of atmosphere

Atmospheric effect on MTCI was evaluated using simulated model data for four atmospheric conditions. They are (i) Rayleigh Atmosphere (it contained only

scattering but no absorption) (atm 1) (ii) Rayleigh atmosphere with gaseous absorption (atm 2) (iii) atmosphere containing average aerosol (aerosol optical thickness 0.1) (atm 3) (iv) atmosphere containing high aerosol (aerosol optical thickness 0.50) (atm 4). Differential MTCI method was used to evaluate the effect of above four atmospheric conditions on MTCI.

Data from model output were used for surface reflectances and data from Holbern and Kimes, (1986) were used for estimating change in reflectances due to different atmospheric conditions. Holbern and Kimes (1986) produced simulated data in red and NIR wavelengths for four different atmospheric conditions (described above) for the AVHRR sensor. Change in reflectance in red was used for band 8 and change in reflectance in NIR was used for band 10, whereas, a linear interpolation between these two was used for change in reflectance in band 9.

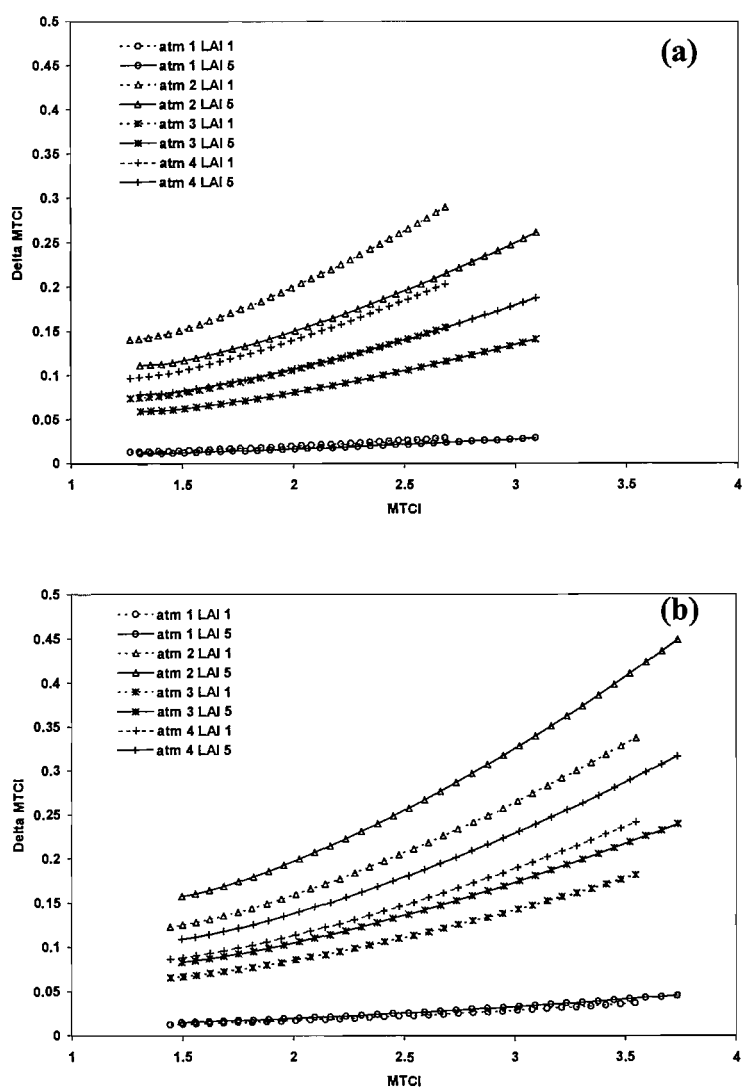
Relation between ΔMTCI and MTCI for four atmospheric conditions and two LAIs, i.e. LAI of 1 and LAI of 5 at nadir viewing is given in figure 4.15a. Similar relationships for viewing angle of -80° and $+80^\circ$ are given in figure 4.15b and 4.15c respectively.

Rayleigh atmosphere (atm 1) produced the lowest ΔMTCI and ΔMTCI remains nearly the same with increase in MTCI. As scattering is inversely proportional to wavelength, therefore, the additive effects due to scattering will decrease from band 8 to 10. These additive effects will minimise by the subtraction of two close bands (i.e. band 10 and band 9 in the numerator, and band 9 and band 8 in the denominator) and there will be less change in MTCI. Therefore, MTCI was limited sensitive to atmospheric scattering.

Atmosphere with both scattering and absorption (atm 2) produced highest ΔMTCI and ΔMTCI had a gradual increase with increase in MTCI. This may be due to the

fact that, different bands respond differently to gaseous absorption in the atmosphere. Therefore, MTCI became sensitive to atmospheric absorption.

Atmosphere containing aerosol (atm 3 and atm 4) produced Δ MTCI values in between the above two atmospheres (atm 1 and atm 2). The atmosphere with more aerosol load produced higher Δ MTCI than atmosphere with less aerosol load. The effect of aerosol optical thickness on MTCI is explained with MERIS data in another section of this chapter.



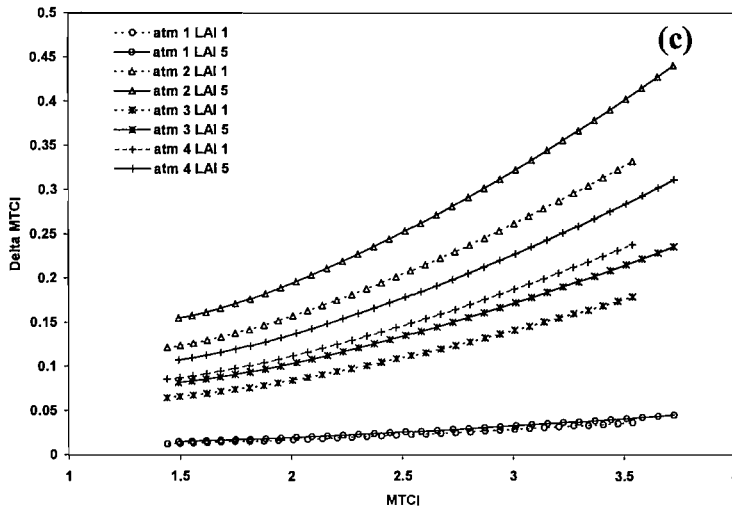


Figure 4.15. MTCI and Delta MTCI (Δ MTCI) for 4 atmospheric conditions and two LAIs: (a) viewing angle of 0° ; (b) viewing angle of -80° ; (c) viewing angle of $+80^\circ$.

Comparison of three figures (figure 4.15a, b and c) reveals four important factors about the atmospheric effect on MTCI: (1) MTCI was limited sensitive to atmospheric scattering, (ii) presence of aerosol and gaseous absorption in atmosphere produced a change in MTCI, however, this change is not significant for average aerosol load, (iii) increase in LAI decreases Δ MTCI, therefore, MTCI estimated over high LAI will be less sensitive to atmosphere than MTCI estimated over low LAI and (iv) there is less change in the relationship between MTCI and Δ MTCI with change in viewing angle.

4.3.3 Using real MERIS data

Real MERIS data were used to study the effect of three features associated with MTCI: (i) data processing (ii) spatial resolution and (iii) change in aerosol load.

4.3.3.1. Effect of data processing on MTCI

Atmospherically corrected level 1(L1) data were used for the design and preliminary evaluation of MTCI. It was later realised that it was not possible to apply a single atmospheric correction for a global data set. Therefore, it was decided to use the best available reflectance data set, i.e. the normalised surface reflectance from level 2 (L2) processing. It was necessary to check the effect of using different level data in the estimation of MTCI. Therefore, MTCI estimated from L1 data and L2 data were compared both spatially and temporally.

Spatial comparison

A reduced resolution (RR) MERIS image of the United Kingdom, Ireland and northern France acquired on 18th April 2004 was used for spatial comparison. Two processing steps were performed to estimate MTCI. First, the data were atmospherically corrected and converted to top-of-canopy reflectance using the Simplified Methods for Atmospheric Correction (SMAC) (Rahman and Dedieu 1994) and MTCI was estimated from these top-of-canopy reflectances (figure 4.16a). Second, the data were processed for standard level-2 products, where the radiances from L-1 products were converted to normalised surface reflectances without atmospheric correction (ESA, 2005) and MTCI was estimated from these normalised surface reflectances (figure 4.16b). Details about the MERIS data processing are given in chapter 7.

Comparison of MTCI estimated from L1 and L2 is presented in two forms: first, images of MTCI estimated from L1 and L2 and second, plots of relations between MTCI estimated from L1 and L2 for both grassland and woodland.

Results from image data

Use of input data from different processing levels (L1 and L2) had very little effect on the MTCI estimation; this can be seen by comparing figure 4.16a and figure 4.16b.

However, use of normalised surface reflectance may produce, in some cases, higher MTCI values. A difference image of the two MTCI images was used to visualise the effect of using different levels (figure 4.16 c). It can be seen for most part of the image (figure 4.16 c) the difference in MTCI between L1 and L2 data is below 0.4, which is less than 10% of the maximum MTCI. This limited sensitivity of change in level of input data on estimation of MTCI can be explained by: a) the closeness of the three bands (band 8, 9 and 10) used in estimation of MTCI and b) the design of MTCI. These three bands were close together and will be similarly affected by the additive constants of atmospheric contamination. These additive constants were cancelled out by the subtraction of two more close bands (i.e. band 10 and band 9 in the numerator, and band 9 and band 8 in the denominator).

It may be noted that there are some vertical lines present in figure 4.16c, these lines are resulted from the 'smile effect' of the MERIS sensor (ESA, 2005).

MERIS sensor is composed of 5 cameras and measures radiances using CCD technique. Each camera is equipped with a two-dimensional CCD array. Each CCD horizontal line provides an image line within a spectral band of 2.5 nm for the swath covered by one camera; the other dimension provides the spectrally dispersed radiance for each pixel along the image line. The spectral measurements of each pixel along an image line are made by its own set of CCD sensors which causes small variations of the spectral wavelength of each pixel along the image that result in the "smile effect". The variation of the wavelength per pixel is in order of 1nm from one camera to another, while they are in the order of 0.1nm within one camera. Even though this variation is small compared to the spectral bandwidth of a band, which is typically 10nm, and can hardly be seen in an image, it can cause disturbances in processing algorithms (ESA, 2005).

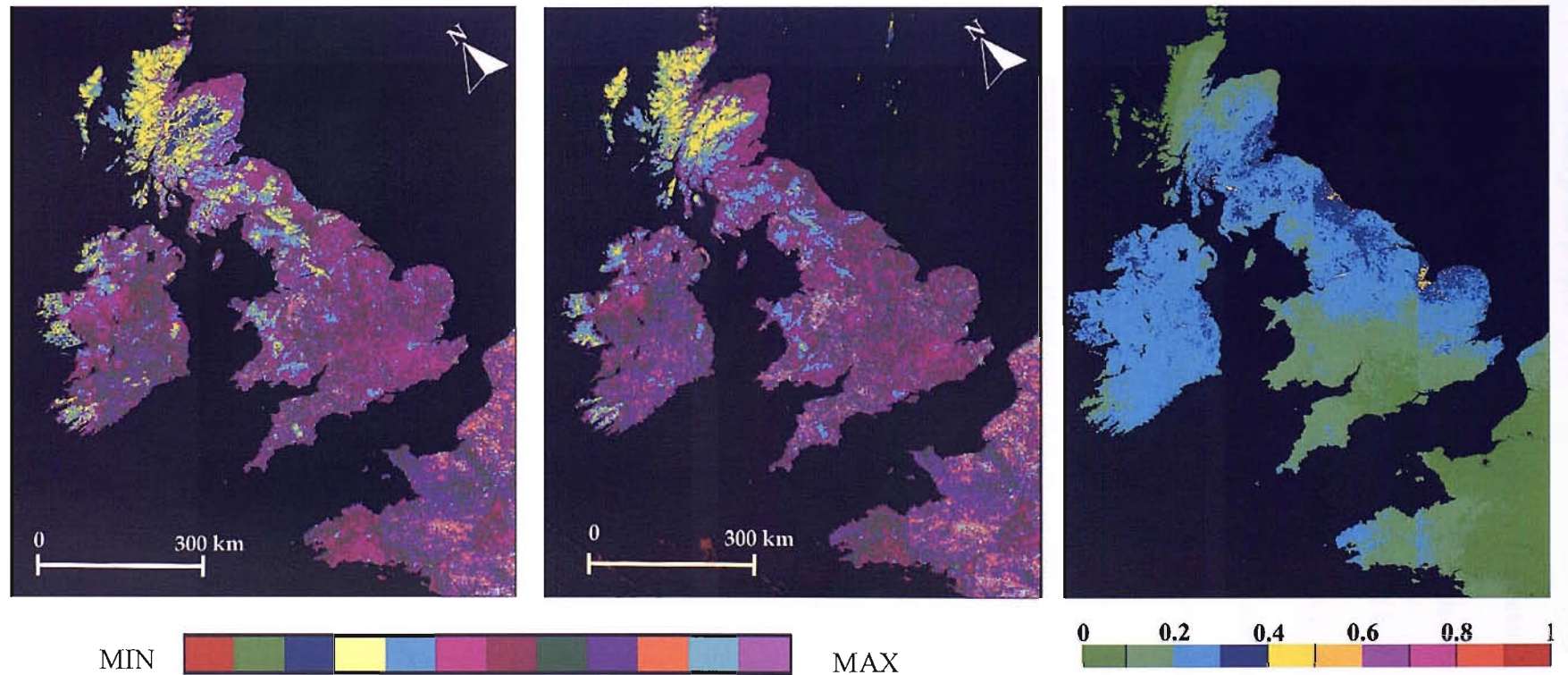


Figure 4.16. Evaluating the effect of data processing on MTCI; (a) MTCI estimated from L1 data, (b) MTCI estimated from normalised surface reflectance data (L2) and (c) difference image.

Results from profile

MTCI estimated using atmospherically corrected L1 data and MTCI estimated using L2 normalised surface reflectance were plotted for grassland (assumed low chlorophyll content) and woodland (assumed high chlorophyll content).

As expected, there was a very strong positive relationship between MTCI estimated from L1 and L2 data for both grassland and woodland. For both grassland and woodland, the coefficient of determination (r^2) was 0.99 between MTCI estimated using L1 data and L2 data, suggesting a strong positive relationship. However, MTCI values over woodland were higher than MTCI values over grassland. This is obvious, because woodland has relatively high chlorophyll content than grassland.

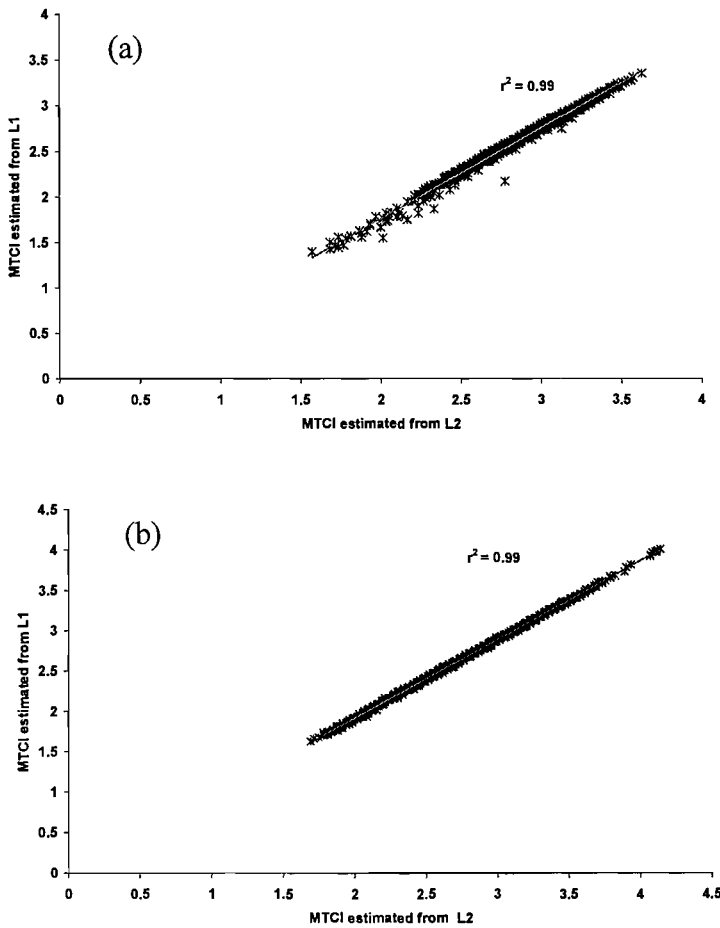


Figure 4.17. Comparison of MTCI estimated from L1 and L2 data for (a) grassland and (b) woodland.

Temporal comparison

Three different sites, representing different vegetation types were selected for temporal comparison of MTCI estimated from L1 and MTCI estimated from L2 (table 4.8).

For each site RR MERIS data were used to generate the time series for the year 2003. MTCI from L1 and L2 data were estimated for cloud free and less atmospherically contaminated pixels. MTCI values of 5X5 pixel around the central pixels were averaged to produce the time series.

Site name	Country	Vegetation type	Dominant species	Soil type
Hainich	Germany	Hardwood forest	Beech	Cambisol
Loobos	Netherlands	Coniferous forest	Pine	Podzol
New Forest	United Kingdom	Mixed forest	Oak, Pine, Heath , Bracken	Pelo-stagnogley

Table 4.8. Test site description.

For Hainich, dominated by deciduous forest, the time series started with low MTCI values, representing low chlorophyll content (figure 4.18a). MTCI increased gradually with the growth period and attended maximum values during June and July. Again from September chlorophyll started to decompose and leaves began changing colour and started falling, producing low MTCI.

For Loobos, dominated by coniferous forest, the time series was different than Hainich. Here the overall variation in MTCI values were less compared to Hainich. Because in coniferous forest there is less change in chlorophyll content in different season (figure 4.18b). However there was a slight increase in chlorophyll during July and August indicated by higher value of MTCI.

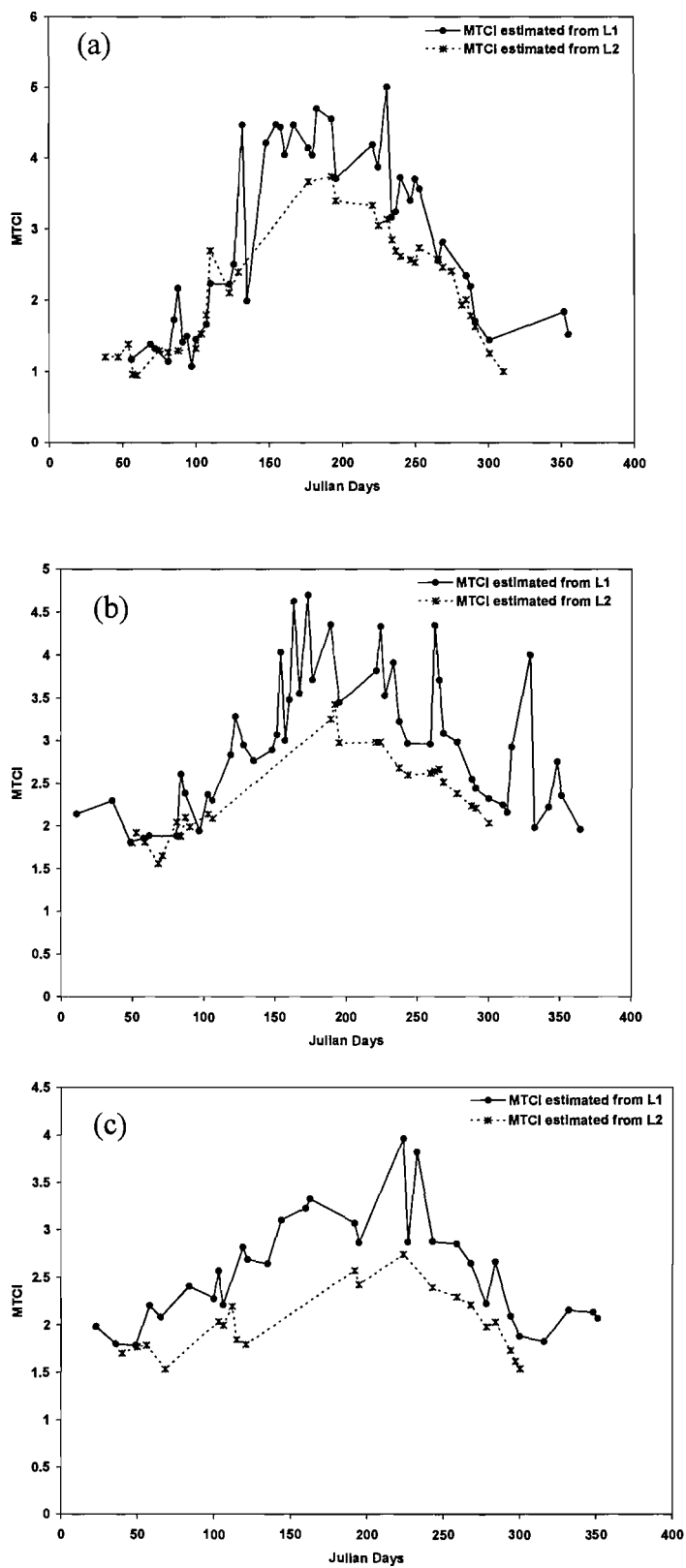


Figure 4.18. Temporal comparison of MTCI estimated from L1 and L2 data for (a) Hainich; (b) Loobos and (c) New Forest.

For New Forest, dominated by coniferous, deciduous forest and heath land, the time series data showed slightly less variation in MTCI (figure 4.18c). Particularly during May to August, there was slight increase in the MTCI values. However, there is not much variation in the MTCI through out the year. This may be due to presence of heath land in the scene, which does not contribute to the total chlorophyll content. In the three study sites described above, MTCI estimated from L1 and L2 were consistent with the growth pattern of the vegetation type in the site. However, in those sites MTCI estimated from L1 is slightly higher than MTCI estimated from L2. This may be due to some atmospheric effect.

4.3.3.2. Effect of spatial resolution

Vegetation biophysical properties are largely scale invariant (Hall et al., 1996; Goodin and Henebry, 2002). However, in some cases (e.g. Sellers et al., 1995) spatial resolution may affect the estimation of any biophysical property. Analyzing the ecosystem functions and their relation to vegetation biophysical processes requires data at regional scale. Estimation of global vegetation condition using MERIS will require data at a coarser spatial resolution than the RR data acquired by MERIS. The effect of spatial resolution on MTCI was evaluated by resampling a full resolution (FR) MERIS data of the southern United Kingdom acquired on 18th October 2002, to various spatial resolutions prior to calculating MTCI. Eight different spatial resolutions, from 300 m to 2400 m were simulated and the standard deviation (SD) of the resultant MTCI was calculated (figure 4.19).

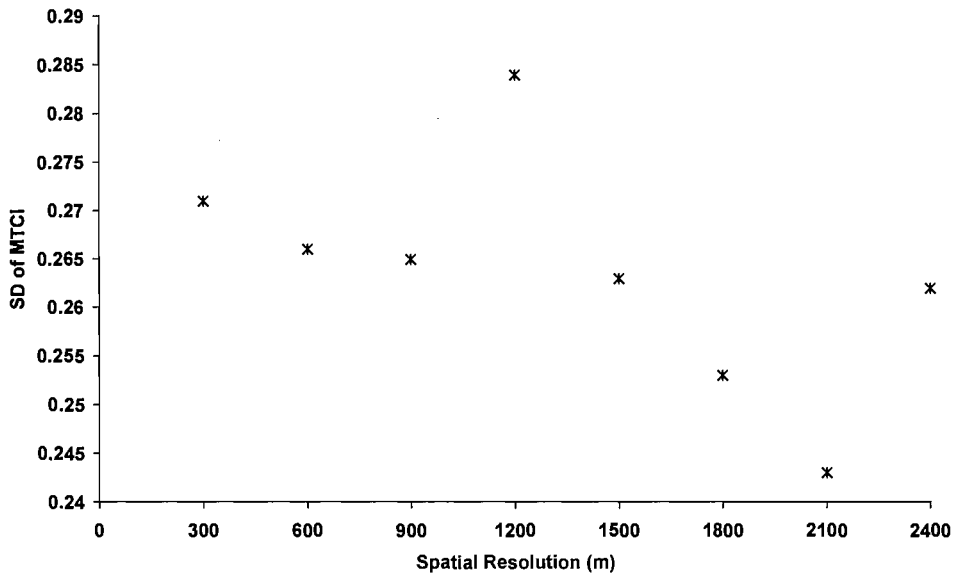


Figure 4.19. SD of MTCI at eight spatial resolutions.

As spatial resolution coarsened SD decreased. This trend was expected, as variability was decreased as a result of averaging of neighbouring pixels. However, variation in the SD of MTCI was very low (less than 1% of the MTCI maximum). Therefore, spatial resolution had very little influence on MTCI. Therefore, MTCI can be scaled up to a coarser spatial resolution for the monitoring global vegetation condition.

4.3.3.3. Effect of aerosol load

Aerosol in the atmosphere is one of the factors which are responsible for change in the incoming signal recorded by any sensor. In turn it affects the estimation of any indices using this signal. Aerosol load in the atmosphere is inversely proportional to horizontal visibility (Petterssen, 1941) and the amount of aerosol is an indicator of the atmospheric condition. Therefore, horizontal visibility can also be used to interpret the atmospheric condition.

RR MERIS data covering part of Europe and Africa were used to evaluate the effect of aerosol load, hence the atmospheric condition on MTCI. Three landcovers i.e. grassland, Mediterranean vegetation and tropical evergreen forest were chosen for this purpose. MTCI was estimated for a misty sky (horizontal visibility 2-4 km) to a clear sky (horizontal visibility 20 km) (Petterssen, 1941) with an increment of 1 km in horizontal visibility using the SMAC processor (ESA,2005) in the BEAM toolbox designed and developed by ESA.

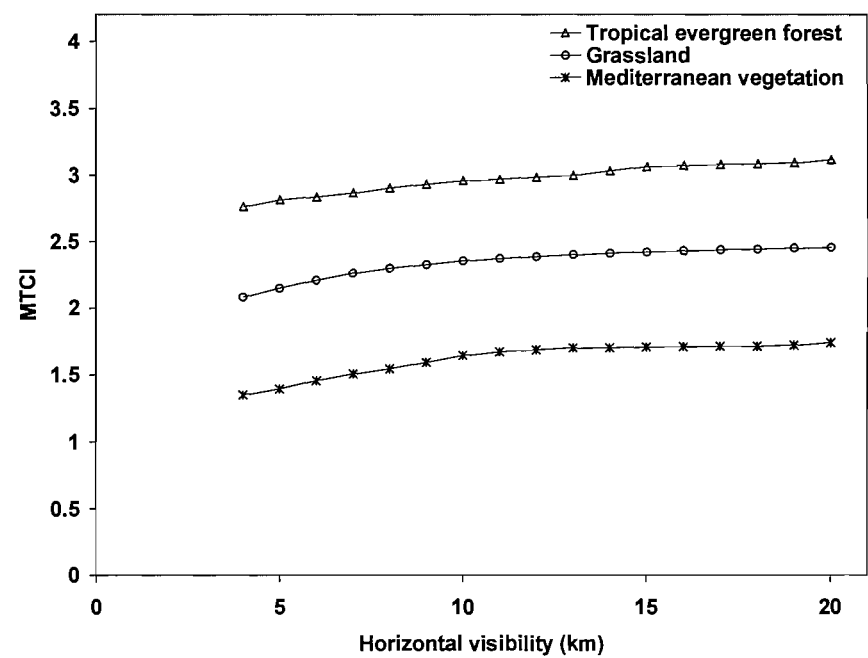


Figure 4.20 Effect of atmospheric aerosol load on MTCI.

MTCI was plotted as a function of horizontal visibility for three landcovers described above (figure 4.20). Tropical evergreen forest (assumed high chlorophyll content) produced high MTCI and Mediterranean vegetation (assumed low chlorophyll content) produced low MTCI. There is very less variation in MTCI values with increase in horizontal visibility for landcovers described above. Therefore, MTCI is limited sensitive to aerosol load in the atmosphere.

The effect of various non-canopy variables on MTCI can be summarised in table 4.9

Variables	Relative influence on MTCI	Notes
Soil brightness	Limited sensitive	MTCI is not affected by change in soil brightness for LAI greater than 2.
Viewing angle	Sensitive	MTCI is limited sensitive to change in viewing angle within -30° to $+30^{\circ}$.
Spatial resolution	Insensitive	
Data processing levels	Insensitive	MTCI estimated using L2 data produced slightly lower value than MTCI estimated using L1 data.
Type of atmosphere	Limited sensitive	MTCI is limited sensitive to atmospheric scattering, but sensitive to change in gaseous absorption.
Change in aerosol load	Limited sensitive	MTCI is not much affected by change in aerosol load in the atmosphere.

Table 4.9. Relative influence of various non-canopy variables on the MTCI.

4.4. Conclusion

In this chapter, the effects of change in various non canopy variables on MTCI were studied. Data at different scales (from leaf to satellite) are influenced by a number of variables, which in turn, affect the MTCI estimation. Followings can be concluded from the chapter

- Spectral reflectance in the red edge region depends on the scale of data. Leaf level data produced a clear REP while canopy level data did not produce a distinct REP.

- At leaf level, the REP depended on the chlorophyll concentration of an individual leaf, where as at canopy level it depended on the chlorophyll content, which is a product of chlorophyll concentration and LAI.
- For MERIS, SNR was random and it was not related directly to the signal, but was related strongly to the sensitivity of the instrument.
- MTCI was limited sensitive to change in soil background reflectance, however it was sensitive to change in view angle.
- MTCI was less sensitive to atmospheric scattering and was limited sensitive to gaseous absorption and increase in aerosol load.
- MTCI was not affected by using different levels of data produced from the MERIS processing chain (level 1 and 2) and any change in spatial resolution.

These results suggested the limited sensitivity of MTCI to most of the non canopy variables using model and real MERIS data. However, model data in most cases assume an ideal condition, which is not always true. Therefore, it is essential to evaluate the performance of MTCI with some real ground data at different scales (leaf to satellite), species and a wide range of biophysical variables.

Chapter 5. Direct MTCI Evaluation

5.1. Introduction

The previous chapter discussed the limited sensitivity of MTCI to change in some of the major non canopy variables using model data. Also, the preliminary evaluation suggested high sensitivity of MTCI to change in chlorophyll content. However, the scale and species used in those evaluations were limited. To obtain a stronger relationship between MTCI and chlorophyll content, it should be evaluated with a large number of chlorophyll content data at various scales and for various species. Therefore, in this chapter the MTCI was evaluated for data recorded at leaf level to satellite level for various species. First part of this chapter explains the MTCI evaluation with data from greenhouse and the second part explains the MTCI evaluation using field data.

5.2. Evaluation of MTCI with greenhouse data

5.2.1 Introduction

To evaluate MTCI with some real foliar biochemical and spectral data a series of experiments was undertaken in a greenhouse located at the School of Biological Sciences, University of Southampton. Two species, spinach (*Spinacia oleracea*) and poplar (*Populus deltoids*) were used; spinach was grown under different levels of fertilisation condition whereas poplar was grown without any fertilisation. For both species spectral and biochemical measurements at leaf and canopy levels were undertaken.

5.2.2 Spinach (*Spinacia oleracea*) data

5.2.2.1. Experimental design

Spinach was grown in 9 trays (30 cm x 50 cm) in a greenhouse under controlled conditions (maximum temperature 20 °C, minimum temperature 12 °C and day light duration 16 hours). A mixture of 30% compost and 70% sand was used as a base soil and equal numbers of spinach seeds were sown on each tray (figure 5.1). Two weeks after sowing and several days after germination the first set of measurements were undertaken and immediately after these measurements fertilisation was carried out using a foliar feed containing NPK (Nitrogen- Phosphorus –Potash). Three trays each were subjected to high fertilisation (100% foliar feed) and low fertilisation (50% diluted foliar feed) treatment and three were unfertilised. Trays were placed on a perforated elevated platform to reduce cross contamination due to seepage of water from the neighbouring trays. Fertilisation was then carried out at 5 day interval up to a week before the end of the experiment.

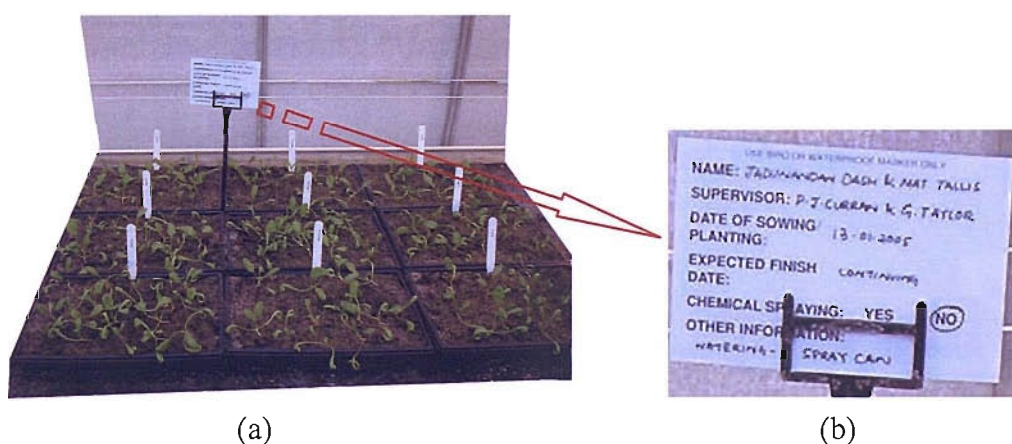


Figure 5.1. (a) One week old spinach seedlings in the greenhouse and (b) information record used in the greenhouse.

5.2.2.2. Canopy measurements

Spectral reflectance, chlorophyll concentration and LAI of spinach tray were measured weekly at canopy level for four weeks.

Spectral measurements

Canopy spectral measurements were undertaken using the Geophysical and Environmental Research Corporation's GER-1500 stand alone field spectrometer. This sensor can acquire data over 350 nm – 1050 nm with a bandwidth of 1.5 nm (table 5.1) (GER, 2005). In this experiment a 4° field-of-view (FOV) lens was used.

Spectral Range	350 nm to 1050 nm
Internal Memory	500 scans
Channels	512
Bandwidth (nominal)	1.5 nm
Scan Time	5 ms and up (selectable)
FOV	4°
Digitization	16 bit
Wavelength Repeatability	+0.1 nm
Noise Equivalent Radiance	0.5 s integration time 400 nm: $6.0 \times 10^{-10} \text{ W} \cdot \text{cm}^{-2} \cdot \text{nm}^{-1} \cdot \text{sr}^{-1}$ 700 nm: $5.7 \times 10^{-10} \text{ W} \cdot \text{cm}^{-2} \cdot \text{nm}^{-1} \cdot \text{sr}^{-1}$ 900 nm: $1.7 \times 10^{-9} \text{ W} \cdot \text{cm}^{-2} \cdot \text{nm}^{-1} \cdot \text{sr}^{-1}$
Maximum Radiance Levels	12 ms integration time 700 nm: $1.5 \times 10^{-4} \text{ W} \cdot \text{cm}^{-2} \cdot \text{nm}^{-1} \cdot \text{sr}^{-1}$
Radiometric Calibration (Traceable to NIST)	400nm : $\pm 5\%$ 700nm : $\pm 4\%$ 1000nm : $\pm 5\%$

Table 5.1 Specification of GER-1500 field spectrometer.

The incoming solar radiation to greenhouse was low and variable because of obstacles in the glass roof and changing weather conditions. Therefore it was decided to carry out measurements at night. An artificial light source, a 1 kw video lamp was used as the source of illumination and it was placed at a zenith angle of 10°. The trays were illuminated from as near to nadir as possible so as to minimise the effect of shadow.

It was intended to keep the instantaneous field-of-view (IFOV) constant. As the trays were of equal height, the height of the sensor was fixed at 1.5 m. This setting produced an IFOV 10.6 cm in diameter. The length of the tray allowed a maximum 3 measurements; hence, 3 points situated at 10 cm apart from each other were marked on the tray as a centre of each IFOV (figure 5.2). During all measurements these point were used as the centre of the IFOV, thus making it sure that the same area was measured on each occasion.

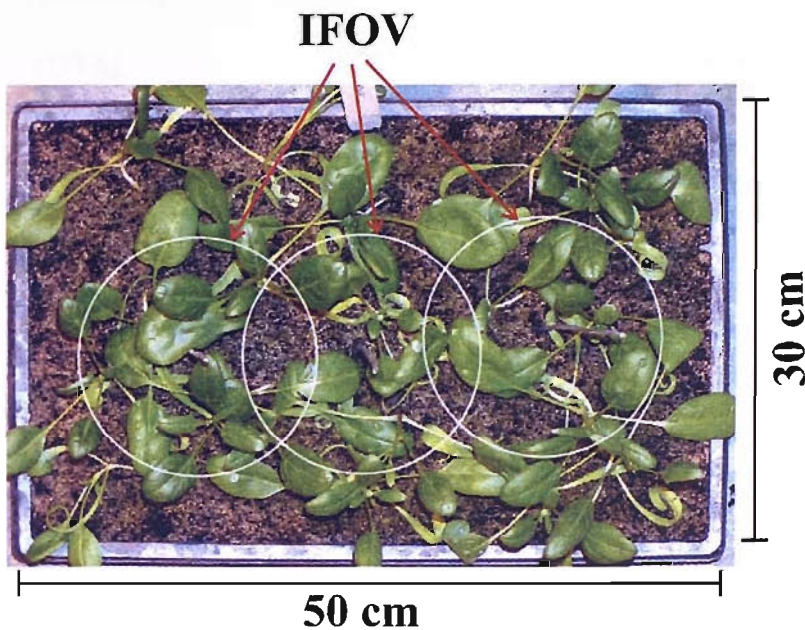


Figure 5.2. Spectral measurement pattern for a tray.

One non-Lamberterian spectralon panel (NERC, 2005) was used as a reference target and spectral measurements were undertaken at regular intervals during the experiment. Each data point was an average of 5 measurements and 27 spectral measurements were taken of the vegetation on each day of measurement (table 5.2).

Date	Fertilisation	LAI (photograph)	Chlorophyll concentration (SPAD)	Spectral reflectance (GER-1500)
Week-1 (03-02-05)	HIGH	1	315	9(each avg 5)
	MEDIUM	1	315	9(each avg 5)
	LOW	1	315	9(each avg 5)
Week-2 (10-02-05)	HIGH	1	315	9(each avg 5)
	MEDIUM	1	315	9(each avg 5)
	LOW	1	315	9(each avg 5)
Week-3 (17-02-05)	HIGH	1	315	9(each avg 5)
	MEDIUM	1	315	9(each avg 5)
	LOW	1	315	9(each avg 5)
Week-4 (24-02-05)	HIGH	1	315	9(each avg 5)
	MEDIUM	1	315	9(each avg 5)
	LOW	1	315	9(each avg 5)
TOTAL		12	3780	108 (540)

Table 5.2. Total number of LAI, chlorophyll concentration and spectral reflectance measurements undertaken during the experiment.

Chlorophyll measurements

Chlorophyll concentration was measured instantaneously and non-destructively using a Minolta chlorophyll meter SPAD-502 (Minolta, 2005). The SPAD values were estimated from the amount of radiation transmitted by a leaf in two wavelengths: red with a peak at 650 nm and NIR with a peak at 940 nm. The illuminating system in the instrument emits radiation in red and NIR wavelengths; a portion of the radiation is absorbed by chlorophyll and the remaining passes through the leaf and strikes the receptor, which converts the radiation into analogue signal (figure 5.3). The analogue signals are boosted and converted to a digital signal, which are used within a microprocessor to calculate the SPAD value. Other technical specifications of the Minolta SPAD-502 are given in table 5.3.

Measurement area	2 mm * 3 mm
Maximum sample thickness	1.2 mm
Insertion depth	12 mm
Minimum interval between measurements	2 seconds
Accuracy	±1 SPAD unit
Repeatability	Within ± 0.3 SPAD units

Table 5.3. Minolta SPAD system specifications.

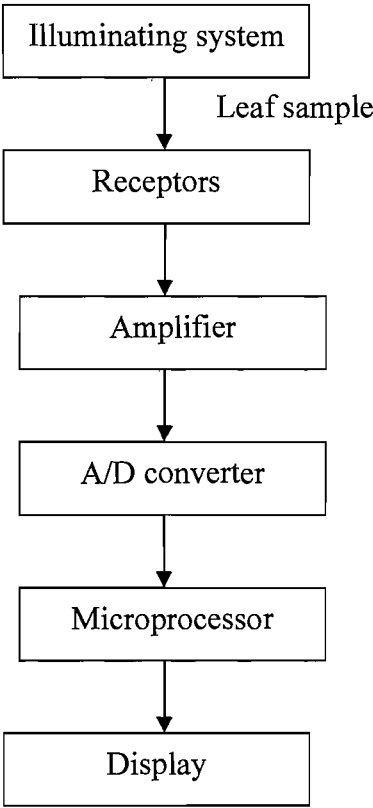


Figure 5.3. Flow diagram of SPAD-502 processing steps.

Chlorophyll concentration varies across a leaf. Therefore, it was decided to find the minimum number of samples to represent the whole leaf. The number of samples required to satisfy a defined level of confidence for a given error may be determined by equation 5.1 (Rao and Ulaby, 1977)

$$SN = (\sigma_s t / a)^2 \tag{5.1}$$

Where,

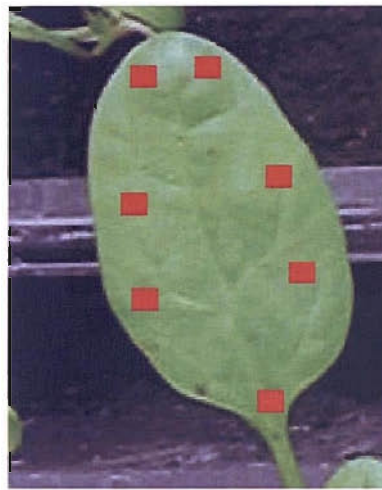
SN= Sample number

σ = standard deviation of the measured value

t= students t value for n-1 at the confidence level of 95%

a= required degree of accuracy

3 leaf samples were collected from the greenhouse, SPAD values were collected at different points on each leaf and sample numbers for each leaf was estimated (appendix). It was found that 7 SPAD measurements for each leaf represented the variability within a leaf with 95% confidence (figure 5.4).



■ SPAD measurement points

Figure 5.4. SPAD measurement points on a leaf.

For each IFOV of GER-1500 5 leaves were chosen representing the maximum variation in chlorophyll concentration and SPAD measurements were taken for each one. A total of 945 SPAD measurements were taken on each day of measurement (table 5.2).

LAI measurement

The size and distribution of spinach plants within the tray were not suitable for measurement using an LAI meter. Therefore, it was decided to use a digital

photograph based estimation of LAI. Digital photographs were taken using an Olympus C-760 digital camera (Olympus, 2005). This uses a charge coupled device to record 3.2 million pixels. The camera was placed at 1 m height and nadir view photographs of each tray were taken for further analysis.

5.2.2.3. Canopy data processing

Spectral data processing

The radiance recorded by the GER-1500 were converted to absolute reflectance by ratioing the target and reference spectral data and then applying a correction using a panel calibration (using REFG1500.EXE (appendix) (NERC, 2005)).

For each disc the following were calculated:

1. Simple Ratio (SR) = $\frac{R_{NIR}}{R_{Red}}$

Where R_{NIR} and R_{Red} are reflectances in NIR and red wavelengths respectively.

2. Normalised Difference Vegetation Index (NDVI) = $\frac{R_{NIR} - R_{Red}}{R_{NIR} + R_{Red}}$

Where R_{NIR} and R_{Red} are reflectances in NIR and red wavelengths respectively.

3. REP estimated using the maximum of first derivative of the reflectance spectra. The derivative spectrum can be estimated by

$$D_{\lambda(i)} = \frac{R_{\lambda(i)} - R_{\lambda(i-1)}}{\Delta\lambda}$$

Where, $R_{\lambda(i)}$ and $R_{\lambda(i-1)}$ are reflectances at wavelength i and $(i-1)$ respectively.

4. REP estimated using the linear interpolation (Guyot et al., 1988).

$$REP = 700 + 40 \frac{(R_i - R_{700})}{(R_{740} - R_{700})}$$

where $R_i = \frac{(R_{670} + R_{780})}{2}$

Where R_{670} , R_{700} , R_{740} and R_{780} are reflectance at wavelength 670 nm, 700 nm, 740 nm and 780nm respectively.

5. REP estimated using Lagrangian interpolation (Dawson and Curran, 1998).

$$REP = \frac{A(\lambda_i + \lambda_{i+1}) + B(\lambda_{i-1} + \lambda_{i+1}) + C(\lambda_{i-1} + \lambda_i)}{2(A + B + C)}$$

$$\text{Where, } A = \frac{D\lambda_{(i-1)}}{(\lambda_{i-1} - \lambda_i)(\lambda_{i-1} - \lambda_{i+1})}, \quad B = \frac{D\lambda_{(i)}}{(\lambda_i - \lambda_{i-1})(\lambda_i - \lambda_{i+1})},$$

$$C = \frac{D\lambda_{(i+1)}}{(\lambda_{i+1} - \lambda_{i-1})(\lambda_{i+1} - \lambda_i)}$$

In this case $D\lambda_{(i-1)}$, $D\lambda_{(i)}$, $D\lambda_{(i+1)}$ are the first derivative reflectances

corresponding to wavebands $\lambda_{(i-1)}$, $\lambda_{(i)}$, $\lambda_{(i+1)}$ respectively ($\lambda_{(i)}$ is the band with maximum first derivative reflectance with $\lambda_{(i-1)}$ and $\lambda_{(i+1)}$ representing the bands either side of it).

6. Medium Resolution Imaging Spectrometer (MERIS) Terrestrial Chlorophyll Index (MTCI) (Dash and Curran, 2004)

$$MTCI = \frac{R_{Band10} - R_{Band9}}{R_{Band9} - R_{Band8}} = \frac{R_{753.75} - R_{708.75}}{R_{708.75} - R_{681.25}}$$

Where $R_{753.75}$, $R_{708.75}$, $R_{681.25}$ are the normalised surface reflectance in the centre wavelengths of band 8, 9 and 10 in the MERIS standard band setting. MTCI is computationally simpler and known to be sensitive to higher values of chlorophyll content than the red edge position.

Only REP estimated by Linear and Lagrangian methods were used here because these two techniques were used earlier to estimate the REP using MERIS standard band setting. These values could then be compared with MTCI.

Chlorophyll concentration data processing

To convert each SPAD values into chlorophyll concentration value, the SAPD was calibrated with chlorophyll concentration data extracted from spinach leaves.

SPAD Calibration

60 discs (diameter 22 mm) were cut from spinach leaves and SPAD measurements were undertaken (5 SPAD measurements per disc) immediately following the SPAD measurement discs were placed in 1 ml of DMF (N, N-dimethylformamide; analytical grade; Fisher Scientific). DMF is a superior solvent to acetone for the purposes of chlorophyll extraction as it overcomes problems such as incomplete extraction and variable evaporation during processes such as maceration, centrifugation, filtration and spectrophotometric analysis (Wellburn, 1994). Direct leaf immersion in DMF resulted in equally efficient chlorophyll extraction as pre-grinding the leaf and then immersing (Moran and Porath, 1980). Therefore, leaf discs were left in DMF and kept at 4 °C in the dark for 48 hrs for the extraction of leaf pigments.

Chlorophyll extraction

Each sample was diluted (1:10 with DMF) to fall within the sensitive and linear range of the spectrophotometer. The mean of the three technical replicate dilutions of each biological sample was used to represent the amount of chlorophyll within that sample and this was the sum of chlorophyll a and chlorophyll b ($\mu\text{g ml}^{-1}$) determined using specific extinction coefficients (Wellburn, 1994) for a spectrophotometer with a 1 - 4 nm spectral resolution as detailed below. With a known sample area (379.94 mm^2) chlorophyll concentration was expressed as mg m^{-2} .

$$\text{Chlorophyll a} = 11.65 * A_{664} - 2.69 * A_{647}$$

$$\text{Chlorophyll b} = 20.81 * A_{647} - 4.53 * A_{664}$$

Where A_{647} and A_{664} are the sample absorptions at 647 nm and 664 nm measured using a Hitachi U-2000 spectrophotometer (Hitachi, 2005).

SPAD values corresponding to each chlorophyll concentration values were correlated with coefficient of determination (r^2) 0.86 for chlorophyll-a concentration and 0.84 for chlorophyll-b concentration (figure 5.5). Chlorophyll concentration can be estimated by

$$\text{Chlorophyll-a concentration (mg m}^{-2}\text{)} = 0.36 * \text{SPAD}^2 - 12.44 * \text{SPAD} + 276.64$$

$$\text{Chlorophyll-b concentration (mg m}^{-2}\text{)} = 0.11 * \text{SPAD}^2 - 4.30 * \text{SPAD} + 100.22$$

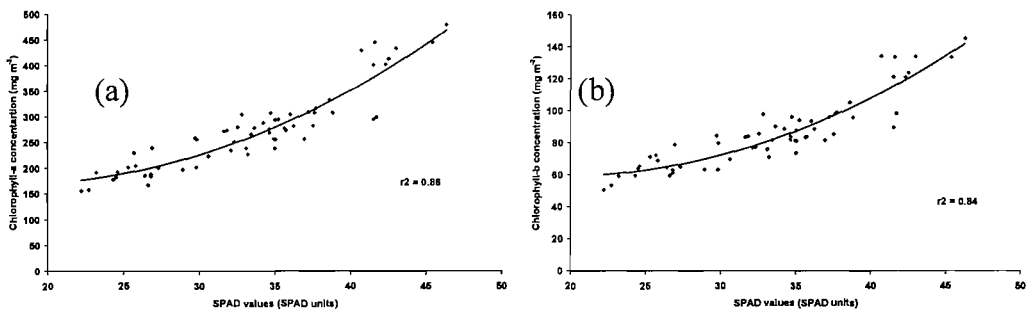


Figure 5.5. Correlation between SPAD values with chlorophyll a concentration (a) and chlorophyll b concentration (b) for spinach.

LAI data processing

Digital image processing was carried out for estimating the LAI for each IFOV of the spectral measurement. Image of each tray was referenced and the region of interest (ROI) corresponding to each IFOV was extracted (figure 5.6). Individual leaf within a single ROI was digitized and the area of each leaf was calculated. For leaves which were not clearly visible from the top approximate digitization was carried out. The sum of all leaf area was divided by the area of the IFOV (88.2 cm^2) to obtain the LAI.

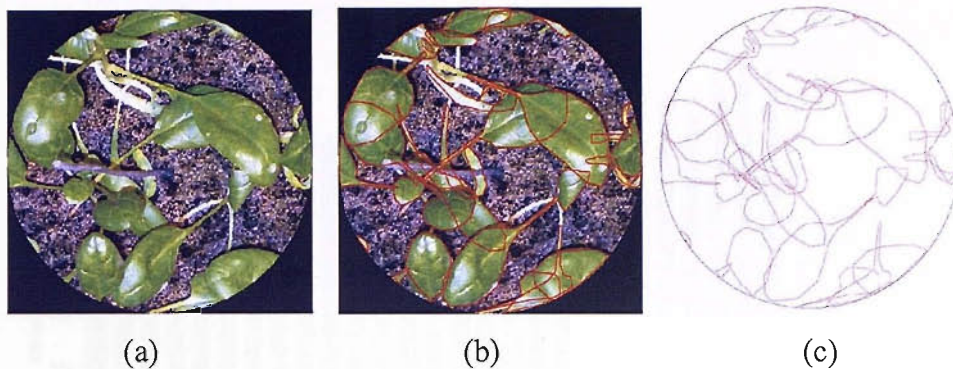


Figure 5.6. Estimation of LAI from a digital photo (a) Extraction of IFOV image, (b) digitisation of individual leaf and (c) estimation of area.

Chlorophyll content was obtained by multiplying the LAI with the chlorophyll concentration of individual IFOV.

5.2.2.4. Statistical significance of data

At the end of the experiment there were 108 spectral measurements, each measurement associated with a chlorophyll concentration, LAI and chlorophyll content. There was no visual difference between chlorophyll concentrations due to the fertilisation treatment, however, for each treatment chlorophyll concentration increased up to the third week and then decreased as leaf chlorophyll started to decompose (figure 5.7a). However, fertilisation made some visual difference in LAI, plants receiving high fertilisation treatment had a higher

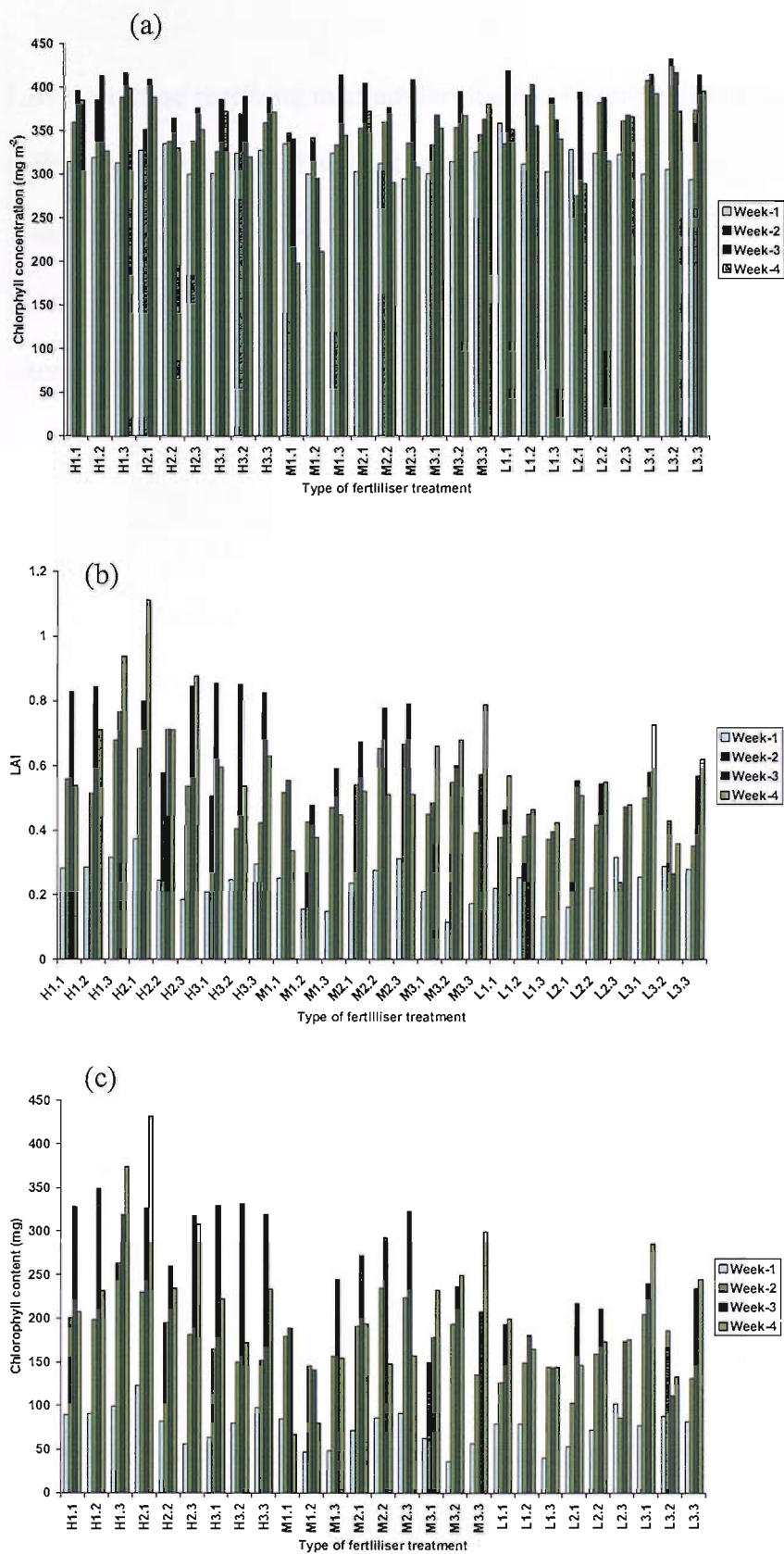


Figure 5.7. Variation of (a) chlorophyll concentration, (b) LAI and (c) chlorophyll content through out the experiment.

LAI than those receiving medium fertilisation (figure 5.7b). As a result there was difference in chlorophyll content among the treatments (figure 5.7c).

Analysis of variance (ANOVA) was undertaken to find the statistical significance between the different treatments on chlorophyll concentration, LAI and chlorophyll content (table 5.4).

Number of week	Chlorophyll concentration (mg m ⁻²)	LAI	Chlorophyll content (mg)
Week-1	0.714	0.112	0.78
Week-2	0.181	0.002	0.027
Week-3	0.164	0.000	0.000
Week-4	0.049	0.005	0.009

Table 5.4. Statistical significance values from ANOVA for chlorophyll concentration, LAI chlorophyll content through out the experiment.

It was found that:

- Before the start of fertilisation (week-1) there was no statistically significant difference in chlorophyll concentration, LAI and chlorophyll content between trays.
- Due to the fertilisation, there was no statistically significant difference between chlorophyll concentrations between each treatment except on week-4 (when chlorophyll started to decompose).
- Due to the fertilisation treatment there was a statistically significant difference in LAI and chlorophyll content.

5.2.2.5. Leaf measurements

Spectral reflectance of and biochemical measurements of spinach leaf were undertaken to study the effect of change in irradiance on the red edge and thereby, on SR, NDVI, REP and MTCI. The amount and distribution of chloroplast which contains chlorophyll within a leaf cell depends on several biophysical and environmental variables (Wada *et al.*, 2003). One of the important variables is the level of irradiance.

When plants are exposed to higher levels of irradiance than those required by photosynthesis, chloroplasts may be damaged in a process termed photoinhibition (Long *et al.*, 1994). To overcome this damage plants have developed several protective mechanisms such as energy dissipation through pigments of the xanthophyll cycle (DemmigAdams & Adams, 1996) and chlorophyll fluorescence (Horton *et al.*, 1994). One among those protective mechanisms is the relocation of chloroplasts from the cell surface to the side walls of the cells, so reducing the area available for light capture (Kasahara *et al.*, 2002). When plants are exposed to low levels of irradiance chloroplasts orientate perpendicular to the light direction in order to increase light absorption (Park *et al.*, 1996). These photorelocations (movements of chloroplast within a cell due to change in the level of irradiance) are species dependent (Brugnoli & Björkman, 1992, Park *et al.*, 1996, Cate & Perkins, 2003; Martínez & Guiamet, 2004; Pandey *et al.*, 2005) and explain the under-estimation of chlorophyll content at high levels of irradiance (Hoel & Solhaug, 1998) using a handheld chlorophyll content meter. Hoel & Solhaug (1998) reported an 8% variation and Martínez & Guiamet (2004) reported a 5% variation in chlorophyll content meter values with varying level of irradiance. However, little information exists on the effect of this photorelocation on the red edge.

The influence of incident irradiance upon leaf function needs to be addressed as it may affect the red edge and so create errors in the remotely sensed estimation of chlorophyll content and thereby, vegetation condition.

Experimental setup

One spinach tray which was grown separately was subjected to two levels of irradiance each for two hours: $150 \mu\text{mol s}^{-1} \text{m}^{-2}$ referred as medium irradiance and $20 \mu\text{mol s}^{-1} \text{m}^{-2}$ referred as low irradiance. Following each irradiance treatment one leaf from each of eight spinach plants were selected and three 22 mm diameter discs were extracted. A total of 24 discs for spinach from each irradiance treatment were extracted; both spectral reflectance and chlorophyll content of each disc were measured.

Spectral reflectance measurement

Spectral reflectance was measured using a GER-1500 field spectrometer. An elevated platform was prepared and covered with a black cloth (~100 % absorption) to minimise background reflectance. The IFOV of the sensor lay well within the perimeter of the disc and three replicate spectral reflectance measurements were taken per disc.

The radiance of each disc recorded by the GER-1500 was converted to absolute reflectance by taking the ratio of the target (leaf) with the reference spectral data, then applying a correction using a panel calibration (NERC, 2005). Each spectral measurement was converted to absolute reflectance (using REFG1500.EXE) and SR, NDVI, REP and MTCI were estimated.

Chlorophyll concentration measurements

Immediately following the spectral measurement discs were placed in 1 ml of DMF and the chlorophyll concentration measurements followed the same pattern as explained in section 5.2.2.3.

5.2.3 Poplar (*Populus deltoids*) data

5.2.3.1. Canopy measurements

Canopy spectral reflectance, chlorophyll concentration and LAI measurements were undertaken for 11 poplar plants.

Spectral measurement

Similar measurement procedure to that followed for spinach was used to take spectral reflectance measurements for each poplar plant. In each pot the height of poplar plant was different; therefore, the height of GER-1500 was changed in each measurement to acquire data at a constant IFOV (10.6 cm diameter). 5 spectral measurements were undertaken per pot.

Chlorophyll measurement

A procedure similar to that used for the spinach analysis (section 5.2.2.3) was used to estimate the chlorophyll concentration; however the equations for calibration SPAD were different. A solution of 1:12 was used for chlorophyll extraction of individual discs.

SPAD values corresponding to each chlorophyll concentration values were correlated with coefficient of determination (r^2) 0.97 for chlorophyll-a concentration and 0.96 for chlorophyll-b concentration (figure 5.8). Chlorophyll concentration can be estimated by

$$\text{Chlorophyll-a concentration (mg m}^{-2}\text{)} = 0.14 * \text{SPAD}^2 + 3.83 * \text{SPAD} + 3.73$$

$$\text{Chlorophyll-b concentration (mg m}^{-2}\text{)} = 0.03 * \text{SPAD}^2 + 1.62 * \text{SPAD} + 1.20$$

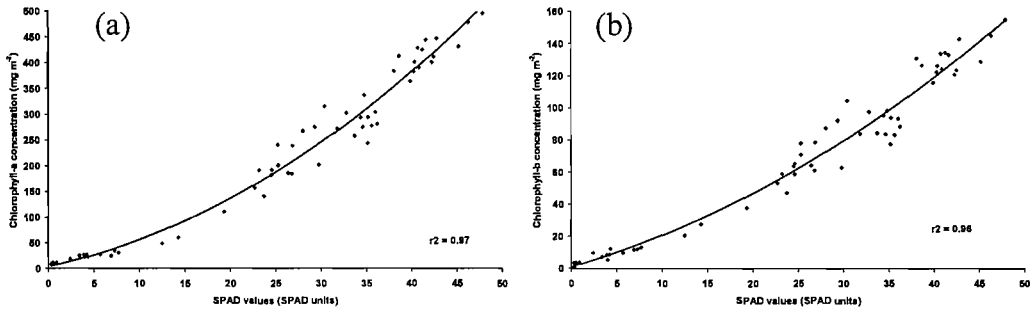


Figure 5.8. Correlation between SPAD values with chlorophyll a concentration (a) and chlorophyll b concentration (b) for poplar.

LAI measurement

Similar procedure to that followed for spinach was used to determine the LAI of an individual poplar plant. Chlorophyll content was obtained by multiplying the LAI with the chlorophyll concentration for each IFOV.

5.2.3.2. Leaf measurements

Like spinach, spectral and biochemical measurements of poplar leaves were also undertaken to study the effect of irradiance on SR, NDVI, REP and MTCI. Eleven trees (selected in previous experiment) were subjected to three levels of irradiance each for two hours: $300 \mu\text{mol m}^{-2} \text{s}^{-1}$ referred to as high irradiance, $150 \mu\text{mol s}^{-1} \text{m}^{-2}$ referred to as medium irradiance and $20 \mu\text{mol s}^{-1} \text{m}^{-2}$ referred to as low irradiance. Following each irradiance treatment one leaf from each of eleven poplar trees and three 22 mm diameter discs from each leaf were extracted. A total of 33 discs for poplar from each irradiance treatment were extracted; both spectral reflectance and chlorophyll concentration similar to spinach leaf for each disc were measured.

5.2.4 Results and discussion for spinach

5.2.4.1. Relation between chlorophyll content and reflectance in individual MERIS Bands

Canopy spectral reflectance for spinach was averaged for individual MERIS bands according to band width of each band. Six spectra for spinach representing a range in chlorophyll content (36 mg to 432 mg) (figure 5.9) at MERIS standard band positions are given here. The spectrum for the highest chlorophyll content (432 mg) had lowest reflectance in band 8 (centered at 681.25 nm) and highest reflectance in band 11 (centered at 760.62 nm). However, band 11 is associated with oxygen absorption and therefore, it is not provided in MERIS standard L2 products (ESA, 2005). So, if it is ignored then the highest reflectance of vegetation spectra was obtained at band 10 (centered at 753.75 nm) (figure 5.9).

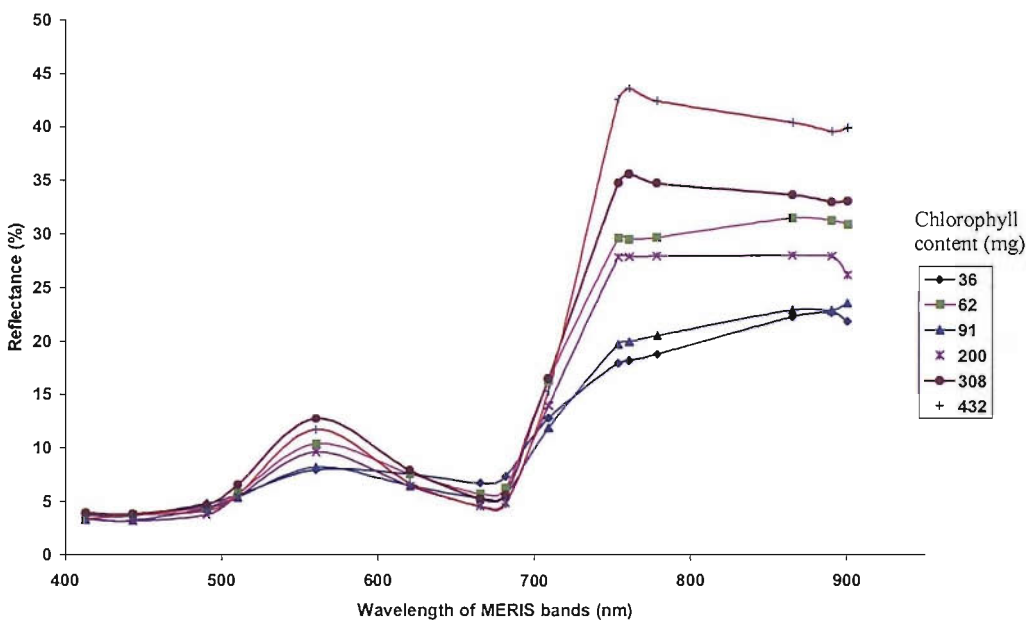


Figure 5.9. Spectral reflectance at MERIS standard band setting for a wide range of chlorophyll content.

In the standard band setting, MERIS has six discontinuous wavebands (Band 7, 8, 9, 10, 11 and 12) in red and near infrared (NIR) wavelengths. Spectral

reflectances of each of the above bands (except band 11) were correlated with chlorophyll content for both species (figure 5.10).

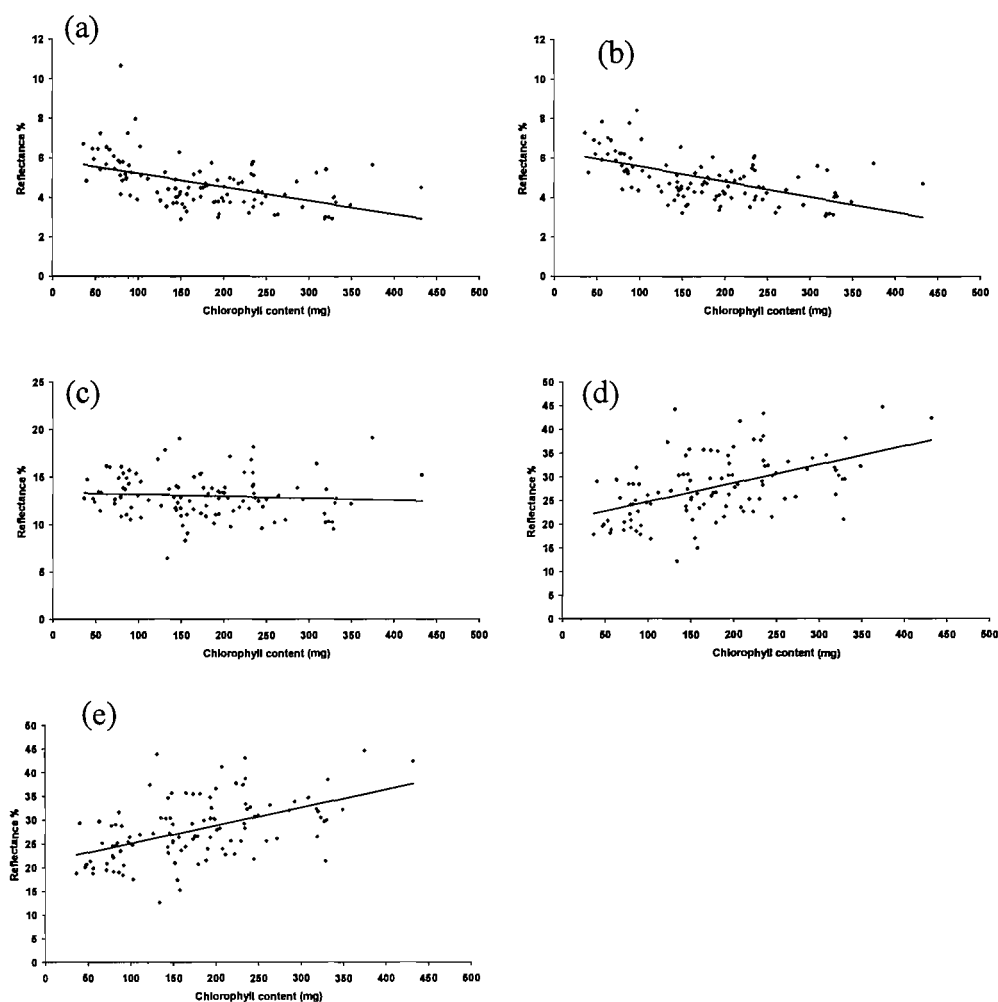


Figure 5.11. Relation between chlorophyll content and reflectance in MERIS band 7(a), band 8 (b), band 9 (c), band 10 (d) and band 12 (e) for spinach.

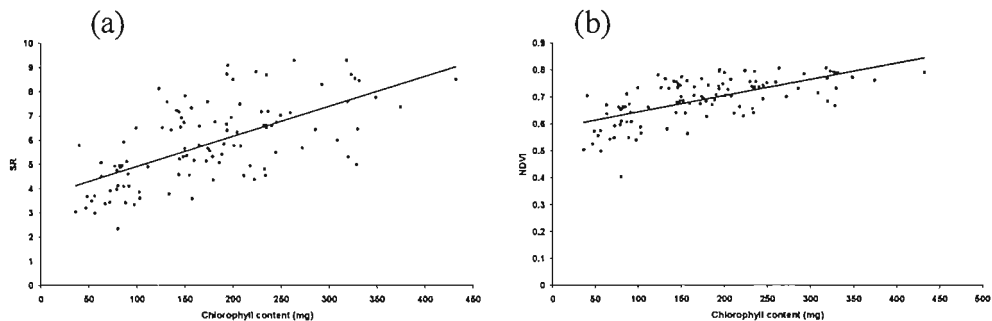
Reflectance in band 7 and band 8 had a negative relationship with chlorophyll content with band 8 having the stronger one. Reflectance in band 9 has a very weak relationship with chlorophyll content. Whereas, band 10 and band 12 has a positive relationship with chlorophyll content with band 10 having the stronger one.

5.2.4.2. Effect of chlorophyll content

The chlorophyll content through the experiment varies from 36.1 mg to 432.3 mg. SR, NDVI, REP and MTCI were related to the total chlorophyll content of all data set (n=106) (2 data were ignored due to problem in them) (figure 5.12).

Reflectance indices	Chlorophyll content (mg)	Chlorophyll a:b	LAI
SR	0.41	0.19	0.42
NDVI	0.4	0.22	0.4
REP (Max first derivative)	0.42	0.22	0.42
REP (linear)	0.55	0.52	0.47
REP (Lagrangian)	0.51	0.46	0.45
MTCI	0.58	0.48	0.49

Table 5.5. Coefficient of determination of different estimators with chlorophyll content, chlorophyll a:b and LAI.



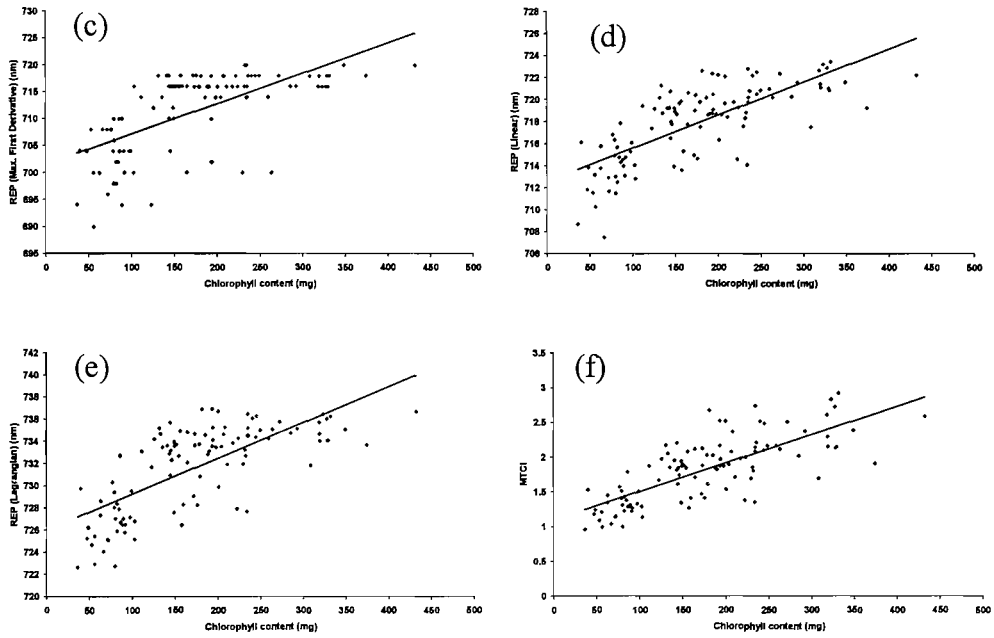


Figure 5.12. Relationship between chlorophyll content and SR (a), NDVI (b), REP estimated by maximum of first derivative (c), REP estimated by linear interpolation (d), REP estimated by Lagrangian interpolation (e) and MTCI (f) for spinach.

MTCI had the strongest ($r^2 = 0.58$) and NDVI had the weakest ($r^2 = 0.4$) positive correlation with chlorophyll content (table 5.5). Among the techniques used to estimate the REP, linear interpolation had the strongest ($r^2 = 0.55$) and maximum of first derivative had the weakest ($r^2 = 0.42$) correlation with chlorophyll content. Among all reflectance indices, the regression line for NDVI had the gentler slope, indicating less sensitivity to a change in chlorophyll content.

5.2.4.3. Problem with the Lagrangian Interpolation technique

While estimating the REP using Lagrangian interpolation technique for the MERIS standard band setting, for some cases, it over estimated the REP (especially at high chlorophyll content). Some of these cases were identified (figure 5.13a) and derivative spectra at MERIS standard band setting were determined (figure 5.13b). Similarly, five canopy spectra where Lagrangian interpolation technique was not over

estimating the REP were also identified for a comparison (figure 5.14a) and derivative spectra were determined (figure 5.14b).

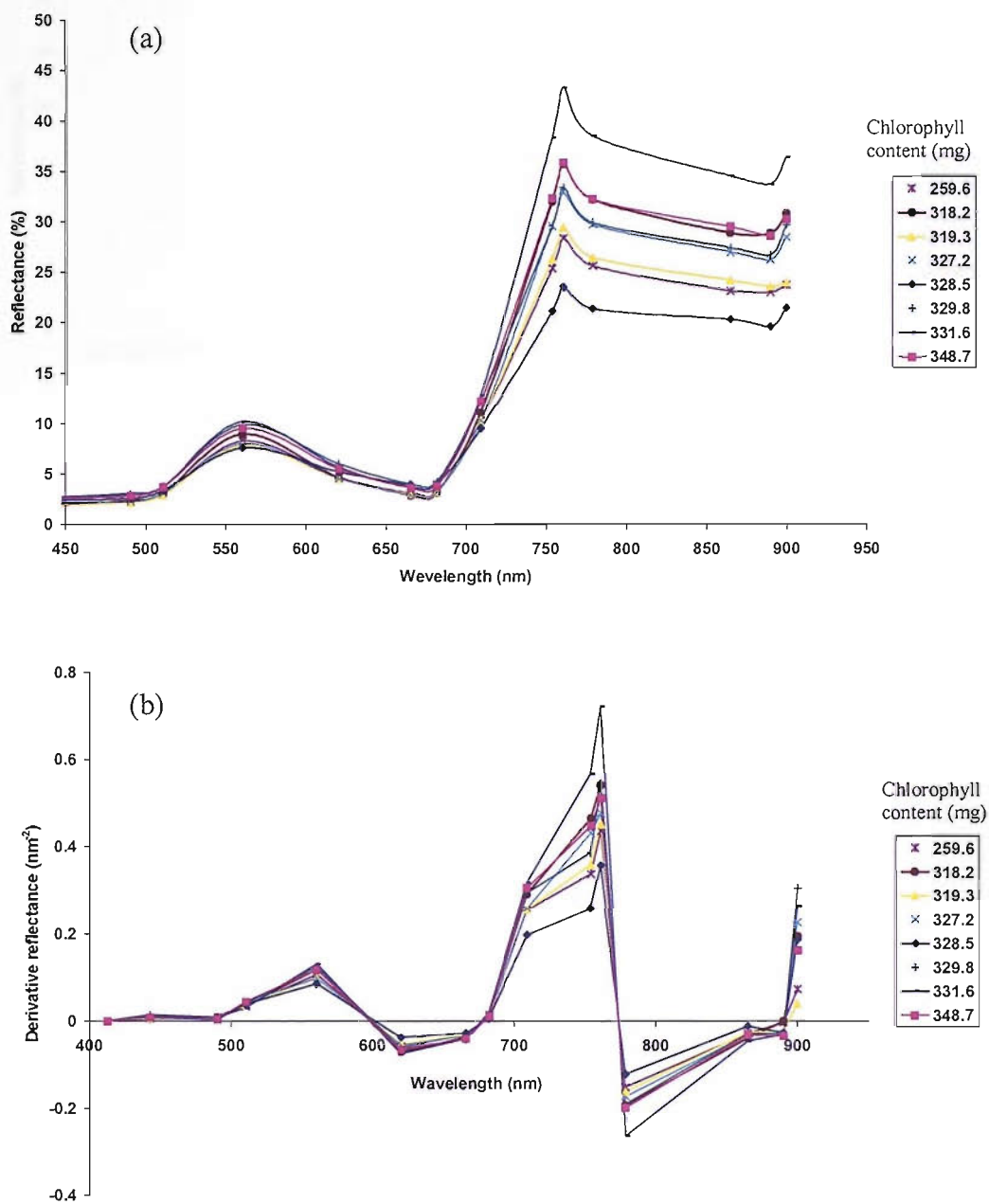


Figure 5.13. Reflectance spectra at MERIS standard band setting for cases where Lagrangian interpolation over estimated the REP (a) and derivative spectra (b).

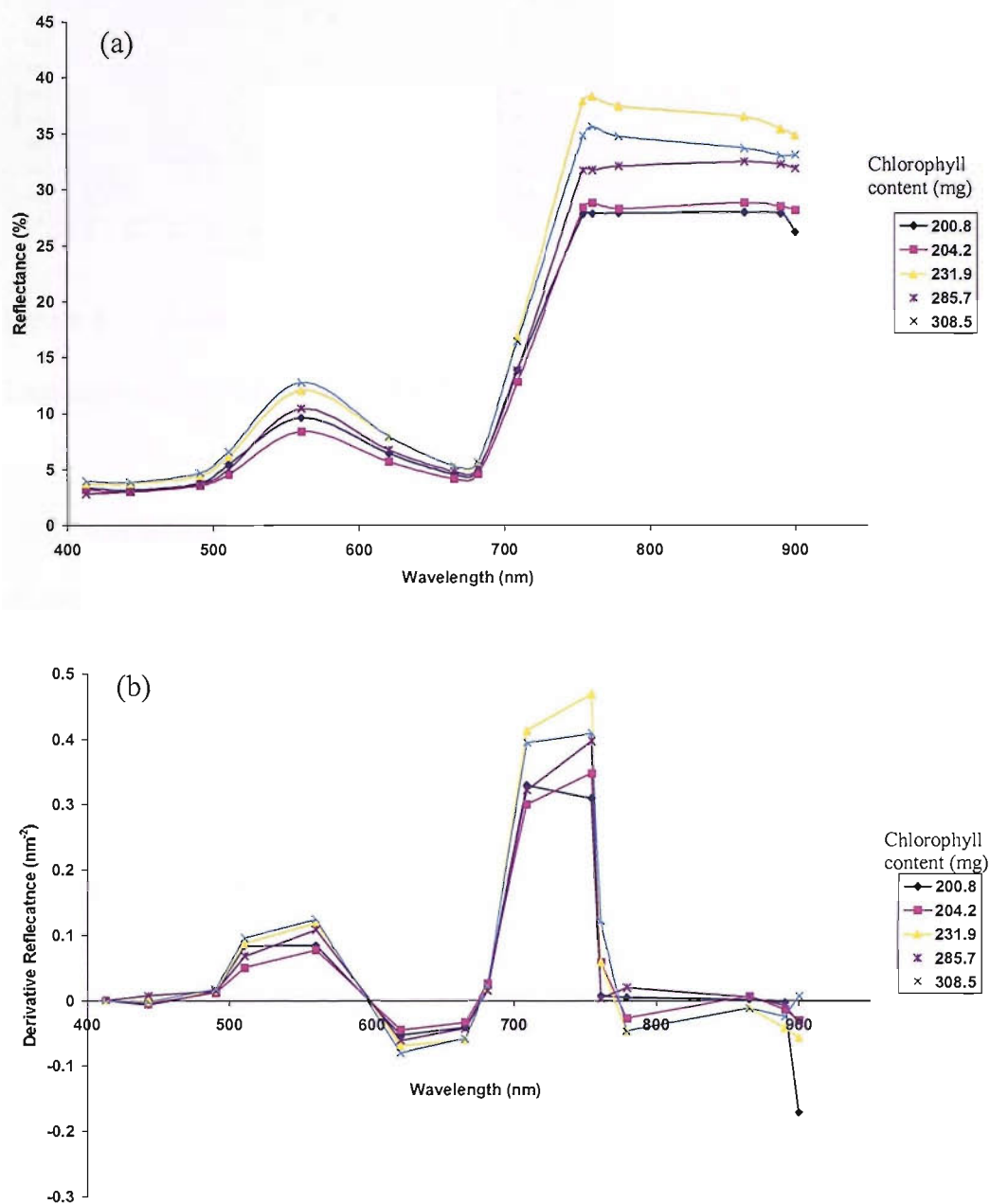


Figure 5.14. Reflectance spectra at MERIS standard band setting for cases where Lagrangian interpolation did not over estimate the REP (a) and derivative spectra (b).

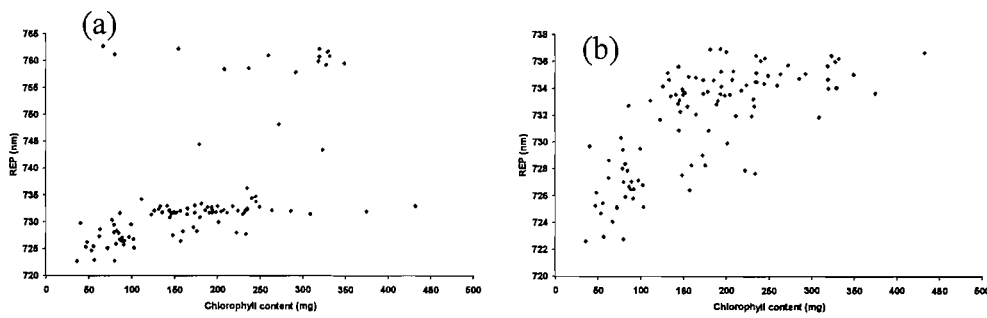


Figure 5.15. Relationship between chlorophyll content and REP estimated by Lagrangian interpolation using band 11 (a) and not using band 11(b).

There was an unusual increase in reflectance at band 11 (figure 5.13a) in MERIS standard band setting for those spectra where there is an over estimation of REP. Interestingly, this small increase in reflectance produced a high derivative reflectance at band 11.

A high derivative reflectance could be produced either by a high difference in reflectance or a low difference in wavelength between neighbouring bands. In this case the latter was true. Because difference between B11 and B10 (6.875 nm) is the lowest among all neighbouring MERIS bands, a little increase in reflectance could produce a higher derivative reflectance. Therefore, for those case where there was an over estimation of REP, B11 produced the maximum of derivative reflectance at MERIS standard band setting.

The Lagrangian interpolation technique uses three wavebands, i.e., the waveband having the maximum of first derivative spectrum, the one preceding it and the one succeeding it. In the cases where there was an over estimation of REP, the Lagrangian interpolation was using band 10, 11 and 12. All of them lie in the NIR region, therefore it overestimated the REP.

It was decided not to include band 11, while estimating REP using Lagrangian interpolation technique for MERIS standard band setting, because

1. Band 11 is not present in the red edge region of the vegetation spectrum.
2. A small increase in reflectance at band 11 produced a large increase in derivative spectra, resulting an over estimation of REP.
3. Band 11 is not present in standard ESA L2 product, because it is associated with oxygen absorption.

REP estimated by Lagrangian interpolation technique without using the band 11 resulted in a robust estimation of REP (figure 5.15).

5.2.4.4. Relation between different REP for MERIS

REP estimated by the maximum of first derivative method was compared with the two techniques that had been used to estimate the REP from MERIS spectra: Lagrangian interpolation and linear interpolation (figure 5.16).

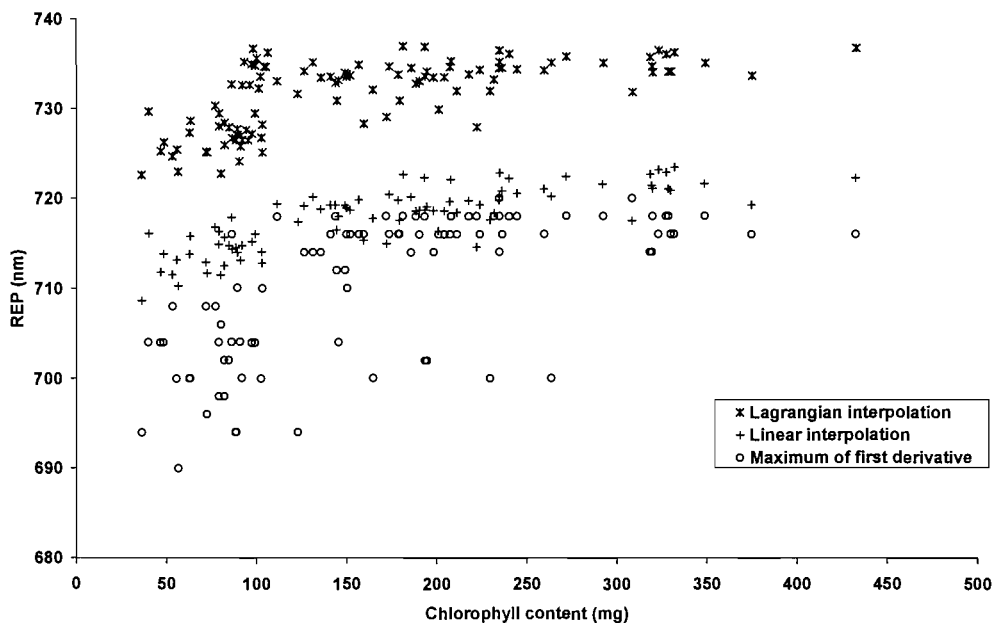


Figure 5.16. Relationship between REP estimated by different methods and chlorophyll content.

Both techniques over-estimated the REP compared to the one estimated using the maximum of first derivative. However, REP estimated by Linear interpolation had slightly stronger correlation ($r^2 = 0.43$) than Lagrangian interpolation ($r^2 = 0.42$) with

REP estimated by maximum of first derivative (figure 5.17). For both techniques REP became saturated with increase in chlorophyll content. It was clear from this result that, even for the same data, one could have different REP. the REP is largely dependent on the method used.

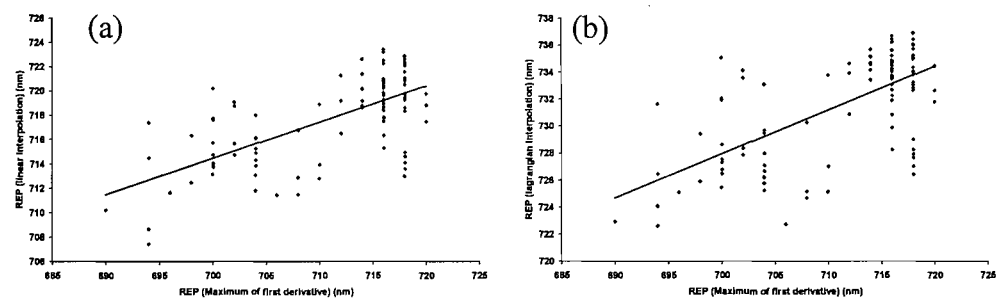


Figure 5.17. Relationship between REP estimated by (a) maximum of first derivative and linear interpolation; (b) maximum of first derivative and Lagrangian interpolation.

5.2.4.5. Effect of chlorophyll a:b

Change in chlorophyll a:b may produce a change in reflectance in the red edge region (section 2.8.3), therefore, the effect of change in chlorophyll a:b on reflectance indices was studied. There was little variation in chlorophyll a:b through out the experiment; it varied from 2.8 to 3.33. Four canopy spectra representing chlorophyll a:b of 2.8, 3.0, 3.1 and 3.3 are given in figure 5.18. It appears that there was an increase in absorption in the red wavelengths due to increase in chlorophyll a:b, however, this effect was not consistent for all spectra. SR, NDVI, REP and MTCI were related to the chlorophyll a:b of all data set (n=106) (figure 5.19).

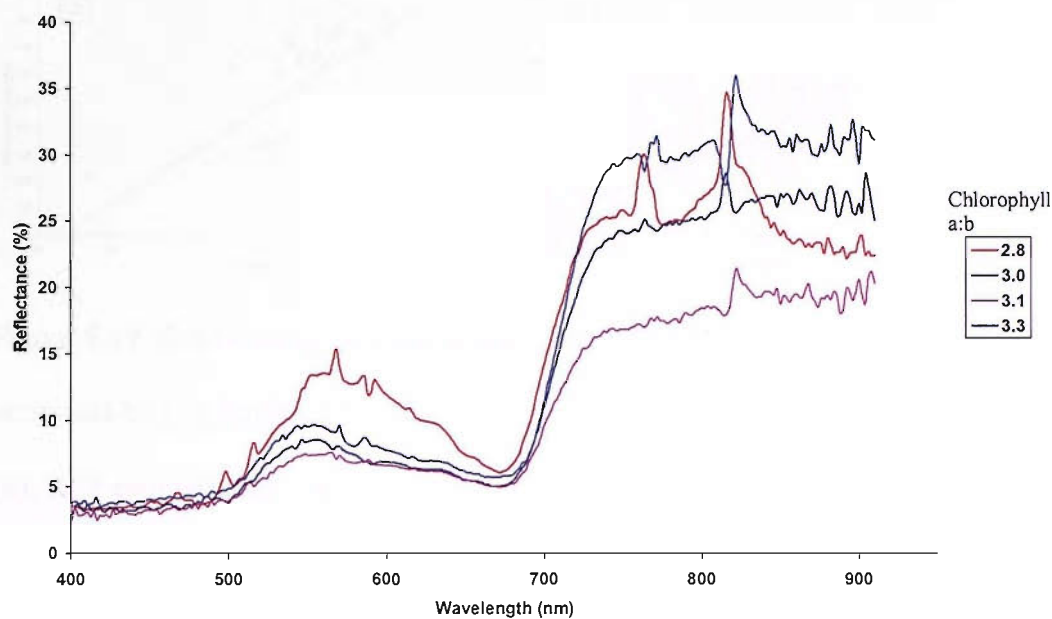
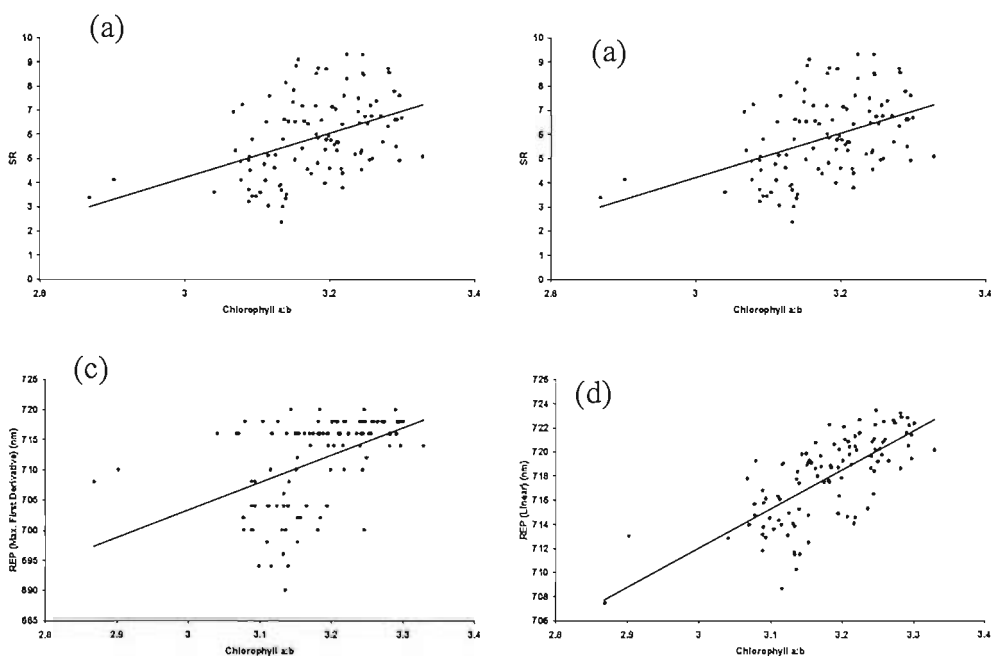


Figure 5.18. Canopy reflectance spectra for different chlorophyll a:b.

REP estimated using linear interpolation technique had the strongest ($r^2 = 0.52$) and SR had the weakest ($r^2 = 0.19$) positive correlation with chlorophyll a:b. MTCI had also a positive relationship with chlorophyll a:b ($r^2 = 0.48$).



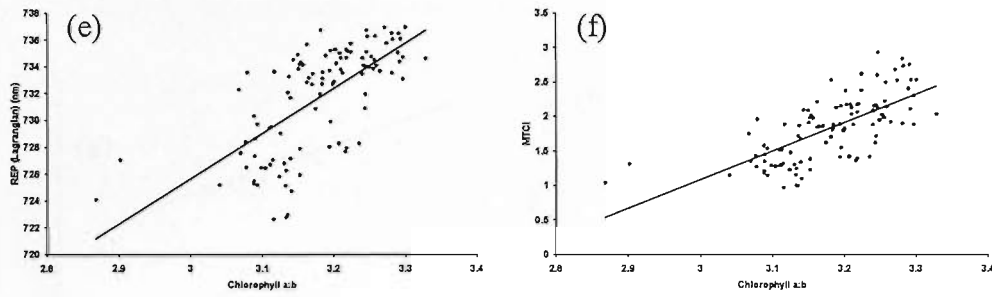


Figure 5.19. Relationship between chlorophyll a:b and SR (a), NDVI (b), REP estimated by maximum of first derivative (c), REP estimated by linear interpolation (d), REP estimated by Lagrangian interpolation (e) and MTCI (f) for spinach.

5.2.4.6. Effect of LAI

Many studies reported the correlation between red and NIR reflectance with LAI (Franklin et al., 1986; Peterson et al., 1988; Gong et al., 1995). Danson and Plummer (1995) found that in addition to chlorophyll content, REP was influenced by LAI (section 2.8.1). During the experiment LAI for the IFOV of the GER-1500 varied from 0.11 to 1.12. Five canopy spectra representing a variation of LAI from 0.16 to 1.12 are given in figure 5.20.

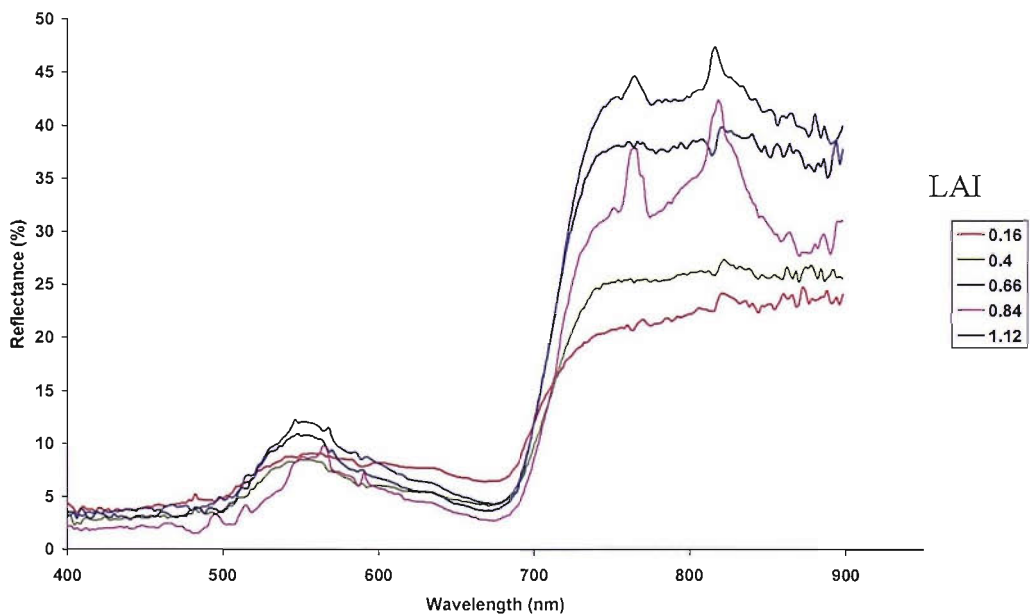


Figure 5.20. Canopy reflectance spectra of spinach for different LAI.

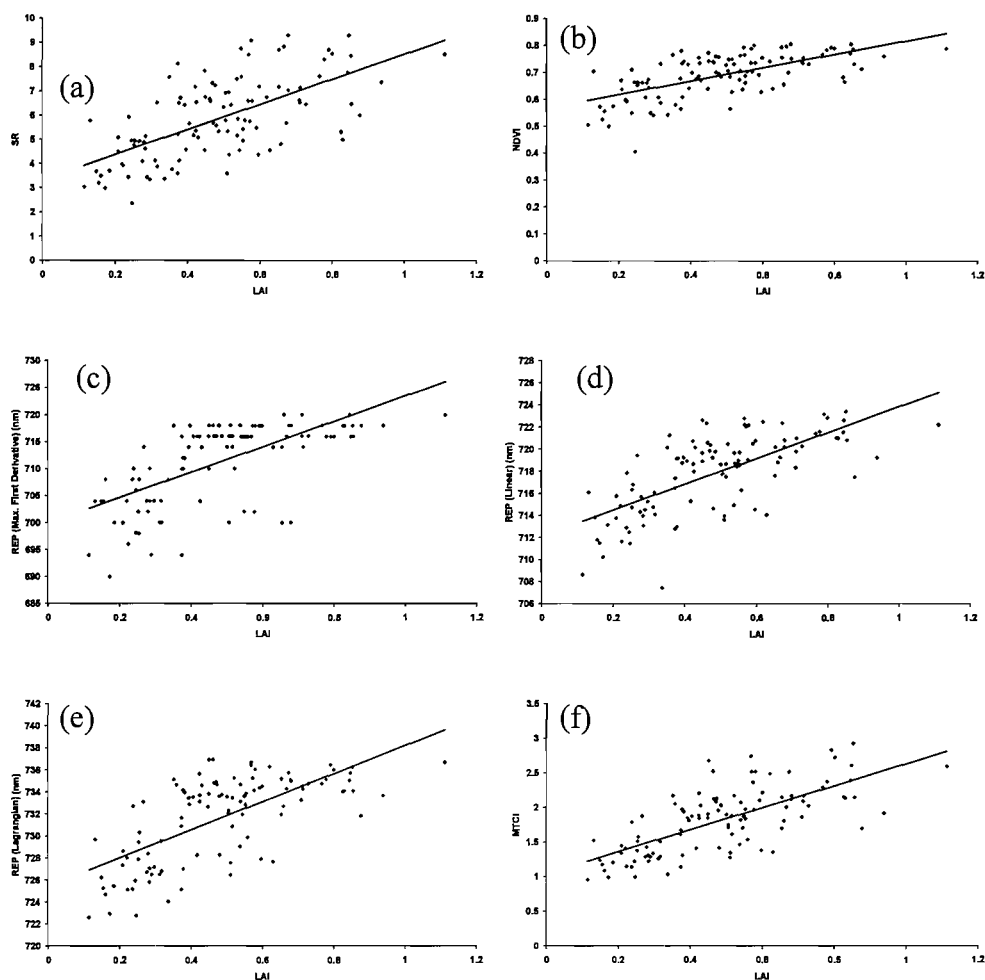


Figure 5.21. Relationship between LAI and SR (a), NDVI (b), REP estimated by maximum of first derivative (c), REP estimated by linear interpolation (d), REP estimated by Lagrangian interpolation (e) and MTCI (f) for spinach.

An increase in LAI resulted in an increase in reflectance in the NIR region. The spectrum with the lowest LAI (0.16) had the lowest NIR reflectance and spectrum with the highest LAI (1.12) had the highest NIR reflectance. However, there was no significant relationship with absorption in the red region. SR, NDVI, REP and MTCI were related to the LAI of all data set (n=106) (figure 5.21).

MTCI had the strongest ($r^2 = 0.49$) and NDVI had the weakest ($r^2 = 0.4$) positive correlation with LAI.

5.2.4.7. Effect of Irradiance

Two reflectance spectra for spinach having very similar chlorophyll concentration (approximately 230 mg m^{-2}) corresponding to low and medium levels of irradiance are presented. (figure 5.22).

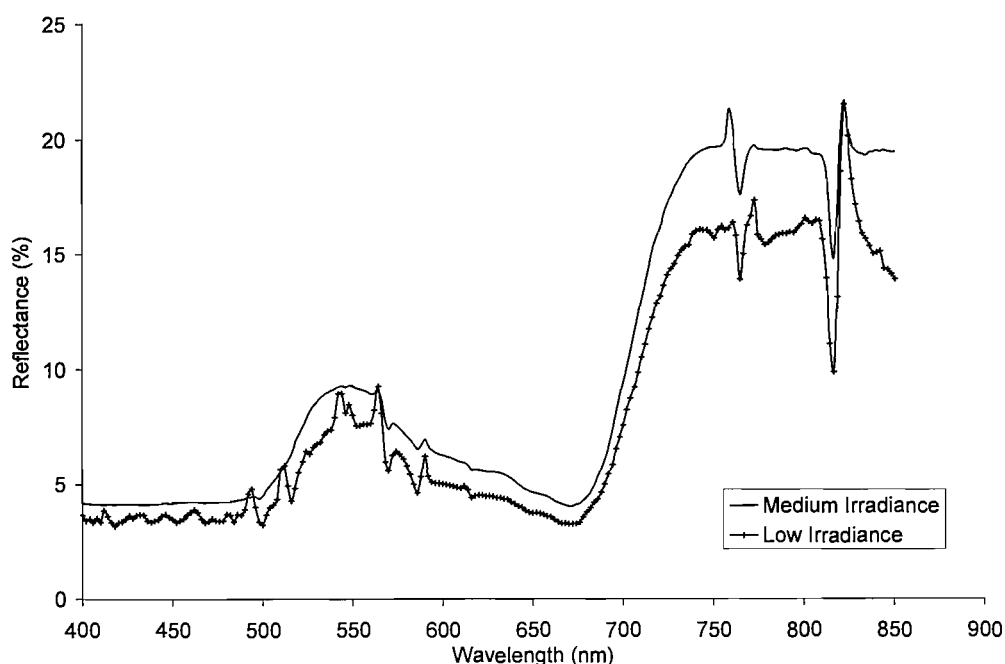


Figure 5.22. Spectral reflectance spectra (a) for spinach at two levels of irradiance

There was an increase in reflectance across all wavelengths of the spectrum with an increase in level of irradiance. In the visible part of the spectrum the absorption was dominated by photosynthetic pigments contained in the chloroplast. With an increase in level of irradiance there was a decrease in absorption, which may be due to the photorelocation of the chloroplast. However, spectral reflectance in the NIR region results from light dissipation due to leaf cellular structure. An increased reflectance in

this region when associated with an increased level of irradiance may be the result of changing cellular turgor and mesophyll airspace, as stomatal conductance responds to the changing irradiance (Will and Teskey, 1999).

Chlorophyll concentration at each level of irradiance was correlated with SR, NDVI, REP and MTCI. A change in the relationship between chlorophyll concentration and these indices were observed due to changes in the level of irradiance (Figure 5.23).

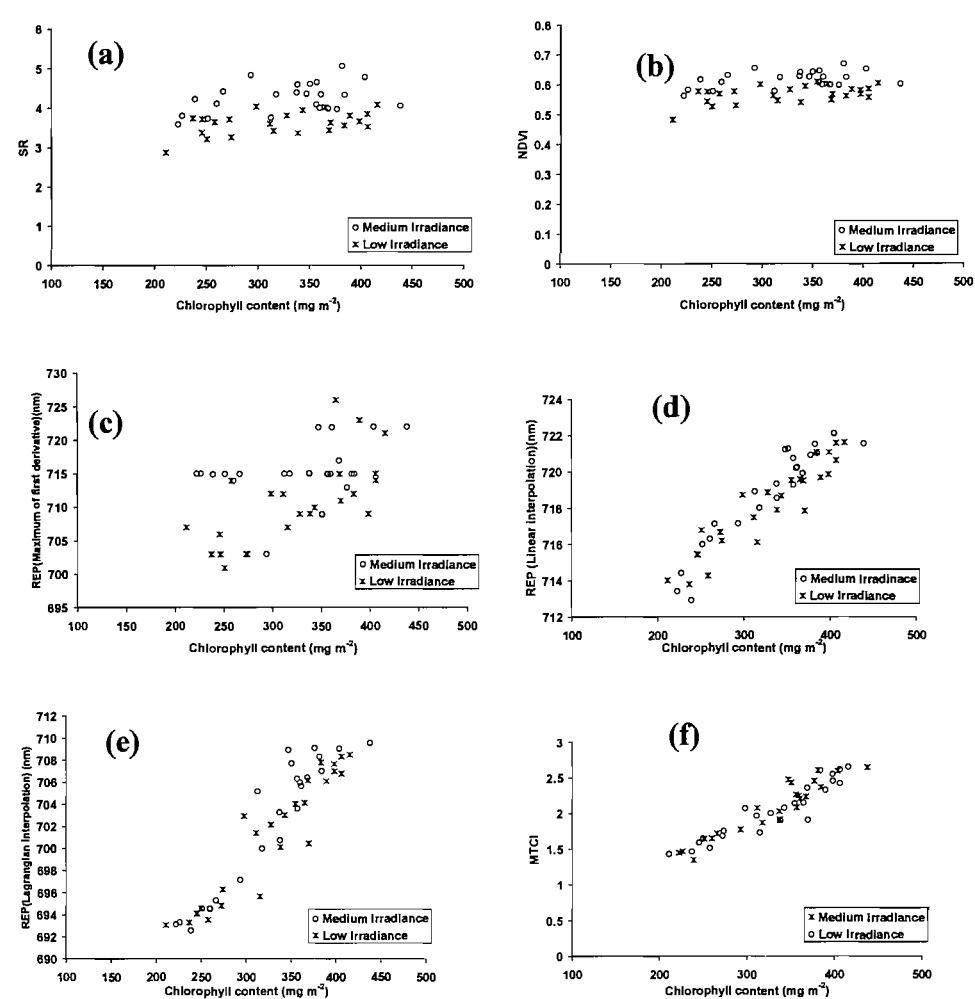


Figure 5.23. Relationships between chlorophyll concentration and SR (a), NDVI (b), REP estimated using the maximum of first derivative (c), REP estimated using linear interpolation (d), REP estimated using Lagrangian interpolation (e) and MTCI (f) at two levels of irradiance for spinach.

At low levels of irradiance SR had the weakest correlation ($r^2 = 0.24$) and both REP estimated using Lagrangian interpolation and MTCI ($r^2 = 0.89$) had the strongest correlations with chlorophyll concentration. At medium levels of irradiance REP estimated using the maximum of first derivative had the weakest correlation ($r^2 = 0.13$) and both REP estimated using Lagrangian interpolation and MTCI ($r^2 = 0.89$) had the strongest correlation with chlorophyll concentration (Table 5.6). At medium levels of irradiance REP estimated using the maximum of the first derivative had a weak correlation with chlorophyll concentration. This appears to result from the superimposition on to the reflectance red edge of an additional reflectance source that interfered with the estimation of derivative spectra. This feature has previously been identified as chlorophyll fluorescence (Zarco-Tejada *et al.*, 2003) and is under further investigation.

Reflectance indices	Coefficient of determination (r^2)		Level of significance
	Low level of irradiance	Medium level of irradiance	
SR	0.22	0.16	0
NDVI	0.24	0.18	0
REP (Max first derivative)	0.49	0.13	0.005
REP (linear)	0.87	0.88	0.24
REP (Lagrangian)	0.89	0.89	0.238
MTCI	0.89	0.89	0.574

Table 5.6. The coefficient of determination for correlations between chlorophyll concentration and reflectance indices at two levels of irradiance (and their statistical significance) for spinach.

Although both REP estimated using the Lagrangian interpolation technique and MTCI had the same coefficient of determination at medium and low irradiance,

the gradients of the regression lines for MTCI were similar to each other at both levels of irradiance. This suggests that, MTCI was less affected by irradiance than other indices by level of irradiance. The statistical significance of the effect of irradiance on relationships between SR, NDVI, REP, MTCI and chlorophyll concentration was evaluated by ANOVA (Table 5.6). Change in irradiance resulted in a statistically significant difference (95% confidence level) on the relationships between SR, NDVI and REP estimated using the maximum of first derivative and chlorophyll concentration. However, a changing level of irradiance did not produce any statistically significant change in the relationship between the other indices and chlorophyll concentration. The REP shifted to a longer wavelength with an increase in level of irradiance for a given chlorophyll concentration. As a result, the REP would underestimate chlorophyll concentration at high levels of irradiance.

5.2.4.8. Moving from leaf to canopy

As we move from leaf to canopy some other variables add to reflectance from the vegetation (section 4.2), therefore, the effect of this scaling-up on REP and MTCI was investigated. Leaf data for REP estimated using linear interpolation and Lagrangian interpolation and MTCI were used, because these data were not significantly affected by change in irradiance.

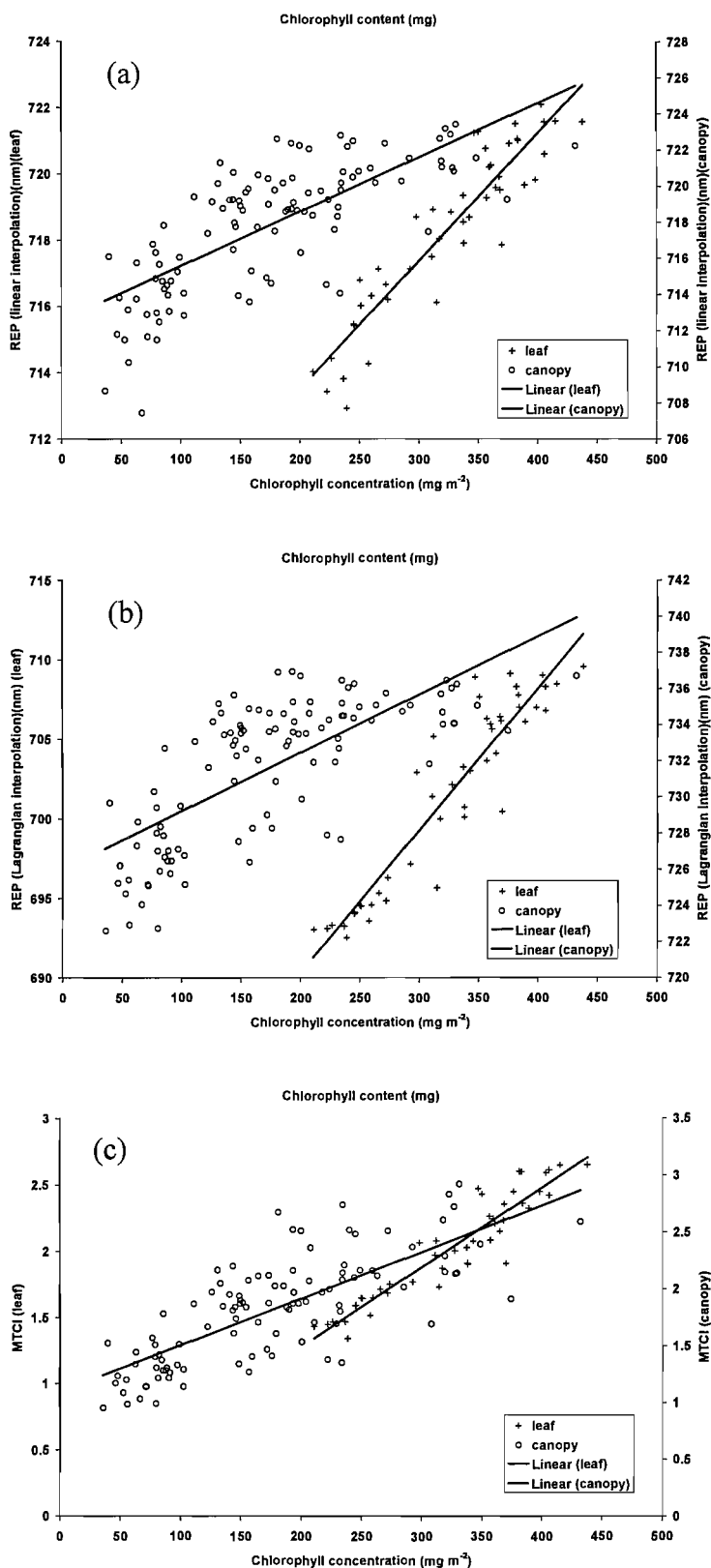


Figure 5.24. Effect of scaling up on relationship between the amount of chlorophyll and REP estimated by linear interpolation (a), Lagrangian interpolation (b) and MTCI (c) for spinach.

While scaling up from leaf to canopy it was observed that, the relationships between chlorophyll content and the reflectance indices (i.e. REP estimated by both linear and Lagrangian interpolation techniques, MTCI) became weaker. All the above reflectance indices at canopy level produced a higher value than leaf level for same chlorophyll content. It was also observed that the regression line for canopy level data was gentler than that for leaf level data. This may be due addition of other variables when moving from leaf to canopy which affects reflectance from the canopy.

5.2.4.9. Conclusions

Followings can be concluded from evaluation of MTCI using spinach data

1. MTCI had the strongest correlation with chlorophyll content and LAI than any other reflectance indices; whereas REP estimated using the linear interpolation technique had the strongest relationship with chlorophyll a:b.
2. Both techniques used to estimate REP using MERIS standard band setting i.e. linear interpolation and Lagrangian interpolation over-estimated the REP.
3. Band 11 in the MERIS standard band setting should be ignored while estimating REP using Lagrangian interpolation techniques to avoid possible over estimation of REP.
4. Change in irradiance resulted in a statistically significant difference on the relationships between SR, NDVI and REP estimated using the maximum of first derivative and chlorophyll content. Care must be taken while estimating those variables at different irradiance.
5. The REP shifted to a longer wavelength with an increase in level of irradiance for given chlorophyll content. As a result the REP would underestimate chlorophyll content at high levels of irradiance.

6. Change in irradiance did not produce a statistically significant difference on the relationships between MTCI and techniques used to estimate REP from MERIS data and chlorophyll content.
7. Scaling up from leaf to canopy weaken the relationship between REP and MTCI with chlorophyll content.

5.2.5 Results and discussion for poplar

There were very few canopy spectral reflectance and chlorophyll content data available for poplar. Therefore, only relationships between canopy chlorophyll content and SR, NDVI, REP and MTCI were studied.

5.2.5.1. Effect of chlorophyll content

Although the number of data points for poplar canopy were less ($n=11$), there was a high variation in chlorophyll content (7.98 mg to 198 mg). All reflectance indices had a stronger relationship (higher coefficient of determinant) with chlorophyll content in poplar than in spinach. MTCI had the strongest correlation ($r^2=0.86$) and NDVI had the weakest ($r^2=0.59$) correlation with chlorophyll content. Among the techniques used to estimate the REP, Lagrangian interpolation had the strongest ($r^2 = 0.84$) and maximum of first derivative had the weakest ($r^2 = 0.56$) correlation with chlorophyll content.

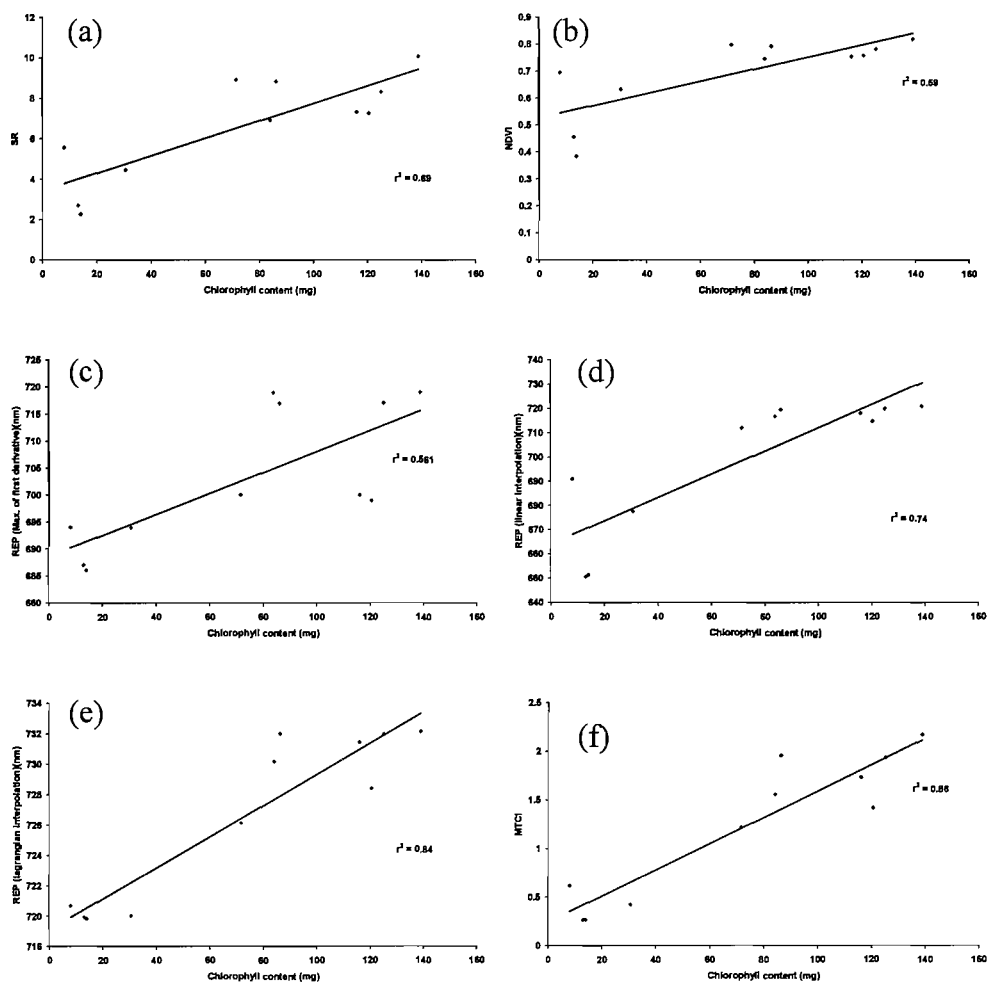


Figure 5.26. Relationship between chlorophyll content and SR (a), NDVI (b), REP estimated by maximum of first derivative (c), REP estimated by linear interpolation (d), REP estimated by Lagrangian interpolation (e) and MTCI (f) for poplar.

5.2.5.2. Effect of irradiance

Three reflectance spectra for poplar having very similar chlorophyll content (approximately 560 mg m^{-2}) corresponding to low, medium and high level of irradiance (Figure 5.27) are presented. Like spinach, there was an increase in reflectance across all wavelengths of the spectrum with an increase in level of irradiance.

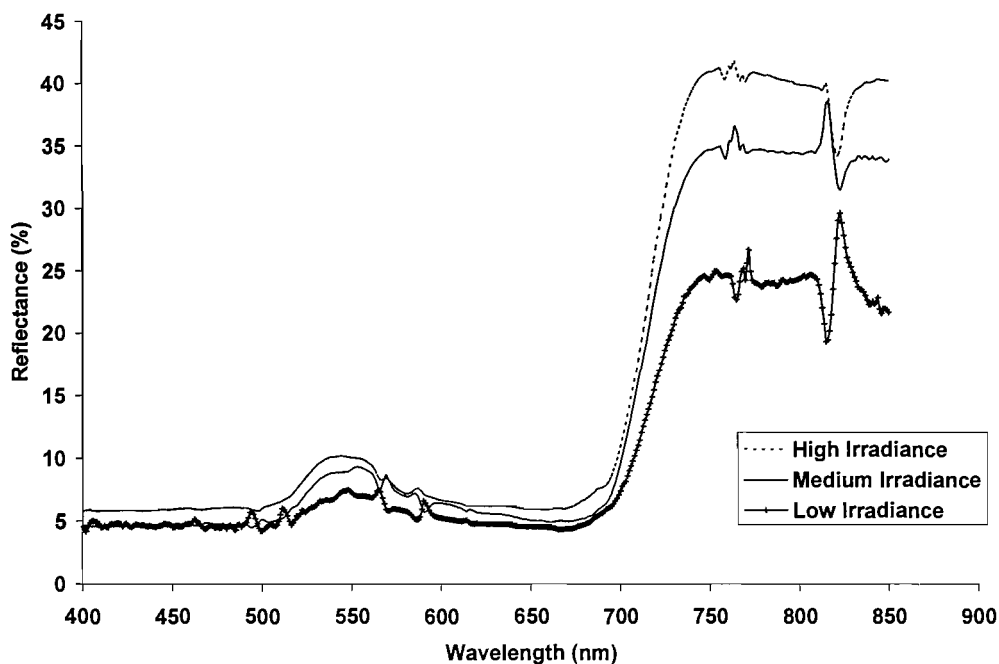
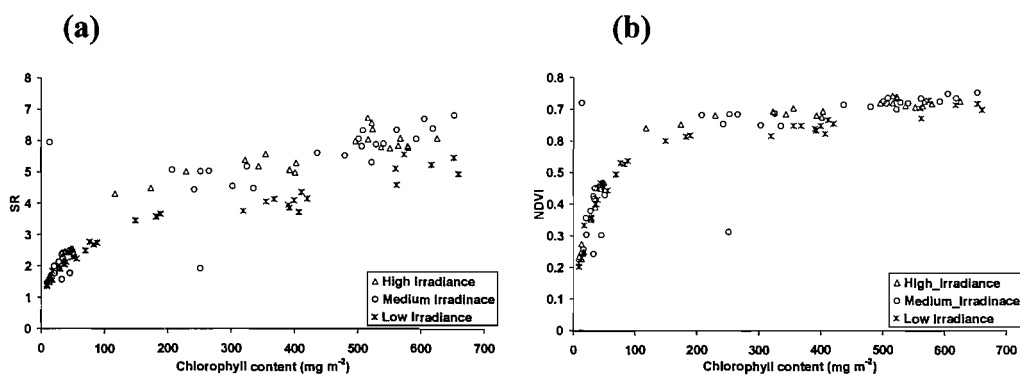


Figure 5.27. Spectral reflectance spectra for poplar at three levels of irradiance.

Chlorophyll concentrations at each level of irradiance were correlated with SR, NDVI, REP and MTCI for poplar. At low levels of irradiance REP estimated using linear interpolation had the weakest correlation ($r^2 = 0.72$) and MTCI had the strongest correlation ($r^2 = 0.98$) with chlorophyll concentration (Figure 5.28).



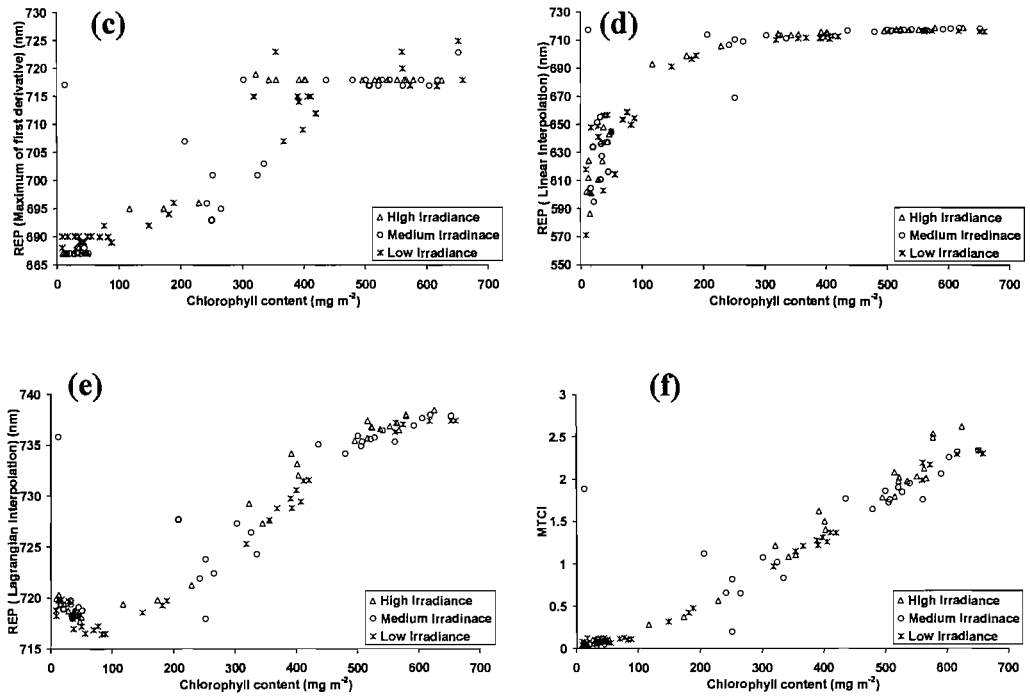


Figure 5.28. Relationships between chlorophyll content and SR (a), NDVI (b), REP estimated using the maximum of first derivative (c), REP estimated using linear interpolation (d), REP estimated using Lagrangian interpolation (e) and MTCI (f) at three levels of irradiance for poplar.

At a medium levels of irradiance NDVI had the weakest correlation ($r^2 = 0.66$) and MTCI had the strongest correlation ($r^2 = 0.82$) with chlorophyll concentration. At high levels of irradiance NDVI had the weakest correlation ($r^2 = 0.77$) and MTCI had the strongest correlation ($r^2 = 0.98$) with chlorophyll concentration (table 5.7). There was no significant difference (95% confidence level) between the three REP and chlorophyll concentration relationships as a result of variation in irradiance. However, like spinach, the REP shifted towards the longer wavelengths with an increase in irradiance. MTCI had the strongest relationship with chlorophyll concentration at all levels of irradiance.

Reflectance indices	Coefficient of determination (r^2)			Level of significance
	Low level of irradiance	Medium level of irradiance	High level of irradiance	
SR	0.93	0.77	0.89	0.016
NDVI	0.74	0.66	0.77	0.537
REP (Max first derivative)	0.90	0.77	0.90	0.478
REP (linear)	0.72	0.67	0.80	0.795
REP (Lagrangian)	0.95	0.77	0.96	0.116
MTCI	0.98	0.82	0.98	0.249

Table 5.7. The coefficient of determination for correlations between chlorophyll content and reflectance indices at three levels of irradiances (and their statistical significance) for poplar.

After exposure to high levels of irradiance a prominent and consistent trough centred around 720 - 722 nm in the first derivative spectra (like spinach) was identified. This trough, a feature absent for spectra recorded at low levels of irradiance, existed across a wide range of chlorophyll concentrations (0 - 450 mg m⁻²) and is being considered in further research.

5.2.5.3. Conclusion

- Due to the small sample size (n=11) it was not possible to relate various canopy bio physical variables to reflectance indices. However, these indices were only casually related to canopy chlorophyll content.
- MTCI had the strongest correlation with the canopy chlorophyll content.

- Like spinach, the REP shifted towards the longer wavelengths with an increase in irradiance. However, there was no significant difference between the reflectance indices and chlorophyll concentration relationships as a result of variation in irradiance.

5.3. Evaluation with field data

5.3.1 Introduction

Ideal evaluation of a satellite sensor product is to evaluate its performance using field data. However, for a coarse spatial resolution data like MERIS it is always difficult to perform the field verification (explained in detail in next chapter). For the purpose of this study MTCI was evaluated for field data obtained at Barrax in the south of Spain as a part of SPectra bARrax Campaign (SPARC) (SPARC, 2005). The SPARC was originally designed for calibrating the CHRIS sensor but later on it was used for validation of other instruments too.

5.3.2 Study site and data used

Barrax, located in south of Spain, covers an area on 10 km x 5 km. The site has different crop types which includes corn, potato, Sugar beat, alfalfa, onion and garlic, each of them grown in separate plots. MERIS data acquired on 14/07/2003 covered the region. Ground measurement of biophysical parameters (LAI, chlorophyll and fraction of vegetation cover) were undertaken two days before the satellite over pass. Further information on the sampling strategy and measurement methods could be found in the SPARC user's manual (SPARC, 2005). MERIS data corresponding to

each crop type were atmospherically corrected to obtain reflectance in individual plots (figure 5.29)

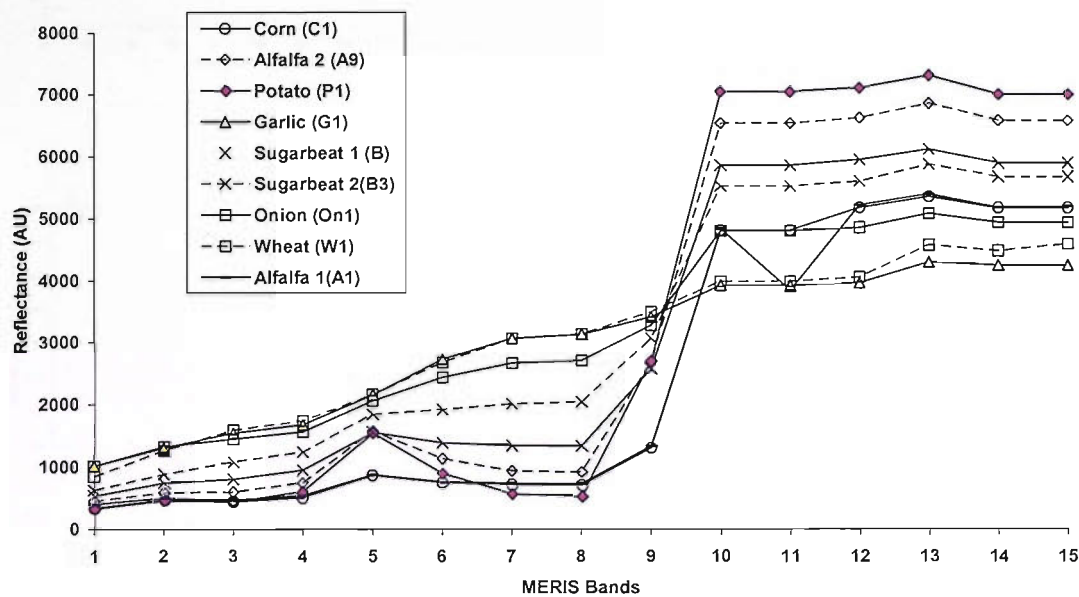


Figure 5.29. MERIS spectral reflectances for different crops.

Reflectance in MERIS wavebands situated in the NIR region was related to LAI; potato having highest LAI (5.41) had the highest NIR reflectance whereas garlic having lowest LAI (0.56) had the lowest. Similarly, absorption in MERIS wavebands situated in the red region was related to chlorophyll content of each plot.

5.3.3 Relation of MTCI and REP with chlorophyll content

SR, NDVI, MTCI and REP (estimated by Lagrangian and linear interpolation) were correlated with total chlorophyll content for each crop in the study area (figure 5.30).

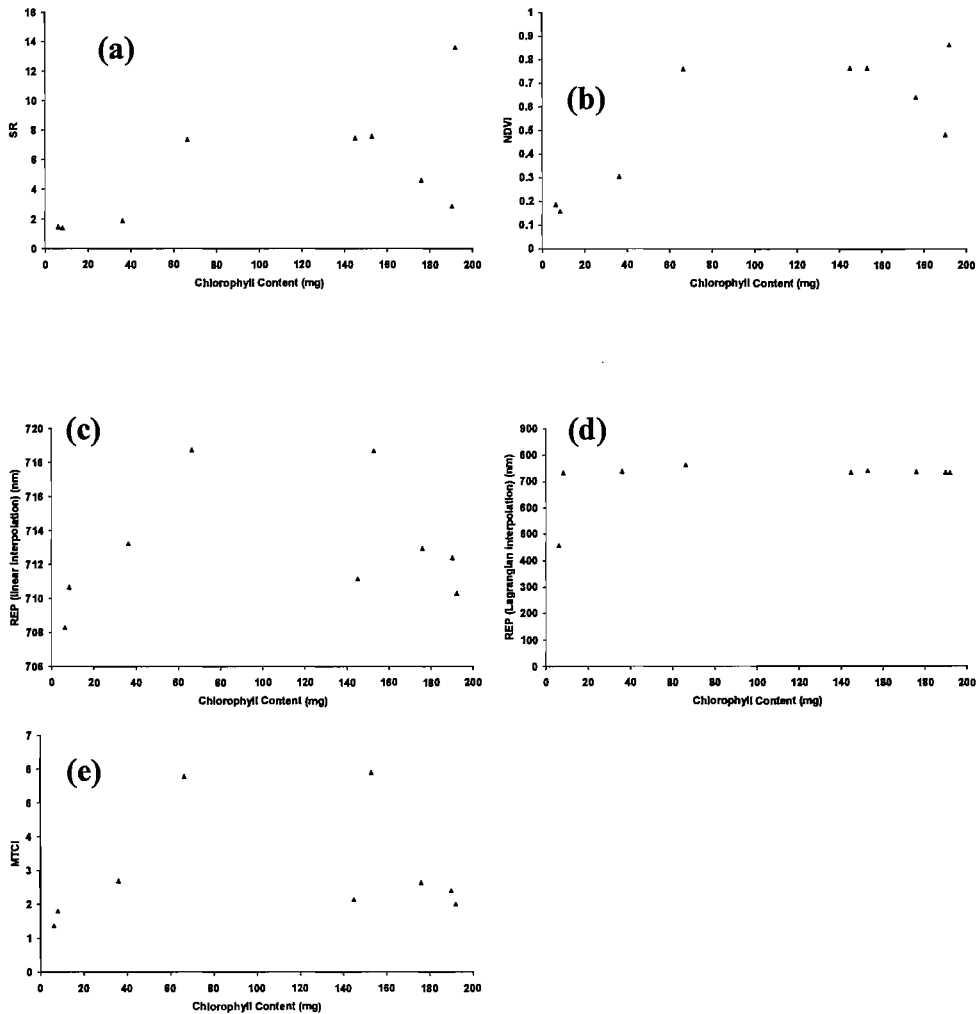


Figure 5.30. Relationship between SR(a); NDVI(b); REP estimated using linear interpolation (c); REP estimated by Lagrangian interpolation(d) and MTCI(e) with chlorophyll content for different crops in the field site.

There was no strong relation observed for any of the reflectance indices and chlorophyll content for the field data. This may be due to three factors: (i) very few samples ($n=9$) available for this study, (ii) uncertainty in the sampling strategy for the foliar biochemical variable at MERIS spatial resolution and (iii) species dependence of MTCI, as dataset consists of several species with different canopy architecture. The species dependence of MTCI should be investigated further. The issue of uncertainty in the sampling of foliar biochemical variable is explained in the next chapter.

5.4. Conclusion

In this chapter MTCI was evaluated with some real spectral reflectance and biophysical data obtained from greenhouse experiment and field. Leaf and canopy data from greenhouse showed a strong relationship between MTCI and chlorophyll content. This chapter could be summarised as:

- MTCI had a stronger correlation with chlorophyll content than all reflectance indices used in this study; this relationship was stronger at leaf level than at canopy level.
- In most cases, REP estimated by Lagrangian interpolation techniques had a stronger correlation with chlorophyll content than all REP. A problem was detected while estimating REP for MERIS bands using Lagrangian interpolation with band 11, which resulted in over estimation of REP. Therefore, band 11 should not be included in the REP estimation for MERIS standard band setting using Lagrangian interpolation.
- The REP of a leaf shifted towards longer wavelength with an increase in irradiance. However, in most cases, this shift was not significant.
- There was no significant difference in MTCI and chlorophyll concentration relationship of a leaf following a change in irradiance.
- Due to very few field data, it was not possible to find any relationship between real MTCI data and chlorophyll content.

In this chapter and the previous chapter MTCI was evaluated using data from model, greenhouse and field at various spatial and spectral resolutions. In most cases it showed a limited sensitivity to various non canopy variables and high sensitivity to change in chlorophyll content. Now, MTCI is a standard MERIS

land product, so it should also be possible to confirm the nature of the MTCI/chlorophyll content relationship with a range of chlorophyll content data at the spatial resolution of MERIS.

Chapter 6. Indirect MTCI Evaluation (Validation)

6.1. Introduction

MTCI is a standard ESA product derived from MERIS data available at two spatial resolutions: 300 m and 1200 m. Therefore, a sustainable validation programme is needed to provide timely feedback on its performance. As a result, the algorithm could be suitably modified to improve the product quality. ‘Validation’ is the process of accessing the accuracy of the data product by independent means (Justice et al., 2000; Privette et al., 2000). However, product validation at a coarse spatial resolution like MERIS or MODIS is not straightforward, because ground measurements can not be easily compared to the spatial resolution of the space-borne sensor. Curran (1988) suggested a semivariogram based approach for determining the spatial resolution and sampling scheme. This approach was used to design the sampling strategy for validating MODIS LAI product at three homogeneous forest sites (Tian et al., 2002). NASA has also developed a validation protocol called ‘BigFoot’ for validation of MODIS landcover, LAI, FPAR and NPP products (Cohen and Justice, 1999). However, there has been little validation of biophysical products at the coarse spatial resolution of MERIS or MODIS.

The main requirement in MTCI validation would be to attain adequate ground sampling of chlorophyll content which could produce spatial and temporal variation at MERIS spatial resolution. However, sampling chlorophyll content at MERIS spatial resolution has logistical difficulties for four major reasons: (i) chlorophyll content varies with vegetation type and condition; (ii) it is difficult to obtain an

uniform vegetation cover for a suitably sized plot ($>10^5 \text{ m}^2$); (iii) there is no existing sampling strategy for chlorophyll content at MERIS spatial resolution and (iv) standard validation sites used for validating coarse spatial resolution products do not have chlorophyll content data.

Therefore the relationship between chlorophyll content and MTCI at satellite level were qualitative for this study. However for indirect evaluation (validation), MTCI was related to other vegetation indices derived from current space-borne spectrometer; they include (i) MGVI from MERIS and (ii) NDVI and EVI from MODIS.

6.2. Comparison with MGVI

The MERIS global vegetation index (MGVI) is another level 2 MERIS vegetation index and it is related to the LAI of the vegetation. Detailed description of this index is given in next chapter. The purpose of MGVI was to identify and monitor the presence of live green vegetation over all terrestrial surface using MERIS data, whereas the purpose of MTCI is to estimate the amount of chlorophyll present in that vegetation and there by giving information about the vegetation condition. It was assumed that for healthy green vegetation MGVI would be positively related MTCI, where as there may be deviation in this relationship for vegetation with stress. Both spatial and temporal comparison between MTCI and MGVI were performed for different study sites representing different vegetation type.

6.2.1 Spatial comparison

Spatial comparison of MTCI and MGVI was performed for image covering (i) United Kingdom, Ireland and northern France and (ii) the State of Wisconsin in the USA.

6.2.1.1. United Kingdom, Ireland and northern France data

Both MGVI and MTCI were compared for RR MERIS data covering United Kingdom, Ireland and northern France acquired on 18th April 2003 (figure 6.1).

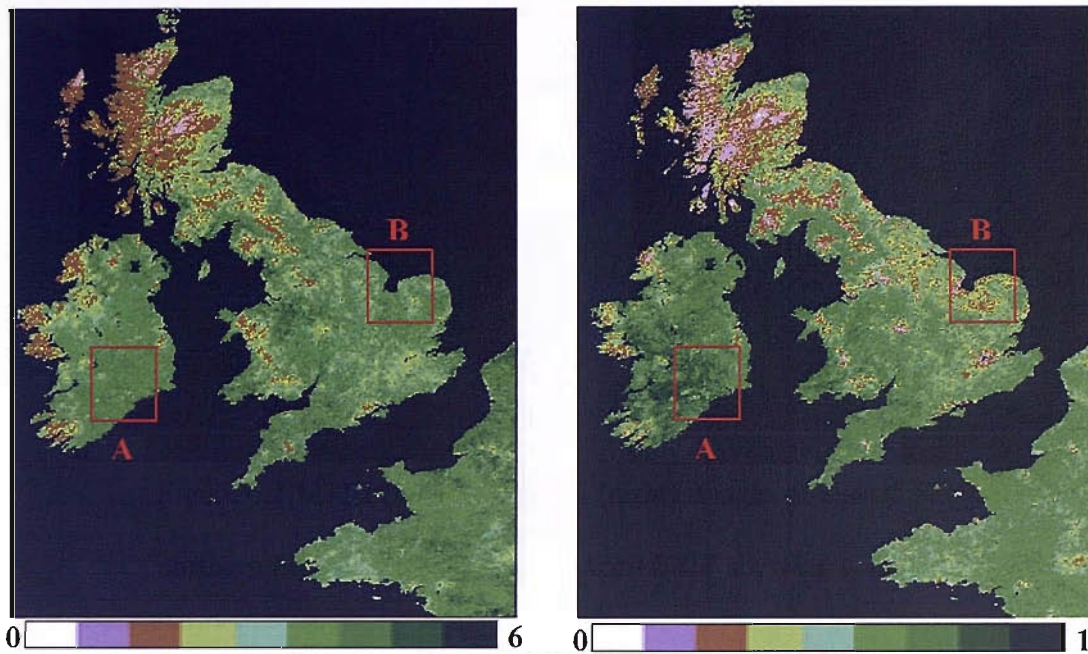


Figure 6.1 MTCI (left) and MGVI (right) images of United Kingdom, Ireland and northern France acquired on 18th April 2003 showing two regions where there was considerable difference between MGVI and MTCI values.

In the major part of the image MTCI is proportional to MGVI. This may be due to the fact that, during this period of time vegetation started to regain canopy cover, hence in both LAI (MGVI) and chlorophyll content (MTCI) were proportional. However, two areas in the image were identified where there was a variation between MGVI and MTCI. Within area A (figure 6.1) MGVI was relatively greater than MTCI, this means this region has high LAI and medium chlorophyll content. This is because, this area is dominated by pastures which do not have high chlorophyll content, but during this time of year they were fully grown with a high LAI. Hence, they also had a high MGVI but medium MTCI. Within area B (figure 6.1) MTCI was relatively greater

than MGVI, which indicate the vegetation here has more chlorophyll content and comparatively less LAI.

6.2.1.2. Analysis with Wisconsin data

Both MGVI and MTCI were compared for FR MERIS data covering the state of Wisconsin, USA acquired on 18th August 2003 (figure 6.2).

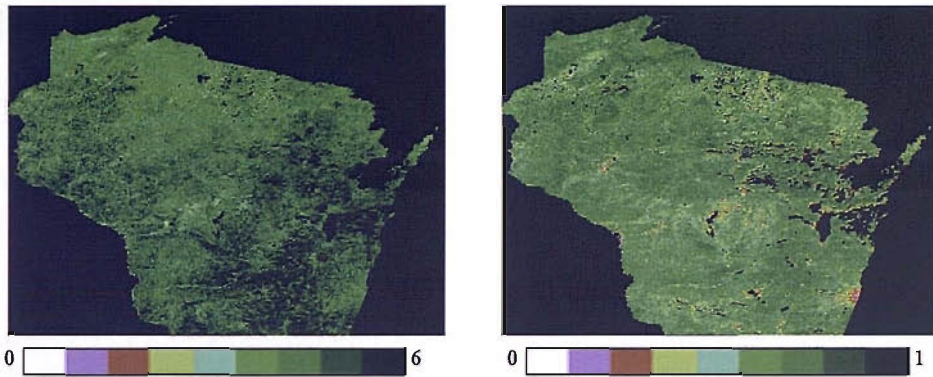


Figure 6.2 MTCI (left) and MGVI (right) images of Wisconsin, USA acquired on 18th August 2003.

For this area the MTCI image was greener than the MGVI image (high MTCI values and medium MGVI values). This was because, by this time of year most vegetation was at the peak of its growing season and so had a high chlorophyll content.

Particularly the south and south east part of the image has higher MTCI than rest of the image; this was because the dominant land use was either agricultural land or deciduous forest, which tend to have higher chlorophyll content in August and thereby higher MTCI, than other vegetation type. Whereas, there was little variation in MGVI, because the LAI tends to be similar for these vegetation types.

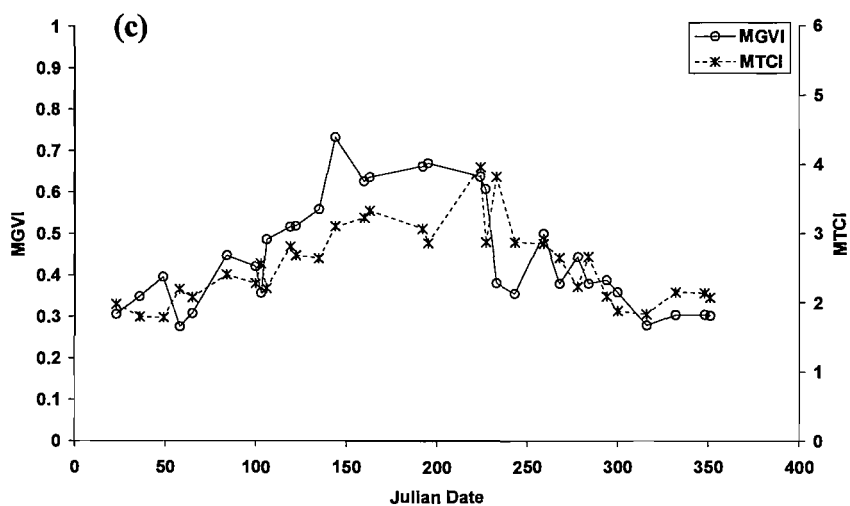
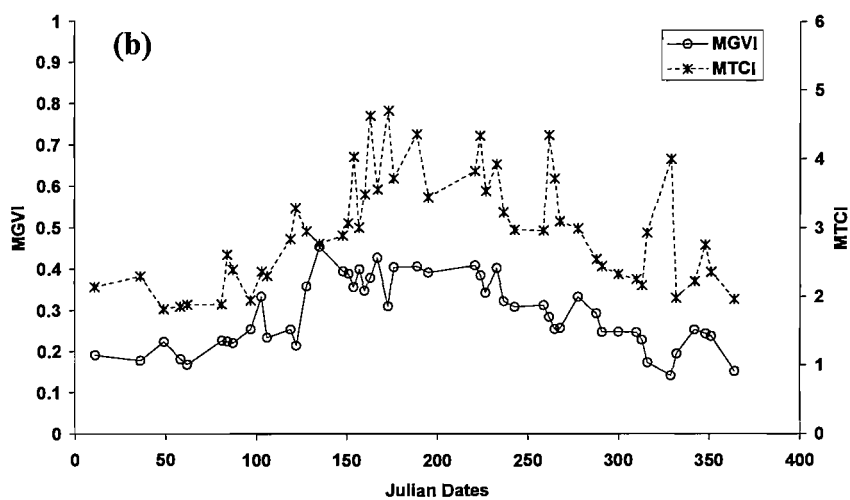
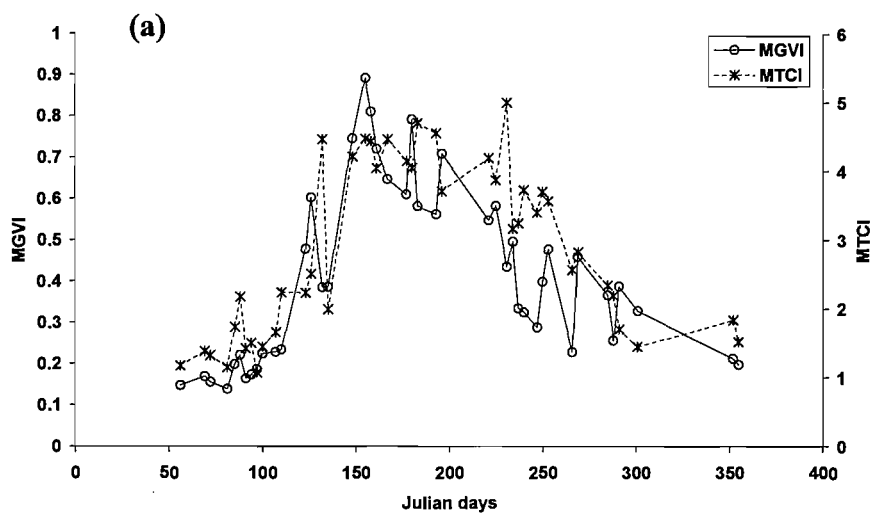
6.2.2 Temporal comparison

Temporal comparison of MTCI and MGVI was performed through time series of data acquired through 2003 for four sites representing different vegetation type (table 6.1).

Site name	Country	Vegetation type	Dominant species	Soil type
Hainich	Germany	Hardwood forest	Beech	Cambisol
Loobos	Netherlands	Coniferous forest	Pine	Podzol
New Forest	United Kingdom	Mixed forest	Oak, Pine, Heath , Bracken	Pelo-stagnogley
Pavia	Italy	Crop	Rice	Alluvial, Sandy

Table 6.1. Description of study sites used for the temporal comparison between MTCI and MGVI.

For each site FR MERIS data acquired through 2003 were used to generate the time series. The orbit and the path of acquisition were different for different dates for a specific site. Therefore, position of the central pixel corresponding to each site was determined and all the images were re-projected with respect to the central pixel. MTCI and MGVI were estimated for cloud free and less atmospherically contaminated pixels. For each index, the average of 5X5 pixel around the central pixels was calculated to represent the vegetation index value at that time.



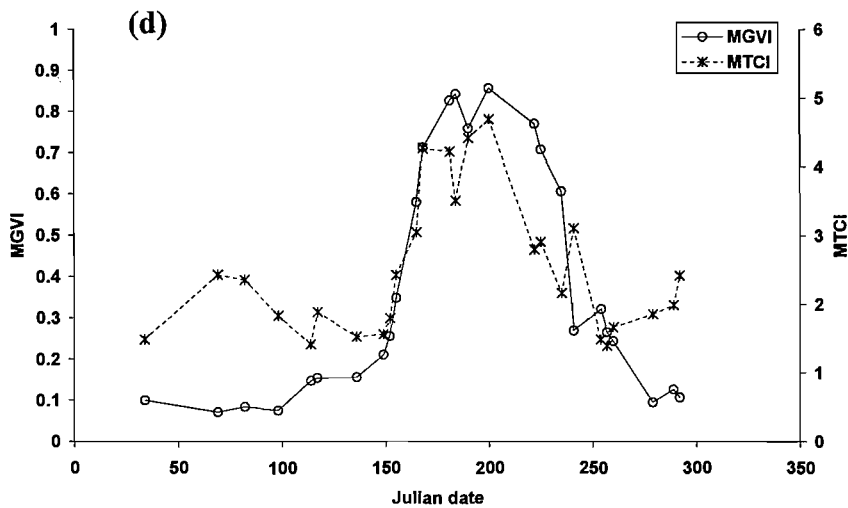


Figure 6.3. Time series of MGVI and MTCI for (a) Hainich; (b) Loobos; (c) New Forest and (d) Pavia.

For Hainich, dominated by deciduous forest, the MTCI time series started with low values, representing low chlorophyll content (figure 6.3a) in February and March. MTCI increased gradually with the growth period and attained maximum values during June and July. Again from September chlorophyll started to decompose and leaves started changing colour and falling, producing low MTCI. MGVI values followed the same trend as MTCI, with lower values in February and March and again in September, whereas higher values during June and July.

For Loobos, dominated by coniferous forest, the time series was different to that for Hainich. Here the overall variation in MTCI values were less compared to Hainich. Because in coniferous forest there is a little seasonal change in chlorophyll content (figure 6.3b). However, there was a slight increase in chlorophyll during July and August indicated by higher value of MTCI. These higher values may be due to presence of understorey vegetation which contributes to the overall chlorophyll content of the area. MGVI values were lower than Hainich site for the time series.

But there was a relative increase in MGVI values from May to August. Since the dominant vegetation type was coniferous forest, there was not much variation in LAI (MGVI) through out the year.

For New Forest, dominated by coniferous, deciduous forest and heath land, the time series data showed slightly less variation in MTCI (figure 6.3c). Particularly during May to August, there was slight increase in the MTCI values. However, there was little variation in the MTCI through the year. This may be due to presence of heath land in the scene, which contributes little to the total chlorophyll content. MGVI followed the same trend as MTCI except from April to July where there was a relative increase in MGVI values.

For Pavia, dominated by agricultural crop (rice), the time series of MTCI (Figure 6.3d) was similar to Hainich. It started with low values from February to May and then MTCI increased sharply to a maximum in July with the growth of rice crop after which there was a sharp decrease in MTCI values with maturity of the crop. During the growth season (between Julian days 150 to 250) there was a sharp increase in MGVI values with maximum in July (like MTCI) but there was a gradual decrease in MGVI values. When the crop started growing chlorophyll content and LAI increased simultaneously but when the crop started maturing the chlorophyll started to decompose first while leaves were still intact. Therefore, the rate of decrease in MGVI was lower than MTCI with crop maturity.

MGVI and MTCI for each available date at each of the four sites were correlated (figure 6.4). For these sites, MTCI was positively related to MGVI with Pavia having the strongest correlation ($r^2=0.65$) and Loobos having the weakest correlation ($r^2=0.34$) between MTCI and MGVI. The nature and strength of this relationship was dependent on the type of vegetation presented in the site.

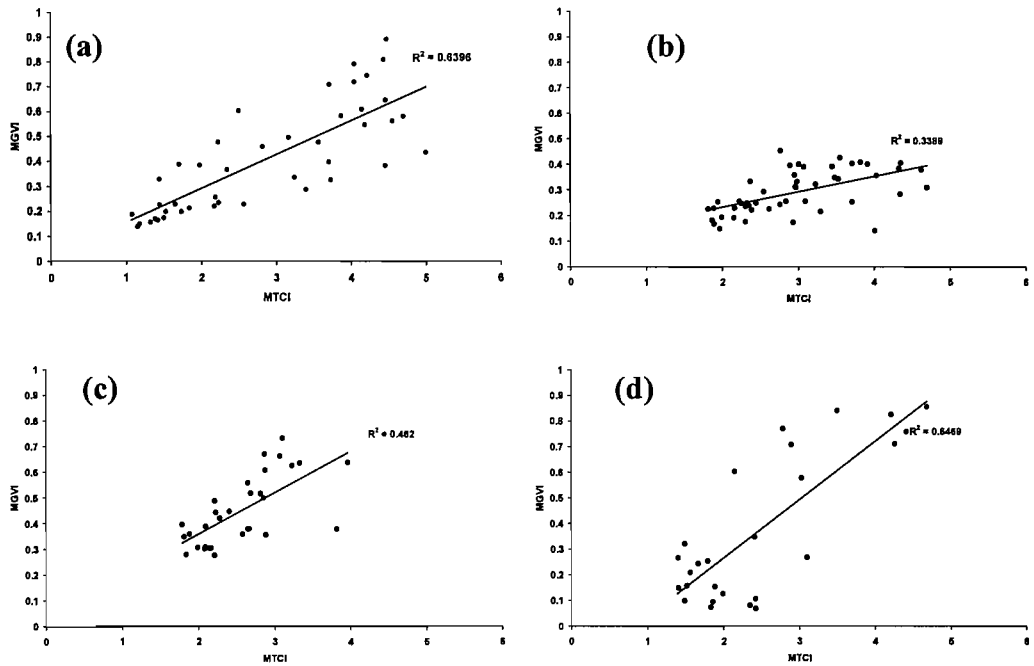


Figure 6.4. Correlation between MGVI and MTCI for (a) Hainich; (b) Loobos; (c) New Forest and (d) Pavia.

6.3. Comparison with MODIS vegetation indices

MODIS is a key instrument aboard the NASA EOS's Terra (launched on 18th December 1999) and Aqua (launched on 4th May 2002) satellites (NASA, 2005). Terra orbits around the Earth passing equator from north to south in the morning while Aqua passes the equator from south to north in the afternoon, allowing the Earth coverage in every 2 days with 36 spectral bands. MODIS provides 44 standard data product that are suitable for observing and monitoring various ecological and environmental processes in land, ocean and atmosphere. For land application MODIS data provided a mean for quantifying land surface characteristics such as mapping land cover type (Hansen et al., 2000; Friedl et al., 2002), snow cover extent (Hall et al, 2002; Klein and Barnett, 2003), surface temperature (Petitcolin and Vermote, 2002), leaf area index (Privette et al., 2002; Wang et al., 2004) and fire

occurrence (Kaufman et al, 2003, Giglio et al., 2003). However, for monitoring vegetation condition MERIS has three advantages compared to MODIS data:

1. Although MODIS has 16 bands in the visible and NIR region of the electromagnetic spectrum, it has fewer bands than MERIS in the red edge region which is the potential zone of information for vegetation condition (figure 6.5). MERIS has 5 bands in the red edge region while, MODIS has only 3 bands.

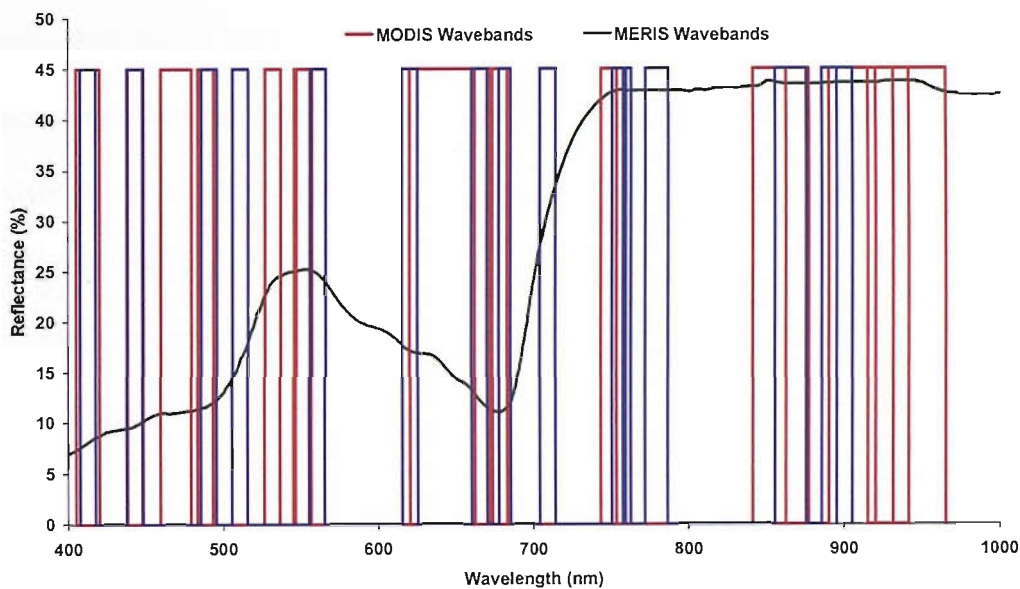


Figure6.5. MERIS and MODIS bands overlain on a modelled vegetation spectrum.

2. Data acquired for three MODIS bands situated in the red edge region has the spatial resolution of 1 km, while, data acquired for five MERIS bands in the red edge region can have spatial resolution of 300 m and 1200 m.
3. Finally, the programmability of MERIS's standard band position could be used to locate more bands in the red edge region and could be used for a detailed study of the relationship between canopy variables and reflectance (Curran and Steele, 2005). This facility is not available for MODIS data.

Therefore, spectrally, spatially and technically MERIS is superior to MODIS in the red edge region.

Two vegetation indices are available from MODIS data at 500 m and 1 km resolution, they are, the normalized difference vegetation index (NDVI) and enhanced vegetation index (EVI) (Huete et al., 2002).

NDVI derived from MODIS data is also referred as “continuity index” to the existing AVHRR NDVI time series over past 20 years. This MODIS NDVI was used successfully as a vegetation measure (Tucker et al., 2005) because it can overcome noise introduced due to illumination differences, cloud shadows, atmospheric attenuation and topographic variations. However, NDVI exhibits scaling problems, saturates over high biomass and is very sensitive to canopy background variations (Huete, 1988).

The enhanced vegetation index (EVI) is an atmospherically resistant index and was optimised to increase sensitivity in high biomass regions (Huete et al., 2002). EVI is estimated by,

$$EVI = G * \frac{\rho_{NIR} - \rho_{Red}}{\rho_{NIR} + C_1 * \rho_{Red} - C_2 * \rho_{Blue} + L}$$

where, ρ_{NIR} , ρ_{Red} and ρ_{Blue} are partially atmosphere corrected (Rayleigh and ozone absorption) surface reflectances for NIR, red and blue MODIS bands, G is gain factor, C_1 and C_2 are the coefficients of the aerosol resistance term in red and blue wavelength and L is the canopy background brightness correction factor. The coefficients used in the EVI algorithm are $G=2.5$, $C_1=6$, $C_2=7.5$ and $L=1$.

EVI is related to canopy structural variables including LAI and leaf angle distribution. EVI derived from MODIS data has been used successfully for determining vegetation status in the Sahelian and Sudanian forest in West Africa

(Fensholt, 2004) and seasonal biophysical dynamics in Amazonian forest in north Brazil (Huete et al., 2003). However, there is no established relationship between canopy chlorophyll content and MODIS vegetation indices. In the absence of a real chlorophyll index for MODIS data, MTCI was related to both EVI and NDVI for study sites in (i) United Kingdom (spatially) and (ii) Wisconsin (temporally).

6.3.1 Spatial comparison

MTCI was estimated from RR MERIS data acquired over the United Kingdom and Ireland on 18th April 2003 and EVI and NDVI were estimated from MODIS data acquired over the same region on 17th April 2003 (figure 6.6).

Among the three vegetation index image, NDVI derived from MODIS data tended to have higher value across the image (Figure 6.6a). In some areas even it had reached the maximum values, which was unusual considering the date of acquisition. The EVI image showed lower values across the image and it successfully captured the variation in different vegetation type (Figure 6.6b). However, it did not capture the variation within a particular vegetation type. The MTCI image showed the greatest variation which indicates it was sensitive to change in chlorophyll content within the vegetation type also (Figure 6.6c). Due to different spatial resolution of these vegetation indices a pixel to pixel comparison was not possible.

6.3.2 Temporal comparison

Temporal comparison of MTCI and MODIS VIs were performed using data acquired for the State of Wisconsin, USA. Due to unavailability of enough cloud free data it was not possible to produce a time series. However, data for different months corresponding to different growth stage were compared using (i) image and (ii) histograms of MTCI and MODIS VIs for the study area.

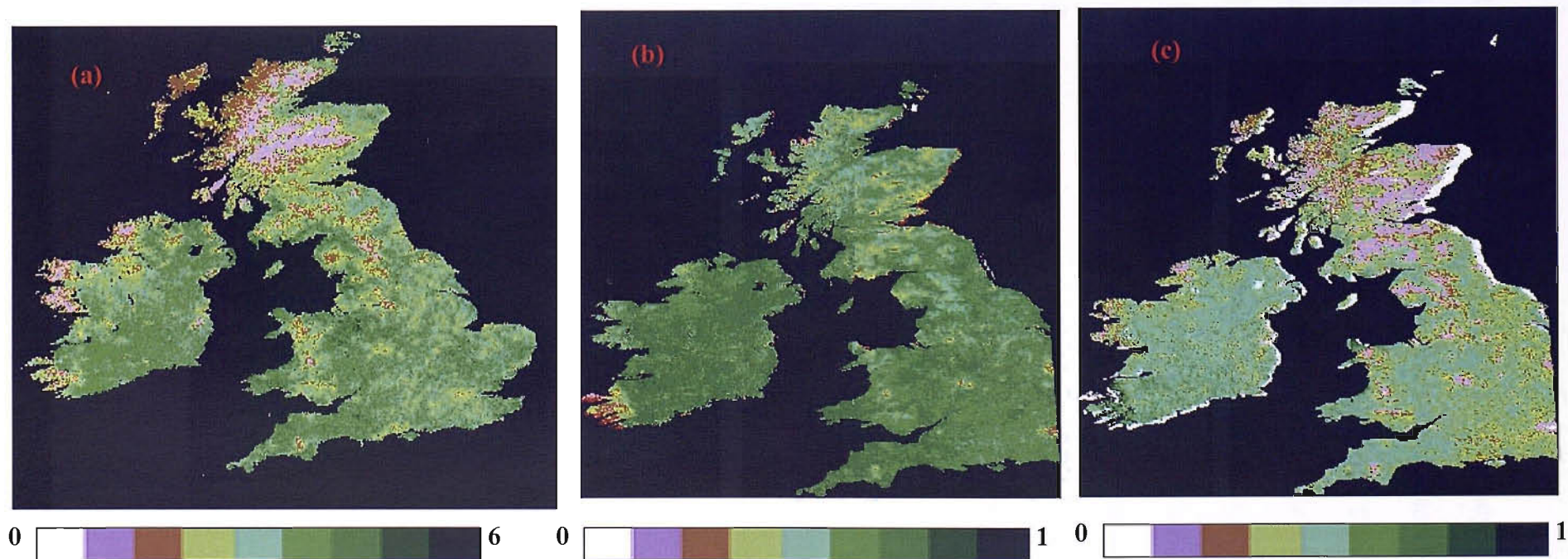


Figure6.6. MTCI and MODIS VI for United Kingdom and Ireland. (a) MTCI estimated from MERIS data acquired on 18th April 2003 , (b) NDVI and (c) EVI for MODIS data acquired on 17th April 2003.

6.3.2.1. Image comparisons

Cloud free MERIS and MODIS data for the study area were available for three dates in 2003: 11th April, 20th September and 19th October. MTCI from FR MERIS data (300 m) and EVI and NDVI from MODIS data (500 m) were estimated for these dates. For the study area MTCI and MODIS VIs estimated in September had the highest value while these indices estimated in April had the lowest value (figure 6.7). This change in the value of vegetation indices through a year was related to vegetation the growth pattern. Because among all available dates (describe above) during September there would be more live green vegetation. However, compared to MODIS VIs MTCI showed a greater variation in its values, particularly in September image. MODIS NDVI image did not capture the variation in both chlorophyll and LAI in vegetation within the study area and most of the NDVI values were high. The EVI image was better than the NDVI image to capture the variation in LAI; still in the north part of the image it did not capture the variation very well. However, the MTCI image captured most of the variation in chlorophyll within the study area. In September some areas corresponded to high EVI but low to medium MTCI, this indicated that the LAI was high but chlorophyll content was low. This is obvious considering the time of the year, when leaves are still present in the plant producing high LAI, in turn high EVI, but chlorophyll had started to decompose, thus low MTCI.

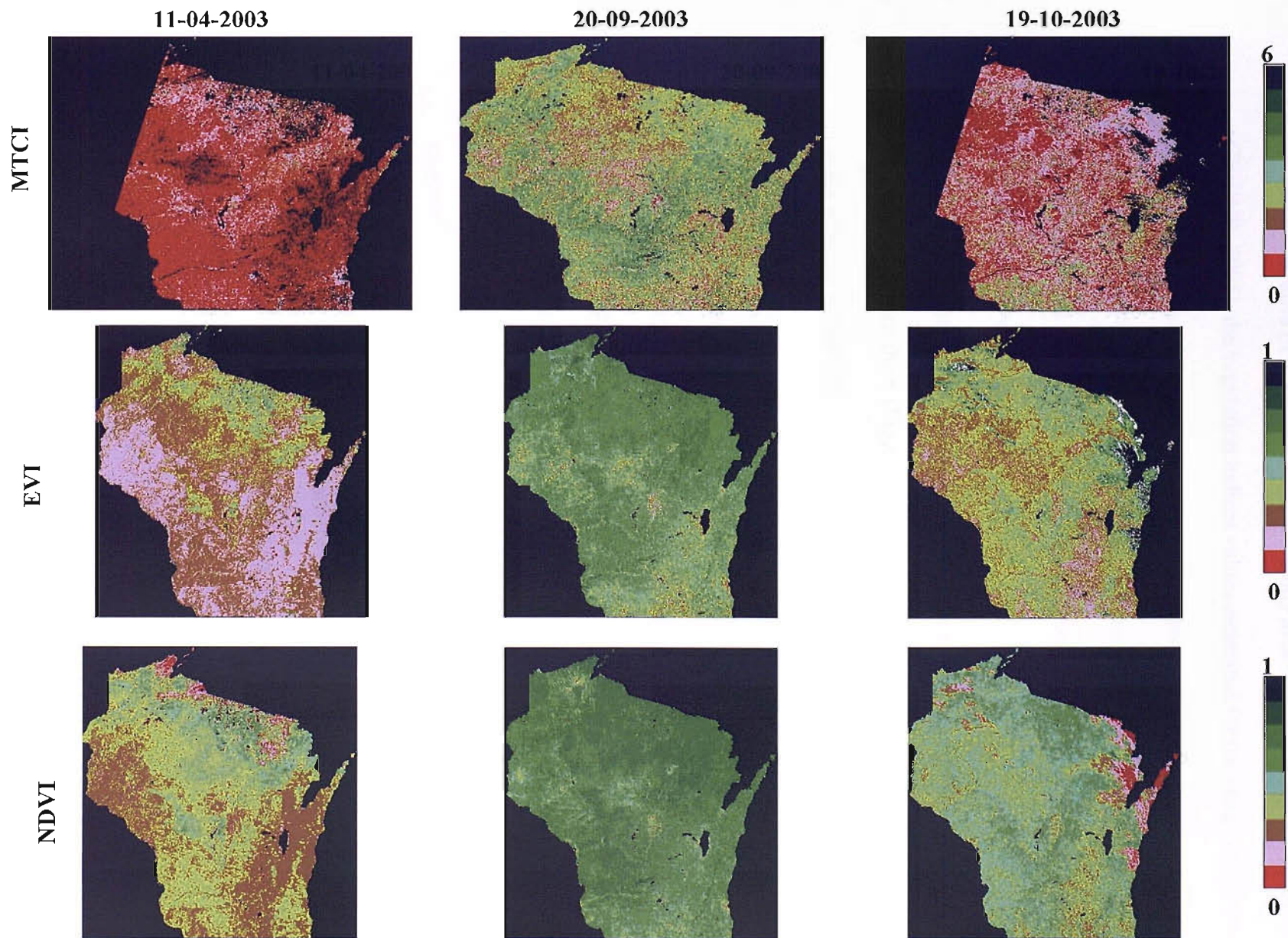


Figure 6.7. MTCI derived from MERIS data, EVI and NDVI derived from MODIS data acquired in three dates for Wisconsin, USA, MTCI and MODIS VIs images are different in size because they have different spatial resolution.

6.3.2.2. Histogram comparison

As more than 80% of the landcover in the study area comprised vegetation classes (WiDNR, 2005), the vegetation indices values estimated for the image of the whole State could represent the amount and condition of different kind of vegetation. Therefore, histograms of MTCI and MODIS VIs for the three dates were computed for the State to provide statistical comparison between these three indices. MTCI values were scaled from 0 to 1 for a better comparison with MODIS VIs.

For MTCI, histograms for the three dates were negatively skewed and there was a clear distinction between them (Figure 6.8a). Histogram for the September data had the highest mode whereas histograms for April data had the lowest mode. This was in accordance with the growth pattern of vegetation, because among the three dates one would expect better vegetation condition in September than April and October and hence, higher MTCI.

For EVI, histograms for September data were positively skewed whereas histograms for April and October data were negatively skewed (Figure 6.8b). There was not much difference between the histograms for April and September data which was of concern. This indicated EVI was unable to distinguish between vegetations at low chlorophyll content.

For NDVI, estimated from MODIS data histograms for September and October data were positively skewed whereas histogram for April data were negatively skewed (Figure 6.8c). The Mode of histogram for September data was close to the maximum value, which indicated that a considerable number of pixels had a very high NDVI.

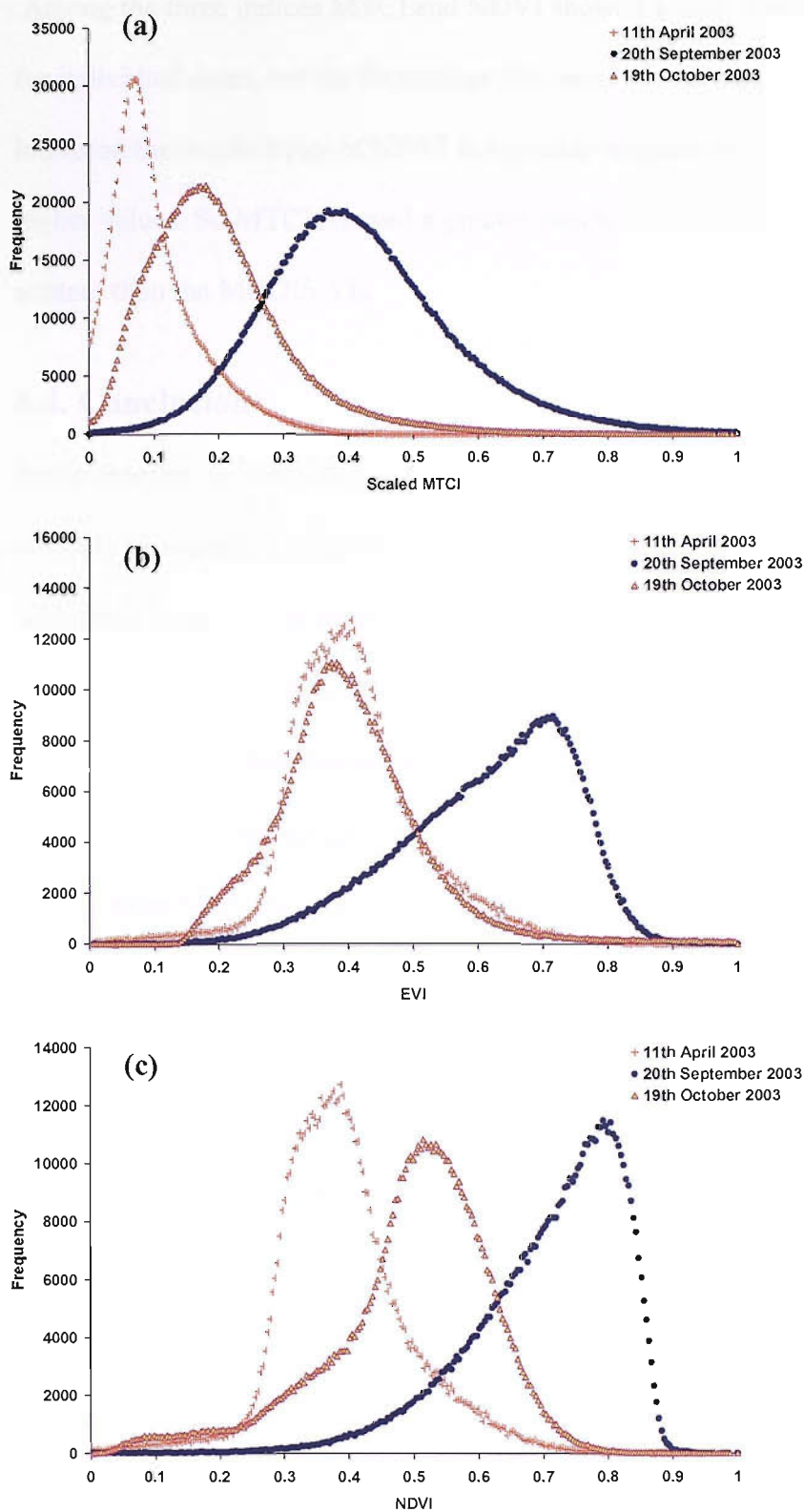


Figure 6.8. Histograms for MTCI (a); EVI (b) and NDVI derived from MODIS data(c) for data acquired in three dates for Wisconsin.

Among the three indices MTCI and NDVI showed a clear distinction between histograms for individual dates, but for September data most of the NDVI values were high. This indicated the insensitivity of NDVI to variation in chlorophyll content particularly at higher values. So MTCI showed a greater sensitivity to temporal variation in chlorophyll content than the MODIS VIs.

6.4. Conclusion

In the absence of adequate ground chlorophyll data at MERIS spatial resolution it was not possible to evaluate (validate) MTCI with real MERIS data. However, indirect evaluation with other vegetation indices available from another contemporary space-borne imaging spectrometer showed that MTCI has higher sensitivity to change in vegetation chlorophyll content than other vegetation indices. The chapter can be summarised as:

- For most vegetation types MTCI was positively related to MGVI, however in some areas MGVI was relatively higher than MTCI; whereas in other areas MTCI was relatively higher than MGVI at a particular time. This variation in MTCI and MGVI relation was also time depended.
- Both spatial and temporal variation in MGVI and MTCI relationship could be used to distinguish different vegetation classes (explained in next chapter).
- MTCI was also more sensitive to changing chlorophyll content than MODIS VIs. The EVI had a problem in distinguishing between different vegetation types at low chlorophyll content whereas NDVI derived from MODIS data had a problem of saturation during the high chlorophyll season. Whereas, MTCI was able to distinguish vegetation types at each available date and did not have saturation problem.

At present MTCI is the only available operational chlorophyll index for terrestrial vegetation from a space-borne imaging spectrometer and this could be used for various

ecological and environmental applications at a regional to global scale. Now ESA is planning to produce MTCI as a level 3 product, which will contain monthly global composites of MTCI. The first MTCI monthly composites will be available in early 2006.

Chapter 7. Application of MTCI-I

7.1. Introduction

MERIS was launched on the ESA's Envisat satellite in March 2002 and is now into its fourth year of data acquisition (ESA, 2005). Within last 3 years of operation several products have been derived from MERIS data for ocean, land and atmospheric application. MERIS data are available at three levels of processing. Level 1 data include calibrated instantaneous radiance estimates in each waveband at both full (300 m) and reduced (1200 m) spatial resolution. Level 2 data include atmospherically-corrected reflectances, geophysical and biophysical products. Level 3 data are derived products (e.g., mosaic of fraction of absorbed photosynthetically active radiation (APAR)). Level 1 and level 2 products are available through the processing chain, while level 3 products are still in the developmental stage.

7.2. Level-2 MERIS Product

MERIS data are being acquired for application over ocean, land and cloud. Therefore, before deriving any product from the raw data it is necessary to classify the pixels into land, ocean and atmosphere to reduce the processing task. The primary task in the level 2 processing is pixel classification followed by atmospheric correction for each category. A processing overview of level 2 products is given in figure 7.1.

For land applications level 2 products provide normalised surface reflectance in all MERIS wavebands and two vegetation indices: MGVI and MTCI. MGVI is an atmospherically resistant vegetation index; therefore, it uses the instantaneous radiances (without atmospheric correction) and so is the top of atmosphere vegetation index (TOAVI). On the

other hand MTCI uses atmospherically-corrected reflectances and is called a bottom of atmosphere vegetation index (BOAVI).

MGVI was designed to exhibit maximum sensitivity to healthy green vegetation (Gobron *et al.*, 1999) and uses a two step approach to separate the reflectances from land and atmosphere. The MGVI uses information from the blue, red and near-infrared (NIR) part of the spectrum (Gobron *et al.* 1999). The information in blue wavelength (MERIS waveband 2) is used to mask pixels contaminated with atmospheric noise, with the index calculated for all other pixels. The normalised red (MERIS waveband 8) and NIR (MERIS waveband 13) wavebands are used to derive information regarding vegetation amount and structure. The magnitude of the MGVI has a positive relationship with fAPAR, which in turn, is related positively to LAI.

7.2.1 Implementation of MTCI in the MERIS processor

Mathematically, MTCI is the ratio of the difference between MERIS band10 and band9 and the difference between band9 and band8. However, implementing MTCI in the MERIS processor first require thresholding to remove unwanted pixels.

MTCI requires atmospherically corrected reflectance, in other words, top-of-canopy reflectance. However, it is not possible within the MERIS processor to perform a full atmospheric correction. The best available data for MTCI calculation is Rayleigh corrected surface reflectance in individual bands. Further description about the atmospheric correction over land can be found in the MERIS user's handbook (ESA, 2005).

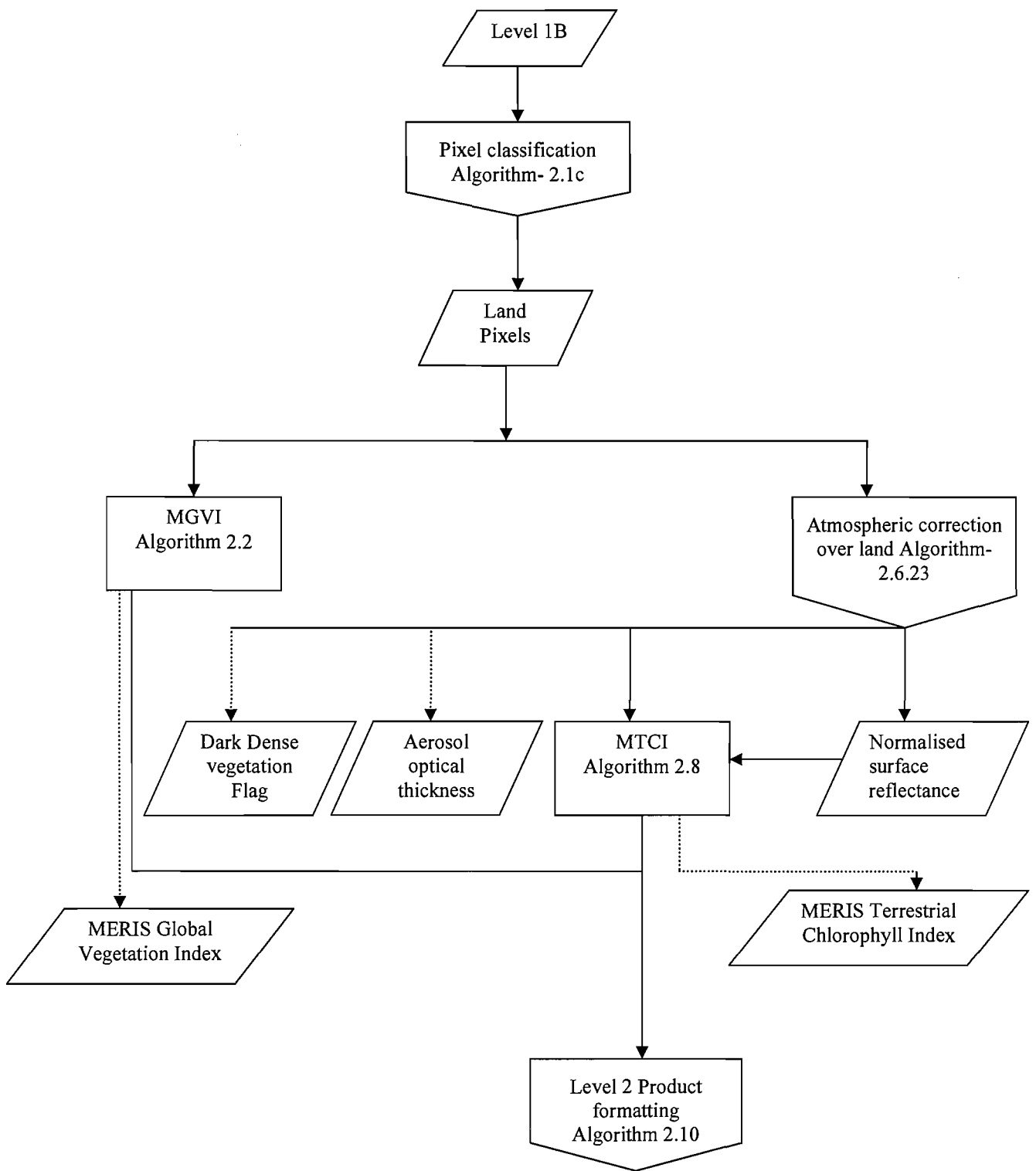


Figure 7.1. MERIS level 2 processing for land.

Three possible features: sediment laden water, barren and low cloud cover could be a source of ambiguity in the MTCI estimation. Therefore, prior to the calculation of MTCI pixels covering these features should be removed.

For sediment laden water, reflectance in MERIS bands 8, 9 and 10 varies with change in sediment concentration (figure 7.2). In most cases MTCI estimated for pixels covering sediment laden water varies with sediment concentration and falls within the MTCI range for vegetation. Therefore, pixels covering sediment laden water should be removed from the scene to avoid confusion with vegetation.

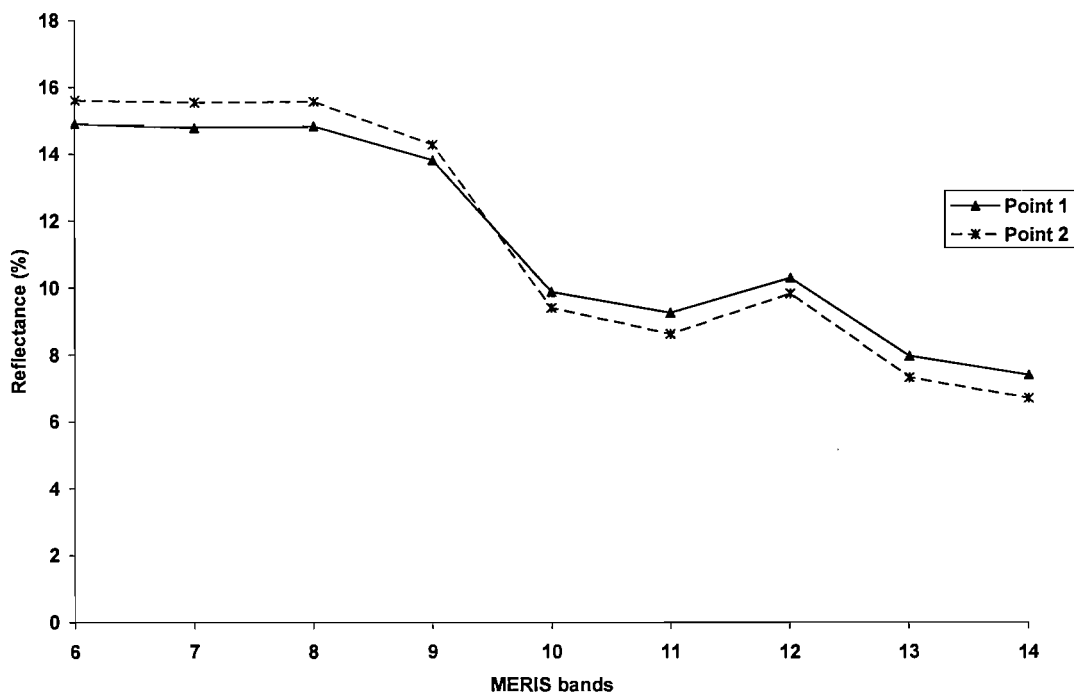


Figure 7.2 Reflectance of sediment laden water in MERIS red and NIR wavebands for two points in the Mekong River, Cambodia.

Unlike vegetated pixel these pixels have very low NIR reflectance; therefore, it was decided to remove pixels with reflectance less than 0.1 NIR (MERIS band 13) in order to keep only land pixels.

Next task was to remove the non-vegetated land pixels. Absorption in the red region was used to distinguish between the vegetated and non-vegetated pixels. It was assumed that pixel having high red reflectance (greater than 0.3) are non-vegetated. Therefore, pixels having reflectance at MERIS band 8 greater than 0.3 were removed.

Pixels with low cloud cover are not removed during atmospheric correction. The reflectance in these pixels is a mixture of reflectance from both ground and the top of cloud. Therefore, MTCI estimated for these pixels are not representative of the ground vegetation condition and should be removed to avoid confusion. It was assumed that, for these pixels there will be a small difference between red and NIR reflectance. Therefore, pixels where difference in reflectances between band 13 and band 8 was less than 0.05 were flagged.

7.2.2 Mathematical description of the algorithm

Figure 7.3 shows the logic of the MTCI computation. The products delivered by the atmospheric correction processing are used as input to the MTCI algorithm (figure 7.4).

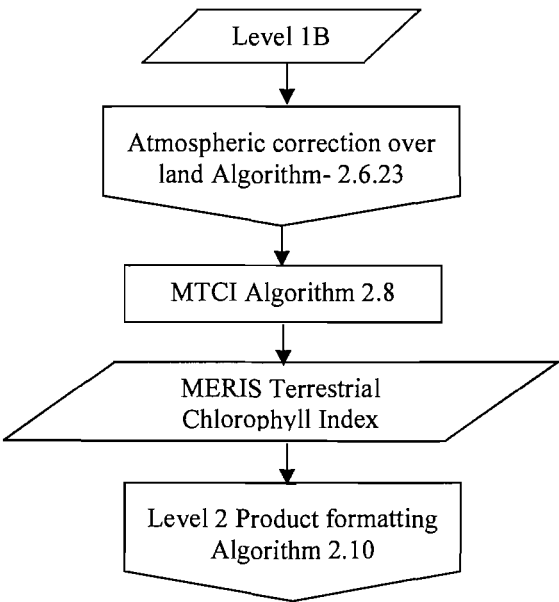


Figure 7.3. MERIS level 2 MTCI computation (step 2.8) in the MERIS processor.

Variable	Descriptive Name	Type	Unit	Range - References
$\rho_{top}(b,j,f)$	Top of aerosol reflectance for land pixels	i	dl	b: 3 bands (b8, b9, b10) specified through external data
INVALID_F(j,f)	Invalid pixel flag	i	-	from previous step
LANDCONS_F(j,f)	Land/water consolidated flag	i	-	from previous step
MTCI_RANGE(0..1)	Range limits for MTCI	s	dl	0: minimum valid value, 1: maximum valid value
mtci_nir1_band	near infrared band #1 for MTCI	s	dl	Nominally b705
mtci_nir2_band	near infrared band #2 for MTCI	s	dl	Nominally b753
mtci_red_band	red band number for MTCI	s	dl	Nominally b681
ρ_{red_max}	Minimum value of ρ_{top} in nir2 band to allow MTCI computation	s	dl	Nominally 0.3
ρ_{nir2_min}	Maximum value of ρ_{top} in red band to allow MTCI computation	s	dl	Nominally 0.1
ρ_{diff_min}	Minimum value of the reflectance difference between nir1 and red to allow MTCI computation	s	dl	Nominally 0.05
BAD_VALUE	Output value when algorithm fails	s	-	Previously defined
MTCI(j,f)	Chlorophyll index	o	dl	to step 2.10, to Breakpoint
ORINP2_F(j,f)	Out of range input flag for MTCI	i/o	-	default: FALSE, to step 2.10, to Breakpoint
OROUT2_F(j,f)	Out of range output flag for MTCI	i/o	-	default: FALSE, to step 2.10, to Breakpoint

Table 7.1. List of Variables used in the MTCI algorithm (figure 7.4) in the MERIS processor.

For each pixel (j,f) such that (INVALID_F(j,f) == FALSE) AND (LANDCONS_F(j,f) = TRUE)

Exception processing

WHEN ($\rho_{top}(mtci_red_band,j,f) \leq 0$) **OR**
 $(\rho_{top}(mtci_nir1_band,j,f) \geq \rho_{red_max})$ **OR**
 $\rho_{top}(mtci_nir2_band,j,f) \geq \rho_{nir2_min}$ **OR**
 $|\rho_{top}(mtci_nir1_band,j,f) - \rho_{top}(mtci_nir2_band,j,f)| < \rho_{diff_min}$:
ORINP2_F(j,f)=TRUE
MTCI(j,f)= BAD_VALUE)

End of exception processing

$$MTCI(j,f) = \frac{\rho_{top}(mtci_nir2_band,j,f) - \rho_{top}(mtci_nir1_band,j,f)}{\rho_{top}(mtci_nir1_band,j,f) - \rho_{top}(mtci_red_band,j,f)}$$

If(MTCI(j,f)<MTCI_RANGE(0))**OR**(MTCI(j,f)>MTCI_RANGE(1)) **THEN**
ORINP2_F(j,f)=TRUE
MTCI(j,f)= BAD_VALUE
ENDIF

Figure 7.4. Description of **Algorithm 2.8** used for MTCI calculation.

A detailed description of this algorithm, including the physical principles and mathematical background can be found in the Algorithm Theoretical Basis Document (ATBD) (ATBD-2.20, Chlorophyll Index, *Version-2*) submitted to the ESA (Curran and Dash, 2004). This ATBD also describes the limitations and assumptions behind this algorithm.

7.2.3 Conclusion

MTCI is a direct indicator of vegetation chlorophyll content, thereby, the vegetation condition and it is the only chlorophyll index available from space-borne imaging spectrometer. Recently ESA has taken initiative to validate MTCI with real ground chlorophyll content data. This validation campaign will start from beginning of 2006 and will continue up to 2008.

MTCI is an operational level 2 product readily available from the standard MERIS processor. It could be used for a number of ecological and environmental applications at regional to global scales. The next section reports on the use of MTCI along with MGVI for mapping eleven broad landcover classes in Wisconsin, USA.

7.3. Land cover classification using multi-temporal MERIS vegetation indices

7.3.1 Introduction

Land cover maps provide key environmental information for environmental understanding, resource management and policy development at a range of spatial scales (Cihlar 2000; Latifovic *et al.* 2004; Treitz and Rogan 2004). Remote sensing has considerable potential for the provision of land cover maps but the accuracy of these maps is sometimes viewed as insufficient (Wilkinson 1996; Foody 2002). There are many factors responsible for this

situation including the nature of classes being studied, the properties of the sensing system used to acquire the imagery and also the techniques used to extract thematic information from the imagery (Steele 2000; Foody 2002; Pal and Mather 2003). Despite recent research into land cover classification, the accuracy with which land cover has been mapped from remotely sensed data often remains low and there does not appear to be an upward trend in accuracy over time. Wilkinson (2005) highlighting the need for further advances if the full potential of remote sensing for land cover is to be realised.

The growing need for land cover information has driven developments in sensing technologies as well as advances in methods to extract information from remotely sensed data. Research over last two decades has, for example, focussed on ways to increase the accuracy of thematic information extraction from remotely sensed data (Benediktsson *et al.* 1990, Friedl and Brodley 1997; Foody and Mathur 2004) often making use of contemporary sensing systems with enhanced spectral, spatial and radiometric properties. Much research has also addressed the potential benefits to be derived from the inclusion of additional information such as (i) image texture, context and ancillary information (e.g., soil, topography) and (ii) waveband transformations such as vegetation indices (Beneditti *et al.* 1994; Krishnaswamy *et al.* 2004; Li and Moon 2004; Mather 2004) into the classification methodology. This section focuses on the use of vegetation indices as discriminating variables for land cover classification.

Vegetation indices, empirical formula derived using reflected radiance in two or more wavelengths, have been used widely to indicate vegetation properties. These vegetation indices may also be used to enhance the contrast between vegetated and non vegetated land cover classes and so be useful as discriminating variables in classification applications.

The most commonly used vegetation indices are the normalised difference vegetation index (NDVI) and simple ratio (SR) (Gaston *et al.* 1994; Myneni *et al.* 1995; Lobo *et al.* 1997). However, many vegetation indices have been developed that are relatively insensitive to soil background, Sun-sensor angular geometry and the atmosphere. For example, widely used indices include the perpendicular vegetation index (PVI) (Richardson and Wiegand 1977), weighted distance vegetation index (WDVI) (Clevers 1988), soil adjusted vegetation index (SAVI) (Huete 1988), transformed soil adjusted vegetation index (TSAVI) (Baret and Guyot 1991), atmospherically resistant vegetation index (ARVI) (Kaufman and Tanré 1992) and the global environmental monitoring index (GEMI) (Pinty and Verstraete 1992). Although often specified to indicate biophysical properties (Tucker *et al.* 1985) vegetation indices have also been used as discriminating variables in image classification (e.g. Justice *et al.* 1989; Lloyd 1990; Hill and Foody 1994; Benedetti *et al.* 1994; Achard and Estreguil 1995).

The NDVI is the most widely used vegetation index for classification applications (Lloyd 1990; Myneni *et al.* 1995; Li and Moon 2004) and has been used both as an additional discriminating variable or used to indicate specific properties of vegetation. For example, using NDVI data Running *et al.* (1995) present a classification based on the permanence of above ground biomass, longevity of leaves and leaf type. Critically, the use of a vegetation index can yield a classification that is more accurate than one derived from the data used in its calculation (Anderson *et al.* 1993, Nemani *et al.* 1993; Hirata *et al.* 1997). This feature, together with the ready availability of NDVI data in major archives (e.g. Smith *et al.* 1997) ensured that the NDVI is used widely in image classification. Indeed, the NDVI derived from a variety of different sensors has been used to classify vegetated terrain at scales ranging from the local to global (Benedetti *et al.* 1994; Lobo *et al.* 1997; Han *et al.* 2004;

Hansen *et al.* 2000). The NDVI is, for example, at the core of major global land cover mapping programmes (e.g. Loveland *et al.* 2000). Typically the data used are a time series of NDVI images which provide a measure of phenological variability in space and time that can facilitate inter-class discrimination (Tucker *et al.* 1985; DeFries and Townsend 1994). However, the use of the NDVI to classify vegetation has some major limitations (described earlier), one of which is insensitive to very high and very low chlorophyll content. The plant chlorophyll content varies with vegetation type (Clark 1995; Smith and Curran 1992; Peterson *et al.* 1988; Curran *et al.* 2001). For example, deciduous trees have higher chlorophyll content than coniferous trees. Not only is the chlorophyll content different for dissimilar vegetation types at a particular time, but also the variation in chlorophyll content for a growing season depends on vegetation type. This indicates that, knowledge of chlorophyll content in space and time may enhance class separability and the production of accurate land cover maps.

The aim of this study was to evaluate the potential of MERIS data, and especially the derived vegetation index products (MERIS VI data set), for land cover mapping. A key feature of the work was to determine if vegetation indices could be used to map land cover at least as accurately as single MERIS bands (MERIS spectral data set). This would be advantageous, as it would reduce the number of discriminating variables in the analysis (which should reduce the size of the training set needed and so the cost of undertaking a classification) as well as allowing researchers to exploit readily available data products.

7.3.2 MERIS vegetation indices

The study was based on the premise that the relationship between chlorophyll concentration varies with vegetation type and time. For example, vegetation with a large temporal range in chlorophyll concentration includes broadleaf forests and crops while

shrubs and pasture have a low chlorophyll range. The range in chlorophyll concentration over a growing season is expected to vary between different land cover classes and is associated with the phenology of the vegetation types. For example, deciduous trees have a higher variation in chlorophyll concentration than coniferous trees. This variation in chlorophyll concentration may also be influenced by geographical location. The range in chlorophyll concentration is, therefore, a function of time, space and land cover type.

The MGVI is related with biophysical variables such as LAI and is calculated from:

$$\text{MGVI} = g_0(\rho_{R681}, \rho_{R865})$$

where g_0 is the generic function (Verstraete and Pinty 1996), ρ_{R681} and ρ_{R865} are rectified bidirectional reflectance values in MERIS bands centred at 681.25 nm and 865 nm (Gobron *et al* 1999).

The MTCI is positively related to the total chlorophyll content of vegetation, which in turn is a product of the chlorophyll concentration (amount of chlorophyll per unit area) and LAI. Consequently, the ratio MTCI/MGVI is approximately equal to chlorophyll concentration.

The temporal variation in chlorophyll concentration of vegetation may provide a valuable discriminating variable. This variation in chlorophyll concentration can be estimated by subtracting chlorophyll concentration estimated in the low chlorophyll season from that estimated in the high chlorophyll season. The ideal dates of MERIS data acquisition for land cover classification should, therefore, be drawn from both the high and low chlorophyll seasons.

7.3.3 Data and methods

The study area comprised part of the State of Wisconsin, USA., where imagery acquired in late July and mid-September would represent high and low chlorophyll seasons.

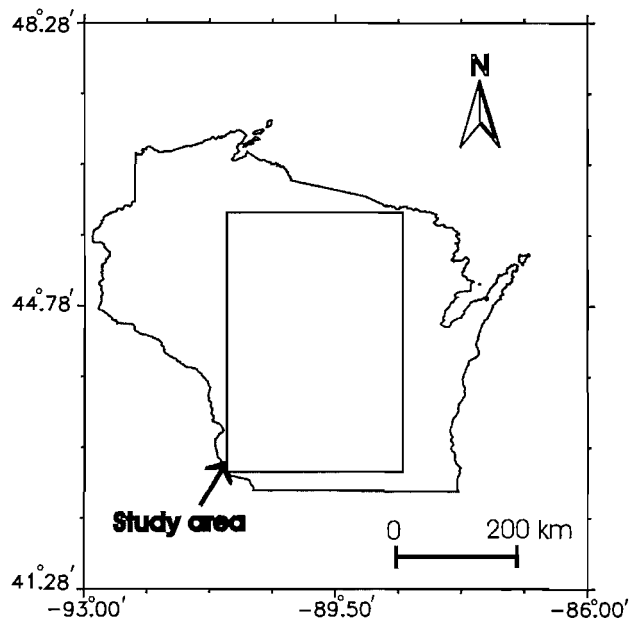


Figure 7.5. Study area for landcover classification

However, suitable cloud-free MERIS data were unavailable and so cloud-free MERIS data (spatial resolution of 300 m) acquired on 18th August 2003 and 20th September 2003 were used to represent a period late in high and early in the low chlorophyll season respectively (Figure 7.5). Although not ideal dates, the first lies near the end of the normal growing season while the second corresponds to the typical date of the first frost in the fall for the study area. Thus, although not widely separated in time, the two sets of imagery provided representations of the land cover at times when chlorophyll condition would be expected to differ markedly and so still be useful as potential discriminating variables.

The ground data set was the Wisconsin Initiative for State wide Cooperation on Landscape Analysis and Data (WISCLAND) land cover map (WiDNR, 1998). The WISCLAND land cover map was derived from the classification of Landsat Thematic Mapper (TM) data acquired during the mid-1990s (Reese *et al.* 2002). Although it is based on data acquired

nearly 10 years prior to that of the MERIS data used in this study, the land cover in the study area was relatively stable in this period except for gradual expansion of urban areas, which was addressed by excluding such regions from the analysis when extracting data from the imagery. Additionally, the WISCLAND data set is the finest spatial resolution, most accurate, and most categorically detailed land cover data set available for the State (Lillesand *et al.* 1998, Reese *et al.* 2002). The WISCLAND data set comprised 7 classes at Anderson level I and 24 classes at Anderson level II/III. The WISCLAND data had an overall accuracy of 94% for Anderson level I upland classes, 77% for Level II/III upland classes and 84% for level II/III wetland classes (WiNDR, 1998). For this study, the Anderson level I set of classes was deemed too generalised while the Anderson level II/III classes too detailed for mapping from MERIS data with a 300 m spatial resolution. The WISLAND detailed land cover classes were, therefore, merged to produce a generalized land cover map depicting a set of land cover classes that could potentially be classified using MERIS data (Table 7.6).

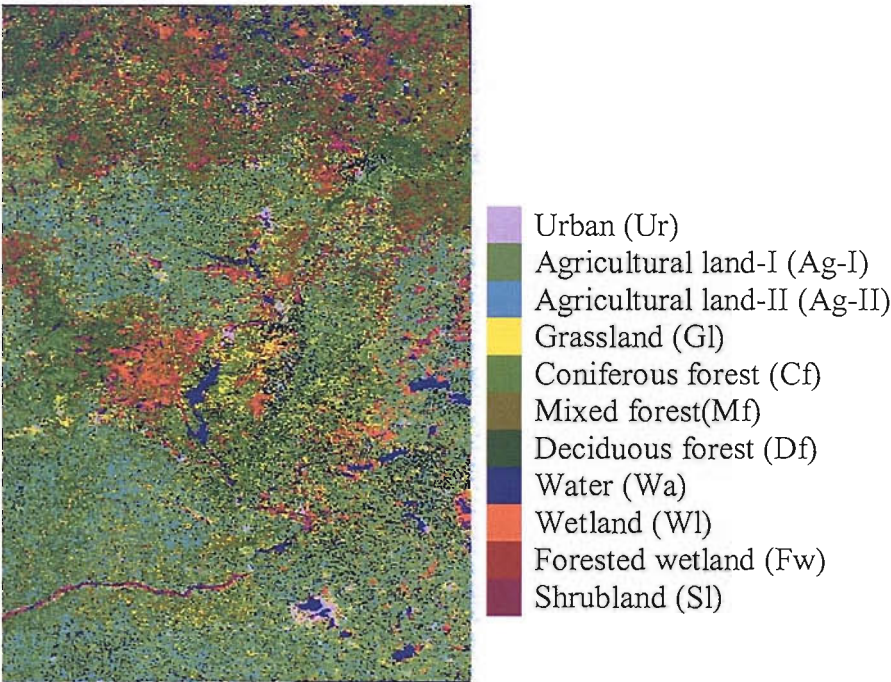


Figure 7.6. Landcover map of the study area derived from Landsat TM data.

Given that the ground data had a fine spatial resolution (30 m) relative to the MERIS data to be classified and the proportion of mixed pixels in an image is positively related to pixel size, action was taken to ensure that only, pure MERIS pixels were selected for the analysis. Training and testing data were, therefore, extracted from large homogenous sites for each of the classes to ensure pixel purity. In total, 962 MERIS pixels were extracted for further analysis, with the relative abundance of the classes at the test site reflected in the number of pixels derived for each class (Table 7.2). The data for each class were divided randomly into equally sized training and testing sets.

Classifications were undertaken using the data acquired in the MERIS spectral wavebands directly and the MERIS vegetation indices. Due to a processing problem, ESA was unable to provide data in MERIS wavebands 11 and 15 but data acquired in all other wavebands were available and included in the analyses. For the classifications using MERIS spectral data set, a feature selection analysis was used to reduce the size of the data set by removing potentially uninformative wavebands. This feature selection was based on a stepwise discriminant analysis applied to the training data set. The Wilks' lambda coefficient was inversely related to the discriminatory power of the variables input to the analysis. Wilks' lambda was used here to select the most discriminating set of the 13 spectral wavebands MERIS for use in the classification. For comparative purposes, the NDVI was also calculated for both image data sets and the separability of the classes in the resulting products assessed with Wilks' lambda. The NDVI was not, however, included in the classification as attention was focused on the potential of the MERIS vegetation index products as discriminating variables.

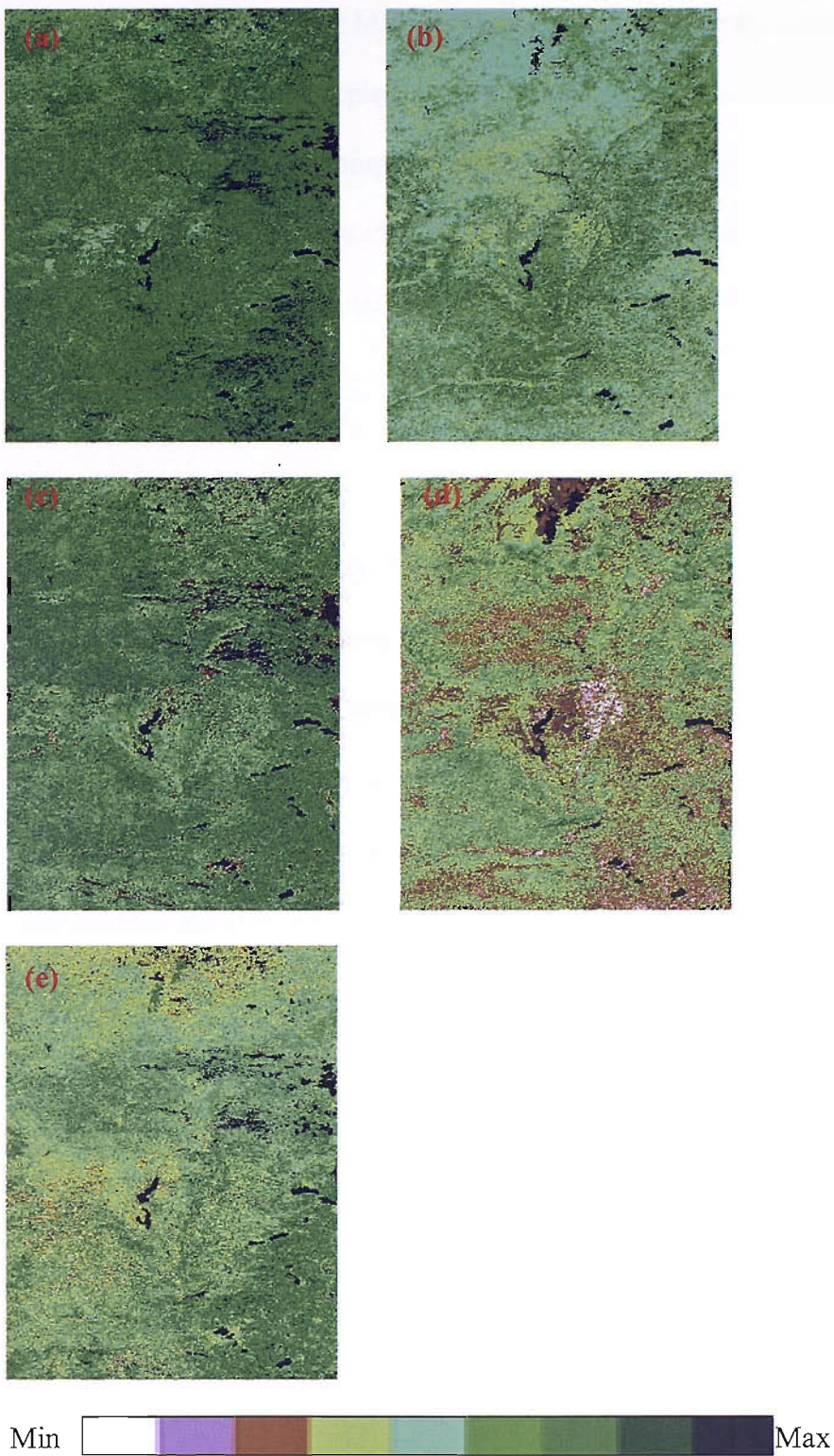


Figure 7.7. Vegetation indices image of the study area: (a) MTCI in August; (b) MTCI in September; (c) MGVI in August and (d) MGVI in September; (e) chlorophyll range.

For the classification using MERIS VI data set, the chlorophyll range, MTCI in high chlorophyll and low chlorophyll season and MGVI in high chlorophyll and low chlorophyll season were computed and used as discriminatory variables (Figure 7.7). The chlorophyll range was defined as the difference between the MTCI/MGVI ratio estimates derived for August and September respectively from,

$$C_{A-S} = \frac{MTCI_A}{MGVI_A} - \frac{MTCI_S}{MGVI_S}$$

where the subscripts identify the month of data acquisition.

An initial set of classifications were undertaken using discriminant analysis. This allocated each case to the class with which it had the highest posterior probability of membership. Since such probabilistic classification analyses may not always be appropriate a further set of classifications was undertaken with a support vector machine (SVM). SVM have attracted the attention of the remote sensing community for supervised image classification applications (Brown *et al.* 1999; Huang *et al.* 2002; Halldorsson *et al.* 2003). The mathematical background to SVM classification is not needed here and is discussed extensively in the literature (e.g. Huang *et al.* 2002; Foody and Mathur 2004). A key attraction of SVM for image classification, however, is that comparative studies have shown that SVM may classify remotely sensed data more accurately than many other classifiers (Huang *et al.* 2002; Pal and Mather 2003; Foody and Mathur 2004). Two parameters, one controlling the balance between the desire to maximise the margin between the classes against the term that penalises cases on the wrong side of the classifier's decision boundary (C) and the other to control the width of the Gaussian kernel used (γ), need to be defined for a SVM classification. Here, a range of parameter settings

were evaluated and the set that yielded the highest classification accuracy reported. This approach was adopted in order to indicate the greatest potential accuracy achievable. For comparative purposes the same training and testing sites were used in the two sets of classifications (MERIS spectral data set and MERIS VI data set).

Land cover class	Number of pixels
Urban	94
Agricultural land-I*	90
Agricultural land-II **	70
Grassland	98
Coniferous forest	104
Mixed forest	92
Deciduous forest	70
Water	60
Wetland	118
Forested wetland	102
Shrubland	64
Total	962

Table 7.2. The land cover classes and number of pixels extracted from each class for the analyses. Note that Agricultural land –I contains the vegetation type present on the field in August and September (e.g. corn) and Agricultural land –II contains the vegetation type harvested from the field by September (e.g. forage crop).

Classifications derived using both data set were compared to evaluate the relative value of the two information sources for mapping the land cover of the study area. In all cases, classification accuracy was expressed as the percentage of testing cases correctly classified (overall accuracy). The statistical significance of differences in the accuracy of the classifications derived was assessed using a McNemar test, without correction for continuity, for related samples (Foody 2004). All testing was undertaken at the 95% level of confidence. Interpretation of the test results is based on the Z statistic, with, for example,

a value $Z \geq |1.96|$ indicating a statistically significance difference in accuracy at the 95% confidence level.

<u>Variable</u>	<u>Wilks' Lambda</u>
NDVI	.106
B13	.155
B12	.156
B10	.160
MGVI	.169
MTCI	.169
B14	.173
Chlorophyll concentration	.254
B9	.274
B5	.350
B6	.365
B8	.372
B7	.373
B4	.423
B3	.446
B2	.468
B1	.488

Table 7.3. Wilks' lambda coefficients derived from the MERIS data acquired in August.

<u>Variable</u>	<u>Wilks' Lambda</u>
MTCI	.166
B14	.235
B13	.240
B12	.262
B10	.267
NDVI	.280
MGVI	.348
B9	.437
Chlorophyll concentration	.493
B5	.568
B6	.585
B7	.596
B8	.596
B4	.630
B3	.642
B2	.649
B1	.654

Table 7.4. Wilks' lambda coefficients derived from the MERIS data acquired in September.

Variable	Wilks Lambda
NDVI-August	.106
B13-August	.155
B12-August	.156
B10-August	.160
MTCI-September	.166
MGVI-August	.169
MTCI-August	.169
B14-August	.173
B14-September	.235
B13-September	.240
Chlorophyll concentration-August	.254
B12-September	.262
B10-September	.267
B9-August	.274
NDVI-September	.280
MGVI-September	.348
B5-August	.350
B6-August	.365
B8-August	.372
B7-August	.373
B4-August	.423
B9-September	.437
B3-August	.446
B2-August	.468
B1-August	.488
Chlorophyll concentration-September	.493
Chlorophyll range	.521
B5-September	.568
B6-September	.585
B7-September	.596
B8-September	.596
B4-September	.630
B3-September	.642
B2-September	.649
B1-September	.654

Table 7.5. Wilks' lambda coefficients derived from the combined August and September MERIS data sets.

7.3.4 Results and discussion

The discriminating ability of the MERIS spectral data set and MERIS VI data set was indicated by the magnitude of the Wilks' lambda coefficient derived from the discriminant analyses (Tables 7.3 to 7.5). It was evident that for both the August and September data

sets, a vegetation index provided the greatest discriminating information. Moreover, in relation to MERIS spectral data set, discriminating ability appeared to be related positively to wavelength. The rank order of the discriminating variables and level of spectral separability of the classes, however, appeared to vary with time. For example, data acquired in August appeared to provide a greater degree of discrimination than those acquired in September. In addition, while the NDVI was the most discriminating variable in August the MTCI provided the greatest degree of discrimination in September. With the data for the two months combined, the vegetation indices, especially the MTCI, were amongst the most discriminating variables (Table 7.5).

Using the data acquired for each month individually and combined, land cover maps of the study area were produced by stepwise discriminant analyses. For the August data set, nine spectral wavebands were selected from the spectral data set for inclusion in the classification and used to derive a map with an estimated accuracy of 66.7% (Table 7.6). Only five spectral wavebands were selected from the corresponding analysis of the data acquired in September and, as expected from the separability analyses, the derived land cover map was less accurate than that derived from the data acquired in August, with an accuracy of 55.9% (Table 7.7). For all classes except grassland, classification accuracy was lower in the September than August data set. Combining the MERIS spectral data set acquired in August and September resulted in an increase in class separability and hence map accuracy. With the eleven selected spectral bands the discriminant analysis classified the land cover the study area to an accuracy of 69.0% (Table 7.8).

Using the set of wavebands selected in the discriminant analyses, the classifications were repeated using the SVM. The SVM was able to classify the data for each month more accurately than was possible with discriminant analysis (Tables 7.9 and 7.10). The main difference was in relation to the September data set and most notably the deciduous forest

class. The classification derived from the combined use of the August and September data sets was, however, of comparable accuracy to that derived from the corresponding discriminant analysis (Table 7.11).

The results of the discriminant analyses indicated an ability to classify land cover to a moderate level of accuracy. However, the provision of the data acquired in all 13 available wavebands as discriminating variables necessitates a large training set. The potential of the MERIS VI data set for classification, which may allow a reduction in the size of the training set required was assessed through classifications by the discriminant analysis and SVM. The discriminant analysis yielded a classification with an overall accuracy of 67.2% (Table 7.12), marginally, but insignificantly ($Z=-0.384$), different from the comparable classification based on the MERIS spectral data set (Table 7.8). The SVM classification was significantly more accurate than that derived from the discriminant analysis ($Z=2.36$), with an overall accuracy of 73.2% (Table 7.13). In general, the accuracy of each class from the producer's perspective was higher in the SVM classification except for three classes for which there were very small decreases in accuracy associated with no more than 4 pixels. Critically, for classification by SVM, the use of MERIS VI data set rather than the MERIS spectral data set resulted in a 4.37% increase in accuracy, although the difference was (marginally) insignificant ($Z=1.86$). The MERIS VI data set, therefore, appear able to provide at least a comparable if not increased ability to discriminate the land cover classes relative to that associated with the MERIS spectral data set and have great potential for use in land cover classification. It is possible that data acquired at different dates, especially in the high chlorophyll season, may provide further discrimination.

	Predicted Class											
Actual Class	Ur	Ag-I	Ag-II	Gl	Cf	Mf	Df	Wa	Wl	Fw	Sl	Total
Urban (Ur)	40				7							47
Agricultural land-I (Ag-I)		39				3	3					45
Agricultural land-II (Ag-II)			27			1			1	6		35
Grassland (Gl)			5	11	26		1		3		3	49
Coniferous forest (Cf)				11	32				2	2	5	52
Mixed forest (Mf)		1		1		28	8			7	1	46
Deciduous forest (Df)						10	25					35
Water (Wa)								30				30
Wetland (Wl)	1		7	1	3				44	1	2	59
Forested wetland (Fw)				4	3	9	3		2	25	5	51
Shrubland (Sl)			1	3	1				3	4	20	32
Total	41	40	40	31	72	51	40	30	55	45	36	481

Table 7.6. Confusion matrix for the classification by discriminant analysis using data acquired in the MERIS spectral wavebands in August. Wavebands selected: B1, B3, B5, B8, B9, B10, B12, B13 and B14. Overall accuracy = 66.74%.

	Predicted Class											
Actual Class	Ur	Ag-I	Ag-II	Gl	Cf	Mf	Df	Wa	Wl	Fw	Sl	Total
Urban (Ur)	35	1	1	4	3			1	1		1	47
Agricultural land-I (Ag-I)	1	20	6			1	10		6	1		45
Agricultural land-II (Ag-II)	1	3	27	1					2	1		35
Grassland (Gl)		3	3	19	15			1	2	5	1	49
Coniferous forest (Cf)	1			12	18				3	13	5	52
Mixed forest (Mf)		1	3	2	2	20	5		1	8	4	46
Deciduous forest (Df)			1	1		6	24				3	35
Water (Wa)								30				30
Wetland (Wl)	1		1	2	3			1	39	6	6	59
Forested wetland (Fw)			5		6	11	1		6	18	4	51
Shrubland (Sl)	1			1	2	1			2	6	19	32
Total	40	28	47	42	49	39	40	33	62	58	43	481

Table 7.7. Confusion matrix for the classification by discriminant analysis using data acquired in the MERIS spectral wavebands in September. Wavebands selected: B1, B2, B10, B12 and B13. Overall accuracy = 55.92%.

	Predicted Class											
Actual Class	Ur	Ag-I	Ag-II	Gl	Cf	Mf	Df	Wa	Wl	Fw	Sl	Total
Urban (Ur)	41				5						1	47
Agricultural land-I (Ag-I)		39	1			1	4					45
Agricultural land-II (Ag-II)			29						3	3		35
Grassland (Gl)			4	13	26				2	2	2	49
Coniferous forest (Cf)				13	31				1	2	5	52
Mixed forest (Mf)		1		1		31	7			6		46
Deciduous forest (Df)						8	25				2	35
Water (Wa)								30				30
Wetland (Wl)	1		1	4	2				49	1	1	59
Forested wetland (Fw)			1	2	6	8	4		1	25	4	51
Shrubland (Sl)	1			1	3				1	7	19	32
Total	43	40	36	48	63	48	40	30	57	46	34	481

Table 7.8. Confusion matrix for the classification by discriminant analysis using data acquired in the MERIS spectral wavebands in August and September. Wavebands selected: B1, B5, B7, B8, B9, B10 and B12 from August and B1, B7, B10 and B12 from September. Overall accuracy = 69.02%.

	Predicted Class											
Actual Class	Ur	Ag-I	Ag-II	Gl	Cf	Mf	Df	Wa	Wl	Fw	Sl	Total
Urban (Ur)	40				5				2			47
Agricultural land-I (Ag-I)		42				2	1					45
Agricultural land-II (Ag-II)			25								10	35
Grassland (Gl)			3	32	5				3		6	49
Coniferous forest (Cf)	2			12	26				6	1	5	52
Mixed forest (Mf)		1				33	2			10		46
Deciduous forest (Df)		4				12	19					35
Water (Wa)								30				30
Wetland (Wl)				1					52	6		59
Forested wetland (Fw)						12			4	34	1	51
Shrubland (Sl)			3	3	3				3	1	19	32
Total	42	47	31	48	39	59	22	30	70	52	41	481

Table 7.9. Confusion matrix for the classification by SVM using data acquired in the MERIS spectral wavebands in August. Wavebands used: B1, B3, B5, B8, B9, B10, B12, B13 and B14. Note $C=14$ and $\gamma=9$. Overall accuracy = 67.57%.

	Predicted Class											
Actual Class	Ur	Ag-I	Ag-II	Gl	Cf	Mf	Df	Wa	Wl	Fw	Sl	Total
Urban (Ur)	38	2		1	2				2		2	47
Agricultural land-I (Ag-I)		31	6	1			2		4	1		45
Agricultural land-II (Ag-II)		1	24		2				6	2		35
Grassland (Gl)			4	18	17				4	5	1	49
Coniferous forest (Cf)	2			11	27				6	4	2	52
Mixed forest (Mf)		2	3	1	2	21	6		1	7	3	46
Deciduous forest (Df)			3			3	25		1	1	2	35
Water (Wa)								30				30
Wetland (Wl)	1		1	2	5				40	5	5	59
Forested wetland (Fw)		1	4	1	7	6	2		4	26		51
Shrubland (Sl)	1				2	1			4	9	15	32
Total	42	37	45	35	64	31	35	30	72	60	30	481

Table 7.10. Confusion matrix for the classification by SVM using data acquired in the MERIS spectral wavebands in September. Wavebands used: B1, B2, B10, B12 and B13. Note $C=250$ and $\gamma=30$. Overall accuracy = 61.33%.

	Predicted Class											
Actual Class	Ur	Ag-I	Ag-II	Gl	Cf	Mf	Df	Wa	Wl	Fw	Sl	Total
Urban (Ur)	37	1	1		2				2	4		47
Agricultural land-I (Ag-I)		40	1			3	1					45
Agricultural land-II (Ag-II)			27	2					6			35
Grassland (Gl)	2		1	27	8				4	4	3	49
Coniferous forest (Cf)	1			17	22				5	3	4	52
Mixed forest (Mf)		1	1			29	5		1	8	1	46
Deciduous forest (Df)		2				5	26			1	1	35
Water (Wa)								30				30
Wetland (Wl)	2		1		3				50	3		59
Forested wetland (Fw)	1	1		4	1	5			2	33	4	51
Shrubland (Sl)			1	3	4	1	2		2	9	10	32
Total	43	45	33	53	40	43	34	30	72	65	23	481

Table 7.11. Confusion matrix for the classification by SVM using data acquired in the MERIS spectral wavebands in August and September. Wavebands used: B1, B5, B7, B8, B9, B10 and B12 from August and B1, B7, B10 and B12 from September. Note $C=400$ and $\gamma=30$. Overall accuracy = 68.81%.

7.3.5 Conclusions

The study investigated the potential of MIP in Agri. and Forests for MIP in Vietnam.

	Predicted Class											
Actual Class	Ur	Ag-I	Ag-II	Gl	Cf	Mf	Df	Wa	Wl	Fw	Sl	Total
Urban (Ur)	37				10							47
Agricultural land-I (Ag-I)		39				1	5					45
Agricultural land-II (Ag-II)			29								6	35
Grassland (Gl)			7	28	4				2	1	7	49
Coniferous forest (Cf)	2		1	9	19				11	5	5	52
Mixed forest (Mf)		3				32				11		46
Deciduous forest (Df)		5				9	21					35
Water (Wa)								30				30
Wetland (Wl)					2			3	43	9	2	59
Forested wetland (Fw)						20	1		2	26	2	51
Shrubland (Sl)			6	4	1				2	1	18	32
Total	39	47	43	41	36	62	27	33	60	53	40	481

Table 7.12. Confusion matrix for the classification by discriminant analysis using the vegetation index product data for August and September. Overall accuracy = 67.20%.

	Predicted Class											
Actual Class	Ur	Ag-I	Ag-II	Gl	Cf	Mf	Df	Wa	Wl	Fw	Sl	Total
Urban (Ur)	40				5				2			47
Agricultural land-I (Ag-I)		42				2	1					45
Agricultural land-II (Ag-II)			25								10	35
Grassland (Gl)			3	32	5				3		6	49
Coniferous forest (Cf)	2			12	26				6	1	5	52
Mixed forest (Mf)		1				33	2			10		46
Deciduous forest (Df)		4				12	19					35
Water (Wa)								30				30
Wetland (Wl)				1					52	6		59
Forested wetland (Fw)						12			4	34	1	51
Shrubland (Sl)			3	3	3				3	1	19	32
Total	42	47	31	48	39	59	22	30	70	52	41	481

Table 7.13. Confusion matrix for the classification by the SVM using the vegetation index product data for August and September. Note $C=3$ and $\gamma=8$. Overall accuracy = 73.18%.

7.3.5 Conclusions

The study highlighted the potential of MERIS data, and especially the MERIS VI data set, for use as discriminating variables in land cover classification. The ability to separate eleven broad land cover classes in Wisconsin using MERIS data acquired on two dates was assessed. The MERIS VI data set was noted to provide a high degree of inter-class separability, more so than many of the spectral wavebands. Separability and classification accuracy were also observed to vary between dates, being higher with data acquired in August rather than September. Using the data acquired in each month together resulted in an increase in classification accuracy. It is possible that the use of data acquired earlier in the growing season may further enhance class separability and this is an issue that could be addressed in future research.

The highest accuracy was obtained using the MERIS VI data set with a SVM, yielding an accuracy of 73.2%. MERIS vegetation index data are now readily accessible as a fine spatial resolution (300 m) European Space Agency level 2 product with a potential for reducing both volume of data and size of training sets used in land cover classification. It is therefore, anticipated that MERIS vegetation index data will be used increasingly for mapping land cover.

7.4. Conclusion

In this chapter the processing steps required for implementing MTCI in the MERIS processor were discussed. Also this chapter demonstrated the ability of multi temporal MERIS vegetation indices to classify landcovers. Which can be summarised as:

- MERIS vegetation indices in the high and low chlorophyll seasons can be used to enhance class separability.

- The vegetation indices were amongst the most discriminating variables, providing a higher degree of inter-class separability than the data acquired in many of the MERIS spectral wavebands.
- The most accurate map (73.2%) was derived from a classification of vegetation index derived data with a support vector machine and was 4.37% more accurate than the corresponding map derived from a classification using the data acquired in the original spectral wavebands.

Chapter 8. Application of MTCI-II

8.1. Introduction

Accurate and repetitive measurements of regional to global scale vegetation condition are required to understand a number of important processes, for example, global carbon cycle. The condition of vegetation is generally related to the amount of chlorophyll presented in the particular vegetation canopy. Therefore, it is essential to estimate terrestrial vegetation chlorophyll content at regional to global scales. For the moment at least this is only possible by using MTCI available from the MERIS data. In an ideal case we would like chlorophyll content data derived from ground data. In the absence of this we looked for sites where chlorophyll content was known to vary.

This chapter represents two regional scale application of MTCI in assessing vegetation condition in : (i) coastal vegetation affected by saltwater inundation due to the Indian Ocean tsunami in 26th December 2004 and (ii) forests of southern Vietnam affected by herbicide spraying during 1960s and 1970s.

8.2. Assessment of vegetation condition in the tsunami affected coastal region

8.2.1 Introduction

On 26th December 2004 Southeast Asia was hit by a tsunami generated by an undersea earthquake with an epicentre located approximately 100 km north of Indonesian province of Sumatra. The earthquake was 9.0 on the Richter scale and the largest since the Alaskan Good Friday earthquake of 1964 (BBC 2005). The earthquake uplifted the sea bed by several meters and displaced water struck the coast of southern India, Sri Lanka, southern Thailand, Indonesia and neighbouring countries. This natural disaster resulted in more than a quarter of a million fatalities and the destruction of roads, buildings and other

infrastructure (SpaceUK 2005). The coastal vegetation was removed in many areas. In addition, some near-coastal and low lying interior regions were inundated by salt water. According to media reports from the region the resultant salt stress reduced the chlorophyll content and led to early senescence of vegetation (Mail and Guardian 2005).

The importance of chlorophyll content to estimate vegetation condition is described in section 2.3 of this thesis.

The aim of this study was to determine if there was a decrease in the MTCI after the tsunami in near-coastal and low lying interior regions of Thailand. The hypothesis was that near-coastal and low lying interior regions, which were stressed due to the salt water inundation, would have decreased chlorophyll content and hence decreased MTCI values after the tsunami.

8.2.2 Study area and remotely sensed data

The study area was the southern part of Phuket province in Thailand (figure 8.1) and was selected because tsunami damage in this area was known to be severe (United Nations News 2005). The study area covers nearly 105 km² and comprises highlands, coastal and near-coastal plains and beaches. The dominant vegetation cover type was tropical rain forest with small strips of mangrove forest along the coast and the analysis that follows is for non-mangrove areas.

Remotely sensed data from two missions (Envisat's MERIS and Shuttle Radar Topography Mission (SRTM)'s Spaceborne Imaging Radar-C (SIR-C)) were employed.

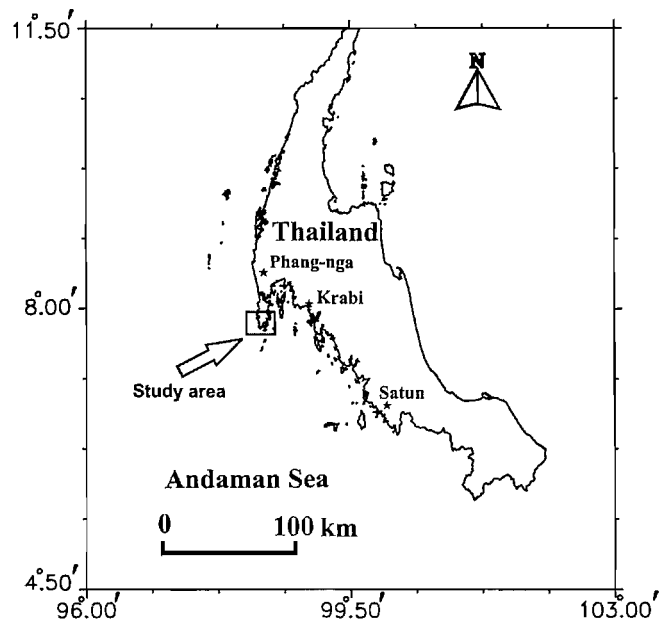


Figure 8.1. Location of the study area in western Thailand.

8.2.2.1. MERIS data

MERIS can sense in 15 programmable visible and NIR wavebands with dual spatial resolutions of 300 m and 1200 m and a three day repeat cycle. Two MERIS full resolution (300 m) images (21st December 2004 and 6th January 2005) were geo-corrected (nearest neighbour) and used to estimate MTCI. Care was taken to minimise any errors caused by both inaccuracies in image co-registration and differences in data acquisition conditions between these pre and post tsunami MERIS images. The same ground control points were used in both images to reduce the probability of registration error. Sun-sensor geometry and atmospheric conditions may affect the radiances recorded by the instrument. However, the difference between both conditions was not large enough to affect MTCI estimation for pre and post tsunami data. There being a 1.1° difference in Sun zenith angle and 4.3° difference in sensor zenith angle at the centre of the study site between both dates. Similarly, there was 3% change in the relative humidity and 5 DU change in ozone concentration for the centre of the study site between both dates.

8.2.2.2. SRTM data

The elevation of the study area ranged from mean sea level to 419 m. SIR-C measures the Earth’s surface from an altitude of 233 km and with a swath of 225 km (Farr and Kobrick 2000). SRTM data were organized and mosaiced into rasterized cells at NASA’s Jet Propulsion Laboratory (JPL). Each cell covered one degree by one degree in latitude and longitude and individual data points were spaced by either 1 arc-second (SRTM-1) or 3 arc-seconds (SRTM-3), and SRTM -3 data were used here.

	Spectral data		Elevation data
	Pre-tsunami	Post-tsunami	
Sensor	MERIS	MERIS	SIR-C
Date of acquisition	21 st Dec. 2004	6 th Jan. 2005	Feb. 2000
Spatial resolution (m)	300	300	90
Instrument	Imaging spectrometer	Imaging spectrometer	Radar

Table 8.1. Remotely sensed data used in this study: MERIS is the Medium Resolution Imaging Spectrometer on board ESA’s Envisat and SIR-C is the Spaceborne Imaging Radar-C on board NASA’s Shuttle Radar Topography Mission (SRTM).

These elevation data were co-registered with the MERIS image for December, resampled to the spatial resolution of MERIS (300 m) and output as a digital elevation map of the study area (figure 8.2).

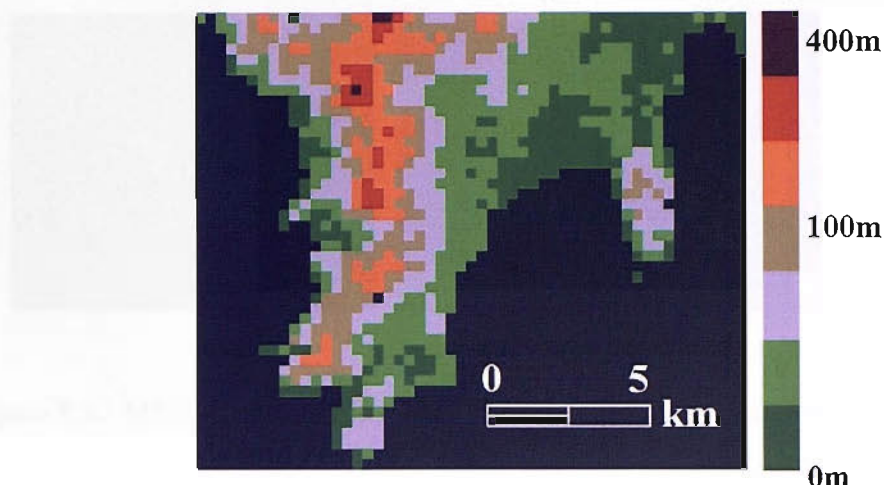


Figure 8.2. Elevation image of the study area generated from SRTM data.

8.2.3 Analysis and results

The analysis was undertaken in two steps: first, a determination of the difference between the two MTCI images and second, a determination of the relationship between these differences and elevation.

8.2.3.1. Change detection

Both tropical rain forest and mangrove forest in south Phuket had a high chlorophyll content, hence they had high MTCI values (represented as dark green on the pre-tsunami MTCI image (figure 8.3a)). In the post-tsunami MTCI image the MTCI values had changed little in the west but had decreased in the east (figure 8.3b).

A change detection map was produced using pre and post-tsunami MTCI images (figure 8.4). This was classified broadly into: (i) where there was a little change in MTCI values after the tsunami; (ii) where there was a small decrease in MTCI values after the tsunami and (iii) where there was a large decrease in MTCI values after the tsunami.

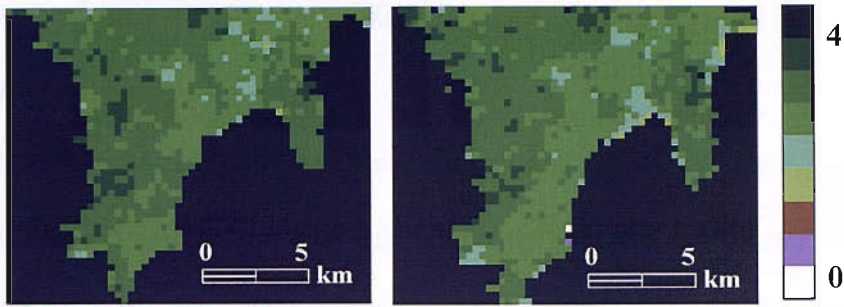


Figure 8.3. MTCI image of the study area (a) pre-tsunami; (b) post-tsunami.

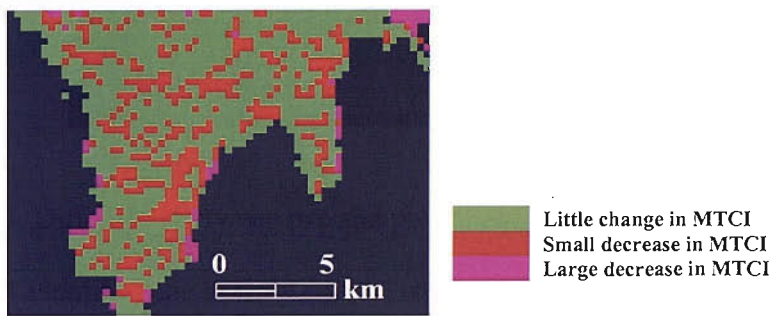


Figure 8.4. Difference between pre and post-tsunami MTCI images.

Figure 8.4 identifies the narrow coastal strip where the removal of some of the vegetation (mainly mangroves) by the tsunami resulted in a considerable decrease in MTCI. However, the majority of the difference image indicated little change or a small decrease in MTCI. It was hypothesised that areas where there was some, albeit a small change in MTCI were at lower elevations.

8.2.3.2. MTCI change in relation to elevation

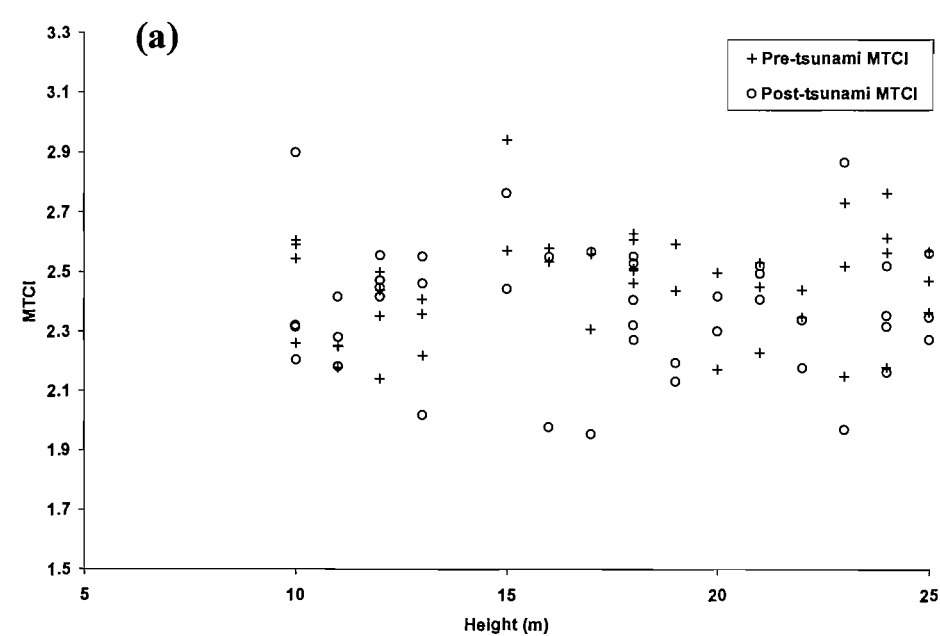
To study the relation between difference in MTCI in the non-near coastal regions and elevation, random points were selected across the image. Severely damaged mangrove vegetations at elevation below 10 m were excluded. The remaining data were then divided by elevations into: (i) between 10 m and 25 m and (ii) greater than 100 m. Both pre-

tsunami and post-tsunami MTCI values were plotted against height estimated using SRTM data.

Vegetation at an elevation between 10 m and 25 m tended to have decreased MTCI values after the tsunami (figure 8.5a). This was consistent with the hypothesis that salt water inundation resulted in salt stressed vegetation and this led to a decrease in chlorophyll content and MTCI values. Some pixels had a little change in MTCI values, even though they had an elevation between 10 m and 25 m. However, these pixels were situated far from the coast and so were less likely to have been inundated by saltwater.

Vegetation at an elevation of greater than 100 m showed little change in MTCI values after the tsunami (figure 8.5b). This was because, these regions were less likely to have been affected by salt water inundation and so would not have experienced either salt stress or a decrease in chlorophyll content.

Analysis of variation (ANOVA) was used to determine if the observed differences were statistically significant. For elevations between 10 m and 25 m, there was a statistically significant ($p=0.02$) decrease in MTCI values and for elevations greater than 100 m there was no significant change ($p=0.305$) in MTCI values following the tsunami.



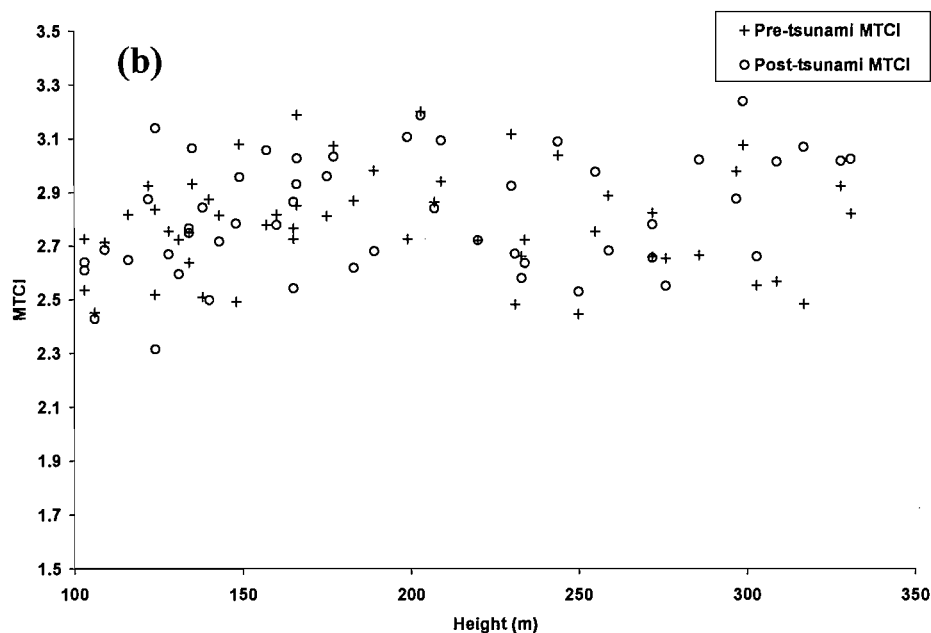


Figure 8.5. Pre and post-tsunami MTCI for terrain with an elevation (a) between 10 m and 25 m and (b) greater than 100 m.

8.2.4 Conclusion

The MTCI was used to examine the reported effect of salt stress on the vegetation of the near-coastal and low lying interior region of Phuket following the Indian Ocean tsunami. From this study it can be concluded that:

- There was a decrease in the MTCI in near-coastal and low lying interior regions. This, it was hypothesised, was the result of salt water stress leading to a decrease in the chlorophyll content of vegetation.
- There was a dramatic decrease in the MTCI of some parts of the coastal strip as vegetation (mainly mangroves) had been removed by the tsunami.
- Inland regions at elevations of over 100 m saw little or no change in MTCI after the tsunami.

- Salt water inundation results in a transient decrease in soil fertility and the recovery time of the near-coastal and low lying interior region will be monitored using the MTCl.

Future work will involve monitoring other affected areas in this region using the MTCl as an indicator of vegetation condition.

8.3. Present vegetation condition in the herbicide sprayed forests of southern Vietnam in the 1960s and early 1970s

8.3.1 Introduction

Herbicides were sprayed over Vietnam between January 1961 and September 1971 (Stellman et al., 2003) to defoliate trees, destroy crops and thereby increase visibility of the ground from the air. Heavily sprayed areas included both *inland forests* (i) near the demarcation line of military zones; (ii) at the borders with Cambodia and Laos and (iii) north and northwest of Saigon and *mangrove forests* (i) on the southernmost peninsula of Vietnam and (ii) along major shipping channels southeast of Saigon. This ‘defoliation mission’ affected over 2.61 million ha of land, of which more than 2 million ha was the forest target. Although the herbicide spraying mission started in 1961 and continued until 1971, the main spraying period was from 1965 to 1971 (with a peak between 1966 and 1969). Over the seven years from 1965 -1971 more than 66 million liters of herbicide were used, of which more than 60% was Agent Orange (a code name derived from the orange band used to mark its storage drums) (Young and Reggiani, 1988) (figure 8.7). Agent Orange was a mix of chemicals with equal amounts of two active ingredients (2,4-D n-butyle ester and 2,4,5-T n-butyle ester). Both Agent Orange and Agent White (table1) contain hormone mimicking compounds which interfere with plant metabolism whereas Agent Blue prevents plants from retaining moisture. Agent Orange and Agent Blue were both effective defoliant of dicotyledonous plants and so were used to spray the forests,

whereas Agent Blue was also an effective defoliant of monocotyledonous plants and so was used to spray grain crops (Young, 1975). These chemicals were dispensed by fixed-wing aircraft and to a much lesser extent by ground troops.

Herbicide concentrations used in the defoliation mission were approximately six to twenty five times greater than for normal agricultural use. Loss of foliage, flower and fruit occurred within two to three weeks of spraying (Buckingham, 1982) and some trees died. The level of such contamination was so high that it led to a long term decrease in chlorophyll of forests that have since regained full canopy cover.

Chemical Agent	Total used (l)	Percent of total used	Chemical constituents
Blue	4263299	6.6%	21% sodium cacodylate cacodylic acid to yield at least 26% total acid equivalent by weight
White	19872200	29.8%	Acid weight basis: 21.2% tri-isopropanolamine salts of 2,4-D and 5.7% picloram
Orange	42279487	63.6%	50% n-Butyl ester 2,4-D; 50% n-Butyl ester 2,4,5-T

Table 8.2 Herbicide sprayed during the defoliation mission.

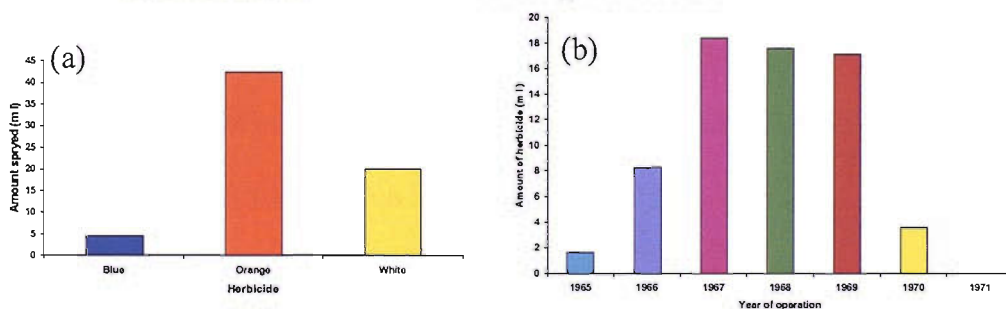


Figure 8.6 Herbicide used during 1965 to 1971 on the forest of southern Vietnam by (a) type and (b) year.

Remotely sensed estimation of foliar biochemical concentration of a vegetation canopy has been used to both understand and manage a wide range of environmental processes (Peterson et al., 1988; Jago et al., 1999; Mutanga and Skidmore, 2004). Chlorophyll is an

important foliar biochemical and is related to both vegetation condition and productivity (Mariotti et al., 1996, Datt, 1998; Gitelson and Merzlyak, 1998; Gitelson et al., 2002).

MTCI can be used to determine the vegetation condition in the herbicide-contaminated forests of southern Vietnam. The regions that received a high concentration of herbicide within forests that have since regained full canopy cover would tend to have a low chlorophyll content and hence low MTCI. In the absence of real chlorophyll content data, the concentration of herbicide previously deposited on the forest was used as a surrogate (inverse) for contemporary chlorophyll content.

This study examined the relationship between the concentration of herbicide sprayed during 1965 to 1971 and the present MTCI for the forests of southern Vietnam.

8.3.2 Data used

Two data set were used : (i) herbicide spraying data (as a surrogate of chlorophyll content) and (ii) full resolution MERIS data (300 m).

8.3.2.1. Herbicide spraying data

Information on the herbicide spraying mission in southern Vietnam has been organised into a database known as the HERBS file (NAS, 2003). Each data point in this file describes a mission in which a specific concentration of herbicide was dispersed along a specified route (copy of a HERBS file is given in the appendix).

Each data point in a HERBS files is broken down into six columns:

- (i) DATE- date of operation.
- (ii) AGN- Type of herbicide used.
- (iii) GALS- Number of gallons of herbicide used during a mission.
- (iv) TYP- Type of mission.

- (v) LEG –Path taken by a mission.
- (vi) UTM- Universal Transverse Mercator grid coordinate of each mission leg.

The spraying path is represented by a sequence of vertices to describe the starting, turning and stopping points. For example, if a flight path consists of three vertices, then spraying begins at 1A and continues until it reaches 1D (figure 8.7), 1B, 1C are intermediate turning points where the aircraft changes direction . Some aircraft which flew multiple paths in a single mission and additional vertices were designated as 2A, 2B, 3A etc. Each of these vertices has a reference UTM coordinate. A database of all missions flown between 1965 to 1971 was created from this HERBS file.

Processing the HERBS file

The aim was to create a herbicide concentration map of southern Vietnam at the same spatial resolution as that of MERIS data. All spraying missions were mapped (software developed at the University of Southampton) (Appendix) and this involved two steps: (i) plotting flight paths and (ii) estimating the concentration of herbicide sprayed per pixel.

Plotting flight paths

During the defoliation mission Vietnam had been divided into 100,000 m X 100,000 m squares. Each coordinate point recorded for a given mission consisted of eight characters: the first two were the label for the square on which an individual vertex fell and the next six were the geographic coordinates of the mission within the square (three marking a distance along the horizontal axis and the last three marking a distance along the vertical axis). For example, if a mission starts at YD 760230 then, YD is the label for the square on the map and 760 is the distance along the horizontal axis from the origin and 230 is the distance along the vertical axis from the origin. Therefore, the first processing task was to convert these local coordinates in the HERBS files to Easting and Northing on a common

grid. To obtain comparability with a full spatial resolution MERIS pixel, the area was divided into a 300 m X 300 m grid, the starting point of an individual mission was located and the subsequent vertices of individual flight were plotted on the grid (figure 8.7).

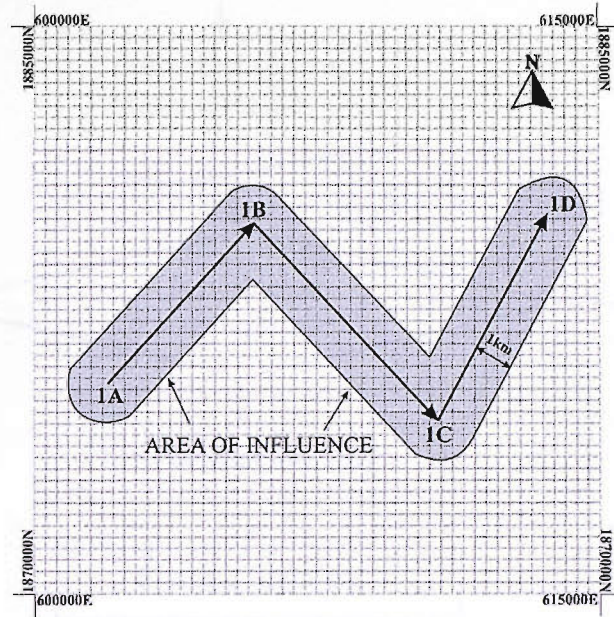


Figure 8.7. Plot of a flight path corresponding to a spraying mission started at (602100E,1875700N) and ended at (614800E,1879900N) of the UTM zone 48N with its estimated area of influence.

Estimating the concentration of herbicide sprayed per pixel

The next step in the processing chain was to estimate the concentration of herbicide sprayed on an individual pixel in a specific mission. It was assumed that (i) pixels within 1km of the flight path would be sprayed and (ii) this area of influence (AOI) was affected evenly.

The concentration of herbicide sprayed on an individual pixel during a particular mission was calculated by dividing the total concentration of herbicide sprayed during a mission by the AOI area (figure 8.8).

All missions were plotted on the predefined grid and all pixels were attributed with a specific concentration of herbicide sprayed for each mission flown. As a result the herbicide concentration map of southern Vietnam was produced (figure 8.9).

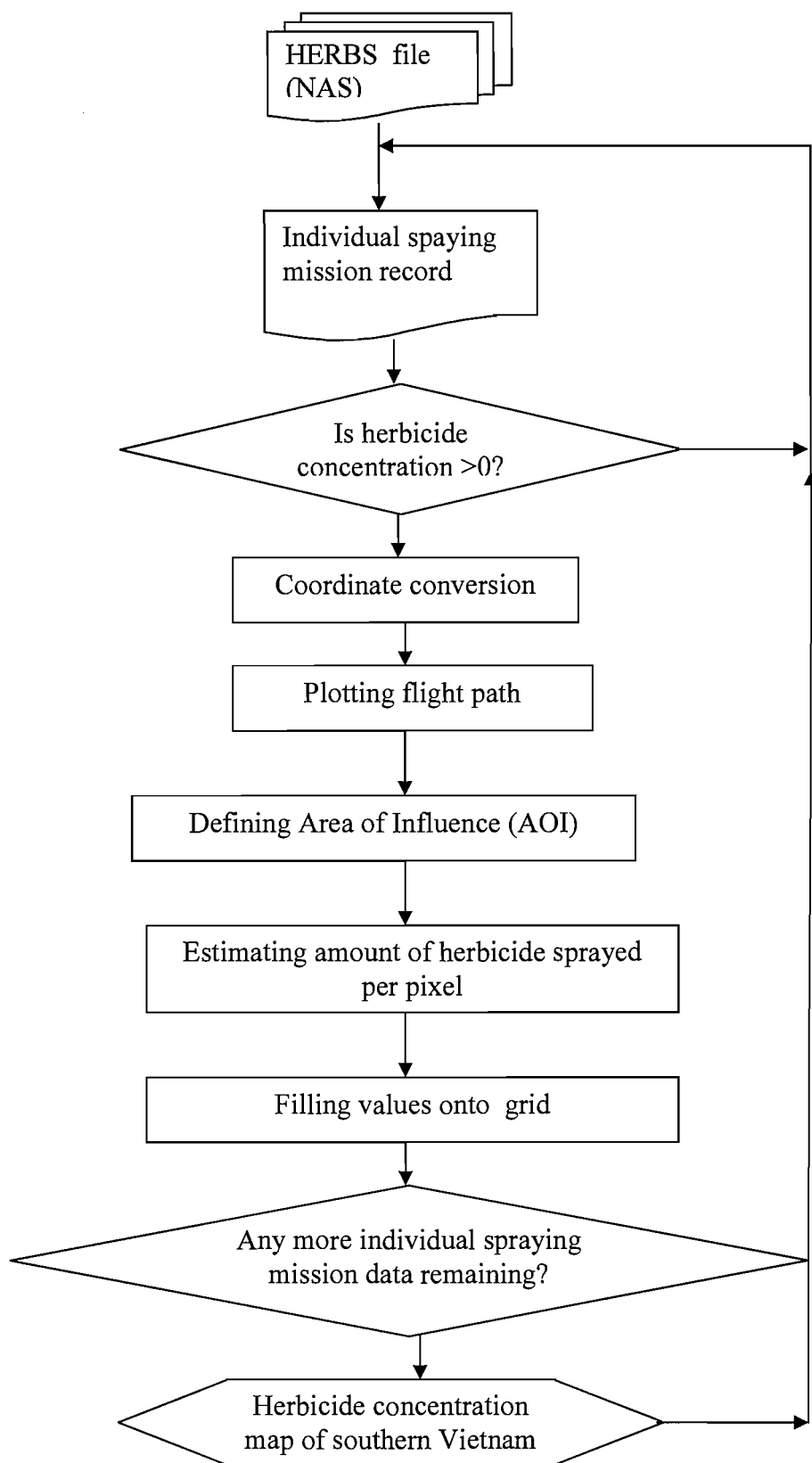


Figure 8.8 Flow diagram of HERBS file processing.

8.3.2.2. MERIS data

Two MERIS full resolution images acquired on 8th June 2003 were used to produce a mosaic of southern Vietnam. These images were (i) geometrically corrected (using the ground control points provided by ESA) and (ii) non forest areas were masked using a landcover map produced as a part of Global Land Cover-2000 (GLC-2000) project (JRC, 2004). Only the forest area was used for further analysis. MTCI was estimated for all forested pixels.

8.3.3 Results and discussion

Visual interpretation of the MTCI map and herbicide concentration map (figure 8.10) and a per pixel correlation between the MTCI and herbicide concentration (figure 8.12) indicated a negative relationship between the two. The nature of the relationship can be seen in the 3 pixel wide transect across an area with high variation in herbicide concentration (figure 8.11). Herbicide concentration increased and then decreased along the transect and MTCI decreased and then increased along the transect.

Initially it was assumed that the forested areas affected by the ‘defoliation mission’ would have lower chlorophyll concentration than the areas which were not affected. Only cloud free forested pixels which have herbicide concentration greater than a threshold of 400 l km⁻² were selected . This was taken to be the minimum concentration of herbicide that would have an influence on contemporary chlorophyll concentration. For these cloud free pixels the relationship between MTCI and herbicide concentration was determined. There was a strong negative relationship with a coefficient of determination (r^2) of 0.74 (figure 8.12).

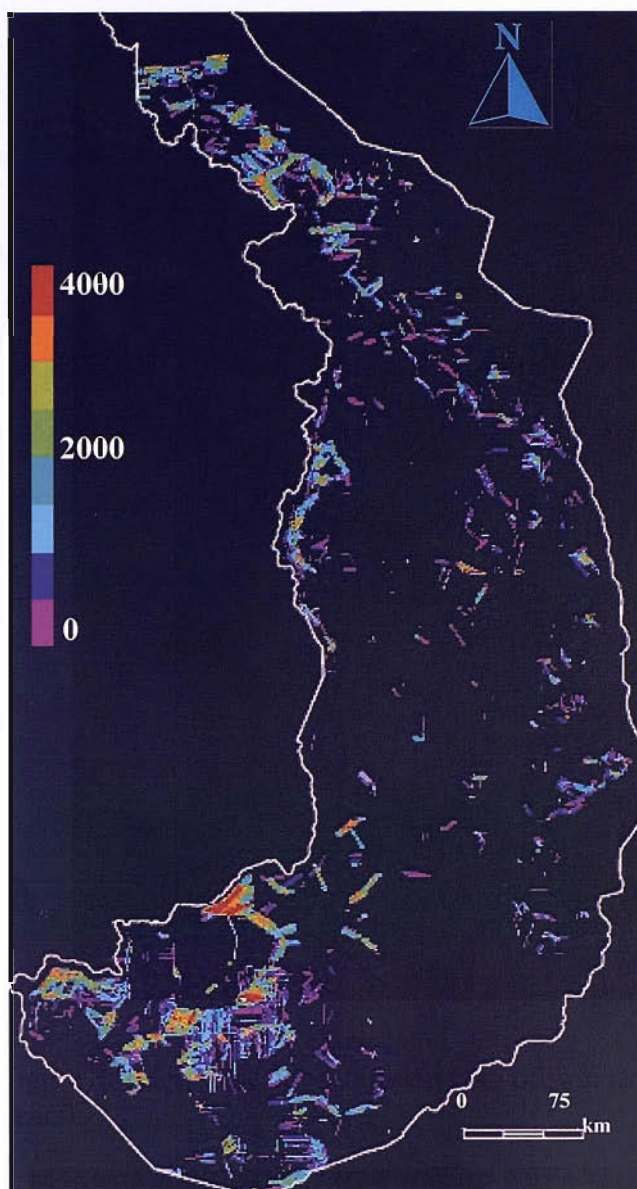


Figure 8.9 Herbicide concentration map of southern Vietnam (units of 1 km^{-2} over 7 years).

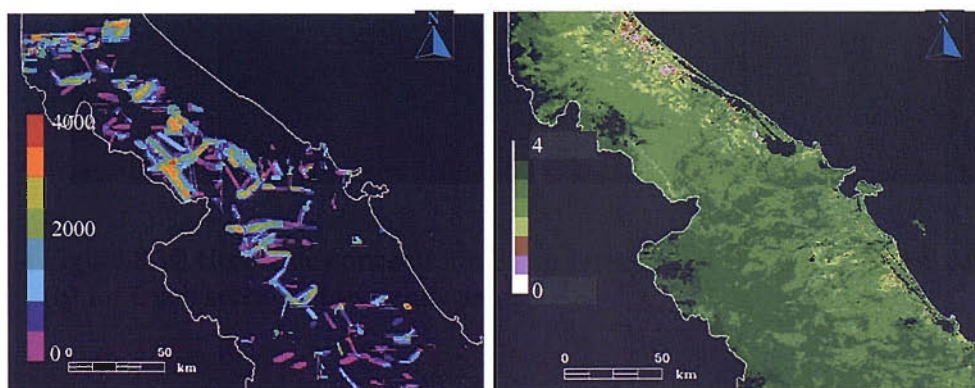


Figure 8.10 Herbicide concentration map (units of 1 km^{-2} over 7 years) (a) and MTCI map (b) for a sub section of the study area.

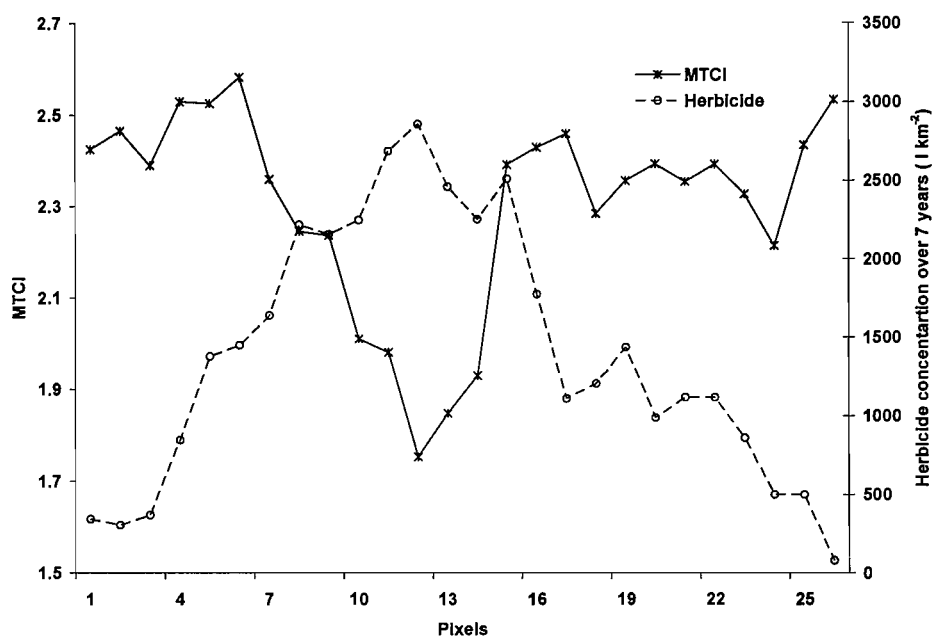


Figure 8.11 Herbicide concentration and MTCI along a transect.

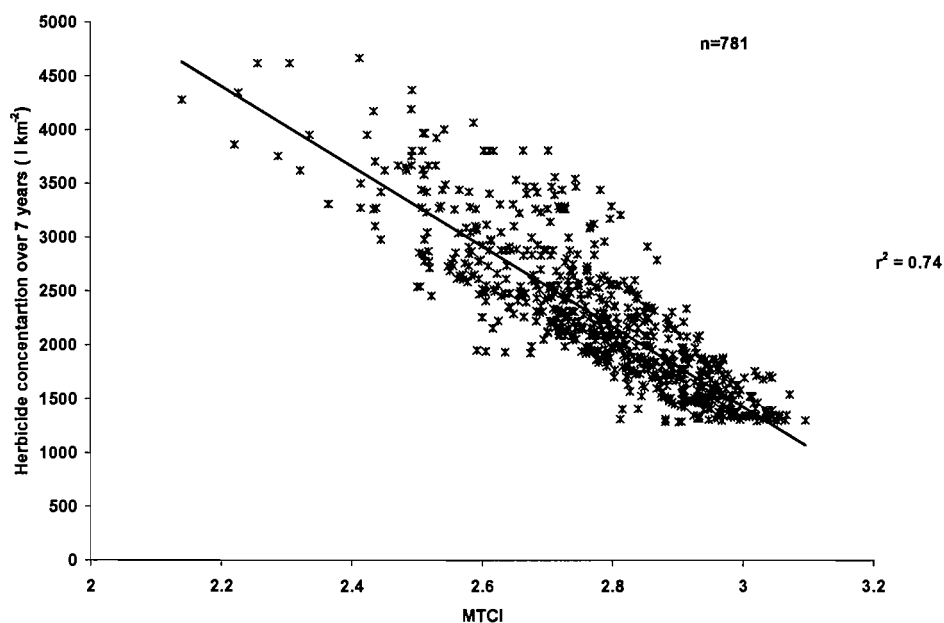


Figure 8.12 Relationship between MTCI and herbicide concentration for selected forested sites in southern Vietnam.

8.3.4 Summary

The concentration of herbicide sprayed onto the forests of Southern Vietnam between 1965 and 1971 was used as a surrogate for contemporary chlorophyll content and was related to current MTCI. The resulting relationship was, as expected, negative ($r^2 = 0.74$). However, presence of cloud in the data restricted the number of forested pixels available for analysis ($n=781$). This study has indicated the strength of the relationship between contemporary MTCI and historical levels of herbicide contamination. Further study will increase the number of forested and cloud free pixels. It will then be possible to move beyond correlation and use contemporary MTCI to estimate historical levels of herbicide contamination across Southern Vietnam.

8.4. Conclusion

Two regional scale application of MTCI were presented in this chapter, in both cases MTCI was able to infer about the vegetation condition. The results from both studies can be summarised as:

- There was a statistically significant (95% confidence level) decrease in the MTCI after the tsunami in near-coastal and low lying interior regions. This decrease was consistent with a reduction in chlorophyll content as a result of the salt stress produced by salt water inundation.
- The relationship between historical levels of herbicide contamination in the forests of southern Vietnam and contemporary MTCI was strong ($r^2 = 0.74$) and negative with high levels of herbicide contamination being associated (via low levels of chlorophyll concentration) with low levels of MTCI.

Chapter 9. Conclusion

9.1. Introduction

This chapter will draw together the design concept, evaluation and application of the MERIS Terrestrial Chlorophyll Index. It will also suggest some points to be considered in future research.

The ‘red edge’, a sudden increase in reflectance in the red and NIR region of the electromagnetic spectrum has been detected in the reflectance spectra of leaves to whole planet. This red edge has been strongly related to the amount of chlorophyll present in the target, therefore, it has been used as a measure of vegetation condition. However, red edge position (REP) is not an accurate indicator of chlorophyll content at high chlorophyll contents and statistical techniques for estimating the REP were designed for small volumes of continuous spectral data rather than the large volume of discontinuous spectral data produced by current space-borne spectrometers. However, since 2004 ESA has been producing an operational level 2 product that estimate the relative location of the red edge. This product employs data from MERIS sensor and is called the MERIS Terrestrial Chlorophyll Index (MTCI).

The MTCI is the only available chlorophyll content product from any space agency and is an estimator of terrestrial vegetation condition. In future it could be used to understand and monitor various environmental and ecological issues.

9.2. Summary

Conclusions from this thesis can be summarised as follows: which includes the description about the importance of REP and its limitations to space-borne spectrometer data, design

of MTCI and its advantage than REP, direct and indirect evaluation of MTCI and finally some regional scale application of MTCI.

9.2.1 Red Edge Position

- **Importance of REP**

Red edge is a potential zone of information about vegetation condition, because, it marks the boundary between two important spectral features. They are chlorophyll absorption in the red region and leaf scattering in the NIR region. This red edge, moves towards longer wavelengths with an increase in chlorophyll content. As a result, the red edge is a commonly used spectral feature for estimating, via remote sensing, the chlorophyll content of terrestrial vegetation. Accurate estimation of the red edge position is required for monitoring vegetation condition at a regional to global scale.

- **Requirement of a chlorophyll index from a space-borne sensor**

Accurate estimation of vegetation condition at a regional to global scale requires a good estimation of chlorophyll content from space borne sensors. This requires proper estimation of the red edge position from the space-borne sensor. However, (i) there remains no generally accepted technique for the estimation of REP, (ii) each technique produces a different value of REP from the same set of data and (iii) neither of the techniques used for estimating REP offer the automated, one-step procedure that would be required for the processing of large volume data at, for example, a ground receiving station. This prompted to develop of a chlorophyll index that could use the data available from present space-borne sensor at the red edge region.

9.2.2 The MERIS Terrestrial Chlorophyll Index

- **Design of the MTCI**

The MTCI was designed to use the variation in reflectance in three available MERIS band situated in the red edge region: centred at 681.25 nm, 708.75 nm and 753.75 nm (bands 8, 9 and 10 in the MERIS standard band setting). It is the ratio of the difference in reflectance between band 10 and band 9 and the difference in reflectance between band 9 and band 8.

- **Advantages of the MTCI**

- (i) MTCI was more sensitive than REP to chlorophyll content, notably at high chlorophyll contents.
- (ii) There was only one MTCI value for each pixel (MTCI is an absolute value derived using a specific method, unlike the REP which is a method specific estimate of an actual value).
- (iii) Calculation of the MTCI could be automated readily, as it involved one step and no manual intervention.
- (iv) Should it be necessary, REP can be estimated from MTCI, as a strong relationship exists between REP and MTCI.

9.2.3 Evaluation of MERIS data

- **Scaling up effect**

Spectral data used in the study comprised data from leaf, canopy and MERIS levels.

Moving from leaf to MERIS level involved the inclusion of various canopy and non canopy factors into the recorded spectral response. At leaf level pigment absorption and leaf structure affected the recorded radiance. At canopy level canopy structure and background reflectance influenced the reflectance. At MERIS level atmosphere and the SNR of the instrument affected the nature of the recorded data.

- **SNR of MERIS data**

It was found that the noise present in the MERIS data was primarily random. The SNR of MERIS was not related directly to the signal but it was indicative of the sensitivity of the sensor.

- **Effect of irradiance on the red edge position**

The effect of irradiance on the relationship between red edge based indices and chlorophyll content was also examined. An increase in reflectance across all wavelengths of the vegetation spectrum was observed with an increase in irradiance. This may be due to the mechanism of photorelocation that would have reduced chlorophyll absorbance in the visible region of the spectrum. The reason for an increase in NIR reflectance with increase in irradiance is still unclear; however, a change in stomatal conductance may be a possibility. A shift in the REP towards longer wavelengths with an increase in irradiance was observed, but, in most cases this shift was not statistically significant (95% confidence level). However, a sudden increase in reflectance near 720 nm was associated with an increase in irradiance and was thought to be due to fluorescence. Detailed investigation of this feature is necessary.

9.2.4 Evaluation of MTCI

- **Direct evaluation of the MTCI**

Model data suggested that MTCI had a limited sensitivity to change in atmospheric condition and soil reflectance, however, it was sensitive to change in Sun-sensor geometry especially to change in viewing angle. Direct MTCI evaluation was undertaken in a greenhouse for spinach and poplar plants under controlled conditions. Reflectance spectra were measured using a GER 1500 spectroradiometer and chlorophyll was extracted and measured using specific absorption coefficients. The coefficients of determination (r^2) between chlorophyll content and first MTCI and second REP were 0.65 and 0.6. This

suggests a stronger MTCI-chlorophyll content relationship than REP-chlorophyll content relationship.

- **Indirect evaluation (Validation) of the MTCI**

During this work MTCI was not validated with real chlorophyll content data at MERIS spatial resolution because (i) ground chlorophyll content data for MERIS pixel sized area are not available and (ii) collecting such data for a considerable number of MERIS pixel (at least 20) is a major task. However, recently ESA has started initiative for the validation of MTCI with ground chlorophyll data.

In this research, MTCI was compared both spatially and temporally with other available vegetation indices from space-borne spectrometers. In some cases MTCI showed a greater variation for vegetated terrain; thus, it is more likely to be sensitive to chlorophyll content than other vegetation indices.

9.2.5 Application of MTCI

During this research MTCI was used to:

- (i) Infer the salt stress in the vegetation of near coastal and low lying interior region affected by the 26th December Indian Ocean tsunami.
- (ii) Monitor the condition of southern Vietnamese forests that had been contaminated by herbicides during the 1960s and 70s
- (iii) Map landcover in the State of Wisconsin, USA.

9.3. Chronology of MTCI development

During the last two and half years MTCI has been developed from a simple reflectance index to a standard ESA product. In this process the MTCI went through a number of direct and indirect evaluations, before it was released as a land product (Table 9.1).

Date	Task	Place
March, 2002	Envisat with MERIS and other 9 instruments onboard was launched	Kourou, French Guiana
March 2003	Concept of MTCI and initial evaluations	University of Southampton
November 2003	MTCI was accepted as a possible standard level 2 products	ESRIN, Frascati, Italy
January 2004 – Till date	MTCI has been calculated by interested users using the BEAM toolbox	Various
March 2004	Various evaluation and validations with other vegetation indices	JRC, Ispra, Italy
July 2004	MTCI became an official ESA level 2 product	ESRIN, Frascati, Italy
August 2004 – January 2005	MTCI was applied to a number of regional scale environmental problem	University Southampton; University of Wisconsin-Madison, WI, USA
February 2005-April 2005	Direct evaluation of MTCI with greenhouse data	University Southampton
August 2005	MTCI was incorporated into MERIS processor and made directly available to users.	ESRIN, Frascati, Italy
October 2005	ESA stated initiative to validate MTCI using ground chlorophyll data following the recommendations from 2 nd MERIS workshop (26-30 September 2005)	ESRIN, Frascati, Italy
January 2006	MTCI validation will start	Various

Table 9.1. Chronology of development of the MTCI.

9.4. Future work

The MTCI is the only land chlorophyll index ever produced; therefore, it has huge potential for various environmental and ecological applications. The future work should focus on the following four sections: further understanding the MTCI, validating the MTCI, continuing on going research and some other possible applications.

9.4.1 Further understanding the MTCI

This research should focus on understanding the characteristic of MTCI and its sensitivity to chlorophyll content under a wide range of conditions and also exploring the relationship between REP and MTCI in detail.

9.4.1.1. Use of other multi angular and fine spectral resolution satellite data

This thesis reports on MTCI in detail but lacks any validation of the MTCI with ground data, because it was difficult to obtain any chlorophyll content data for a pixel with ground resolution of 300m. However, the availability of Compact High Resolution Imaging Spectrometer (CHRIS) data currently at a spatial resolution of 17 m and the potential availability of Venus data at spatial resolution of 5.3 m offer the possibility of evaluating the MTCI and chlorophyll content relationship for field data.

Compact High Resolution Imaging Spectrometer (CHRIS)

CHRIS can acquire data in 5 modes; one among these is the chlorophyll mode (CHRIS, 2005). In the chlorophyll mode it can have 18 bands along the red edge region and can acquire data from 5 angular positions. These data could be used for accurate calculation of the red edge position and to optimise MTCI for sensor view angle effect (change in sensor view angle resulted in a change in the MTCI/chlorophyll content relationship). CHRIS data, acquired at five different angles will provide a potential dataset for testing the sensor view angle effect on MTCI/chlorophyll content relationship.

Venus

Venus, a multispectral imaging spectrometer proposed for launch in August, 2008 will be able to provide data in 18 bands in the visible and NIR region with a spatial resolution of 5.3 m and two day repeat cycle (Karnieli, 2005). It will have four spectral bands nearly

equivalent to MERIS band 8, band 9, band 10 and band 12 in the red edge region (figure 9.1). Therefore, the data from Venùs could be used to estimate the MTCI and with a spatial resolution of 5.3 m, it would be easier to validate with ground data.

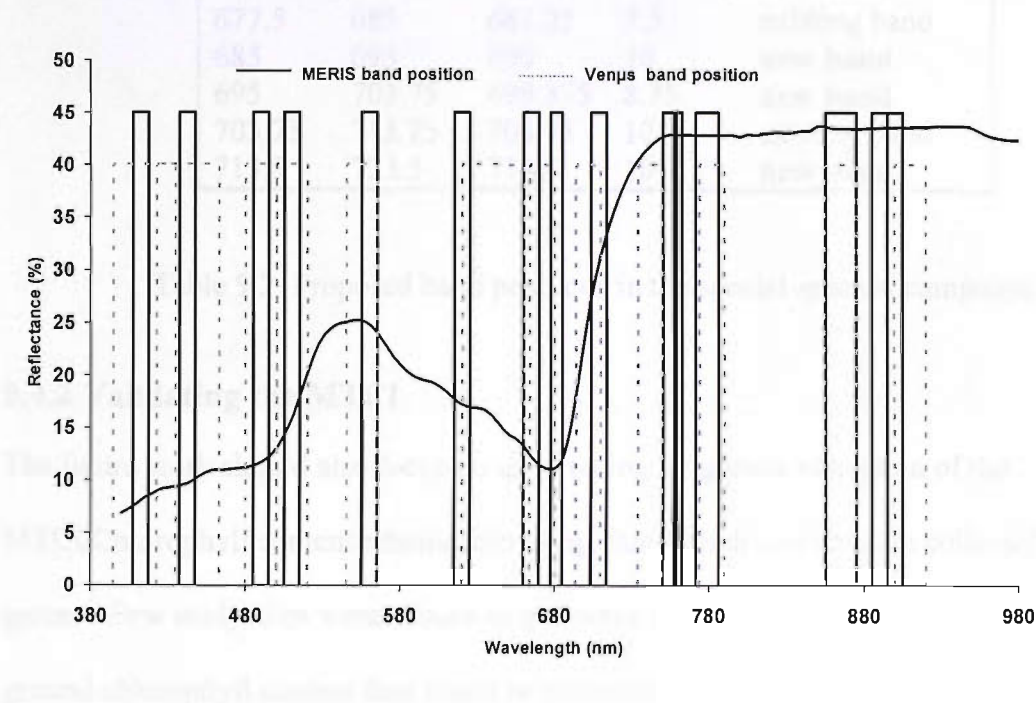


Figure 9.1. MERIS standard bands and proposed Venùs bands are overlain on model vegetation spectra

9.4.1.2. MERIS spectral campaign

The programmability of MERIS’s default band could be used to acquire data in more spectral bands with in the red edge region. ESA has a provision for special campaigns and one proposal has been approved for this purpose. In this spectral campaign five bands will be repositioned to provide contiguous coverage of the wavelength range 650 to 720 nm with a resolution of 7.5 to 10 nm (table 9.2). This data set will be useful to compare REP calculated using continuous data with MTCI.

Start	End	Centre	Width	New/existing
650	660	655	10	new band
660	670	665	10	existing band
670	677.5	673.75	7.5	new band
677.5	685	681.25	7.5	existing band
685	695	690	10	new band
695	703.75	699.375	8.75	new band
703.75	713.75	708.75	10	existing band
713.5	723.5	718.5	10	new band

Table 9.2 Proposed band positions in the special spectral campaign.

9.4.2 Validating the MTCI

The future work should also focus on undertaking a rigorous validation of the MTCI/Chlorophyll content relationship using chlorophyll content data collected on the ground. Few study sites were chosen (e.g. Barrax in southern Spain) for this purpose where ground chlorophyll content data could be collected in future.

9.4.3 Continuing on going research

Studies which were started in thesis should continue in future to evaluate the potential of MTCI. This includes long term monitoring the vegetation conditions in the tsunami affected regions and comparison with MODIS data.

9.4.3.1. Long term monitoring of tsunami region

A decrease in MTCI was reported in the near coastal and low lying interior vegetation of Phuket, Thailand as a result of saltwater inundation by the Indian Ocean tsunami occurred on 26th December, 2004 (Curran et al., 2005). This tsunami affected the coast of southern India, Sri Lanka, southern Thailand, Indonesia and neighbouring countries. Future work should involve monitoring other affected areas in this region. This should include identifying costal vegetation affected by the tsunami and monitoring the recovery time using the MTCI as an indicator of vegetation condition. Considering the size of the

affected area, it would be impractical to monitor directly; therefore, indirect monitoring should be undertaken through a time series of MERIS data.

Figure 9.2. Tsunami affected area in Sri Lanka (a), MTCI before tsunami (22-12-2004) (b) and MTCI after tsunami (17-02-2005) (c).

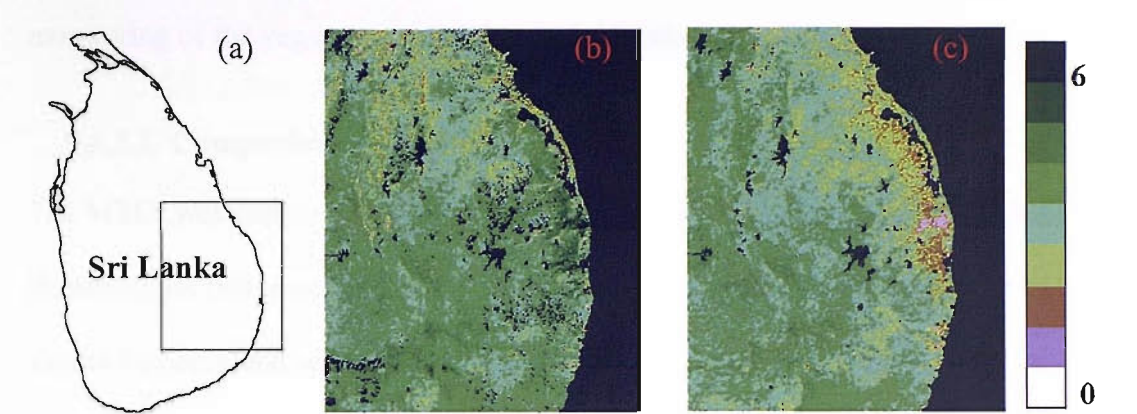


Figure 9.2. Tsunami affected area in Sri Lanka (a), MTCI before tsunami (22-12-2004) (b) and MTCI after tsunami (17-02-2005) (c).

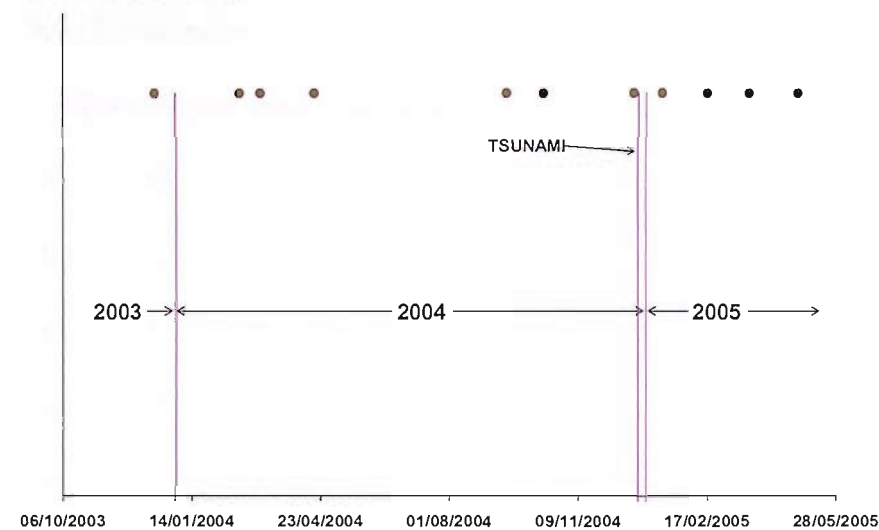


Figure 9.3. Cloud free MERIS data available for the eastern Sri Lanka (figure 9.2.).

One of the worst affected areas was the eastern part of Sri Lanka (figure 9.2). Initial evaluation of MTCI for pre and post tsunami data showed a decrease in MTCI (figure 9.2). However, it is not yet clear if this decrease in MTCI was due to the effect of tsunami or the time difference between the images. A timeseries of MTCI and other vegetation indices

would be able to indicate if there was a change in vegetation condition in this region. For this region there are at least 11 cloud free MERIS images available from December 2003 to April 2005 (figure 9.3). Future research should focus on using these data for a long term monitoring of the vegetation condition in Sri Lanka and other affected areas.

9.4.3.2. Comparison with MODIS

The MTCI was compared with two MODIS vegetation indices, they are, EVI and NDVI. However, for better understanding the similarity and differences between these indices should be compared with a range of spatial and temporal data. Future study should emphasis on comparison of MTCI with MODIS vegetation indices for major vegetation types through time series of data.

9.5. Conclusion

Results obtained from this research suggested the higher sensitivity of MTCI to canopy chlorophyll content and limited sensitivity to most of the non-canopy variables that may affect the data recorded at MERIS. The steps which should be followed to evaluate any index from a space-borne sensor were discussed. A number of applications of MTCI to regional scale environmental problem were also demonstrated. Furthermore, evidence was shown that MTCI could be used to understand, classify, manage and monitor the dynamics of terrestrial vegetation.

References

- ACHARD, F. and ESTREGUIL, C., 1995, Forest classification of southeast Asia using NOAA AVHRR data. *Remote Sensing of Environment*, **54**, 198-208.
- ADAMS, M. L., PHILPOT, W. D. and NORVELL, W. A., 1999, Yellowness Index: an application of spectral second derivatives to estimate chlorosis of leaves in stressed vegetation. *International Journal of Remote Sensing*, **20**, 3663-3675.
- ALLEN, W. A. and RICHARDSON, A. J., 1970, Interaction of light with plant canopy. *Journal of the Optical Society of America*, **58**, 1023-1028.
- ALLEN, W. A., GAUSMANN, H. W., RICHARDSON, A. J. and THOMAS, J. R., 1969, Interaction of isotropic light with a compact plant leaf. *Journal of Optical Society of America*, **59**, 1376-1379.
- ANDERSON, G. L., HANSON, J. D. and HAAS, R. H., 1993, Evaluating Landsat Thematic Mapper derived vegetation indexes for estimating aboveground biomass on semiarid rangelands. *Remote Sensing of Environment*, **45**, 165-175.
- ANDERSON, J. M., 1986, Photoregulation of the composition, function, and structure of Thylakoid membranes. *Annual Review of Plant Physiology and Plant Molecular Biology*, **37**, 93-136.
- ANGER, C. D., ACHAL, S., IVANCO, T., MAH, S. and PRICE, R., 1996, Extended operational capabilities of CASI. In *Proceedings of the Second International Airborne Remote Sensing Conference*, San Francisco, California, 124-133.
- ARNOLD, L., GILLET, S., LARDIERE, O., RIAUD, P. and SCHNEIDER, J., 2002, A test for the search for life on extra solar planets - Looking for the terrestrial vegetation signature in the Earthshine spectrum. *Astronomy and Astrophysics*, **392**, 231-237.
- ASD, 2005, Vis/NIR Spectroradiometers - FieldSpec® HandHeld and HandHeld Pro, Analytical Spectral Devices, Inc. Available online at : <http://www.asdi.com/products-FSHH-FSHHP.asp> (Last accessed 19th Sept 2005).
- BANNINGER, C., 1991, Phenological changes in the red edge shift of Norway spruce needles and their relationship to needle chlorophyll content. In *Proceedings of the 5th International Colloquium - Physical Measurements and Signatures in Remote Sensing*, Courcheval, France, 155-158.
- BANWELL, C. N., 1994, *Fundamentals of Molecular Spectroscopy*, (London: McGrawHill).

- BARANOSKI, G. V. G. and ROKNE, J. G., 2005, A practical approach for estimating the red edge position of plant leaf reflectance. *International Journal of Remote Sensing*, **26**, 503-521.
- BARET, F. and FOURTY, T., 1997, Radiometric estimates of nitrogen status of leaves and canopies. In *Diagnosis of the Nitrogen status in crops*, edited by G. Lemaire, pp. 207-227 (Berlin: Springer-Verlag).
- BARET, F. and GUYOT, G., 1991, Potentials and limits of vegetation indexes for LAI and APAR assessment. *Remote Sensing of Environment*, **35**, 161-173.
- BARET, F., JACQUEMOUD, S., GUYOT, G. and LEPRIEUR, C., 1992, Modelled analysis of the biophysical nature of spectral shifts and comparison with information content of broad band. *Remote Sensing of Environment*, **41**, 133-142.
- BARNES, W. L., PAGANO, T. S. and SALOMONSON, V. V., 1998, Prelaunch characteristics of the Moderate Resolution Imaging Spectroradiometer (MODIS) on EOS-AM1. *IEEE Transactions on Geoscience and Remote Sensing*, **36**, 1088-1100.
- BARTON, C. V. M., 2001, A theoretical analysis of the influence of heterogeneity in chlorophyll distribution on the leaf reflectance. *Tree Physiology*, **21**, 789-795.
- BBC NEWS, 2005, Reporters' log: Asian quake disaster. Available online at: www.bbc.co.uk (accessed 20 March, 2005).
- BENEDETTI, R., ROSSINI, P. and TADDEI, R., 1994, Vegetation classification in the middle Mediterranean area by satellite data. *International Journal of Remote Sensing*, **15**, 583-596.
- BENEDIKTSSON, J. A., SWAIN, P. H. and ERSOY, O. K., 1990, Neural network approaches versus statistical-methods in classification of multi-source remote-sensing data. *IEEE Transactions on Geoscience and Remote Sensing*, **28**, 540-552.
- BERMYN, J., 2000, PROBA-PRoject for On-Board Autonomy. *Air and Space Europe*, **2**, 70-76.
- BÉZY, J. L., DELWART, S. and RAST, M., 2000, MERIS- A new generation of ocean colour sensor onboard Envisat. *ESA bulletin* 103, 48-56.
- BIRTH, G. S. and HECHT, H. G., 1987, The physics of near infrared reflectance. In *Near-Infrared Technology in Agricultural and Food Industry*, edited by P. Williams and K. Norris, (St. Paul, MN: American Association of Cereal Chemists Inc.).
- BLACKBURN, G. A. and MILTON, E. J., 1995, Seasonal variations in the spectral reflectance of deciduous tree canopies. *International Journal of Remote Sensing*, **16**, 709-720.

- BLACKBURN, G. A., 1998, Quantifying chlorophyll and carotenoids at leaf and canopy scales: an evaluation of some hyperspectral data. *Remote Sensing of Environment*, **66**, 273-285.
- BOARDMAN, J. W. and GOETZ, A. F. H., 1991, Sedimentary facies analysis using AVIRIS data: A geophysical inverse problem. In *Proceeding of the Third AVIRIS workshop*, Pasadena, CA , 4-13.
- BONHAM-CARTER, G. F., 1988, Numerical procedures and computer program for fitting an inverted Gaussian model to vegetation reflectance data. *Computers and Geosciences*, **14**, 339-356.
- BOOCHS, F., KUPFER, G., DOCKTER, K. and KÜHBAUCH, W., 1990, Shape of red edge vitality indicator for plants. *International Journal of Remote Sensing*, **11**, 1741-1753.
- BOYD, D. S. and DANSON, F. M., 2005, Satellite remote sensing of forest resources: three decades of research development. *Progress in Physical Geography*, **29**, 1-26.
- BROGE, N. H. and LEBLANC, E., 2001, Comparing prediction power and stability of broadband and hyperspectral vegetation indices for estimation of green leaf area index and canopy chlorophyll density. *Remote Sensing of Environment*, **76**, 156-172.
- BROWN, M., GUNN, S. R. and LEWIS, H. G., 1999, Support vector machines for optimal classification and spectral unmixing. *Ecological Modelling*, **120**, 167-179.
- BRUGNOLI, E. and BJORKMAN, O., 1992, Chloroplast Movements in leaves - influence on chlorophyll fluorescence and measurements of light-induced absorbency changes related to Delta-Ph and Zeaxanthin formation. *Photosynthesis Research*, **32**, 23-35.
- BUCKINGHAM, W. A., 1982, *Operation Ranch Hand: the air force and herbicides in Southeast Asia, 1961-1971*, (Washington, D.C.: Office of Air Force History, United States Air Force).
- BUSCHMANN, C. and LICHTENTHALER, H. K., 1998, Principles and characteristics of multi-colour fluorescence imaging of plants. *Journal of Plant Physiology*, **152**, 297-314.
- CARTER, G. A., 1993, Responses of leaf spectral reflectance to plant stress. *American Journal of Botany*, **80**, 239-243.
- CATE, T. M. and PERKINS, T. D., 2003, Chlorophyll content monitoring in sugar maple (*Acer Saccharum*). *Tree Physiology*, **23**, 1077-1079.
- CHANDRASEKHAR, S., 1978, *Radiative transfer*, (Oxford: Clarendon Press).
- CHAURASIA, S. and DADHWAL, V. K., 2002, A simulation study on retrieval of leaf area index using principal component inversion technique. In *Proceeding of*

- CHEN, J. M., RICH, P. M., GOWER, S. T., NORMAN, J. M. and PLUMMER, S., 1997, Leaf area index of boreal forests: Theory, techniques, and measurements. *Journal of Geophysical Research-Atmospheres*, **102**, 29429-29443.
- CHOUDHURI, B. J., 1987, Relationship between vegetation indices, radiation absorption and net photo synthesis evaluated by a sensitivity analysis. *Remote Sensing of Environment*, **22**, 209-233.
- CHRIS, 2005, The CHRIS Instrument, Available online at: <http://www.chris-proba.org.uk/frames/index2.html> (Last accessed 19th Sept 2005).
- CIHLAR, J., 2000, Land cover mapping of large areas from satellites: status and research priorities. *International Journal of Remote Sensing*, **21**, 1093-1114.
- CLARK, R. N., KING, T. V. V., AGER, C. and SWAYZE, G. A., 1995, Initial vegetation species and senescence/Stress indicator mapping in the San Luis valley, Colorado using imaging spectrometer data. In *Proceeding of the AVIRIS Airborne Geoscience Workshop*, Pasadena, CA.
- CLEVERS, J. G. P. W., 1988, The derivation of a simplified reflectance model for the estimation of leaf area index. *Remote Sensing of Environment*, **35**, 53-70.
- CLEVERS, J. G. P. W., DE JONG, S. M., EPEMA, G. F., VAN DER MEER, F., BAKKER, W. H., SKIDMORE, A. K. and SCHOLTE, K. H., 2002, Derivation of the red edge index using the MERIS standard band setting. *International Journal of Remote Sensing*, **23**, 3169-3184.
- CLEVERS, J. G. P. W., JONG, S. M., EPEMA, G. F., VAN DER MEER, F., BAKKER, W. H., SKIDMORE, A. K. and ADDINK, E. A., 2001, MERIS and the red-edge position. *International Journal of Applied Earth Observation and Geoinformation*, **3**, 313-320.
- CLEVERS, J. G. P. W., KOOISTRA, L. and SALAS, E. A. L., 2004, Study of heavy metal contamination in river floodplains using the red-edge position in spectroscopic data. *International Journal of Remote Sensing*, **25**, 3883-3895.
- COHEN, W. B. and JUSTICE, C. O., 1999, Validating MODIS terrestrial ecology products: Linking in situ and satellite measurements. *Remote Sensing of Environment*, **70**, 1-3.
- CURRAN, P. J. and DASH, J., 2004, *Report on Algorithm theoretical basis document (ATBD): Chlorophyll Index- Version 2.2*. pp.22 (Noordwijk, the Netherlands: ESA).
- CURRAN, P. J. and DUNGAN, J. L., 1989, Estimation of signal-to-noise - a new procedure applied to AVIRIS data. *IEEE Transactions on Geoscience and Remote Sensing*, **27**, 620-628.

- CURRAN, P. J. and STEELE, C. M., 2002, MERIS for terrestrial remote sensing. In *Observing our Environment from Space: New Solutions for a New Millennium*, edited by G. Begni, pp. 179-183 (Lisse: Swets & Zeitlinger).
- CURRAN, P. J. and STEELE, C. M., 2005, MERIS: The re-branding of an ocean sensor. *International Journal of Remote Sensing*, **26**, 1781-1798.
- CURRAN, P. J., 1980, Multispectral remote sensing of vegetation amount. *Progress in Physical Geography*, **4**, 315-341.
- CURRAN, P. J., 1982, Multispectral photographic remote sensing of green vegetation biomass and productivity. *Photogrammetric Engineering and Remote Sensing*, **48**, 243-250.
- CURRAN, P. J., 1987, Remote sensing methodologies and geography. *International Journal of Remote Sensing*, **8**, 1255-1275.
- CURRAN, P. J., 1988, The semivariogram in remote-sensing - An introduction. *Remote Sensing of Environment*, **24**, 493-507.
- CURRAN, P. J., 1989, Remote Sensing of foliar chemistry. *Remote Sensing of Environment*, **30**, 271-278.
- CURRAN, P. J., 2001, Imaging spectrometry for ecological applications. *International Journal of Applied Earth Observation and Geoinformation*, **3**, 305-312.
- CURRAN, P. J., DASH, J. and LLEWELLYN, G. M., 2005, Indian Ocean tsunami: The use of MERIS (MTCI) data to infer salt stress in coastal vegetation. *International Journal of Remote Sensing* (accepted).
- CURRAN, P. J., DUNGAN, J. L. and GHOLZ, H. L., 1990, Exploring the relationship between reflectance red edge and chlorophyll content in slash pine. *Tree Physiology*, **7**, 33-48.
- CURRAN, P. J., DUNGAN, J. L. and PETERSON, D. L., 2001, Estimating the foliar biochemical concentration of leaves with reflectance spectrometry testing the Kokaly and Clark methodologies. *Remote Sensing of Environment*, **76**, 349-359.
- CURRAN, P. J., DUNGAN, J. L. MACLER, B. A. and PLUMMER, S. E., 1991, The effect of a red leaf pigment on the relationship between red edge and chlorophyll concentration. *Remote Sensing of Environment*, **35**, 69-76.
- CURRAN, P. J., DUNGAN, J. L., MACLER, B. A., PLUMMER, S. E. and PETERSON, D. L., 1992, Reflectance spectroscopy of fresh whole leaves for the estimation of chemical concentration. *Remote Sensing of Environment*, **39**, 153-166.
- CURRAN, P. J., KUPIEC, J. A. and SMITH, G. M., 1997, Remote Sensing the biochemical composition of a slash pine canopy. *IEEE Transactions on Geoscience and Remote Sensing*, **35**, 415-420.

- CURRAN, P. J., WINDHAM, W. R. and GHOLZ, H. L., 1995, Exploring the relationship between reflectance red edge and chlorophyll concentration in slash pine leaves. *Tree Physiology*, **15**, 203-206.
- CUTTER, M., 2004, Review of Aspects Associated With the Chris Calibration. In *Proceedings of the Second CHRIS Proba Workshop*, Frascati, Italy.
- DANSON, F. M and CURRAN, P. J., 1993, Factors affecting the remotely sensed response of coniferous forest plantation. *Remote Sensing of Environment*, **43**, 55-65.
- DANSON, F. M, 1998, Teaching the physical principle of vegetation canopy reflectance using the SAIL model. *Photogrammetric Engineering & Remote Sensing*, **64**, 809-812.
- DANSON, F. M. and CURRAN, P. J., 1993, Factors Affecting the Remotely Sensed Response of Coniferous Forest Plantations. *Remote Sensing of Environment*, **43**, 55-65.
- DANSON, F. M. and PLUMMER, S. E., 1995, Red edge response to forest leaf area index. *International Journal of Remote Sensing*, **16**, 183-188.
- DASH, J. and CURRAN, P. J., 2004, The MERIS Terrestrial Chlorophyll Index. *International Journal of Remote Sensing*, **25**, 5003-5013.
- DATT, B., 1998, Remote Sensing of chlorophyll a, chlorophyll b, chlorophyll a+b, and total carotenoid content in Eucalyptus leaves. *Remote Sensing of Environment*, **66**, 111-121.
- DAUGHTRY, C. S. T., WALTHALL, C. L., KIM, M. S., BROWN DE COLSTOUN, E. and MCMURTREY III, J. E., 2000, Estimating corn leaf chlorophyll concentration from leaf and canopy reflectance. *Remote Sensing of Environment*, **74**, 229-239.
- DAWSON, T. P. and CURRAN, P. J., 1998, A new technique for interpolating the reflectance red edge position. *International Journal of Remote Sensing*, **19**, 2133-2139.
- DAWSON, T. P., 2000, The potential of estimating chlorophyll content from a vegetation canopy using the Medium Resolution Imaging Spectrometer (MERIS). *International Journal of Remote Sensing*, **21**, 2043-2051.
- DAWSON, T. P., CURRAN, P. J. and KUPIEC, J. A., 1995, Casual correlation of foliar biochemical concentration with AVIRIS spectra using forced entry linear regression. In *Fifth AVIRIS Airborne Geoscience Workshop Proceedings*, Pasadena, CA.
- DAWSON, T. P., CURRAN, P. J. and PLUMMER, S. E., 1998, LIBERTY - Modelling the effects of leaf biochemical concentration on reflectance spectra. *Remote Sensing of Environment*, **65**, 50-60.
- DAWSON, T. P., CURRAN, P. J., NORTH, P. R. J. and PLUMMER, S. E., 1997, The potential for understanding the biochemical signals in the spectra of forest

- canopies using a coupled leaf and canopy model. In *Physical Measurements and Signatures in Remote Sensing*, edited by G. Guyot and D. Vidal-Madjar, (Rotterdam: A. A. Balkema).
- DAWSON, T. P., CURRAN, P. J., NORTH, P. R. J. and PLUMMER, S. E., 1999, The propagation of foliar biochemical absorption features in forest canopy reflectance: A theoretical analysis. *Remote Sensing of Environment*, **67**, 147-159.
- DEFRIES, R. S. and TOWNSHEND, J. R. G., 1994, NDVI-derived landcover classifications at a global scale. *International Journal of Remote Sensing*, **15**, 3567-3586.
- DEMETRIADES-SHAH, T. H., STEVEN, M. D. and CLARK, J. A., 1990, High resolution derivative spectra in remote sensing. *Remote Sensing of Environment*, **33**, 55-64.
- DEMMIGADAMS, B. and ADAMS, W. W., 1996, The role of xanthophyll cycle carotenoids in the protection of photosynthesis. *Trends in Plant Science*, **1**, 21-26.
- ELVIDGE, C. D., CHEN, Z. and GROENEVELD, D. P., 1993, Detection of trace quantities of green vegetation in 1990 AVIRIS data. *Remote Sensing of Environment*, **44**, 271-279.
- EPIPHANIO, J. C. N. and HUETE, A. R., 1995, Dependence of NDVI and SAVI on Sun sensor geometry and its effect on fAPAR Relationships in Alfalfa. *Remote Sensing of Environment*, **51**, 351-360.
- ESA, 2005, MERIS product handbook. Available online at: <http://envisat.esa.int/dataproducts/meris/CNTR.htm> (Last accessed 19th Sept 2005).
- FARR, T. G. and KOBRICK, M., 2000, Shuttle Radar Topographic Mission produces a wealth of data. *EOS, Transactions American Geophysical Union*, **81**, 583-581.
- FENSHOLT, R., 2004, Earth observation of vegetation status in the Sahelian and Sudanian West Africa: comparison of terra MODIS and NOAA AVHRR satellite data. *International Journal of Remote Sensing*, **25**, 1641-1659.
- FERREIRA, L. G., YOSHIOKA, H., HUETE, A. and SANO, E. E., 2003, Seasonal landscape and spectral vegetation index dynamics in the Brazilian Cerrado: An analysis within the Large-Scale Biosphere-Atmosphere Experiment in Amazonia (LBA). *Remote Sensing of Environment*, **87**, 534-550.
- FILELLA, I. and PEÑUELAS, J., 1994, The red edge position and shape as indicator of plant chlorophyll content, biomass and hydric status. *International Journal of Remote Sensing*, **15**, 1459-1470.

- FOODY, G. M. and MATHUR, A., 2004, A relative evaluation of multiclass image classification by support vector machines. *IEEE Transactions on Geoscience and Remote Sensing*, **42**, 1335-1343.
- FOODY, G. M. and MATHUR, A., 2004, Toward intelligent training of supervised image classifications: directing training data acquisition for SVM classification. *Remote Sensing of Environment*, **93**, 107-117.
- FOODY, G. M., 2002, Status of land cover classification accuracy assessment. *Remote Sensing of Environment*, **80**, 185-201.
- FOODY, G. M., 2004, Thematic map comparison: evaluating the statistical significance of differences in classification accuracy. *Photogrammetric Engineering and Remote Sensing*,
- FRANKLIN, J., 1986, Thematic Mapper analysis of coniferous forest structure and composition. *International Journal of Remote Sensing*, **7**, 1287-1301.
- FRANKLIN, S. E., 1994, Discrimination of subalpine forest and canopy density using digital CASI, SPOT PLA, and Landsat TM data. *Photogrammetric Engineering & Remote Sensing*, **60**, 1233-1241.
- FRIEDL, M. A. and BRODLEY, C. E., 1997, Decision tree classification of land cover from remotely sensed data. *Remote Sensing of Environment*, **61**, 399-409.
- FRIEDL, M. A., MCIVER, D. K., HODGES, J. C. F., ZHANG, X. Y., MUCHONEY, D., STRAHLER, A. H., WOODCOCK, C. E., GOPAL, S., SCHNEIDER, A., COOPER, A., BACCINI, A., GAO, F. and SCHAAF, C., 2002, Global land cover mapping from MODIS: algorithms and early results. *Remote Sensing of Environment*, **83**, 287-302.
- FUJIMOTO, N., TAKAHASHI, Y., MORIYAMA, T. and SHIMADA, M., 1989, Evaluation of SPOT HRV image data received in Japan. In *Quantitative Remote Sensing: an Ecological Tool for the Nineties*, 463-466 (Vancouver: IEEE).
- GANAPOL, B. D., JOHNSON, L. F., HAMMER, P. D., HLAVKA, C. A. and PETERSON, D. L., 1998, LEAFMOD: A new within leaf radiative transfer model. *Remote Sensing of Environment*, **63**, 182-193.
- GAO, B. C., 1993, An operational method for estimating signal to noise ratios from data acquired with imaging spectrometers. *Remote Sensing of Environment*, **43**, 23-33.
- GASTELLU-ETCHEGORRY, J. P., ZAGOLSKI, F., MOUGIN, E., MARTY, G. and GIORDANO, G., 1995, An assessment of canopy chemistry with AVIRIS-a case study in the Landes forest, South-west France. *International Journal of Remote Sensing*, **16**, 487-501.
- GASTON, G. G., JACKSON, P. L., VINSON, T. S., KOLCHUGINA, T. P., BOTCH, M. and KOBAK, K., 1994, Identification of carbon quantifiable regions in the former Soviet-union using unsupervised classification of AVHRR global

- vegetation index images. *International Journal of Remote Sensing*, **15**, 3199-3221.
- GAUSMANN, H. W., 1974, Leaf reflectance of near-infrared. *Photogrammetric Engineering*, **40**, 183-191.
- GER, 2005, Group for Environmental Research, Field Portable Spectroradiometers. Available online at: <http://www.ger.com/ground.html> (Last access 11th July, 2005).
- GIBSON, L. J. and ASHBY, M. F., 1997, *Cellular Solids: Structure and Properties* (Cambridge, UK: Cambridge University Press).
- GIGLIO, L., DESCLOITRES, J., JUSTICE, C. O. and KAUFMAN, Y. J., 2003, An enhanced contextual fire detection algorithm for MODIS. *Remote Sensing of Environment*, **87**, 273-282.
- GITELSON, A. A. and MERZLYAK, M. N., 1997, Remote estimation of chlorophyll content in higher plant leaves. *International Journal of Remote Sensing*, **18**,
- GITELSON, A. A. and MERZLYAK, M. N., 1998, Remote sensing of chlorophyll concentration in higher plant leaves. *Advances in Space Research*, **22**, 689-692.
- GITELSON, A. A., KAUFMAN, Y. J., STARK, R. and RUNDQUIST, D., 2002, Novel algorithms for remote estimation of vegetation fraction. *Remote Sensing of Environment*, **80**, 76-87(12).
- GLASSNER, A. S., 1989, *Surface physics for ray tracing*, pp. 121-160 (London: Academic press).
- GOBRON, N., MÉLIN, F., PINTY, B., TABERNER, M. and VERSTRAETE, M. M., 2003, MERIS Global Vegetation Index: Evaluation and Performance. *Proceeding of MERIS User Workshop*, Frascati, Italy.
- GOBRON, N., PINTY, B., VERSTRAETE, M. and GOVAERTS, Y., 1999, The MERIS global vegetation index (MGVI): description and preliminary application. *International Journal of Remote Sensing*, **20**, 1917-1927.
- GOBRON, N., PINTY, B., VERSTRAETE, M. M. and GOVAERTS, Y., 1997, A semidiscrete model for the scattering of light by vegetation. *Journal of Geophysical Research-Atmospheres*, **102**, 9431-9446.
- GOEL, N. S. and THOMPSON, R. L., 1984, Inversion of vegetation canopy reflectance models for estimating agronomic variables. *Remote Sensing of Environment*, **16**, 69-85.
- GOEL, P. K., PRASHER, S. O., PATEL, R. M., LANDRY, J. A., BONNELL, R. B. and VIAU, A. A., 2003, Classification of hyperspectral data by decision trees and artificial neural networks to identify weed stress and nitrogen status of corn. *Computers and Electronics in Agriculture*, **39**, 67-93.

- GONG, P., PU, R. and MILLER, J. R., 1995, Coniferous forest leaf area index estimation along the Oregon transect using compact airborne spectrographic imager data. *Photogrammetric Engineering & Remote Sensing*, **61**, 1107-1117.
- GOODIN, D. G. and HENEERY, G. M., 2002, The effect of rescaling on fine spatial resolution NDVI data: a test using multi-resolution aircraft sensor data. *International Journal of Remote Sensing*, **23**, 3865-3871.
- GORGE, D. C., 1997, Cover bathymetry mapping using a Compact Airborne Spectrographic Imager (CASI). *International Journal of Remote Sensing*, **18**, 2067-2071.
- GOVAERTS, Y. and VERSTRAETE, M., 1994, Applications of the L-systems to canopy reflectance modeling in a Monte Carlo ray tracing technique. In *Fractals in Geoscience and Remote Sensing*, edited by G. G. Wilkinson, L. Kanellopoulos, and J. Megier, pp. 211-236 (Ispra, Italy: Joint Research Centre of the European Commission).
- GOVAERTS, Y. M. and VERSTRAETE, M. M., 1998, Raytran: A Monte Carlo ray-tracing model to compute light scattering in three-dimensional heterogeneous media. *IEEE Transactions on Geoscience and Remote Sensing*, **36**, 493-505.
- GOVAERTS, Y. M., VERSTRAETE, M. M., PINTY, B. and GOBRON, N., 1999, Designing optimal spectral indices: a feasibility and proof of concept study. *International Journal of Remote Sensing*, **20**, 1853-1873.
- GOWER, J. F. R. and BORSTAD, G. A., 2004, On the potential of MODIS and MERIS for imaging chlorophyll fluorescence from space. *International Journal of Remote Sensing*, **25**, 1459-1464.
- GUERIF, M. and DUKE, C., 1998, Spatial calibration of a crop model using optical remote sensing data. A case study on sugar beet emergence and early growth. In *Proceeding of 1st International Conference on Geospatial Information in Agriculture and Forestry*, Lake Buena Vista, Florida, USA.
- GUPTA, R. K., VIJAYAN, D. and PRASAD, T. S., 2001, Characterization of red-near infrared transition for wheat and chickpea using 3 nm bandwidth data. *Advances in Space Research*, **28**, 189-194.
- GUYOT, G., BARET, F. and MAJOR, D. J., 1988, High spectral resolution: Determination of spectral shifts between the red and the near infrared. *International Archives of Photogrammetry and Remote Sensing*, **11**, 740-760.
- HALL, D. K., RIGGS, G. A., SALOMONSON, V. V., DIGIROLAMO, N. E. and BAYR, K. J., 2002, MODIS snow-cover products. *Remote Sensing of Environment*, **83**, 181-194.
- HALL, F. G., PEDDLE, D. R. and LEDREW, E. F., 1996, Remote Sensing of biophysical variables in boreal forest stands of *Picea mariana*. *International Journal of Remote Sensing*, **17**, 3077-3081.

- HALLDORSSON, G. H., BENEDIKTSSON, J. A. and SVEINSSON, J. R., 2003, Support Vector Machines in multisource Classification. In *Proceeding of IEEE Remote Sensing and Geosciences Conference*, Toulouse, France.
- HAN, K. S., CHAMPEAUX, J. L. and ROUJEAN, J. L., 2004, A land cover classification product over France at 1 km resolution using SPOT4/VEGETATION data. *Remote Sensing of Environment*, **92**, 52-66.
- HANSEN, M. C., DEFRIES, R. S., TOWNSHEND, J. R. G. and SOHLBERG, R., 2000, Global land cover classification at 1km spatial resolution using a classification tree approach. *International Journal of Remote Sensing*, **21**, 1331-1364.
- HARE, E. W., MILLER, J. R. and EDWARDS, G. R., 1984, Studies of the vegetation red reflectance edge in geobotanical remote sensing in eastern Canada. In *Proceedings of the 9th Canadian Symposium on Remote Sensing*, Newfoundland, 433-440.
- HERRING, M., 1987, Shuttle Imaging Spectrometer Experiment (SISEX). *SPIE 384, Imaging Spectroscopy II*, 181-187.
- HERWITZ, S. R., PETERSON, D. L. and EASTMAN, J. R., 1989, Thematic mapper detection of changes in the leaf area of closed canopy pine plantations in central Massachusetts. *Remote Sensing of Environment*, **30**, 129-140.
- HEYMSFIELD, A. J., BANSEMER, A., LEWIS, S., IAQUINTA, J., KAJIKAWA, M., TWOHY, C., POELLOT, M. R. and MILOSHEVICH, L. M., 2002, A general approach for deriving the properties of cirrus and stratiform ice cloud particles. *Journal of Atmospheric Science*, **59**, 3-29.
- HILL, R. A. and FOODY, G. M., 1994, Separability of tropical rain-forest types in the Tambopata- Candamo Reserved Zone, Peru. *International Journal of Remote Sensing*, **15**, 2687-2693.
- HIRATA, M., KOGA, N., SHINJO, H., FUJITA, H., GINTZBURGER, G. and MIYAZAKI, A., 2001, Vegetation classification by satellite image processing in a dry area of north-eastern Syria. *International Journal of Remote Sensing*, **22**, 507-516.
- HITACHI, 2005, Hitachi High-Technologies Corporation, U-2800 Double-Beam Spectrophotometer. Available online at: http://www.hitachi-hitec.com/science/english/uv_vis/u2800.html (Last accessed 11th July 2005).
- HOEL, B. O. and SOLHAUG, K. A., 1998, Effect of irradiance on chlorophyll estimation with the Minolta SPAD-502 leaf chlorophyll meter. *Annals of Botany*, **82**, 389-392.
- HOGUE, F. E. and LYON, P. E., 2002, Satellite observation of chromophoric dissolved organic matter (CDOM) variability in the wake of hurricanes and typhoons. *Geophysical Research Letters*, **29**, 90-92.
- HOLLAS, J. M., 1992, *Modern Spectroscopy*, (Chichester: John Wiley and Sons).

- HORLER, D. N. H., BARBER, J. and BARRINGER, A. R., 1980, Effect of heavy metals on the absorption and reflectance spectra of plants. *International Journal of Remote Sensing*, **1**, 121-136.
- HORLER, D. N. H., DOCKRAY, M. and BARBER, J., 1983, The red edge of plant leaf reflectance. *International Journal of Remote Sensing*, **4**, 273-288.
- HORTON, P., RUBAN, A. V. and WALTERS, R. G., 1994, Regulation of light-harvesting in green plants - indication by nonphotochemical quenching of chlorophyll fluorescence. *Plant Physiology*, **106**, 415-420.
- HOSGOOD, B., JACQUEMOUD, S., ANDREOLI, G., VERDEBOUT, J., PERDRINI, G. and SCHMUCK, G., 1995, Leaf optical properties experiment 93 (LOPEX93). *Joint Research Centre European Commission publication no. EUR 16095 EN, Luxembourg.*
- HUANG, C., DAVIS, L. S. and TOWNSHEND, J. R. G., 2002, An assessment of support vector machines for land cover classification. *International Journal of Remote Sensing*, **23**, 725-749.
- HUETE, A. R. and JACKSON, R. D., 1987, Suitability of spectral indexes for evaluating vegetation characteristics on arid rangelands. *Remote Sensing of Environment*, **23**, 213-&.
- HUETE, A. R., 1988, A soil-adjusted vegetation index (SAVI). *Remote Sensing of Environment*, **25**, 295-309.
- HUETE, A. R., HUA, G., QI, J., CHEHBOUNI, A. and VANLEEUEWEN, W. J. D., 1992, Normalization of multidirectional red and NIR reflectances with the SAVI. *Remote Sensing of Environment*, **41**, 143-154.
- HUETE, A., DIDAN, K., MIURA, T., RODRIGUEZ, E. P., GAO, X. and FERREIRA, L. G., 2002, Overview of the radiometric and biophysical performance of the MODIS vegetation indices. *Remote Sensing of Environment*, **83**, 195-213.
- ISAAKS, E. H. and SRIVASTAVA, R. M., 1989, *Applied Geostatistics*, (New York: Oxford University Press).
- JACQUEMOUD, S. and BARET, F., 1990, PROSPECT: A model of leaf optical properties spectra. *Remote Sensing of Environment*, **34**, 75-91.
- JACQUEMOUD, S., BARET, F., ANDRIEU, B., DANSON, F. M. and JAGGARD, K., 1995, Extraction of vegetation biophysical parameters by inversion of the PROSPECT plus SAIL models on sugar-beet canopy reflectance data - application to TM and AVIRIS sensors. *Remote Sensing of Environment*, **52**, 163-172.
- JACQUEMOUD, S., USTIN, S. L., VERDEBOUT, J., SCHMUCK, G., ANDREOLI, G. and HOSGOOD, B., 1996, Estimating leaf biochemistry using the PROSPECT leaf optical properties model. *Remote Sensing of Environment*, **56**, 194-202.

- JAGO, R. A., CUTLER, M. E. and CURRAN, P. J., 1999, Estimation of canopy chlorophyll concentration from field and airborne spectra. *Remote Sensing of Environment*, **68**, 217-224.
- JASINSKI, M. F. and EAGLESON, P. S., 1989, The structure of red-infrared scattergrams of semivegetated landscapes. *IEEE Transactions on Geoscience and Remote Sensing*, **27**, 441-451.
- JASINSKI, M. F. and EAGLESON, P. S., 1990, Estimation of subpixel vegetation cover using red-infrared scattergrams. *IEEE Transactions on Geoscience and Remote Sensing*, **28**, 253-267.
- JASINSKI, M. F., 1990, Functional relation among subpixel canopy cover, ground shadow, and illuminated ground at large sampling scales. *Society of Photo Optical Instrumentation Engineers annual report*.
- JEFFREY, A., 1985, *Mathematics for Engineers and Scientists*. 708-709 (Workingham, UK: Van Nostrand Reinhol).
- JOHNSON, L. F., 1999, Response of grape leaf spectra to Phylloxera infestation. *NASA Report#CR-208765, NASA Center for AeroSpace Information, Hanover, MD 21076-1320*.
- JOHNSON, L. F., 2001, Nitrogen influence on fresh-leaf NIR spectra. *Remote Sensing of Environment*, **78**, 314-320.
- JORDAN, C. F., 1969, Derivation of leaf area index from quality of light on the forest floor. *Ecology*, **50**, 663-666.
- JRC, 2004, *Global Land Cover-2000*, Joint Research centre ,Ispra, Italy, 2004. Data set available on-line at <http://www.gvm.sai.jrc.it/glc2000/defaultGLC2000.htm>.(Accessed 10 May 2005)
- JUSTICE, C. and TOWNSHEND, J., 2002, Special issue on the moderate resolution imaging spectroradiometer (MODIS): a new generation of land surface monitoring. *Remote Sensing of Environment*, **83**, 1-2.
- JUSTICE, C. O., TOWNSHEND, J. R. G. and CHOUDHURY, B. J., 1989, Comparison of AVHRR and SMMR data for monitoring vegetation phenology on a continental scale. *International Journal of Remote Sensing*, **10**, 1607-1632.
- JUSTICE, C., BELWARD, A., MORISETTE, J., LEWIS, P., PRIVETTE, J. and BARET, F., 2000, Developments in the validation of satellite sensor products for the study of the land surface. *International Journal of Remote Sensing*, **21**, 3383-3390.
- JUSTICE, C., TOWNSHEND, J., VERMOTE, E. F., MASUOKA, E. and WOLFE, R. E., 2002, An overview of MODIS Land data processing and product status. *Remote Sensing of Environment*, **83**, 3-15.
- KARNIELI, A., 2005, *The Venus System* (Personal Communication).

- KASAHARA, M., KAGAWA, T., OIKAWA, K., SUETSUGU, N., MIYAO, M. and WADA, M., 2002, Chloroplast avoidance movement reduces photodamage in plants. *Nature*, **420**, 829-832.
- KAUFMAN, Y. J. and TANRE, D., 1992, Atmospherically resistant vegetation index (ARVI) for EOS-MODIS. *IEEE Transactions on Geoscience and Remote Sensing*, **30**, 261-270.
- KAUFMAN, Y. J., HAYWOOD, J. M., HOBBS, P. V., HART, W., KLEIDMAN, R. and SCHMID, B., 2003, Remote Sensing of vertical distributions of smoke aerosol off the coast of Africa. *Geophysical Research Letters*, **30**, art-1831.
- KAUFMAN, Y. J., ICHOKU, C., GIGLIO, L., KORONTZI, S., CHU, D. A., HAO, W. M., LI, R. R. and JUSTICE, C. O., 2003, Fire and smoke observed from the Earth Observing System MODIS instrument - products, validation, and operational use. *International Journal of Remote Sensing*, **24**, 1765-1781.
- KIRCHNER, J. A., YOUKHANA, S. and SMITH, J. A., 1982, Influence of sky radiance distribution on the ratio technique for estimating bidirectional reflectance. *Photogrammetric Engineering and Remote Sensing*, **48**, 955-959.
- KLEIN, A. G. and BARNETT, A. C., 2003, Validation of daily MODIS snow cover maps of the upper Rio Grande River basin for the 2000-2001 snow year. *Remote Sensing of Environment*, **86**, 162-176.
- KRISHNASWAMY, J., KIRAN, M. C. and GANESHAIAH, K. N., 2004, Tree model based eco-climatic vegetation classification and fuzzy mapping in diverse tropical deciduous ecosystems using multi-season NDVI. *International Journal of Remote Sensing*, **25**, 1185-1205.
- KUBELKA, P. and MUNK, F., 1931, Ein Beitrag zur Optik der Farbanstriche. *Zeitschrift für Technischen Physik*, **12**, 593-601.
- KUPIEC, J. and CURRAN, P. J., 1995, Decoupling effect of the canopy and foliar biochemicals in AVIRIS spectra. *International Journal of Remote Sensing*, **16**, 1731-1739.
- KUUSK, A. and RENHUA, Z., 1997, Monitoring of LAI and chlorophyll content by the inversion of a CR analytical model. *Journal of Remote Sensing*, **1**, 166-170.
- KUUSK, A., 1994, A multispectral canopy reflectance model. *Remote Sensing of Environment*, **50**, 75-82.
- LAMB, D. W., STEYN-ROSS, M., SCHAAARE, P., HANNA, M. M., SILVESTER, W. and STEYN-ROSS, A., 2002, Estimating leaf nitrogen concentration in ryegrass (*Lolium* spp) pasture using chlorophyll red-edge: theoretical modelling and experimental observation. *International Journal of Remote Sensing*, **23**, 3619-3648.
- LATIFOVIC, R., ZHU, Z. L., CIHLAR, J., GIRI, C. and OLTTHOF, I., 2004, Land cover mapping of north and central America - Global land cover 2000. *Remote Sensing of Environment*, **89**, 116-127.

- LAWLOR, D. W., 1993, *Photosynthesis (2nd Edition)*, (Essex: Longman Scientific and Technical).
- LEON C.T., SHAW, D.R., COX, M.S., ABSHIRE, M.J., WARD, B., WARDLAW III, M.C. and WATSON, C., 2003, Utility of remote sensing in predicting crop and soil characteristics. *Precision Agriculture*, **4**, 81-87.
- LEPRIEUR, C, VERSTRAETE, M. and PINTY, B., 1994, Of the performance of various vegetation indices to retrieve vegetation cover from AVHRR data. *Remote Sensing Reviews*, **10**, 265-284.
- LI, L., USTIN, S. L. and LAY, M., 2005, Application of AVIRIS data in detection of oil-induced vegetation stress and cover change at Jornada, New Mexico. *Remote Sensing of Environment*, **94**, 1-16.
- LI, P. J. and MOON, W. M., 2004, Land cover classification using MODIS-ASTER airborne simulator (MASTER) data and NDVI: a case study of the Kochang area, Korea. *Canadian Journal of Remote Sensing*, **30**, 123-136.
- LICHTENHALER, H. K., 1987, Chlorophyll and carotinoids: pigments of photosynthetic biomembranes. *Methods of Enzymology*, **184**, 350-382.
- LILLESAND, T. M. and KIEFER, R. W., 1987, *Remote Sensing and Image Interpretation*, (New York: John Wiley & Sons Inc).
- LILLESAND, T. M., CHIPMAN, J. W., NAGEL, D. E., REESE, H. M., BOBO, M. R and GOLDMANN, R. A., 1998, Upper Midwest Gap Analysis Program image processing protocol. *Environmental Management Technical Center report EMTC-98-G001*, (Onalaska, WI: Environmental Management Technical Center, US Geological Survey).
- LLLEWELLYN, G. M. and CURRAN, P. J., 2001, The effect of mixing overstorey and understorey grass land spectra on vegetation indices explored using a combined leaf and canopy model. In *Proceeding of RSPS2001: Geomatics, Earth Observation and the Information Society*, DTI Conference Centre, London.
- LLLEWELLYN, G. M., KOOISTRA, L. and CURRAN, P. J., 2000, The effect of soil contamination on grassland spectra. In *Proceeding of RSS 2000: Adding Values to Remotely Sensed Data*, Leicester, UK.
- LLLEWELLYN, G. M., KOOISTRA, L. and CURRAN, P. J., 2001, The red-edge of soil contaminated grassland. In *Proceeding of Physical measurement and signature in remote sensing: 8th International Symposium of the international society for photogrammetry and remote sensing*, Aussoi, France.
- LLOYD, D., 1990, A Phenological classification of terrestrial vegetation cover using shortwave vegetation index imagery. *International Journal of Remote Sensing*, **11**, 2269-2279.

- LOBO, A., MARTI, J. J. I. and GIMENEZCASSINA, C. C., 1997, Regional scale hierarchical classification of temporal series of AVHRR vegetation index. *International Journal of Remote Sensing*, **18**, 3167-3193.
- LONG, S. P., HUMPHRIES, S. and FALKOWSKI, P. G., 1994, Photoinhibition of photosynthesis in nature. *Annual Review of Plant Physiology and Plant Molecular Biology*, **45**, 633-662.
- LOVELAND, T. R., REED, B. C., BROWN, J. F., OHLEN, D. O., ZHU, Z., YANG, L. and MERCHANT, J. W., 2000, Development of a global land cover characteristics database and IGBP DISCover from 1 km AVHRR data. *International Journal of Remote Sensing*, **21**, 1303-1330.
- LUCAS, N. S., CURRAN, P. J., PLUMMER, S. E. and DANSON, F. M., 2000, Estimating the stem carbon production of a coniferous forest using an ecosystem simulation model driven by the remotely sensed red edge. *International Journal of Remote Sensing*, **21**, 619-631.
- MAIER, S. W., LUDEKER, W. and GUNTHER, K. P., 1999, SLOP: A revised version of the stochastic model for leaf optical properties. *Remote Sensing of Environment*, **68**, 273-280.
- MAIL and GUARDIAN, 2005, Tsunami forms salty crust over farmland. Available online at: www.mg.co.za (accessed 20 March 2005).
- MARIOTTI, M., ERCOLI, L. and MASONI, A., 1996, Spectral properties of Iron-deficient corn and sunflower leaves. *Remote Sensing of Environment*, **58**, 282-288.
- MARTÍNEZ, D. E. and GUIAMET, J. J., 2004, Distortion of the SPAD 502 chlorophyll meter readings by changes in irradiance and leaf water status. *Agronomie*, **24**, 41-46.
- MATHER, P. M., 2004, *Computer Processing of Remotely-Sensed Images: An Introduction*, (Chichester, UK: John Wiley & Sons).
- MCCARTNEY, E. J., 1976, *Optics of the Atmosphere*, (New York: Wiley and Sons).
- MELAMED, M. T., 1963, Optical properties of powders. Part-I. Optical absorption coefficients and the absolute value of the diffuse reflectance. *Journal of Applied Physics*, **34**, 560-570.
- MERTON, R., 1998, Monitoring community hysteresis using spectral shift analysis and the red-edge vegetation stress index. *AVIRIS Airborne Geosciences Workshop Proceedings*, JPL Publication 97-21, Pasadena, CA.
- MIDDLETON, E. M., 1991, Solar zenith angle effects on vegetation indices in tallgrass Prairie. *Remote Sensing of Environment*, **38**, 45-62.
- MILLER, J. R., HARE, E. W. and WU, J., 1990, Quantitative characterization of the vegetation red edge reflectance 1. An inverted-Gaussian reflectance model. *International Journal of Remote Sensing*, **11**, 1755-1773.

- MILLER, J. R., WU, J., BOYER, M. G., BELANGER, M. and HARE, E. W., 1991, Seasonal pattern in leaf reflectance red-edge characteristic. *International Journal of Remote Sensing*, **12**, 1509-1523.
- MILTON, E. J., 2000, Practical methodologies for the reflectance calibration of CASI data. *Activities of the NERC EPFS in support of the NERC ARSF. ARSF Annual Meeting, Keyworth, Nottingham, UK*,
- MILTON, E. J., RIEDMANN, M. and LAWRENCE, D. J., 2001, A novel scene recording spectroradiometer. In *proceeding of the 8th International Symposium on Physical Measurements and Signatures in Remote Sensing ISPRS, Aussois, France*.
- MILTON, N. M., AGER, C. M., EISWERTH, B. A. and POWER, M. S., 1989, Aresenic and selenium induced changes in spectral reflectance and morphology of soyabean plants. *Remote Sensing of Environment*, **30**, 263-269.
- MINOLTA, 2005, Minolta SPAD 502 Meter, Spectrum Technologies, Inc. Available online at : http://www.specmeters.com/Chlorophyll_Meters/Minolta_SPAD_502_Meter.html (Last accessed 19th Sept 2005).
- MORAN, R. and PORATH, D., 1980, Chlorophyll determination in intact tissues using N,N- Dimethylformamide. *Plant Physiology*, **65**, 478-479.
- MUNDEN, R., CURRAN, P. J. and CATT, J. A., 1994, The relationship between red edge and chlorophyll concentration in the Broadbalk winter wheat experiment at Rothamsted. *International Journal of Remote Sensing*, **15**, 705-709.
- MUTANGA, O. and SKIDMORE, A. K., 2004, Narrow band vegetation indices overcome the saturation problem in biomass estimation. *International Journal of Remote Sensing*, **25**, 3999 4014(16).
- MYNENEI, R. B., HOFFMAN, S., KNYAZIKHIN, Y., PRIVETTE, J., GLASSY, J., TIAN, Y., WANG, Y., SONG, X., ZHANG, Y., SMITH, G. R., LOTSCH, A., FRIEDL, M., MORISETTE, J., VTAVA, P., NEMANI, R. R. and RUNNING, S. W., 2002, Global products of vegetation leaf area and fraction absorbed PAR from year one of MODIS data. *Remote Sensing of Environment*, **83**, 214-231.
- MYNENI, R. B., MAGGION, S., IAQUINTO, J., PRIVETTE, J. L., GOBRON, N., PINTY, B., KIMES, D. S., VERSTRAETE, M. M. and WILLIAMS, D. L., 1995, Optical remote-sensing of vegetation - modelling, caveats, and algorithms. *Remote Sensing of Environment*, **51**, 169-188.
- NAS, 2003, Characterizing exposure of veterans to Agent Orange and other herbicides used in Vietnam: Final Report, pp 59 (Washington: The National Academies Press).
- NASA, 2005, Moderate Resolution Imaging Spectroradiometer, Available online at: http://modis.gsfc.nasa.gov/about/media/modis_brochure.pdf (Last accessed 19th Sept 2005).

- NEMANI, R., PIERCE, L. L., RUNNING, S. and BAND, L., 1993, Forest ecosystem process at the watershed scale: Sensitivity to remotely-sensed leaf area index estimates. *International Journal of Remote Sensing*, **14**, 2519-2534.
- NERC, 2005, National Environmental Research Council, Field Spectroscopy Facility. Available online at: <http://fsf.nerc.ac.uk/> (Last accessed 11th July 2005).
- NIEMANN, K. O., 1995, Remote Sensing of forest stands age using airborne spectrometer data. *Photogrammetric Engineering & Remote Sensing*, **61**, 1119-1127.
- NORTH, P. R. J., 1996, Three-dimensional forest light interaction model using a Monte Carlo method. *IEEE Transactions on Geoscience and Remote Sensing*, **34**, 946-956.
- OLYMPUS, 2005, Olympus c700 Users manual, Available online at: http://www.olympusamerica.com/cpg_section/cpg_archived_product_detail_s.asp?fl=2&id=677 (Last accessed 19th Sept 2005).
- O'NEILL, A. L., KUPIEC, J. A. and CURRAN, P. J., 2002, Biochemical and reflectance variation throughout a Stika spruce canopy. *Remote Sensing of Environment*, **80**, 134-142.
- OTTERMAN, J., 1981, Reflection from soil with sparse vegetation. *Advances in Space Research*, **1**, 115-119.
- PAL, M. and MATHER, P. M., 2003, An assessment of the effectiveness of decision tree methods for land cover classification. *Remote Sensing of Environment*, **86**, 554-565.
- PANDEY, D. M., KANG, K. H. and YEO, U. D., 2005, Effects of excessive photon on the photosynthetic pigments and violaxanthin de-epoxidase activity in the xanthophyll cycle of spinach leaf. *Plant Science*, **168**, 161-166.
- PARK S., FEDDEMA J.J. and EGBERT S.L, 2004, Impacts of hydrologic soil properties on drought detection with MODIS thermal data. *Remote Sensing of Environment*, **89**, 53-62.
- PARK, Y. I., CHOW, W. S. and ANDERSON, J. M., 1996, Chloroplast movement in the shade plant *Tradescantia albiflora* helps protect photosystem II against light stress. *Plant Physiology*, **111**, 867-875.
- PATEL, N. K., PATNAIK, C., DUTTA, S., SHEKH, A. M. and DAVE, A. J., 2001, Study of crop growth parameters using Airborne Imaging Spectrometer data. *International Journal of Remote Sensing*, **22**, 2401-2411.
- PERKIN ELMER, 2005, Lambda 800 systems. Available online at: <http://las.perkinelmer.com/default.htm> (Last accessed 19th Sept 2005)
- PETERSON, A. L. and WIEGAND, C. L., 1977, Distinguishing vegetation from soil background information. *Photogrammetric Engineering & Remote Sensing*, **43**, 1541-1552.

- PETERSON, D. L., ABER, J. D., MATSON, P. A., CARD, D. H., SWANBERG, N., WESSMAN, C. and SPANNER, M., 1988, Remote sensing of forest canopy and leaf biochemical content. *Remote Sensing of Environment*, **24**, 85-108.
- PETITCOLIN, F. and VERMOTE, E., 2002, Land surface reflectance, emissivity and temperature from MODIS middle and thermal infrared data. *Remote Sensing of Environment*, **83**, 112-134.
- PETTERSSSEN, S., 1941, *Introduction to Meteorology* (London: McGraw-Hill Book Company Inc).
- PINAR, A. and CURRAN, P. J., 1996, Grass chlorophyll and the reflectance red edge. *International Journal of Remote Sensing*, **17**, 351-357.
- PINTY, B. and VERSTRAETE, M. M., 1992, GEMI - a nonlinear index to monitor global vegetation from satellites. *Vegetatio*, **101**, 15-20.
- PORTER, W. M. and ENMARK, H. T., 1987, A system overview of the Airborne Visible/Infrared Imaging Spectrometer (AVIRIS). *Proceeding of SPIE*-834.
- PRICE, J., 1990, On the information content of soil reflectance spectra. *Remote Sensing of Environment*, **33**, 113-121.
- PRIVETTE, J. L., ASNER, G. P., CONEL, J., HUENNRICH, K. F., OLSON, R., RANGO, A., RAHMAN, A. F., THOME, K. and WALTER-SHEA, E. A., 2000, The EOS prototype validation exercise (PROVE) at Jornada: Overview and lessons learned. *Remote Sensing of Environment*, **74**, 1-12.
- PRIVETTE, J. L., MYNENI, R. B., KNYAZIKHIN, Y., MUKELABAI, M., ROBERTS, G., TIAN, Y., WANG, Y. and LEBLANC, S. G., 2002, Early spatial and temporal validation of MODIS LAI product in the southern Africa Kalahari. *Remote Sensing of Environment*, **83**, 232-243.
- PU, R., GONG, P. and BIGING, G. S., 2003, Simple calibration of AVIRIS data and LAI mapping of forest plantation in southern Argentina. *International Journal of Remote Sensing*, **24**, 4699-4714.
- RAHMAN, H. and DEDIEU, G., 1994, SMAC: A simplified method for the atmospheric correction of satellite measurements in the solar spectrum. *International Journal of Remote Sensing*, **15**, 123-143.
- RAILYAN, Y. and KOROBV, R. M., 1993, Red edge structure of canopy reflectance spectra of triticale. *Remote Sensing of Environment*, **46**, 173-182.
- RANSON, K. J., BIEHL, L. L. and BAUER, M. E., 1985, Variation in spectral response of soybeans with respect to illumination, view and canopy geometry. *International Journal of Remote Sensing*, **6**, 1827-1842.

- RAO, R. G. S and ULABY, F. T., 1977, Optimal spatial sampling techniques for ground truth data in microwave remote sensing of soil moisture. *Remote Sensing of Environment*, **6**, 289-301.
- RAST, M., BÉZY, J. L. and BRUZZI, S., 1999, The ESA medium resolution imaging spectrometer MERIS: a review of the instrument and its mission. *International Journal of Remote Sensing*, **20**, 1681-1702.
- RAUTIAINEN, M., STENBERG, P., NILSON, T., KUUSK, A. and SMOLANDER, H., 2003, Application of a forest reflectance model in estimating leaf area index of Scots pine stands using Landsat-7 ETM reflectance data. *Canadian Journal of Remote Sensing*, **29**, 314-323.
- REESE, H. M., LILLESAND, T. M., NAGEL, D. E., STEWART, J. S., GOLDMANN, R. A., SIMMONS, T. E., CHIPMAN, J. W. and TESSAR, P. A., 2002, Statewide land cover derived from multiseasonal Landsat TM data - A retrospective of the WISCLAND project. *Remote Sensing of Environment*, **82**, 224-237.
- REEVES, D. W., MASK, P. L., WOOD, C. W. and DELANEY, D. P., 1993, Determination of wheat nitrogen status with a hand-held chlorophyll meter influence of management-practices. *Journal of Plant Nutrition*, **16**, 781-796.
- REEVES, M. C., ZHAO, M. and RUNNING, S. W., 2005, Usefulness and limits of MODIS GPP for estimating wheat yield. *International Journal of Remote Sensing*, **26**, 1403-1421.
- ROBERTS, D. A., SMITH, M. O. and ADAMS, J. B., 1993, Green vegetation, nonphotosynthetic vegetation and soil in AVIRIS data. *Remote Sensing of Environment*, **44**, 225-269.
- ROGER, R. E. and ARNOLD, J. F., 1996, Reliably estimating the noise in AVIRIS hyperspectral images. *International Journal of Remote Sensing*, **17**, 1951-1962.
- ROSS, J. K. and MARSHAK, A. L., 1988, Calculation of canopy bidirectional reflectance using the Monte Carlo method. *Remote Sensing of Environment*, **24**, 213-225.
- ROUSE, J. W., HAAS, R. H., SCHELL, J. A. and DEERING, D. W., 1974, Monitoring vegetation systems in the Great Plains with ERTS. In *Proceedings of the Third EarthResources Technology Satellite-1 Symposium*, pp. 301-317 (Greenbelt: NASA).
- ROWLAND, C. S., DANSON, F. M., NORTH, P. R. J. and PLUMMER, S. E., 2000, Retrieval of forest LAI using neural network inversion methods and GeoSAIL. In *Proceeding of RSS 2000: Adding Values to Remotely Sensed Data*, Leicester, UK.
- ROY, D. P., LEWIS, P. and JUSTICE, C., 2002, Burned area mapping using multi-temporal moderate spatial resolution data—a bi-directional reflectance

- model-based expectation approach. *Remote Sensing of Environment*, **83**, 263-286.
- RUNNING, S. W., LOVELAND, T. R., PIERCE, L. L., NEMANI, R. and HUNT, E. R., 1995, A remote sensing based vegetation classification logic for global land-cover analysis. *Remote Sensing of Environment*, **51**, 39-48.
- SAGAN, C., THOMPSON, W. R., CARLSON, R., GURNETT, D. and HORD, C., 1993, A search for life on Earth from the Galileo spacecraft. *Nature*, **365**, 715-721.
- SCHLERF, M. and ATZBERGER, C., 2003, Use of a forest reflectance model for empirical estimation of Norway spruce characteristics from hyperspectral remote sensing imagery.
- SCHLERF, M., ATZBERGER, C. and HILL, J., 2005, Remote sensing of forest biophysical variables using HyMap imaging spectrometer data. *Remote Sensing of Environment*, **95**, 177-194.
- SEAGER, S., TURNER, E. L., SCHAFER, J. and FORD, E. B., 2005, Vegetation's red edge: A possible spectroscopic biosignature of extraterrestrial plants. *Astrobiology*, **5**, 372-390.
- SELLERS, P. J., HEISER, M. D., HALL, F. G., GOETZ, S. J., STREBEL, D. E., VERMA, S. B., DESJARDINS, R. L., SCHUEPP, P. M. and MACPHERSON, J. I., 1995, Effects of spatial variability in topography, vegetation cover and soil moisture on area-averaged surface fluxes: A case study using the FIFE 1989 data. *Journal of Geophysical Research-Atmospheres*, **100**, 25607-25629.
- SHARP, J. H., 1983, The distribution of inorganic nitrogen and dissolved and particulate organic nitrogen in the sea. In *Nitrogen in the marine environment*, edited by E. J. Carpenter and D. G. Capone, pp. 1-32 (New York: Academic Press).
- SHAW, D. T., MALTHUS, T. J. and KUPIEC, J. A., 1998, High-spectral resolution data for monitoring Scots pine (*Pinus Sylvestris*) regeneration. *International Journal of Remote Sensing*, **19**, 2601-2608.
- SINGH, R. P., OLBERT, C., LINDEMANN, C., SCHAALE, M. and FURRER, R., 1997, Atmospheric monitoring with a spectrographic imager. *International Journal of Remote Sensing*, **18**, 1183-1188.
- SMITH, G. M. and CURRAN, P. J., 1992, Exploring the remote sensing of foliar biochemical concentration with AVIRIS data. In *AVIRIS Airborne Geoscience Workshop Proceedings*, Pasadena, CA.
- SMITH, G. M. and CURRAN, P. J., 1999, Methods for estimating image signal-to-noise ratio (SNR). In *Advances in Remote Sensing and GIS Analysis*, edited by P. M. Atkinson and N. J. Tate, pp. 61-74 (Chichester: John Wiley and Sons Ltd.).

- SMITH, K. L., STEVEN, M. D. and COLLS, J. J., 2004, Use of hyperspectral derivative ratios in the red-edge region to identify plant stress responses to gas leaks. *Remote Sensing of Environment*, **92**, 207-217.
- SMITH, P. M., KALLURI, S. N. V., PRINCE, S. D. and DEFRIES, R., 1997, The NOAA/NASA pathfinder AVHRR 8-km land data set. *Photogrammetric Engineering and Remote Sensing*, **63**, 12-&.
- SPACE UK, 2005, Satellites respond to disaster relief. *SPACE:UK*, **15**, 4-5.
- SPARC, 2005, SPARC experimenters' handbook. Available online at: http://gpds.uv.es/sparc/docs/SPARC_Experimenters_Handbook_2004_DR_AFT_5.pdf (Last accessed 19th Sept 2005).
- STEELE, B. M., 2000, Combining multiple classifiers: An application using spatial and remotely sensed information for land cover type mapping. *Remote Sensing of Environment*, **74**, 545-556.
- STELLMAN, J., STELLMAN, M., CHRISTIAN, S. D., WEBER, R. and TOMASALLO, C., 2003, The extent and patterns of usage of Agent Orange and other herbicides in Vietnam. *Nature*, **422**, 681-687.
- STENBACK, J. M. and CONGALTON, R. G., 1990, Using thematic mapper imagery to examine forest understory. *Photogrammetric Engineering & Remote Sensing*, **56**, 1285-1290.
- STEVEN, M. D., MALTHUS, T. J., DEMETRIADES-SHAH, T. H., DANSON, F. M. and CLARK, J. A., 1990, High-spectral resolution indices for crop stress. In *Applications of remote sensing in agriculture*, edited by M. D. Steven and J. A. Clark, pp. 201-228 (London: Butterworths).
- SU, H., RANSOM, M. D. and KANEMASU, E. T., 1997, Simulating wheat crop residue reflectance with the SAIL model. *International Journal of Remote Sensing*, **18**, 2261-2267.
- SUDBRINK JR1, D. L., HARRIS, F. A., ROBBINS, J. T., ENGLISH, P. J. and WILLERS, J. L., 2003, Evaluation of remote sensing to identify variability in cotton plant growth and correlation with larval densities of beet armyworm and cabbage looper (lepidoptera: noctuidae). *Florida Entomologist*, **86**, 290-294.
- SUITS, G. H., 1972, The calculation of the directional reflectance of vegetative canopies. *Remote Sensing of Environment*, **2**, 117-125.
- SVANBERG, S., 1992, *Atomic and Molecular Spectroscopy* (Berlin: Springer-Vrlag).
- TESTON, F., BARNESLEY, M., SETTLE, J., VUILLEUMIER, P. and SANTANDREA, S., 2003, PROBA: An ESA technology demonstration mission with earth imaging payload. First year of in orbit result. In *Proceeding of 4th IAA Symposium on Small Satellites for Earth Observation*, Berlin, Germany.

- THENKABAIL, P. S., SMITH, R. B. and PAUW, E. D., 2000, Hyperspectral Vegetation Indices and Their Relationships with Agricultural Crop Characteristics. *Remote Sensing of Environment*, **71**, 158-182.
- TIAN, Y. H., WOODCOCK, C. E., WANG, Y. J., PRIVETTE, J. L., SHABANOV, N. V., ZHOU, L. M., ZHANG, Y., BUERMANN, W., DONG, J. R., VEIKKANEN, B., HAME, T., ANDERSSON, K., OZDOGAN, M., KNYAZIKHIN, Y. and MYNENI, R. B., 2002, Multiscale analysis and validation of the MODIS LAI product - I. Uncertainty assessment. *Remote Sensing of Environment*, **83**, 414-430.
- TOBEHN, C., KASSEBOHM, M. and SCHMÄLTER, E., 2003, SPECTRA – ESA candidate Earth explorer core mission – feasibility, results and outlook. In *Proceeding of 4th IAA Symposium on Small Satellites for Earth Observation*, Berlin, Germany.
- TOOD, S. W., HOFFER, R. M. and MILCHUNAS, D. G., 1998, Biomass estimation on grazed and ungrazed rangelands using spectral indices. *International Journal of Remote Sensing*, **19**, 427-438.
- TOWNSHEND, J. and JUSTICE, C., 2002, Special issue on the moderate resolution imaging spectroradiometer (MODIS): a new generation of land surface monitoring. *Remote Sensing of Environment*, **83**, 1-2.
- TREITZ, P. and ROGAN, J., 2004, Remote Sensing for mapping and monitoring land-cover and land- use change. *Progress in Planning*, **61**, 267-278.
- TREITZ, P. M. and HOWARTH, P. J., 1999, Hyperspectral remote sensing for estimating biophysical parameters of forest ecosystems. *Progress in Physical Geography*, **23**, 359-390.
- TSAI, F. and PHILPOT, W., 1998, Derivative analysis of hyperspectral data. *Remote Sensing of Environment*, **66**, 41-51.
- TSENG, Y., 1999, Spectral mixture analysis for hyperspectral data. In *Proceeding of the 20th Asian Conference on Remote Sensing*, Hong Kong.
- TUCKER, C. J. and GARRAT, M. W., 1977, Leaf optical system modelled as a stochastic process. *Applied Optics*, **16**, 635-642.
- TUCKER, C. J., PINZON, J. E., BROWN, M. E., SLAYBACK, D. A., PAK, E. W. and MAHONEY, R., 2005, An extended AVHRR 8-km NDVI data set compatible with MODIS and SPOT Vegetation NDVI data. *International Journal of Remote Sensing*,
- TUCKER, C. J., TOWNSHEND, J. R. G. and GOFF, T. E., 1985, African landcover classification using satellite data. *Science*, **227**, 369-375.
- UNITED NATIONS NEWS, 2005, Available online at: www.un.org/News/ (accessed 20 March 2005).
- USTIN, S. L., SMITH, M. O., JACQUEMOUD, S., VERSTRAETE, M. and GOVAERTS, Y., 1999, Geobotany: Vegetation mapping for Earth science. In *Remote*

Sensing for the Earth Science: Manual of Remote Sensing, edited by A. N. Rencz, pp. 189-247 (New York: John Wiley & sons, Inc.).

- VANE, G., 1987, Earth Observing System: a platform for imaging spectrometers. *SPIE 834, Imaging Spectroscopy II*, pp. 176-180.
- VANE, G., GOETZ, A. F. H. and WELLMAN, J. B., 1984, Airborne imaging spectrometer - A new tool for remote-sensing. *IEEE Transactions on Geoscience and Remote Sensing*, **22**, 546-549.
- VANE, G., GREEN, R. O., CHRIEN, T. G., ENMARK, H. T., HANSEN, E. G and PORTER, W. M, 1993, The Airborne visible/infrared imaging spectrometer (AVIRIS). *Remote Sensing of Environment*, **44**, 127-143.
- VERHOEF, W., 1984, Light scattering by leaf layers with application to canopy reflectance modelling: The SAIL model. *Remote Sensing of Environment*, **16**, 125-141.
- VERHOEF, W., 1985, Earth observation modeling based on layer scattering matrices. *Remote Sensing of Environment*, **17**, 165-178.
- VERMA, K. S., SAXENA, R. K., HAJARE, T. N., KHARCHE, V. K. and KUMARI, P. A., 2002, Spectral response of gram varieties under variable soil conditions. *International Journal of Remote Sensing*, **23**, 313-324.
- VERSTRAETE, M. M. and PINTY, B., 1996, Designing optimal spectral indexes for remote sensing applications. *IEEE Transactions on Geoscience and Remote Sensing*, **34**, 1254-1265.
- VERSTRAETE, M. M., PINTY, B. and CURRAN, P. J., 1999, MERIS potential for land application. *International Journal of Remote Sensing*, **20**, 1747-1756.
- VOGELMANN, J. E., ROCK, B. N. and MOSS, D. M., 1993, Red edge spectral measurements from sugar maple leaves. *International Journal of Remote Sensing*, **14**, 1563-1575.
- WADA, M., KAGAWA, T. and SATO, Y., 2003, Chloroplast movement. *Annual Review of Plant Biology*, **54**, 455-468.
- WANG, Y. J., WOODCOCK, C. E., BUERMANN, W., STENBERG, P., VOIPIO, P., SMOLANDER, H., HAME, T., TIAN, Y. H., HU, J. N., KNYAZIKHIN, Y. and MYNENI, R. B., 2004, Evaluation of the MODIS LAI algorithm at a coniferous forest site in Finland. *Remote Sensing of Environment*, **91**, 114-127.
- WEBSTER, R. and OLIVER, M., 2000, *Geostatistics for Environmental Scientist*, (Chichester: John Wiley and Sons Ltd.).
- WEBSTER, R., 1985, Quantitative spatial analysis of soil in the field. *Advances in Soil Science*, **3**, 1-70.

- WELLBURN, A. R., 1994, The spectral determination of chlorophyll-a and chlorophyll-b, as well as total carotenoids, using various solvents with spectrophotometers of different resolution. *Journal of Plant Physiology*, **144**, 307-313.
- WIDNR, 1998, User's Guide to WISCLAND Land Cover data. *Wisconsin Department of Natural Resources*.
- WILKINSON, G. G., 2005, Results and implications of a study of fifteen years of satellite image classification experiments. *IEEE Transactions on Geoscience and Remote Sensing*, **43**, 433-440.
- WILL, R. E. and TESKEY, R. O., 1999, Influence of rate of change in stomatal conductance to fluctuating irradiance on estimates of daily water use by *Pinus taeda* leaves. *Tree physiology*, **19**, 761-765.
- WOOLF, N. J., SMITH, P. S., TRAUB, W. A. and JUCKS, K. W., 2002, The spectrum of earthshine: A pale blue dot observed from the ground. *Astrophysical Journal*, **574**, 430-433.
- WULDER, M., 1998, Optical remote sensing techniques for the assessment of forest inventory and biophysical parameters. *Progress in Physical Geography*, **22**, 449-476.
- WYLIE, B. K., DENDA, I., PIEPER, R. D., HARRINGTON, J. A., REED, B. C. and SOUTHWARD, G. M., 1995, Satellite based herbaceous biomass estimates in the pastoral zone of Niger. *Journal of Range Management*, **48**, 159-164.
- YANG, C and SU, M., 2000, Analysis of spectral characteristics of rice canopy under water deficiency. In *Proceeding of The 21st Asian Conference on Remote Sensing*, Taipei, Taiwan.
- YODER, B. and JOHNSON, L., 1999, Seedling Canopy Chemistry, 1992-1993 (ACCP) (Accelerated Canopy Chemistry Program). *Data set. Available on-line [http://www.daac.ornl.gov] from Oak Ridge National Laboratory Distributed Active Archive Center, Oak Ridge, Tennessee, U.S.A.*,
- YODER, B. J and PETTIGREW-CROSBY, R. E., 1995, Predicting nitrogen and chlorophyll content and concentration from reflectance spectra (400-2500 nm) at leaf and canopy scale. *Remote Sensing of Environment*, **53**, 199-211.
- YOUNG, A. L. and REGGIANI, G. M., 1988, *Agent Orange and Its Associated Dioxin: Assessment of a Controversy* (Amsterdam: Elsevier).
- YOUNG, A. L., 1975, Studies of the ecological impact of repetitive aerial applications of herbicides on the ecosystem of test area C-52A, Eglin AFB, Florida. *United States Air Force Academy, Department of Chemistry and Physiology, Colorado*.
- ZAGOLSKI, F., PINEL, V., ROMIER, R., ALCAYDE, D., FONTANRI, J., GASTELLU-ETCHEGORRY, J. P., GIORDANO, G., MARTY, G., MOUGIN, E. and

- JOFFRE, R., 1996, Forest canopy chemistry with high spectral resolution remote sensing. *International Journal of Remote Sensing*, **17**, 1107-1128.
- ZARCO-TEJADA, P. J. and MILLER, J. R., 1999, Land cover mapping at BOREAS using red edge spectral parameters from CASI imagery. *Journal of Geophysical Research*, **104**, 921-933.
- ZARCO-TEJADA, P. J., MILLER, J. R., MOHAMMED, G. H. and NOLAND, T. L., 2000, Chlorophyll fluorescence effect on vegetation apparent reflectance: I. Leaf level measurements and model simulation. *Remote Sensing of Environment*, **74**, 582-595.
- ZARCO-TEJADA, P. J., MILLER, J. R., MOHAMMED, G. H., NOLAND, T. L. and SAMPSON, P. H., 2001, Estimation of chlorophyll fluorescence under natural illumination from hyperspectral data. *International Journal of Applied Earth Observation and Geoinformation*, **3**, 321-327.
- ZARCO-TEJADA, P. J., PUSHNIK, J. C., DOBROWSKI, S. and USTIN, S. L., 2003, Steady- state chlorophyll a fluorescence detection from the canopy reflectance and double-peak red-edge effects. *Remote Sensing of Environment*, **84**, 283-294.

Appendix-1

User note for the programme refg1500, which was used to obtain reflectance spectra from radiance recorded by the GER-1500.

NERC FSF GER 1500 USER NOTE PRIMARY PROCESSING SOFTWARE - REFG1500.EXE v1.3

C. H. Kerr, April 1998

REFG1500.EXE is a MS-DOS program which performs an absolute reflectance calculation on a GER 1500 signature format spectrum by ratioing the target/reference spectral pair, then applying a correction using a panel calibration. An optional correction for low sun-angle may also be applied. The output data is written in two-column comma-delimited (CSV) format, wavelength and reflectance, to an ASCII (text) file specified in the command line. Wildcards cannot be used.

Usage :

```
refg1500 [-a d h] [-sX] [-o] <signature> <panel> <output>
```

where <signature> is the name of the GER 1500 signature format spectra filename, and <panel> is the name of an ASCII-format panel calibration file; <output> is the name of the text file to be created. If no extension is specified, **REFG1500** will append the extension .ABS (for absolute reflectance) to the filename. The panel calibration file will be in a form similar to the file **ST13160A.PAN** and should be in the current directory when running **REFG1500**.

Flags :

- a write FSF header and reflectance data to file (recommended ¹),
- d write reflectance data only,
- h write GER header data only (default),
- sX apply a sun-angle correction factor of value X ²
- o allows the output file to overwrite pre-existing files but NOT any of the input files.

Example :

```
refg1500 -a -s1.25 -o grass.001 st13160a.pan sample
```

Using these command line parameters, **REFG1500** will ratio the target and reference spectra in the GER signature file 'grass.001', apply a correction using the data in the panel calibration file 'st13160a.pan', with a sun-angle factor of 1.25, and write the resulting reflectance data to a text file 'sample.abs'. The program will overwrite the output file if it already exists. Header information will be included.

Note :

1. It is recommended that all absolute reflectance data files created with REFG1500 should contain the FSF header (using the **-a** flag). This will ensure compatibility with current and future post processing software developed by the NERC FSF.
2. For further details on the use of the sun-angle correction factor, see FSF user note **GEN/98/SW3**.

Disclaimer :

REFG1500.EXE is the property of the UK National Environment Research Council Field Spectroscopy Facility. It is supplied "as is". The NERC FSF will not be held responsible for any loss of data, damage to hardware or software incurred through use of this program. The NERC FSF make no claims as to the accuracy, performance or functionality of this program.

Appendix-2

Data to estimate the sample number of a leaf for SPAD measurements

Sample no	Data	Data	Data	Calculation
Sample-1	41	43.7	41.2	Number of data points= 47
	39.9	40.9	39.4	
	38.4	38.6	39.4	Standard deviation =
	44.7	41.7	43.2	2.61017
	40.5	41.2	41.1	
	44.2	42.9	46.7	Students t from table =
	44.2	40.8	44	2.012
	41	40.5	42.3	(http://www.itl.nist.gov/div898/handbook/eda/section3/eda3672.htm)
	44.8	43.7	41	
	46.5	41	40.9	
	39.5	39.9	38.9	
	43.6	38.4	39.1	accuracy level= ± 1.5
	42.9	46.8	40.5	
	39.7	42.6		Number of Samples (SN)=
	38.1			6.894989(7)
	47			
	48.1			
	43.6			
	41.6			
	46.6			
Sample-2	48.5	48.5	45.9	Number of data points= 44
	48.4	47.8	50	
	46.6	49.7	47.2	Standard deviation = 2.26
	46.2	50.2	50.1	
	50.7	48.1	47.2	Students t from table =
	42.5	48.8	49.7	2.015
	45.5	48	46.7	(http://www.itl.nist.gov/div898/handbook/eda/section3/eda3672.htm)
	50.5	43.6	45.9	
	50.2	40.7	49.7	
	47.9	50	43.7	
	45.7	49.1		accuracy level= ± 1.5
	47.5	47.7		
	47.9	45.5		Number of Samples (SN)=
	51	48		5.196374(6)
	48.4	49.2		
	45.7	48.3		
	49.1	49.5		

Sample-3	46.4	48.2	47.7	Number of data points= 42
	44.8	44.3	44.7	
	42.6	42.5	44.5	Standard deviation = 2.68
	39.1	47.3	49.5	
	48.1	47	46.9	Students t from table =
	48.7	47.5	43.9	2.018
	44.4	44.7	43.9	(http://www.itl.nist.gov/div898/handbook/eda/section3/eda3672.htm)
	48.6	41.9	45.6	
	48.9	46.9	45.9	
	46.6	41.7	48.6	
	45.8	40		accuracy level= ± 1.5
	39.6	40.6		
	46.2	46.2		Number of Samples (SN)=
	44.9	44.5		7.334937(8)
	47.1	46.3		
	47.3	42.1		

Appendix-3

Programme for making the herbicide concentration map from HERBS tapes (file containing information about the herbicide spraying missions in southern Vietnam.

Programme created: 20-02-2004

Programme Language: Perl

Support from: S. S. Modi, School of Electronics and Computer Science, University of Southampton.

Entering Input and output file name

```
print ("\n\n\n Enter the path and name of input file:") ;
```

```
chomp( $filename=<STDIN> ) ;
```

```
open(INFILE,$filename) or die "Can't open the file: $!\n";
```

```
print ("\n\n\n Enter the path and name of output file:") ;
```

```
chomp( $filename=<STDIN> ) ;
```

```
open(OUTFILE1,">$filename") or die "Can't open the file for writing: $!\n";
```

```
$flight_path_no =1;
```

```
print OUTFILE "$flight_path_no ----- \n";
```

Entering the maximum and minimum Easting and Northing in UTM of the area.

```
print " Enter Min Grid x coordinate;;
```

```
chomp( $grid_min_x=<STDIN> ) ;
```

```
print " Enter Min Grid y coordinate;;
```

```
chomp( $grid_min_y=<STDIN> ) ;
```

```
print " Enter Max Grid x coordinate;;
```

```
chomp( $grid_max_x=<STDIN> ) ;
```

```
print " Enter Max Grid y coordinate;;
```

```
chomp( $grid_max_y=<STDIN> ) ;
```

```
$grid_spacing = 300 ;
```

```
$r = 2000 ;
```

Generating the 300 m X 300 m grid

```
$workgrid_max_x=$grid_max_x-$grid_min_x;
```

```
$workgrid_min_x=0;
```

```
$workgrid_max_y=$grid_max_y-$grid_min_y;
```

```
$workgrid_min_y=0;
```

```
$ct=0;
```

```
print ("\n\n\n\n initialising:") ;
```

```

for ( $cell_y=$workgrid_min_y;$cell_y<=$workgrid_max_y;$cell_y=$cell_y+
$grid_spacing) {
    for (
$cell_x=$workgrid_min_x;$cell_x<=$workgrid_max_x;$cell_x=$cell_x+$grid_spaci
ng) {
        # $temp_x=$cell_x+$grid_min_x;$temp_y=$cell_y+$grid_min_y;
        # print " grid_matrix[$temp_x][$temp_y] = 0\n";
        $grid_matrix[$cell_x][$cell_y]=0;
        }
        print"$ct\n";
        $ct=$ct+1;
    }

print ("\n\n\n\n initialising finish:" );

*****
Giving each grid cell one identification number
*****

$line=<INFILE>;
chomp($line);
$line=~ s/(s)+/ /g; ##--- removing extra white spaces
$line=~ s/^\s+//g;    ##--- removing first white spaces
@split_line= split ( /\s/, $line);

$old_id = $split_line[0];
$old_id =~ /\^(d+)/; $old_n_id = $1; # print "$current_n_id ";
$old_s_id = $old_id; $old_s_id =~ s/^\(d+)///; # print "$current_s_id \n ";

$coord_cnt = 0 ;
$flight_start_at = 0 ;
$x_coord_set[$coord_cnt] = $split_line[1]; print
OUTFILE "$x_coord_set[$coord_cnt] ";
$y_coord_set[$coord_cnt] = $split_line[2]; print
OUTFILE "$y_coord_set[$coord_cnt] ";
if ( defined $split_line[3]) {
    $cons_set[$coord_cnt] = $split_line[3]; print
OUTFILE "$cons_set[$coord_cnt] ";
}
else {
    $cons_set[$coord_cnt] = [0];
}
print OUTFILE "\n";
$coord_cnt++;

```

```
*****
Reading the input file and assigning each cell the concentration
*****
```

```
while(<INFILE>)
{
    chomp;
    $line=$_;
    $line=~ s/(\s)+/ /g; ##--- removing extra white spaces
    $line=~ s/^\s+//g;    ##--- removing first white spaces
    @split_line= split ( /\s/, $line);
    $current_id = $split_line[0];
    $current_id =~ /^(\d+)/; $current_n_id = $1; #print "$current_n_id ";
    $current_s_id = $current_id; $current_s_id =~ s/^\d+//; # print
"$current_s_id \n ";

    if ( $current_n_id != $old_n_id ) {
        unless ( $flight_start_at == $coord_cnt - 1 ) {
            $temp = $coord_cnt - 1 ;
            print OUTFILE "\n lenght from $flight_start_at to $temp ";
            $flight_point1=$flight_start_at;
            $flight_point2=$flight_start_at+1;
            $total_length=0;
            do {
                $total_length = $total_length + line_r (
$flight_point1,$flight_point2);
                #find_poly($flight_ppoint1,$flight_point2);
                $flight_point1++;$flight_point2++;
            } while ( $flight_point2 + 1 <= $coord_cnt );
            print OUTFILE "= $total_length ";
            $cons = $cons_set[$flight_start_at] / $total_length ;
            print OUTFILE " hence conscentration = $cons \n";
            $flight_point1=$flight_start_at;
            $flight_point2=$flight_start_at+1;
            $total_length=0;
            do {
                #print " calling update grid\n";

                update_grid($flight_point1,$flight_point2,$cons);
                $flight_point1++;$flight_point2++;
            } while ( $flight_point2 + 1 <= $coord_cnt );

        }

        $flight_start_at = $coord_cnt;
        $flight_path_no++;
        print OUTFILE "$flight_path_no ----- \n";
    }
    else
    {
        if ( $current_s_id le $old_s_id ) {
```

```

unless ( $flight_start_at == $coord_cnt -1 ) {

    $temp = $coord_cnt- 1 ;
    print OUTFILE "\n lenght from $flight_start_at
to $temp ";

    $flight_point1=$flight_start_at;
    $flight_point2=$flight_start_at+1;
    $total_length=0;
    do {
        $total_length = $total_length + line_r (
$flight_point1,$flight_point2);

        $flight_point1++;$flight_point2++;
    } while ( $flight_point2 +1 <= $coord_cnt ) ;
    print OUTFILE "= $total_length ";
    $cons = $cons_set[$flight_start_at] /

$total_length ;

\n";

    $flight_point1=$flight_start_at;
    $flight_point2=$flight_start_at+1;
    $total_length=0;
    do {
        print " calling update grid\n";

        update_grid($flight_point1,$flight_point2,$cons);
        $flight_point1++;$flight_point2++;
    } while ( $flight_point2 +1 <= $coord_cnt ) ;

    }

    $flight_start_at = $coord_cnt;
    $flight_path_no++;

    print OUTFILE "$flight_path_no ----- \n";

}

}

    $x_coord_set[$coord_cnt] = $split_line[1];print
OUTFILE"$x_coord_set[$coord_cnt] ";
    $y_coord_set[$coord_cnt] = $split_line[2];print
OUTFILE"$y_coord_set[$coord_cnt] ";
    if ( defined $split_line[3]) {
        $cons_set[$coord_cnt] = $split_line[3];print
OUTFILE"$cons_set[$coord_cnt] ";
    }
    else {
        $cons_set[$coord_cnt] = [0];
    }
    print OUTFILE "\n";

```

```

Sold_n_id = $current_n_id; Sold_s_id = $current_s_id;

$coord_cnt++;
};

sub line_r {

    my ($x,$y );
    $point1 = $_[0]; $point2 = $_[1];
    $x = $x_coord_set[$point1] - $x_coord_set[$point2];
    $y = $y_coord_set[$point1] - $y_coord_set[$point2];
    return ( sqrt ( ( $x*$x ) + ( $y*$y ) ) ) ;
}

print "@x_coord_set \n";

```

MainLoop;

```

sub find_poly {
    my ( $x1,$y1,$x2,$y2,$m1,$m2 ) ;
    $point1 = $_[0]; $point2 = $_[1];
    $x1 = $x_coord_set[$point1];
    $y1 = $y_coord_set[$point1];
    $x2 = $x_coord_set[$point2];
    $y2 = $y_coord_set[$point2];

    $m1 = ($y2-$y1)/($x2-$x1);
    $m2 = -1 / $m1 ;
}

```

Subroutine for updating the grid cell with concentration values

```

sub update_grid{
    my ($point1, $point2,$conc);

my($max_x,$min_x,$max_y,$min_y,$cell_x,$cell_y,$x1,$x2,$y1,$y2,$tmp_x1,$tmp_x2,$tmp_y1,$tmp_y2);
    $point1 = $_[0]; $point2 = $_[1]; $conc = $_[2];
    $x1 = $x_coord_set[$point1];
    $y1 = $y_coord_set[$point1];
    $x2 = $x_coord_set[$point2];
    $y2 = $y_coord_set[$point2];

    $x1=(int ($x1/$grid_spacing))*$grid_spacing;
    $x2=(int ($x2/$grid_spacing))*$grid_spacing;
    $y1=(int ($y1/$grid_spacing))*$grid_spacing;

```

```

$y2=(int ($y2/$grid_spacing))*$grid_spacing;
## findind relevent cell range##

if($x1> $x2) {
    $max_x=$x1;$min_x=$x2;
}
else {
    $max_x=$x2;$min_x=$x1;
}
if($y1> $y2) {
    $max_y=$y1;$min_y=$y2;
}
else {
    $max_y=$y2;$min_y=$y1;
}

$tmp_x1=(int ($grid_min_x/$grid_spacing))*$grid_spacing;
$tmp_y1=(int ($grid_min_y/$grid_spacing))*$grid_spacing;

$max_x = $max_x - $tmp_x1;
$min_x = $min_x - $tmp_x1;
$max_y = $max_y - $tmp_y1;
$min_y = $min_y - $tmp_y1;

print OUTFILE "\n updating cells ($min_x,$min_y) to ($max_x,$max_y)
with $conc\n";
for ( $cell_y=$min_y;$cell_y<=$max_y;$cell_y+= $grid_spacing) {
    for ( $cell_x=$min_x;$cell_x<=$max_x;$cell_x+= $grid_spacing) {
        if ( $r> find_cell_dist
($x1,$x2,$y1,$y2,($cell_x+$grid_min_x),($cell_y+$grid_min_y))) {
            $grid_matrix[$cell_x][$cell_y] += $conc;

            $temp_x=$cell_x+$grid_min_x;$temp_y=$cell_y+$grid_min_y;
            print OUTFILE" going in $cell_x,$cell_y,
$grid_matrix[$cell_x][$cell_y]\n";
        }
    }
}

print OUTFILE" completing line --- \n";
}

*****
Sub routine for estimating area of Influence for individual mission
*****

sub find_cell_dist {
    my ($line_x1,$line_x2,$line_y1,$line_y2,$point_x,$point_y);
    my ($m1,$m2,$intersect_x,$intersect_y,$dist,$temp1,$temp2);

```

```

$line_x1=$_[0]; $line_x2=$_[1];$line_y1
=$_[2];$line_y2=$_[3];$point_x=$_[4];$point_y=$_[5];
  if (($line_x2 !=$line_x1)&& ($line_y2 !=$line_y1)){

    $m1=($line_y2-$line_y1)/($line_x2-$line_x1);
    $m2=-1/$m1;
    $intersect_x=($point_y-($m2*$point_x)-
$line_y2+($m1*$line_x2))/($m1-$m2);
    $intersect_y=$line_y2-($m1*($line_x2-$point_x));
    $temp1=$intersect_x-$point_x;
    $temp2=$intersect_y-$point_y;
    $dist= sqrt ((($intersect_x-$point_x)*($intersect_x-
$point_x))+(($intersect_y-$point_y)*($intersect_y-$point_y)));
    #print OUTFILE1
"$line_x1,$line_x2,$line_y1,$line_y2,$point_x,$point_y,$intersect_x,$intersect_y,$t
emp1,$temp2,$dist\n";
    return $dist;

  }
  else {
    return 0;
  }

}

*****
END
*****

```


Appendix- 4

One of the log sheets used to record spectral measurements for spinach trays.

SPINACH

double peak appearing f. flowering stress.
17.02.05

NERC EPFS DATA LOG
G15/97/LG1

GER 1500

tray label on left for all measurements

SERIAL No.

SHEET No.

1/4

SITE	Greenhouse	REFERENCE PANEL			
DATE	17.02.05	MODE	STAND ALONE	COMPUTER	DUAL BEAM
OPERATOR	Sadu + Mat	OPTIC	STANDARD	15°	Cosine
ILLUMINATION	Artificial	OPTIC			

TIME	REF. ID	TARG ID	IT	AVG	FILENAME		DESCRIPTION	SKY	PROCESSED FILENAME
					ROOT	EXT.			
					g-170205	000	Low 1.1		
						001	Low 1.2		
						002	Low 1.3		
						003	Low 2.1		
						004	Low 2.2		
						005	Low 2.3		
						006	Low 3.1		
						007	Low 3.2		
						008	Low 3.3		
						009	Medium 1.1		
						010	Medium 1.2		
						011	Medium 1.3		
						012	Medium 2.1		
						013	Medium 2.2		
						014	Medium 2.3		
						015	Medium 3.1		
						016	Medium 3.2		
						017	Medium 3.3		
						018	High 1.1		
						019	High 1.2		
						020	High 1.3		
						021	High 2.1		
						022	High 2.2		
						023	High 2.3		
						024	High 3.1		

SKY CODES : [0] Clear sky; [1] Haze; [2] Thin cirrus - sun not obscured; [3] Thin cirrus - sun obscured; [4] Scattered cumulus - sun not obscured; [5] Cumulus over most of the sky - sun not obscured; [6] Cumulus - sun obscured; [7] complete cumulus cover; [8] Stratus - sun obscured; [9] Drizzle.

tray label = on left at all times

label

← 1

← 2

← 3

so on right

label

← 1

← 2

← 3

Appendix- 5

One of the log sheets used to record spectral measurements for poplar plants.

FOPLAR

GER 1500 at 1.40m above tree

NERC FSF DATA LOG
G15/97/LG1

SERIAL No. P. deltoides cuttings SHEET No.

V2

SITE	Greenhouse	REFERENCE PANEL			
DATE	01.03.05	MODE	STAND ALONE	COMPUTER	DUAL BEAM
OPERATOR	Met + Jordan	OPTIC	STANDARD	15°	Cosine
ILLUMINATION	Artificial	OPTIC			

TIME	REF. ID	TARG ID	IT	AVG	FILENAME		DESCRIPTION	SKY	PROCESSED FILENAME
					ROOT	EXT.			
					g100305	000	black cloth.		
	ref					001	tree 1		
						002	" 1		
						003	" 1		
	ref					004	Tree 2		
						005	" 2		
						006	" 2		
	ref					007	Tree 3		
						008	" 3		
						009	" 3		
	ref					010	Tree 4		
						011	" 4		
						012	" 4		
	ref					013	Tree 5		
						014	" 5		
						015	" 5		
	ref					016	Tree 6		
						017	Tree 6		
						018	" 6		
	ref					019	Tree 7		
						020	" 7		
						021			
	ref					022	Tree 8		
						023	" 8		

STRESSED!

GOOD.

SKY CODES : [0] Clear sky; [1] Haze; [2] Thin cirrus - sun not obscured; [3] Thin cirrus - sun obscured; [4] Scattered cumulus - sun not obscured; [5] Cumulus over most of the sky - sun not obscured; [6] Cumulus - sun obscured; [7] complete cumulus cover; [8] Stratus - sun obscured; [9] Drizzle.

ref = reference taken